Development of Potent and Selective Small-Molecule PROTAC Degraders of SMARCA2 Protein

by

Wenbin Tu

A dissertation submitted in partial fulfillment
of the requirements for the degree of
Doctor of Philosophy
(Medicinal Chemistry)
in The University of Michigan
2024

Doctoral Committee:

Professor Shaomeng Wang, Chair
Associate Professor Amanda Garner
Professor Nouri Neamati
Professor Zaneta Nikolovska-Coleska

Wenbin Tu

tuwenbin@umich.edu

ORCID iD: 0009-0001-8733-9386

© Wenbin Tu 2024

ACKNOWLEDGEMENTS

First and foremost, I would like to express my utmost gratitude to my PhD advisor Dr. Shaomeng Wang. I could still remember the time when I visited the Wang lab and met Dr. Wang for the first time in the summer of 2017 when I was still an undergrad. At that time, I had no idea that this would be the destination that I was going to devote my next 5 years to. As I reflect on my PhD journey, I indeed feel that the Wang lab was such an unparalleled place where real drug discovery is happening, and it was such a privilege for me to have been part of the team in the past 5 years. As my mentor, Dr. Wang not only taught me the state-of-art medicinal chemistry practices, but more importantly, his insights and expertise really had a profound impact on me that transformed my understanding of every drug discovery project in a more in-depth and holistic perspective. These experiences are invaluable for me and my career development in the future. I would also like to thank my thesis committee members, Dr. Nouri Neamati, Dr. Amanda Garner and Dr. Zaneta Nikolovska-Coleska for their advice on my research and their supports for my graduate life.

Next, I would like to thank my former and present colleagues in the Wang lab. I would never have gone this far without their help in the lab. I have been working with the SMARCA project since I joined the Wang lab in May 2019, and I was fortunate enough to have worked with and learned from two of the former lab members who pioneered the SMARCA project: Dr. Bukeyan Miao for his expertise in synthetic organic chemistry, and Dr. Jianfeng Lu for his hands-

on guidance for running Western blots and cell growth inhibition assay on me. I also feel humbled to have worked with some talented chemists, Dr. Lin Yang, Dr. Lingying Leng, Dr. Rohan Rej, Dr. Srinivasa Rao Allu and Dr. Weiguo Xiang, as well as experienced biologists, Dr. Mi Wang, Dr. Liyue Huang and Dr. Wei Jiang, to make so many incredible progresses in the SMARCA project. I was also beyond grateful for my roommates in G393, Dr. Meng Zhang and Dr. Dimin Wu, for their solid and critical advice on every challenging synthetic problem I encountered.

There are also so many thanks that go to my friends in the Wang lab aside from research. I want to express my gratitude to Dr. Bukeyan Miao, Dr. Jiantao Hu, Dr. Fuming Xu, Dr. Lijie Zhao, Dr. Renqi Xu and Yuzhi Wang, for their kind help in my early days in Ann Arbor. I had so much fun fishing with Dr. Lin Yang, Dr. Lingying Leng and Dr. Yukming Siu in Traverse City in 2021, and travelling with Dr. Dimin Wu in the upper peninsula, Chicago, Buffalo, New York City, Princeton, Boston, and Denver.

Last but not least, I would like to thank my parents, relatives and friends in China for their immense support. Even though I was not able to meet them during my PhD due to the great pandemic and China-US political turbulence, I still felt that I was accompanied by their encouragement and care, and we stayed mentally connected.

TABLE OF CONTENTS

ACKNOWLEDGEMENTS ii
LIST OF FIGURES vi
LIST OF TABLES viii
LIST OF SCHEMES x
ABSTRACT xi
Chapter 1 SMARCA2 Targeted Therapies and Targeted Protein Degradation 1
1.1 SMARCA2 as an attractive therapeutic target in SMARCA4-deficient cancers 1
1.2 Small Molecule Inhibitors Targeting SMARCA2 5
1.3 Targeted Protein Degradation as a New Therapeutic Strategy 11
1.4 PROTAC Degraders Targeting SMARCA2 22
Chapter 2 Development of SMD-3040 as a Potent and Selective SMARCA2 PROTAC Degrader 27
2.1 Introduction 27
2.2 Results and discussion 30
2.2.1 Design of Potent and Selective SMARCA2 PROTAC Degraders 30
2.2.2 Evaluation of Degradation Kinetics and the Mechanism of Action of SMD-3040 37
2.2.3 Evaluation of Degradation Potency and Selectivity of SMD-3040 in Different Cell Lines 39
2.2.4 Evaluation of Cell Growth Inhibition of SMD-3040 in Different Cell Lines 42
2.2.5 Pharmacodynamic evaluation of SMD-3040 45
2.2.6 Evaluation of the Efficacy of SMD-3040 in SK-Mel-5 and H838 Xenograft Tumor Models 50
2.3 Chemical Synthesis 53
2.4 Summary 57
2.5 Experimental section 58
Chapter 3 Development of Novel Spiro SMARCA Bromodomain Ligands and Spiro SMARCA2 Selective PROTAC Degraders 82
3.1 Introduction 82
3.2 Results and discussion 85

3.2.1 Structure guided design of novel spiro SMARCA bromodomain ligands 85
3.2.2 Design of selective SMARCA2 PROTAC degraders based on novel spiro SMARCA bromodomain ligands 94
3.2.3 Evaluation of Degradation Kinetics and the Mechanism of Action of SMD-3040. 102
3.2.4 Evaluation of Cell Growth Inhibition of SMD-3040 in Different Cell Lines 105
3.2.5 Pharmacodynamic evaluation of SMD-3236 106
3.2.6 Stability, CYP inhibition, hERG inhibition and Pharmacokinetic (PK) Evaluation of SMD-3236 110
3.2.7 Antitumor Efficacy of SMD-3236 in H838 and H1299 Mice Xenograft Tumor Models 112
3.3 Chemical synthesis 114
3.4 Summary 122
3.5 Experimental section 123
Chapter 4 General Discussion and Future Directions 150
4.1 Achievements in this dissertation 150
4.2 Future directions 151
4.2.1 Development of orally available SMARCA2 selective degraders 151
4.2.2 SMARCA2 selectivity: from serendipity to rational design 152
4.2.3 Toxicity related to SMARCA2 selective PROTAC degraders 154
4.2.4 Clinical development considerations 156
References 158

LIST OF FIGURES

Figure 1. Chemical structure of PFI-3 and the co-crystal structure of PFI-3 in complex with SMARCA4 bromodomain (PDB: 5DKC) 7

Figure 2. Chemical structure of GNE-064 and the co-crystal structure of GNE-064 in complex with SMARCA4 bromodomain. 8

Figure 3. Chemical structures of representative SMARCA2/4 bromodomain ligand reported by Kymera Therapeutics 8

Figure 4. Chemical structure of University of Cambridge/SGC SMARCA2/4 bromodomain ligand 26 and the co-crystal structure of analog compound 18 in complex with the fifth bromodomain of PBRM1. 9

Figure 5. Chemical structure of Novartis's SMARCA2/4 ATPase domain inhibitor compound 14 10

Figure 6. Chemical structure of FHT-2344 and the clinical candidate FHD-286. 11

Figure 7. Peptide-based PROTACs. 15

Figure 8. Chemical structure of the first small-molecule based PROTAC. 16

Figure 9. Chemical structure of the first SNIPER molecule. 16

Figure 10. Chemical structures of VHL ligand VH032 and RIPK2 PROTAC. 18

Figure 11. Chemical structures of CRBN-recruiting PROTACs. 19

Figure 12. Chemical structures of SMARCA2/4 dual PROTAC degraders. 24

Figure 13. Chemical structures of selective SMARCA2 PROTAC degraders. 26

Figure 14. Structures of representative SMARCA bromodomain inhibitors 28

Figure 15. Structures of reported SMARCA degraders 29

Figure 16. Time course of SMD-3040 in degrading SMARCA2 and SMARCA4 in Hela cells using HiBit assay. 38

Figure 17. Mechanistic study of SMD-3040 degrading SMARCA2 and SMARCA4 proteins in Hela cells using a HiBit assay. 39

Figure 18. SMARCA2 and SMARCA4 DC50 and Dmax value determination in SK-Mel-28 cell line. 40

Figure 19. SMARCA2 DC50 and Dmax value determination of SMD-3040 in H838 and SK-Mel-5 cell lines. 42

Figure 20. Cell growth inhibition assay results of SMD-3040. 44

Figure 21. PD effect of SMD-3040 on SMARCA2 protein level in H838 tumors. 46

Figure 22. PD effect of SMD-3040 on SMARCA2 and SMARCA4 protein levels in MV4;11 tumors. 48

Figure 23. Efficacy study of SMD-3040 in the SK-Mel-5 xenograft tumor model in SCID mice. 52

Figure 24. Efficacy study of SMD-3040 in the H838 xenograft tumor model in SCID mice. 53

Figure 25. Modeled structure of compound 2 docked into SMARCA2 bromodomain. 87

Figure 26. Chemical structure of new small molecule ligand (4) for SMARCA bromodomain from Boehringer Ingelheim. 88

Figure 27. Co-crystal structure of SMARCA2 bromodomain complexed with compound 17. 93

Figure 28. Time course of SMD-3236 in degrading SMARCA2 and SMARCA4 in Hela cells using HiBit assay. 103

Figure 29. Mechanistic study of SMD-3236 degrading SMARCA2 protein in Hela cells using a HiBit assay. 105

Figure 30. Efficacy study of SMD-3236 in the H838 xenograft tumor model in SCID mice. 113

Figure 31. Efficacy study of SMD-3236 in the H1299 xenograft tumor model in SCID mice. 114

Figure 32. Chemical structures of representative novel E3 ligase ligands. 152

LIST OF TABLES

Table 1. Ongoing clinical trials of PROTAC degraders as of Oct 2023. 20
Table 2. Determination of the optimal linker length in PROTAC SMARCA2/4 degraders. 31
Table 3. Investigation of a different linking position in VHL ligand for the design of PROTAC degraders 33
Table 4. Optimization of the linker composition 34
Table 5. Optimization of the linker composition 36
Table 6. Cell growth inhibition activity of SMD-3040, compound 15, A947 and ACBI2..... 45
Table 7. PD data of SMD-3040 on SMARCA2 protein level in H838 tumors. 46
Table 8. PD data of SMD-3040 on SMARCA2 and SMARCA4 protein levels in MV4;11 tumors. 48
Table 9. Drug concentrations of SMD-3040 in plasma and tumor..... 50
Table 10. Design of spiro-containing SMARCA bromodomain ligands. 86
Table 11. Desing and binding affinity testing of compound 5. 88
Table 12. Design and binding affinity testing of compounds 6-10. 89
Table 13. Design and binding affinity testing of compounds 11-13. 91
Table 14. Design and binding affinity testing of compounds 14-17. 92
Table 15. Investigation of the optimal linker length in PROTAC SMARCA2/4 degraders. 95
Table 16. Investigation of the linker composition in PROTAC SMARCA2/4 degraders. 96
Table 17. Investigation of the exit vector positions in the SMARCA bromodomain. 97
Table 18. Comparison of the binding affinity of VHL ligands. 99
Table 19. Optimization of the VHL ligands in PROTAC SMARCA2/4 degraders. 99
Table 20. Optimization of the solubility of PROTAC SMARCA2/4 degraders. 101
Table 21. SMD-3236 kinetic degradation data. 103
Table 22. Cell growth inhibition activity of SMD-3236 and SMD-3040 in 5 SMARCA4 deficient and 3 SMARCA4 wild-type cancer cell lines. 106
Table 23. PD data of SMARCA2 protein level upon treatment of SMD-3236 in H838 tumors..... 107
Table 24. PD data of SMARCA2 protein level upon treatment of SMD-3236 in H1299 tumors..... 107

Table 25. PD data of SMARCA2 and SMARCA4 protein level upon treatment of SMD-3236 in MV4-11 tumors. 109
Table 26. Plasma and liver microsomal stability data of SMD-3236. 110
Table 27. CYP and hERG inhibition data of SMD-3236. 111
Table 28. Summary of PK data for SMD-3236 in mice and rats. 111

LIST OF SCHEMES

Scheme 1. Synthesis of Compound 38 in chapter 2. 54
Scheme 2. Synthesis of Compounds 8-17, 24-27 in chapter 2 55
Scheme 3. Synthesis of Compounds 18-23 in chapter 2. 55
Scheme 4. Synthesis of Compounds 28-32 in chapter 2. 56
Scheme 5. Synthesis of Compounds 2-3 in chapter 3. 115
Scheme 6. Synthesis of Compounds 5-6, 8-11 in chapter 3. 116
Scheme 7. Synthesis of Compound 7 in chapter 3. 117
Scheme 8. Synthesis of Compounds 12-13 in chapter 3. 117
Scheme 9. Synthesis of Compounds 14-17 in chapter 3. 118
Scheme 10. Synthesis of Compounds 19-23 in chapter 3. 119
Scheme 11. Synthesis of Compounds 24-26 in chapter 3. 120
Scheme 12. Synthesis of Compounds 27 and 28 in chapter 3. 120
Scheme 13. Synthesis of Compounds 30-37 in chapter 3. 121

ABSTRACT

Epigenetic dysregulation is a prominent feature involved in almost all human cancers. Therefore, targeting key epigenetic regulators that promote tumor progression has been recognized as potential therapeutic strategies for cancer treatment. In particular, the mammalian SWItch/Sucrose Non-Fermentable (mSWI/SNF) complexes play a crucial role in regulating gene expression and have been found to be mutated in approximately 20% of all human cancers. One ATPase subunit of mSWI/SNF complex, SMARCA4, is frequently mutated in various types of cancers including ovarian cancer, melanoma and non-small-cell lung cancer with an average mutation rate of 11%. Multiple studies have established the synthetic lethal relationship between SMARCA4 and its mutually exclusive ATPase subunit SMARCA2, thus making SMARCA2 an attractive therapeutic target for cancers with SMARCA4 deficiency. Early efforts have been focused on developing small molecule inhibitors of SMARCA2 bromodomain and ATPase domain, but neither strategy was proved to be successful. The bromodomain inhibitors exhibit no antiproliferative effects against SMARCA4-deficient cancer cells, while the ATPase inhibitors demonstrate dose limiting toxicities in vivo due to the co-inhibition of SMARCA4. These findings suggest that selective targeting of SMARCA2 is a must to avoid SMARCA4-related toxicities and achieve anti-cancer efficacy in patients with SMARCA4-deficient cancers, which redirected us to pursue the proteolysis targeting chimera (PROTAC) strategy to develop efficacious and selective SMARCA2 targeting agents.

In this thesis, we report the design, synthesis, and biological evaluation of potent and selective SMARCA2 PROTAC degraders. Our efforts have yielded several potent and selective SMARCA2 degraders, with the most promising one named SMD-3040. SMD-3040 achieves DC_{50} = 12 nM and D_{max} > 90 % for SMARCA2 protein in our HiBit degradation assay and importantly, only degrades around 50% of SMARCA4 protein. These data demonstrate the best selectivity profile among all SMARCA degraders reported so far to the best of our knowledge. SMD-3040 selectively inhibits cell growth in SMARCA4-deficient cancer cell lines while sparing SMARCA4-wild type cancer in cell growth inhibition studies. SMD-3040 effectively inhibited tumor growth in two SMARCA4-deficient xenograft tumor models in mice with well-tolerated dose schedules. However, the suboptimal potency and poor in vivo DMPK properties of SMD-3040 make it unsuitable for further development.

To optimize the degradation potency and DMPK properties, we next designed and synthesized a new class of spiro SMARCA bromodomain ligands through structure-based drug design. Following medicinal chemistry efforts have led to the discovery of a set of extremely potent and highly selective SMARCA2 PROTAC degraders, exemplified by SMD-3236. SMD-3236 achieves DC_{50} = 0.5 nM and D_{max} = 96% for SMARCA2 protein and only a D_{max} = 41% for SMARCA4 protein in HiBit degradation assay, which translates into a S2/S4 DC_{50} ratio of over 1000 folds and a ΔD_{max} of 55%. SMD-3236 demonstrates potent antiproliferative effects only in SMARCA4-deficient cancer cells, and is 9-16 times more potent than SMD-3040. SMD-3236 achieves durable and effective PD effect, excellent PK profile in vivo with little CYP inhibition or hERG liability. SMD-3236 exhibits strong anti-tumor activity in two SMARCA4-deficient xenograft tumor models and is well tolerated. Collectively, our data demonstrate that SMD-3236

is a promising candidate for advanced preclinical studies. Future optimization of SMD-3236 might lead to development candidates for the treatment of human cancers with SMARCA4 deficiency.

Chapter 1 SMARCA2 Targeted Therapies and Targeted Protein Degradation

1.1 SMARCA2 as an attractive therapeutic target in SMARCA4-deficient cancers

Epigenetics describes inheritable changes of gene expression and cell function that do not involve alterations in the primary DNA sequence. Epigenetic changes alter the accessibility of chromatin and DNA to transcription factors and thus regulate gene transcription. Genes encoding key epigenetic regulation proteins are frequently mutated in human cancers and therefore, targeting epigenetic regulators is being increasingly recognized as an attractive strategy to combat cancers, as well as other diseases, such as metabolic diseases, neurological disorders and ageing.[1]

In the past few years, therapeutic agents have been developed to target three major classes of epigenetic proteins, the writers, readers and erasers, among which several inhibitors are approved by the FDA for the treatment of hematologic malignancies. 5-Azacitidine (azacitidine) and 5-aza-2′-deoxycytidine (decitabine), the two chemotherapeutic agents, inhibit the function of DNA methyl transferases (DNMTs) by covalently binding to DNMTs and disrupting the transfer of methyl to hemimethylated DNA.[2-3] Vorinostat, an inhibitor of histone deacetylases (HDACs), was first approved by the FDA in 2006 for the treatment of cutaneous T-cell lymphoma (CTCL),[4] followed by a number of next-generation HDAC inhibitors with better selectivity and safety profile. More recently, Tazemetostat, an inhibitor of a histone methyl transferase enhancer of zeste homolog 2 (EZH2), was approved in 2020 for the treatment of epithelioid sarcoma.[5] Apart from

the previously mentioned approved drugs, there are numerous epigenetic targeting agents in different clinical development stages, such as telomeric silencing 1-like (DOT1L) inhibitors, BRD and extraterminal domain (BET) inhibitors, lysine-specific demethylase 1 (LSD1) inhibitors and so on.[6]

However, from a mechanistic point of view, most of the epigenetic inhibitors are developed to target gain-of-function mutations, while the loss-of-function mutations in the epigenetic regulators remain a largely unexplored area, exemplified by the frequently mutated switch/sucrose non-fermentable (SWI/SNF) chromatin remodeling complex.

SWI/SNF family chromatin-remodeling complexes, also known as BRG/BRM-associated factor (BAF) complexes, are key chromatin remodelers that regulate nucleosome positioning.[7] SWI/SNF complexes utilize the energy generated in the hydrolysis of ATP to slide or eject nucleosomes from DNAs, creating accessibility of enhancers and promotors to transcription factors and thereby initiate subsequent expression of target genes.[8-14] In addition to transcription, SWI/SNF complexes have been implicated in other cellular processes, such as DNA-damage repair, replication, sister chromatid cohesion, as well as chromatin topology organization.[15-19]

Mammalian SWI/SNF complexes are comprised of multiple subunits, and are characterized into three subfamilies: canonical BAF (cBAF),[20-21] polybromo-associated BAF (PBAF),[22-23] and the GLTSCR1 or GLTSCR1L-containing and BRD9-containing (GBAF) complex.[24-27] All three complexes share the some of the same core subunits SMARCC1, SMARCC2, SMARCD1, and the ATPase SMARCA2 or SMARCA4, which are mutually exclusive. The subtype of each BAF complex is defined by the unique subunits the only present in one specific complex. For example, ARID1A/B and DPF1/2/3 are cBAF-exclusive subunits, while

PBAF complex contains unique subunits ARID2, PHF, BRD7 and PBRM1.[28-31] GBAF was not discovered until 2018,[24] and it differs from cBAF and PBAF by lacking many core subunits that are shared in those two complexes. For example, SMARCB1, SMARCE1, DPF or PHF10 subunits in cBAF and PBAF are not incorporated in GBAF. The ARID subunits in cBAF and PBAF are substituted by GBAF-specific subunits BICRA (GLTSCR1) or BICRAL (GLTSCR1L) and BRD7 in PBAF is substituted by BRD9. Recently reported single-particle cryo-electron microscopy (cryo-EM) structures of cBAF and PBAF complexes bound to nucleosome further helped to elucidate their compositions and architectures and provides novel insights in investigating the function of SWI/SNF family complexes.[32-35]

Generally, BAF complexes are divided into three different modules: ATPase module, ARP module and core module.[37] In cBAF complexes, the core module comprises of subunits SMARCC1/2, SMARCD1/2/3, SMARCE1, SMARCB1, DPF1/2/3, and ARID1A/B. SMARCC1/2 heterodimer, SMARCD1/2/3 and SMARCE1 form a helices-containing V-shaped structure, bridged by ARID1A. The following assemble of ATPase module is recruited by SMARCC and SMARCD subunits. The core not only functions in complex assembly, but also participates in chromatin binding and nucleosome remodeling. SMARCB1 binds to an acidic patch of the nucleosome via a highly conserved arginine-rich sequence. SS18 subunit also interacts with SMARCA4 in the N-terminus region.[32-33] The ARP module consists of subunits ACTL6, ACTB and BCL7. Importantly, the ARP module interacts with the long helix region formed by SMARCA2/4 helicase–SANT-associated (HSA) domain, as well as other subunits in the core module, such as SMARCC and ARID1A, and bridges the two other modules.[32-33] The ATPase module, which only contains SMARCA2/4, serves as the machinery of chromatin remodeling. Upon nucleosome engagement of the BAF complexes, the SnAc/post-SnAc domain of the ATPase

and the C-terminal α-helix of SMARCB1 adopt a bilateral interaction to the nucleosome by movement of the ATPase and ARP modules, which causes a major conformational change of the whole complexes.[32-33] The ATPase then ejects nucleosomes along the DNA utilizing the energy produces by ATP hydrolysis.

Large-scale, systematic cancer genome sequencing studies have revealed that, at least 9 different BAF subunits have been identified to be mutated recurrently in more than 20% of all human cancers.[38-41] Among the mutated subunits, ARID1A is the most frequently mutated one, followed by SMARCA4 and PBRM1. Some of these mutations are found in various types of cancers with different mutational frequency, while certain mutations tend to cluster in specific malignancies. For example, ARID1A mutation is discovered in around 50% of ovarian clear cell carcinomas (OCCCs) and ovarian endometrioid carcinomas.[42-43] Similarly, PBRM1 mutation is prevalent in 41% of clear cell renal cell carcinoma (ccRCC) patients.[44] SMARCB1 inactivation is found in nearly all cases of rhabdoid tumors.[45-47] Another type of rare form of ovarian cancer, small-cell carcinoma of the ovary, hyper-calcaemic type (SCCOHT), harbor inactivating mutations of SMARCA4 in 90% cases.[48]

The majority of mutations in BAF subunit, including missense, frameshift and deletion mutations, often confer a loss-of-function (LOF) phenotype, which impedes the development of therapeutics that can directly target the mutated proteins. Of note, in cases where there are paralog subunits in the complexes, the loss of function in one paralog will be compensated by the substitution of the other paralog that retains its normal function, which partially rescue the LOF paralog and thus allow cell survival, even that could lead to differentiated gene expression activities.[9] This compensatory effect of the loss of the BAF subunits by incorporation of its paralog makes the cells harboring these mutations exquisitely dependent to the function of the alternative

paralog, creating unique vulnerabilities in these cancers for the development of therapeutics leveraging this synthetic lethal relationship.

Synthetic lethality was first proposed in 1997 as a basis of drug discovery[49] and was clinically validated by the approval of PARP inhibitors for the treatment of BRCA-mutant ovarian cancers in 2015.[50-51] In BAF complex, synthetic lethalities exist in a number of mutually exclusive paralog subunit pairs. For example, ARID1A-deficient cancers are sensitive to the loss of its paralog, ARID1B, which leads to the destabilization of cBAF complex and impairs proliferation in those cancer cells.[52-53] Systematic RNAi-based functional genomic screenings have identified a synthetic lethal relationship between the two mutually exclusive ATPase subunits, SMARCA2 and SMARCA4, that cancers with SMARCA4 deficiency are exquisitely dependent on SMARCA2 for their survival in in vitro and in vivo models.[54-56] LOF mutations of SMARCA4 occur in various types of cancers including ovarian cancer, melanoma, and importantly, in non-small cell lung cancer (NSCLC)[38, 54-55, 57-61] with frequencies of around 11% reported in a large-scale targeted patient sample exome sequencing,[62] representing a significantly unmet clinical need. Therefore, SMARCA2 emerges as an attractive therapeutic target for the treatment of SMARCA4-deficient cancers and accordingly, small molecule inhibitors have been made against SMARCA proteins by the drug discovery community.

1.2 Small Molecule Inhibitors Targeting SMARCA2

The two mutually exclusive ATPase subunits of mSWI/SNF complexes, SMARCA2 and SMARCA4, contain two major functional domains, the bromodomains (BD) and the ATPase domains. The bromodomains of SMARCA2 and SMARCA4, together with that of PBAF-specific

subunit PBRM1, belong to the family VIII branch of the human bromodomain phylogenetic tree.[63] Targeting bromodomains was considered as a potential therapeutic strategy by the herald of highly potent and specific bromodomain and extraterminal domain (BET) inhibitors.[64] Boosted by the encouraging preclinical results of BET inhibitors, multiple clinical trials of BET inhibitors on hematological malignancies and solid tumors were initiated from 2012,[65] with large setbacks in the coming years due to toxicity issues resulted from the lack of mechanistic understanding of their biology.[66] In contrast, the family VIII bromodomains were originally considered to the least druggable, characterized by small pocket occupied with conserved water molecules.[67]

In 2015, the first chemical probe of SMARCA2/4 bromodomain, PFI-3, was reported by Structural Genomics Consortium (SGC) and Pfizer.[68] (Figure 1) Initial screening of drug-like fragments has identified salicylic acid as a highly ligand-efficient hit molecule which possesses good selectivity against 48 other bromodomains using thermal shift assay. Two rounds of structure-based medicinal chemistry efforts led to the discovery of PFI-3 as a chemically stable, high quality chemical probe of SMARCA2/4.[69] The K_D values of PFI-3 binding to SMARCA2/4 bromodomains were between 54 and 97 nM, determined in solution using isothermal titration calorimetry (ITC). The co-crystal structure of PFI-3 binding to the bromodomain of SMARA4 (PDB: 5DKC) showed that PFI-3 bound deeply into a pocket of the bromodomain. (Figure 1) The phenol group in PFI-3 formed a hydrogen bond with Tyr1497, and the carbonyl group formed a second hydrogen bond with Asn1540, with the pyridine ring positioned in a hydrophobic pocket created by the ZA-loop. However, in SMARCA4-deficient lung cancer cell lines (A549, H1299, H157), PFI-3 didn't exhibit antiproliferative effects in cell viability or clonogenic assays and thus failed to phenocopy the cell growth inhibition by RNAi mediated SMARCA2 knockdown.[70] Further testing of PFI-3 in synovial sarcoma, rhabdoid cancer and leukemia cells also showed

similar results. Detailed cDNA complementary rescue experiments validated that the ATPase domain surpassed the bromodomain in SMARCA2 as the therapeutic tractable target against SMARCA4-deficient cancers.

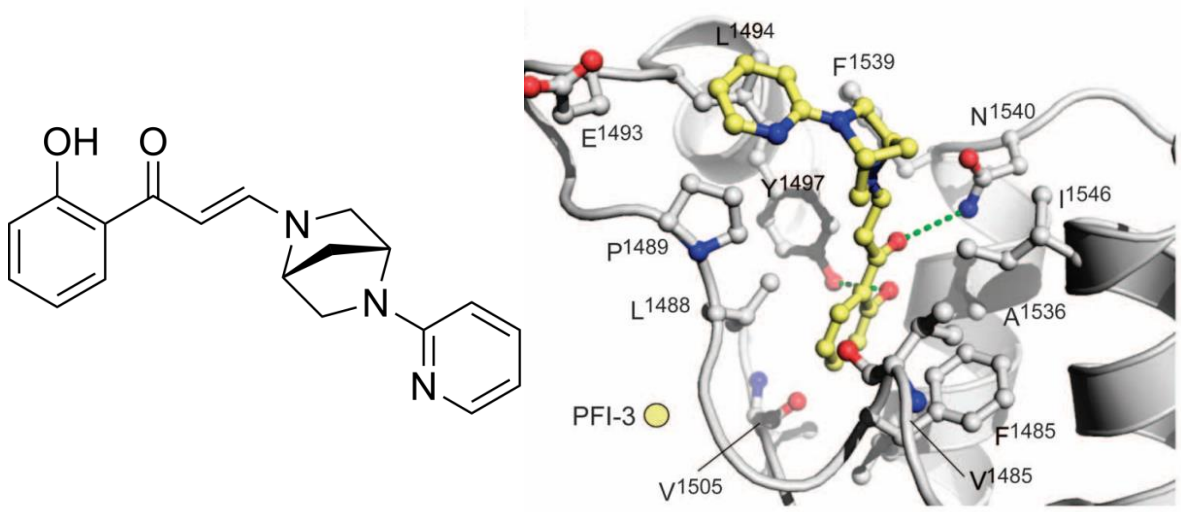


Figure 1. Chemical structure of PFI-3 and the co-crystal structure of PFI-3 in complex with SMARCA4 bromodomain (PDB: 5DKC)

In the meantime, scientists from Genentech disclosed a different type SMARCA2/4 bromodomain ligands.[71] These compounds have the same phenol moiety as PFI-3, while introduction of the pyridazine rings avoided the potential hydrolysis concern on the imine group in PFI-3. GNE-064, one exemplary compound from this series, was reported recently.[72] (Figure 2) GNE-064 demonstrated a K_D value of 47 nM in ITC and an IC_{50} value of 35 nM in a TR-FRET peptide competition assay. Comparison of the binding mode of PFI-3 and an analog of GNE-064 in the co-crystal structure with SMARCA4 showed that the phenol motif interacts with Tyr1497 in a similar manner as that of PFI-3, while the Asn1540 formed double hydrogen bond with one of the nitrogen atoms in the pyridazine and the aniline group. (PDB: 7TAB) (Figure 2) GNE-064 displayed excellent ADME properties by achieving low hepatocellular clarence, reasonable plasma protein binding and volume of distribution, and a bioavailability of 59% in mouse. Following this

work, Kymera Therapeutics conducted extensive medicinal chemistry campaigns on modifying the piperazine part of GNE-064 and reported a series of novel SMARCA bromodomain ligands with better biological activities and their own intellectual properties.[73-74] (Figure 3)

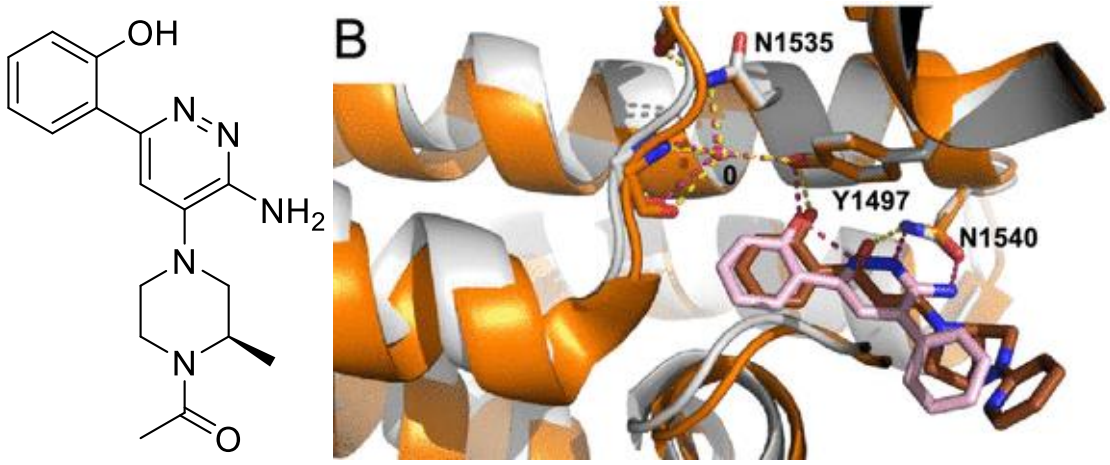


Figure 2. Chemical structure of GNE-064 and the co-crystal structure of GNE-064 in complex with SMARCA4 bromodomain.

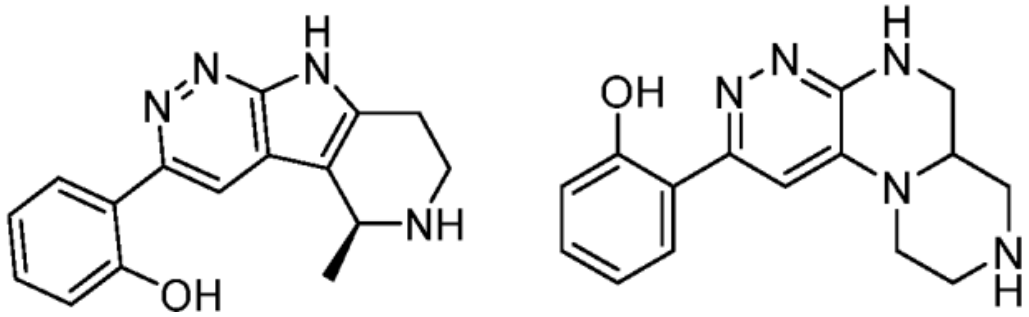


Figure 3. Chemical structures of representative SMARCA2/4 bromodomain ligand reported by Kymera Therapeutics

Another series of quinazolinone-containing SMARCA bromodomain ligands with a distinct chemotype were reported by University of Cambridge and the Structural Genomics Consortium in 2016. Initial screening against the fifth bromodomain of the PBAF specific subunit PBRM1 by differential scanning fluorimetry (DSF) has identified a hit molecule with poor solubility, and subsequent medicinal chemistry optimizations led to compound 26.[75] (Figure 4) Compound 26 binds to the fifth bromodomain of PBRM1 (PB1(5)) with a K_D value of 124 nM.

However, further characterization suggested that it also interacts with SMARCA2 and SMARCA4, giving K_D values of 262 and 417 nM, respectively. The co-crystal structure compound 18, an analog of compound 26, with PB1(5), (Figure 4) indicates an unusual halogen bonding interaction between the chlorine atom and the backbone carbonyl of Met731. The core quinazolinone also forms a hydrogen bond with Asn739. Although further investigations of PB5(1) were impeded by the elusiveness of PBRM1 biological functions, compound 26 was shown to be able to displace SMARCA2 from chromatin in an in vitro setting.

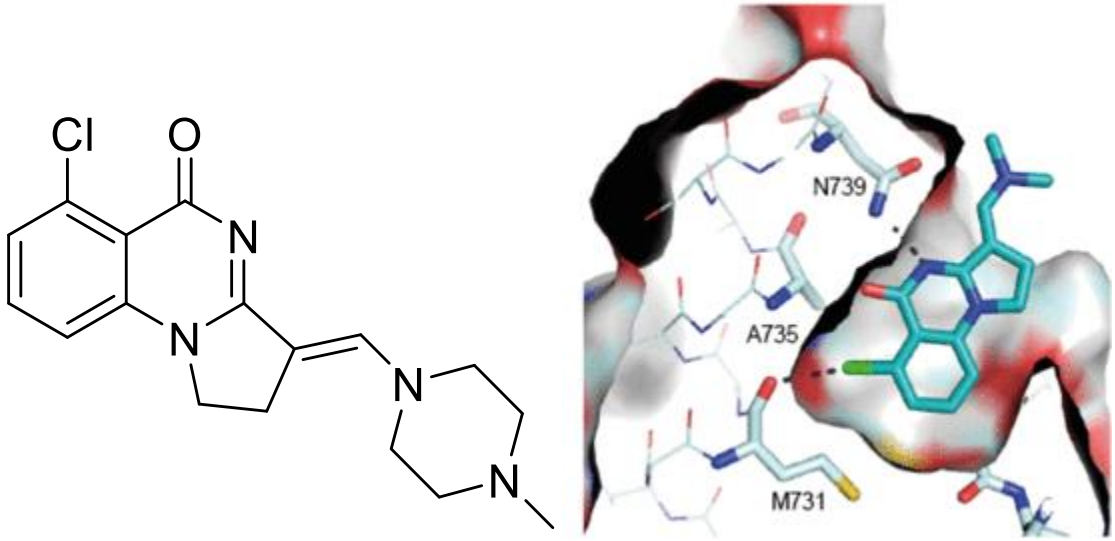


Figure 4. Chemical structure of University of Cambridge/SGC SMARCA2/4 bromodomain ligand 26 and the co-crystal structure of analog compound 18 in complex with the fifth bromodomain of PBRM1.

After the bromodomain of SMARCA proteins was invalidated as a viable drug target, a number of dual inhibitors targeting the ATPase domain of SMARCA2 and SMARCA4 were reported. In 2018, Novartis reported for the first time allosteric dual SMARCA2/4 ATPase inhibitors.[76] (Figure 5) Hit compound 1 was discovered through a focus screening using an ATP-turnover assay against the ATPase-SnAC construct of SMARCA2, and was validated for its binding affinity in the orthogonal surface plasmon resonance (SPR) assay against closely related SMARCA4 ATPase-SnAC construct. Detailed optimization efforts led to compound 14, which

potently inhibited the ATPase activity of both SMARCA2 and SMARCA4 with IC_{50} values of less than 5 nM. Compound 14 down regulated the expression of KRG80 gene in the gene reporter assay, and importantly, showed anti-proliferative effect against SMARCA4-deficient SK-Mel-5 melanoma cell line with an IC_{50} value of 4 nM while no significant cell growth inhibition was observed in the SMARCA2-SMARCA4-deficient cell line SBC5. In vivo studies showed that compound 14 had strong PD effect and inhibited the expression of downstream gene KRT 80 in RERF-LC-AI model. A 55% of tumor growth inhibition was achieved in the efficacy studies with 20mg/kg daily doses. However, dose limiting toxicities were observed in mice with a 4 days on–3 days off, 30 mg/kg oral dosing regimen, that 3 out of 12 animals in the treatment group exhibited body weight loss. Genetic studies in animal models have revealed the indispensable role of SMARCA2 and SMARCA4 in maintaining cardiomyocyte and intestine homeostasis,[77-78] even though these two paralogs have a partial redundancy relationship.

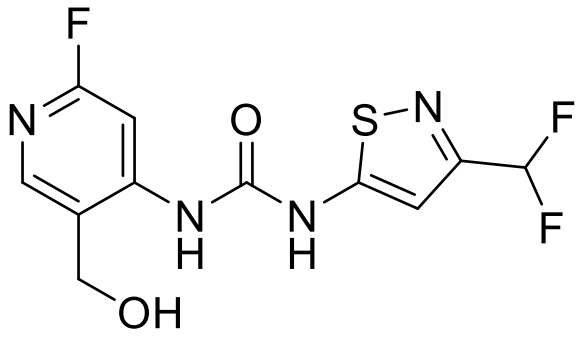


Figure 5. Chemical structure of Novartis's SMARCA2/4 ATPase domain inhibitor compound 14

Recently, Foghorn Therapeutics disclosed the discovery efforts of a novel class of dual SMARCA2/4 ATPase inhibitors.[79] Optimization of potency and ADME properties from initial screening hit led to the identification of FHD-2344 (Figure 6), with biochemical ATPase IC_{50} values of 26 nM and 13 nM for SMARCA2 and SMARCA4, respectively. Profiling of FHD-2344 in a panel of cancer cell lines from different lineages found uveal melanoma (UM) as the most

sensitive and fast-responding cell line group. Detailed CHIP-seq and ATAC-seq analysis showed significant changes of chromatin landscape caused by altered accessibility of enhancer regions to transcriptional factors SOX10, TFAP2A and MITF, which led to the disruption of SOX10-MITF transcriptional axis showed by further RNA-seq analysis. Oral dosing of FHT-2344 at 6.7 mpk daily resulted in 92% tumor growth inhibition and suppression of SOX10 and a SOX10 target genes in 92-1 UM xenograft models. The clinical candidate compound FHD-286 (Figure 6) was advanced into clinical trial in 2021 as a monotherapy or in combination with chemotherapies.[80] In 2022, FDA put a clinical hold on FDH-286 in acute myeloid leukemia (AML) after 1 patient died of severe differentiation syndrome caused by on-target toxicity, and more recently, Foghorn discontinued the uveal melanoma clinical studies due to lack of efficacy.[81] The pre-clinical and clinical evidence of the toxicity caused by dual inhibition of SMARCA2/4 suggests that selective targeting of SMARCA2 is indeed crucial to achieve a necessary safety profile.

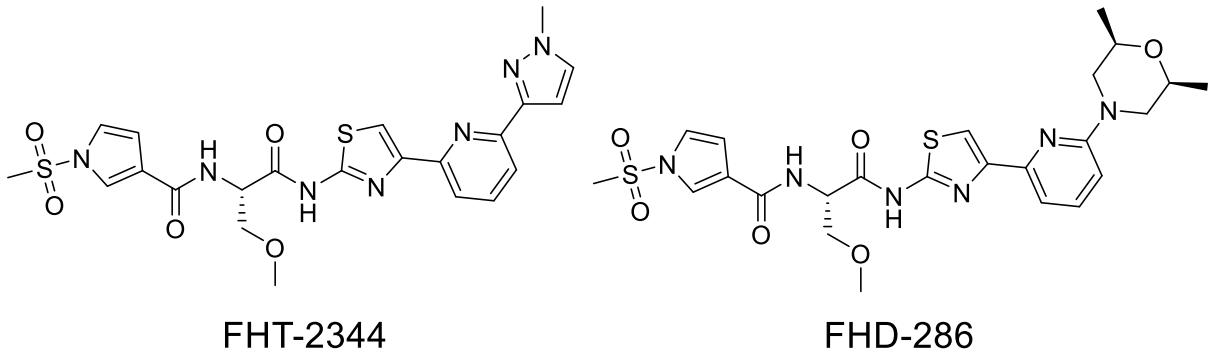


Figure 6. Chemical structure of FHT-2344 and the clinical candidate FHD-286.

1.3 Targeted Protein Degradation as a New Therapeutic Strategy

In the past quarter century, chemically induced proximity (CIP) has evolved from a pure chemical biology concept to study biologic mechanisms into a method with translational potential

for developing medicines.[82] One technology that concurrently advanced with the surging of CIP both in academia and industry is proteolysis targeting chimera (PROTAC).

PROTACs are bifunctional molecules that are able to remove target proteins by hijacking the naturally occurring ubiquitin-proteasome system (UPS). Mechanistically, the process of ubiquitination involves three steps: the ubiquitin activation mediated through E1 ligase, ubiquitin conjugation through E2, and ubiquitin ligation to target proteins through E3.[83] The polyubiquitinated protein is then recognized by the proteasome and allowed for degradation. PROTACs consist of two ligands joined together by a linker: one ligand recruits the protein of interest (POI) and the other binds to a specific E3 ligase. Simultaneous binding to the POI and E3 ligase by the PROTAC molecule drives the proximity of POI and E3 ligase by formation of a ternary complex, and induces subsequent polyubiquitination and degradation of the POI through the UPS.

PROTACs offer several advantages when compared with traditional small molecule inhibitors. Firstly, PROTACs utilize the event-driven pharmacology[84] to stoichiometrically remove target proteins with a low, catalytical concentration, which contrasts with the occupancy-driven pharmacology in small molecules inhibitors where high concentrations are usually needed to achieve functional target protein inhibition. Due to the catalytic mode of action of PROTACs, degraders with low nanomolar potency could be achieved even using weak binding affinity ligands of either the POI or E3 ligase.[85-86] From the pharmacokinetics perspective, the catalytic nature of PROTACs could be translated into a lower drug exposures and longer dosing intervals[87] required to achieve similar pharmacologic effect compared to small molecule inhibitors, thus creating a broader therapeutic window that would otherwise be impeded by the likelihood of off-target toxic effects at high doses. Secondly, PROTACs offer opportunities to target undruggable proteins.

Many drug targets that are traditionally deemed undruggable often do not have a functional catalytic site that could be blocked, such as transcriptional factors. In the case of signal transducer and activator of transcription 3 (STAT3), small molecule inhibitors failed to suppress its gene transcriptional activity, while the corresponding PROTAC degrader, SD-36, exhibited potent cellular activity and tumor growth inhibition efficacy.[88] In some proteins that possess multiple functional and catalytic domains, inhibition of one of these domains with high affinity ligands might have partial or no efficacy. However, these potent yet functionally inactive binders could be utilized for the development of PROTAC degraders. While pharmacologically targeting the bromodomain of SMARCA proteins has been invalidated as a therapeutic strategy, those potent SMARCA bromodomain ligands have been exploited to develop potent SMARCA protein PROTAC degraders, exemplified by ACBI1.[89] ACBI1 induces ternary complex formation of SMARCA proteins with VHL E3 ligases and induces degradation of SMARCA proteins and cell growth inhibition in a panel of cancer cell lines. What's more, removal of the entire protein instead of inhibition of certain function, especially in muti-domain proteins, could lead to more profound activities that phenocopies the genetic knockdown effect, as noted with the much improved antiproliferative activity of BET degraders compared with BET inhibitors.[90] Lastly, PROTACs possess the ability to selectively degrade a specific protein among its highly homologous protein family. Preferential degradation of BRD4 over other BET family members with PROTAC degraders based on non-selective BET inhibitors was reported by several research groups.[91-92] Detailed X-ray crystallographic analyses suggest that the linker of PROTAC molecule may contribute to secondary interactions for the selective BRD4-VHL ternary complex stabilization.[92] More recently studies demonstrated that precise conformational control of the PROTAC linker could turn pan BET degraders into highly potent and exceptionally selective BRD4 degraders.[93]

In 2001, the first fully synthetic PROTAC molecule, Protac-1, was reported by the Crews and Deshaies groups.[94] Protac-1 (Figure 7) used ovalicin as the ligand to covalently recruit its POI methionyl aminopeptidase 2 (MetAP-2), and a 10- amino acid phosphopeptide (DRHDpSGLDpSM) from nuclear factor-κB inhibitor- α (IκBα) as the β-transducin repeat containing ($SCF^{\beta\text{-}TRCP}$) E3 ubiquitin protein ligase. Biochemical assays showed that MetAP-2 was recruited to SCF by Protac-1 and ubiquitinated by SCF E3 ligase. The covalent MetAP-2-ovacilin complex was able to be degraded in extracts of xenopus laevis eggs, which marks the first in vitro proof of concept for the PROTAC technology. Following this work, in 2003 the same groups reported PROTAC degraders of androgen receptor (AR) and estrogen receptor (ER). These PROTAC molecules employed dihydrotestosterone (DHT) as the AR targeting ligand and estradiol as the ER targeting ligand, and the same IκBα phosphopeptide fragment used in Protac-1 to recruit $SCF^{\beta\text{-}TRCP}$ E3 ubiquitin ligase. Microinjection was then used in introducing these PROTACs into the 293T cells for the degradation of GFP-AR or ER, because the phosphopeptide moiety PROTACs impedes their penetration into the cells.

The first cell permeable PROTAC was reported subsequently in 2004.[95] A seven amino acid sequence from hypoxia inducible factor 1α (HIF1α), ALAPYIP, coupled with a poly-d-Arg tag, was adopted for the recruitment of von Hippel-Lindau (VHL) E3 ligase. Cell permeable Protac-4 and Protac-5 (Figure 7) were designed to degrade F36V FKBP12 variant and AR by incorporating the ALAPYIP-poly-d-Arg sequence with F36V FKBP12 ligand AP21998 and DHT, respectively. These two molecules were shown to degrade GFP-fused F36V FKBP12 and AR using both fluorescence microscopy detection and western blot.

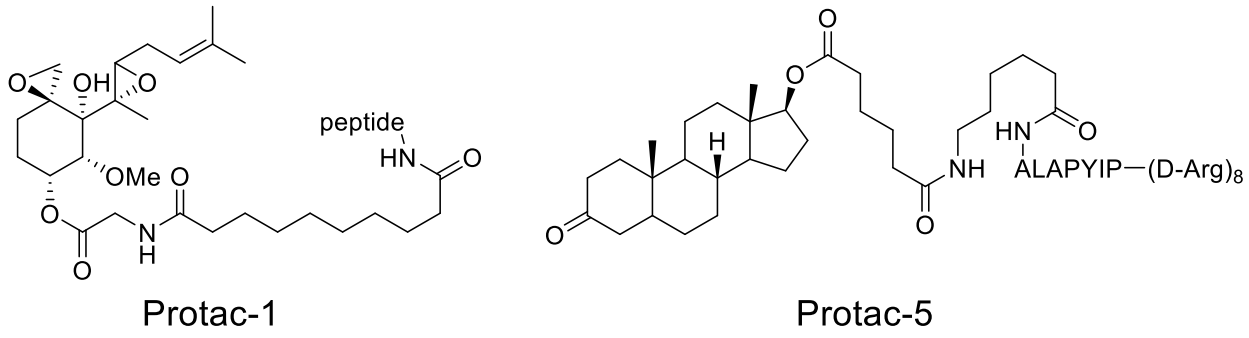


Figure 7. Peptide-based PROTACs.

The first-generation peptide-based PROTACs served as valuable proof-of-concept tool molecules demonstrating that using E3 ligases to modulate protein homeostasis is a feasible strategy. However, the poor cell permeability, low cellular activity and stability preclude these molecules from translating into potential therapeutics. Therefore, the next step is the development of non-peptidic and more drug-like PROTACs, which requires the identification and application of small molecule ligands for E3 ligases. Examples of these E3 ligase for which small molecule ligands are developed for the discovery of small molecule PROTACs include, but are not limited to mouse double minute 2 homolog (MDM2), cellular inhibitor of apoptosis protein 1 (clAP1), cereblon (CRBN) and VHL.[96]

In 2008, the Crews group reported the identification of the first small-molecule based PROTAC.[97](Figure 8) Nutlin, a MDM2-p53 protein-protein interaction (PPI) inhibitor reported by Roche[98] was used as the recruiting moiety to recruit MDM2 as the E3 ligase. Conjugating of nutlin to a selective androgen receptor modulator that recruits AR using a PEG-containing linker yielded the small molecule PROTAC that could induce the degradation of AR in Hela cells at micromolar concentrations.

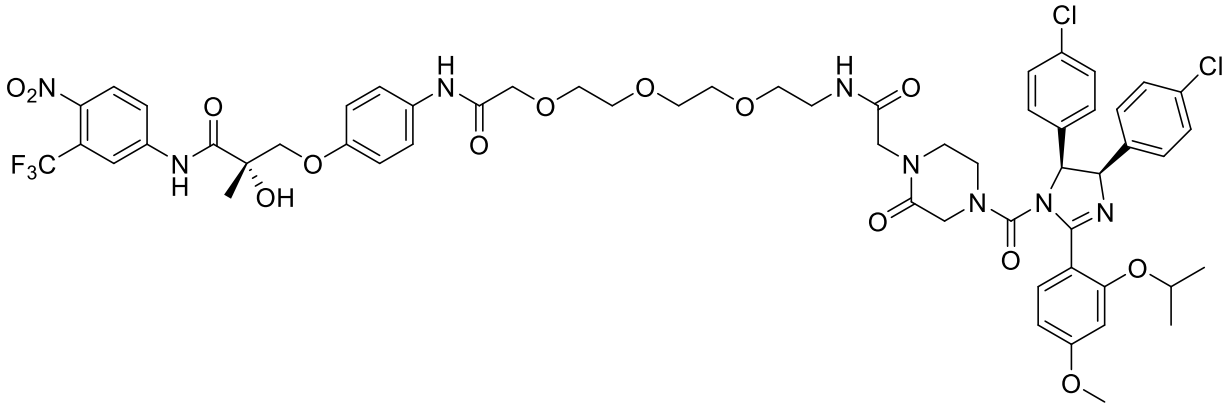


Figure 8. Chemical structure of the first small-molecule based PROTAC.

The first cIAP-based PROTAC molecule was reported in 2010 by the Hashimoto group, for which they also developed a specific name called specific and non-genetic inhibitors of apoptosis protein dependent protein erasers (SNIPER).[99] (Figure 9) The SNIPER molecules employed bestatin as the binder of cIAP1 and was developed to degrade rand retinoic acid binding proteins CRABP-I and II. Later, the substrate scope of SNIPER was expanded to AR, ER and Bcr-Abl.[100-101] Several drawbacks, such as off-target effects of the bestatin, low potency and autoubiquitination and degradation of the IAP proteins limited the further developmental potential of SNIPERs as therapeutics.

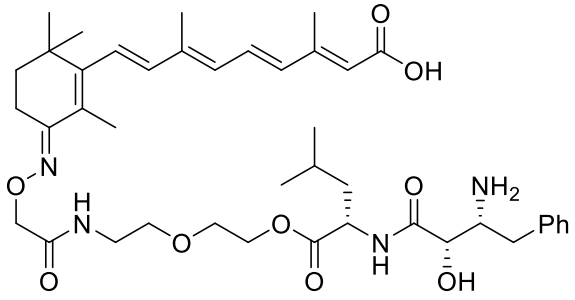


Figure 9. Chemical structure of the first SNIPER molecule.

Works on peptide-based VHL-recruiting PROTACs paved the way for the successful discovery of small molecule VHL ligands. The hydroxyproline in the HIF-1α peptide ALA(P-

OH)YIP motif of earlier VHL PROTACs served as a starting point for further optimization because the configuration I of the hydroxyl is key for VHL binding.[102] In 2012, structure-based drug design performed by the Crews lab led to the discovery of small molecule peptidomimetic VHL ligands with micromolar binding affinity.[103-104] This series of VHL ligands were further optimized by the Ciulli group through extensive structure-activity relationship, leading to VH032 (Figure 10) and VH298 with improved binding affinity and physicochemical properties.[105] These small molecule VHL ligands greatly facilitated the medicinal chemistry community to discover PROTACs with real translational potential into therapeutics. In 2015, the Crews group and GSK in collaboration reported the development of highly potent and selective VHL PROTAC, PROTAC_RIPK2, to target the receptor-Interacting serine/threonine-protein kinase 2 (RIPK2).[86] (Figure 10) PROTAC_RIPK2 contains a PEG-4 linker that connects the RIPK2 ligand with VHL ligand. PROTAC_RIPK2 effectively induced the ubiquitination of proteasome mediated degradation of RIPK2 in THP-1 monocytes, giving a Dmax of >95% at concentrations of 10 nM and higher, and DC50 of 1.4 nM. While no in vivo characterization data of PROTAC_RIPK2 was included, another PROTAC, PROTAC_ERRα that degrades estrogen-related receptor alpha, was reported in the same literature. Importantly, treatment of PROTAC_ERRα reduced ERRa levels by approximately 44%, 44%, and 39% in mouse heart, kidney, and MDA-MB-231 tumors, respectively. Although high dose (100 mg/kg, 3 times/day) and intraperitoneal injection were used, this proves that VHL-based PROTACs could offer robust pharmacodynamic (PD) effect by in vivo protein knockdown. During the same time, the Ciulli group reported the first BET PROTACs, MZ1, based on VH032 and a pan-BET bromodomain inhibitor, JQ1.[106] Since the discovery of small molecule VHL ligand, multiple VHL-based PROTACs have been reported targeting a variety of different classes of

targets including BRD7/9,[107] AR,[108-109] ER,[110] PTK2,[111] FAK,[112] WDR5,[113-114] Bcl-xL,[115] EGFR[116] and SMARCA2/4.[89, 117-118]

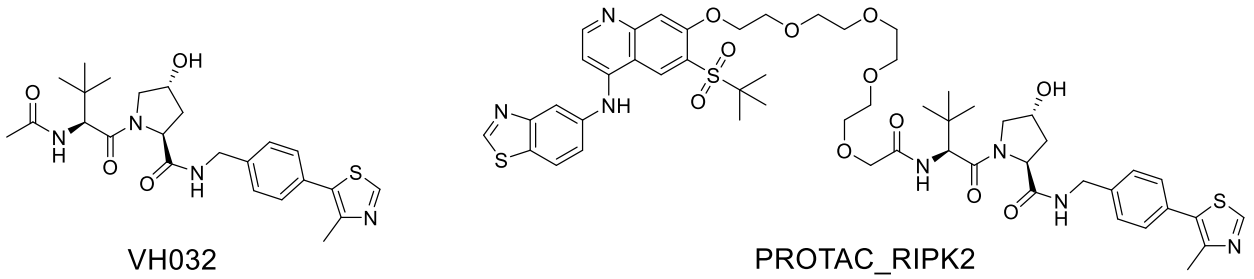


Figure 10. Chemical structures of VHL ligand VH032 and RIPK2 PROTAC.

The adoption of VHL as a viable E3 ligase for the development of PROTACs is realized by the rational design of potent small molecule VHL ligands. Nonetheless, the other type of dominant E3 ligase in the PROTAC field, the substrate receptor of Cullin Ring E3 ubiquitin ligase 4 (CRL4), cereblon (CRBN), was not widely appreciated until CRBN was identified as a direct target of thalidomide by the Ito group in 2010.[119] Binding of immunomodulatory imide drugs (IMiDs), such as thalidomide, lenalidomide and pomalidomide to CRBN was found to promote the recruitment and degradation of neosubstrates to CRBN, such as Ikaros (IKZF1), Aiolos (IKZF3) and casein kinase 1A1 (CK1α).[120-121] The first PROTAC molecules that utilized CRBN as the E3 ligase was reported by the Bradner group (dBET1)[122] and Arvinas (ARV-825)[123] in 2015. (Figure 11) dBET1, comprised of JQ1 and thalidomide connected with an alkyl linker, was able to induce 87% and 95% degradation of BRD4 at 100 nM and 1 uM, respectively, in MV4-11 cells after 18 h treatment time. dBET1 induced stronger apoptosis signals and cell growth inhibitory effects in MV4-11 and DHL4 cells, compared to the parent BET inhibitor JQ1, and showed anti-tumor activity in MV4-11 xenograft model in a 14-day efficacy study upon 50mg/kg daily dosing of dBET1 intraperitoneally. ARV-825 consists of another BET inhibitor OTX015, coupled to

pomalidomide via a PEG linker. ARV-825 potently and rapidly induced BRD4 protein degradation with subnanomolar DC50s in two Burkitt's lymphoma cell lines, which is 10 times more potent than dBET1. ARV-825 also inhibited the cell growth of a number of Burkitt's lymphoma cell lines with a greater effect than the inhibitor OTX015. Because the IMiDs serve as readily available cereblon E3 ligase ligands due to their clinical applications and druglikeliness compared to VHL ligands, developing cereblon-recruiting PROTACs has gained tremendous interests in both academia and industry in the past few years, exemplified by the CRBN-recruiting PROTACs targeting BET proteins,[124-125] cyclin-dependent kinases (CDK6 and CDK9),[126-128] Bruton's tyrosine kinase (BTK),[129-130] STAT transcription factors (STAT3 and STAT5),[88, 131] MCL-1,[132] BCL-XL,[133] Anaplastic lymphoma kinase (ALK),[134] AR,[135-136] ER,[137] BCR-ABL,[138] Sirtuin 2 (Sirt2),[139] Histone deacetylase 6 (HDAC6)[140] and EGFR.[141-142]

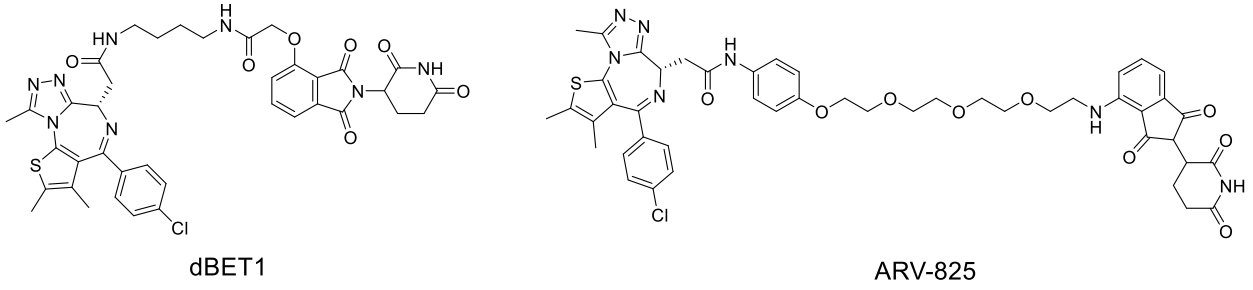


Figure 11. Chemical structures of CRBN-recruiting PROTACs.

The era of PROTACs being not just chemical biology tools but potential human therapeutics was marked by the milestone event that two heterobifunctional degraders, ARV-110 targeting AR and ARV-471 targeting ER, were advanced into first-in-human trials in 2019. The current landscape of PROTAC clinical development status, as of Oct 2023, is summarized in Table 1. Most of the PROTAC programs are in the early clinical stages, with ARV-471 being the only one that just entered phase III recently. The target scope includes AR, ER, BTK, STAT3, BRD9,

MDM2, IRAK4, BRAF V600X, BCL-XL, KRAS G12D and SMARCA2. While PROTAC molecules usually are out of the Lipinski/Veber's rules and are categorized into so called 'beyond rule-of-5' (bRo5) drugs, the wave of clinic success for these PROTAC molecules demonstrates that oral bioavailability is no longer considered a hurdle. Although PROTACs just entered clinical trial 4 years ago, they hold substantial promise in the future for the treatment of a spectrum of diseases as this field rapidly advances.

Table 1. Ongoing clinical trials of PROTAC degraders as of Oct 2023.

Company	Degrader	Target	Indications	E3 ligase	ROA	Highest Phase	Clinical trial no.
Arvinas	ARV-471	ER	Breast cancer	CRBN	Oral	Phase III	NCT05654623
Accutar Biotech	AC682	ER	Breast cancer	CRBN	Oral	Phase I/II	NCT05080842
Arvinas	ARV-110	AR	Prostate cancer	CRBN	Oral	Phase II	NCT03888612
Arvinas	ARV-766	AR	Prostate cancer	CRBN	Oral	Phase I/II	NCT05067140
Celgene	CC-94676	AR	Prostate cancer	Undisclosed	Oral	Phase I	NCT04428788
Accutar Biotech	AC176	AR	Prostate cancer	Undisclosed	Oral	Phase I	NCT05241613
Hinova Pharmaceuticals	HP518	AR	Prostate cancer	Undisclosed	Oral	Phase I	NCT05252364

Nurix Therapeutics	NX-2127	BTK	B cell malignancies	CRBN	Oral	Phase I	NCT04830137
Nurix Therapeutics	NX-5948	BTK	B cell malignancies	CRBN	Oral	Phase I	NCT05131022
Beigene	BGB-16673	BTK	B cell malignancies	CRBN	Oral	Phase I/II	NCT05006716
Haisco Pharmaceutical	HSK29116	BTK	B cell malignancies	CRBN	Oral	Phase I	NCT04861779
Accutar Biotech	AC0676	BTK	B cell malignancies	undisclosed	Oral	Phase I	NCT05780034
C4 Therapeutics	CFT8634	BRD9	synovial sarcoma & SMARCB1-Loss Tumors	CRBN	Oral	Phase I/II	NCT05355753
Foghorn Therapeutics	FHD-609	BRD9	synovial sarcoma & SMARCB1-Loss Tumors	CRBN	I.v.	Phase I	NCT04965753
C4 Therapeutics	CFT1946	BRAF V600X	BRAF V600 mutant solid tumors	CRBN	Oral	Phase I/II	NCT05668585

Kymera	KT-474	IRAK4	Autoimmune diseases	CRBN	Oral	Entering Phase II	NCT04772885
Kymera	KT-413	IRAK4	B cell non-Hodgkin lymphoma	CRBN	I.v.	Phase I	NCT05233033
Kymera	KT-333	STAT3	Liquid and solid tumours	Undisclosed	I.v.	Phase I	NCT05233033
Kymera	KT-253	MDM2	Liquid and solid tumours	Undisclosed	I.v.	Phase I	NCT05775406
Dialectic Therapeutics	DT2216	BCL-XL	Relapsed and/or refractory malignancies	VHL	I.v.	Phase I	NCT04886622
Astellas	ASP3082	KRAS G12D	KRAS G12D-mutant solid tumors	Undisclosed	I.v.	Phase I	NCT05382559
Prelude Therapeutics	PRT3789	SMARCA2	SMARCA4 mutant solid tumors	Undisclosed	I.v.	Phase I	NCT05639751

1.4 PROTAC Degraders Targeting SMARCA2

Despite the efforts in making potent yet unselective SMARCA2/4 small molecule inhibitors, PROTAC approach offers an alternative but potentially attractive strategy to the

selective targeting of SMARCA2 protein for its ability to selectively degrade one protein over its highly homologous proteins using the non-selective protein ligands.

In 2019, a SMARCA2/4 dual PROTAC degrader ACBI1, was first reported in literature by the Ciulli group and Boehringer Ingelheim.[89] (Figure 12) ACBI1 comprised of a known SMARCA2/4 bromodomain ligand previously reported by Genentech[71] and a highly potent VHL ligand VH101 developed by the Ciulli group,[143] with a linker attached at the phenyl group in VHL101. Structure guided design efforts by the elucidation of SMARCA-PROTAC-VHL ternary complex structure were conducted, leading to the discovery of ACBI1. A phenyl ring was incorporated into the linker portion of ACBI1, which formed a pi-pi stacking interaction to VHL Y98 residue at the interface SMARCA-VHL interaction. ACBI1 potently and completely depleted SMARCA2 (DC_{50} = 6 nM) and SMARCA4 (DC_{50} =11 nM) in MV-4-11 leukemia cells with 18 h treatment time, as well as in SMARCA4-deficient NCI-1568 non small cell lung cancer (NSCLC) cells for depletion of SMARCA2 (DC_{50} = 3.3 nM). Kinetic studies showed that half maximal degradation of SMARCA2/4 was achieved within 2 h in MV-4-11 cells. ACBI2 exerted potent anti-proliferative effects in MV-4-11 cells and SMARCA4-deficient SK-Mel-5 and H1568 cells in a 7-day cell growth inhibition assay, with IC_{50} values of 28 nM, 77 nM and 44 nM, respectively. Although ACBI1 caused the degradation of PBRM1, another subunit in PBAF complex, rescue studies by overexpressing PBRM1 in H1568 cells did not impact the anti-proliferative effect of ACBI1. Importantly, ACBI1 had no anti-proliferative activity in NCI-H1703 cell line deficient in both SMARCA2 and SMARCA4, indicating low or no off-target activity of ACBI1.

Another dual SMARCA2/4 PROTAC degrader, AU-15330, was reported later in 2021 by Aurigene and the Chinnaiyan group.[144] (Figure 12) AU-15330 contained the same 2-(6-aminopyridazin-3-yl)pheno SMARCA2/4 bromodomain ligand used in ACBI1, but a structurally

distinct short linker that connects VHL ligand. AU-15330 induced rapid and complete degradation of SMARCA2 and SMARCA4 proteins in HEK293 and HeLa cells within 4 h at 1 uM concentration. The screening of AU-15330 in a panel of 63 normal and cancer cell lines from 14 distinct lineages showed prostate cancer cells driven by AR and FOXA1 to be preferentially sensitive ones. Detailed sequencing studies revealed that the cell growth inhibitory effect of AU-15330 in AR and FOXA1-dependent prostate cancer cell lines was driven by loss of chromatin accessibility to AR, FOXA1, and ERG leading to significant downregulation of AR and FOXA1-regulated genes, as well as the disruption of super enhancer-promoter interactions on AR, FOXA1 and MYC regions that collapse these oncogene transcription programs. AU-15330 promoted potent inhibition of tumor growth in castration resistant prostate cancer (CRPC) tumor models and synergized with AR antagonist enzalutamide which led to tumor regression. Notably, no evident toxicity was observed after prolonged treatments of the dual SMARCA2 and SMARCA4 degrader AU-15330 either in immuno-competent mice or in xenograft models.

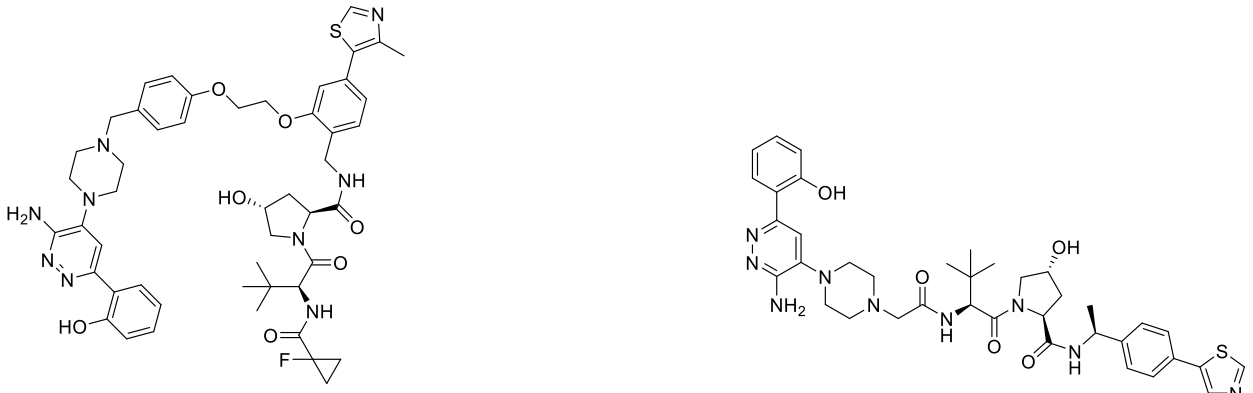


Figure 12. Chemical structures of SMARCA2/4 dual PROTAC degraders.

Recently, two SMARCA2-selective PROTAC degraders ACBI2 and A947 were reported by Boehringer Ingelheim/U of Dundee and Genentech/Arvinas, respectively.[117-118] (Figure 13) In

ACBI2, a potent SMARCA bromodomain binder with reasonable physicochemical properties was first discovered through structure-based optimization of a previously reported bromodomain binder of SMARCA and PBRM1.[76] Subsequent linker optimization has yielded the SMARCA2 selective and orally bioavailable VHL PROTACs ACBI2. ACBI2 had a DC50 of 1 nM and a Dmax of 81% for SMARCA2 in RKO cells, and a DC_{50} of 32 nM and a Dmax of 67% for SMARCA4, demonstrating a 32-fold selectivity in terms of DC_{50} values. Oral dosing of 100mg/kg ACBI2 daily decreased SMARCA2 protein level by 89% in NCI-H1568 tumor xenograft models, and inhibited the tumor growth by 76% at day 17 after treatment start. Significantly, ACBI2 achieved an oral bioavailability of 22% in mice. A947 utilized a previously reported SMARCA bromodomain ligand and a structurally differentiated VHL ligand tethered by a well optimized conformationally rigid linker. A947 is an exceedingly potent SMARCA2 degrader with a DC_{50} value of 39 pM and a Dmax of 96% achieved at 10 nM in SW1573 cells. The DC50 for SMARCA4 is 1.1 nM, demonstrating a 28-fold selectivity. Profiling of A947 in a panel of lung cancer models characterized by SMARCA4mutation status showed that SMARCA4-mutant lung cancer cell lines were sensitive to A947 treatment with a median IC_{50} of 7 nM, and MARCA4-WT cells were significantly less sensitive with a median IC_{50} of 86 nM. Dosing of A947 at 40mg/kg intravenously strongly depleted SMARCA2 protein as well as downstream transcription biomarkers, and resulted in near complete tumor growth inhibition in SMARCA4-mutant HCC515 xenograft model. Additional studies identified potential synergistic effect of SMARCA2 degraders with MCL1 inhibitors.

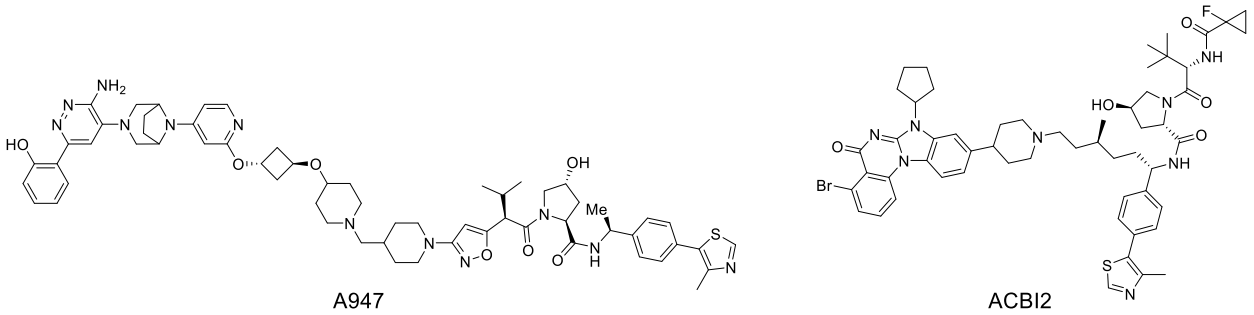


Figure 13. Chemical structures of selective SMARCA2 PROTAC degraders.

While selective degradation of SMARCA2 as a therapeutic strategy has been pursued by multiple pharmaceutical companies and biotechs, most of these discovery programs are still in the early stages. To date, only one selective SMARCA2 degrader, PRT3789, has been advanced into clinical trial. PRT3789 is developed by Prelude Therapeutics and is currently evaluated in Ph. I clinical trial for patients with advanced or metastatic solid tumors with a SMARCA4 mutation.[145]

Chapter 2 Development of SMD-3040 as a Potent and Selective SMARCA2 PROTAC Degrader

2.1 Introduction

The SWItch/Sucrose Non-Fermentable (SWI/SNF) chromatin remodeling complexes play a crucial role in mobilizing nucleosomes to regulate gene transcription and DNA replication/repair.[7] Mutations related to SWI/SNF complexes are present in approximately 20% of all human cancers.[38, 68] The SWI/SNF complex contains two mutually exclusive catalytic ATPase subunits, SMARCA2 and SMARCA4. Studies have shown that SMARCA4 is frequently mutated, primarily through gene deletion, in various types of cancers including ovarian cancer, melanoma and non-small-cell lung cancer.[57-61, 68, 146] Systematic RNAi-based screenings have demonstrated an exquisite dependence of SMARCA2 in SMARCA4-deficient cells for their survival by RNAi-mediated silence of SMARCA2 in vitro and in vivo, indicating a synthetic-lethal relationship between SMARCA2 and SMARCA4.[54-56] These findings strongly suggest that SMARCA2 is a promising therapeutic target cancers harboring SMARCA4 LOF mutations.

Both SMARCA2 and SMARCA4 contain two major functional domains, the bromodomains (BD) that recognizes acetylated lysine residues of histones and the ATPase domains that drive the chromatin-remodeling activity.[29] Early efforts have been focused on discovering SMARCA bromodomain inhibitors.[69, 71, 75, 147] However, these bromodomain inhibitors did not

exhibit antiproliferative effects in SMARCA4-deficient cell line, indicating that bromodomain in SMARCA2 is not the tractable therapeutic target as against SMARCA4-deficient cancers.[70] In 2018, Novartis reported for the first time allosteric dual inhibitors against SMARCA2/4 ATPase activity.[76] While these inhibitors demonstrated antiproliferative activity against SMARCA4-deficient cell lines and xenograft models in mice, dose-limiting toxicity was observed when doing efficacy studies in mice. These on-target toxicities caused by dual inhibition of SMARCA2/4 call for therapies targeting SMARCA2 selectively to achieve a necessary safety profile.

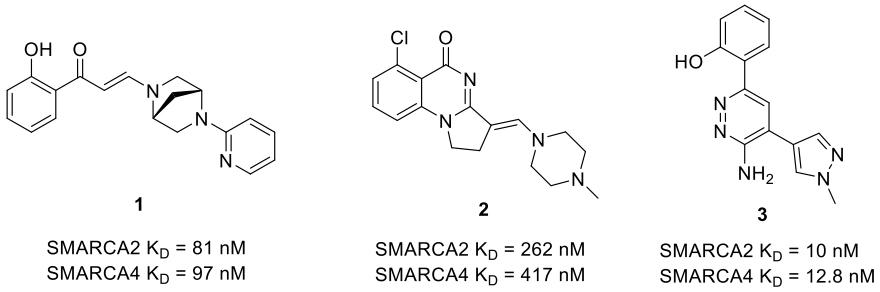
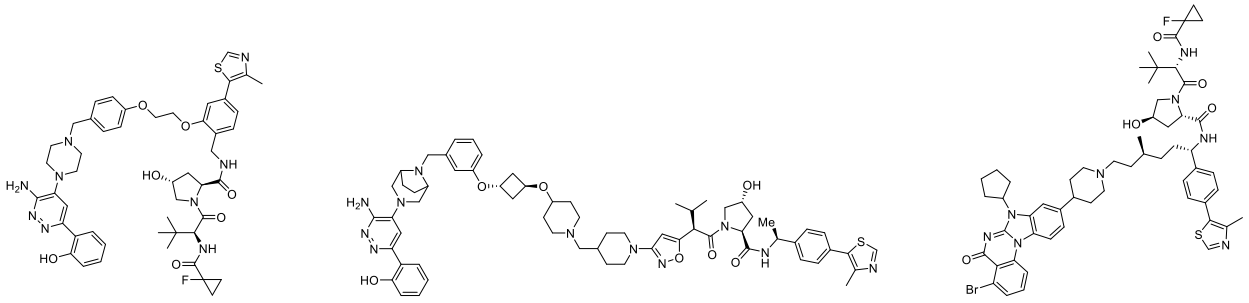


Figure 14. Structures of representative SMARCA bromodomain inhibitors

In addition to small molecule inhibitors, another approach to selective targeting SMARCA2 protein is to leverage targeted protein degradation upon the small molecule proteolysis targeting chimera (PROTAC) concept. One of the advantages of PROTACs over traditional small molecule inhibitors is their ability to selectively degrade one specific protein among its highly homologous proteins.[148-149] Therefore, we elected to pursue the development of selective SMARCA2 PROTAC degraders over its paralog SMARCA4.

Several PROTAC degraders of SMARCA proteins have been reported. ACBI1,[89] the first SMARCA2/4 dual PROTAC degrader, induces rapid degradation of both proteins. A947[118] and ACBI2[117] are two SMARCA2 selective PROTACs recently reported (Figure 15), but they lack a clear differentiation in the Dmax values as over 90% of protein degradation for both SMARCA2

and SMARCA4 are observed for these two molecules. In this chapter, we report the design, synthesis, and biological evaluation of selective SMARCA2 degraders based upon PROTAC strategy. A potent but non-selective SMARCA2/4 bromodomain ligand was used and detailed linker optimization has yielded a number of potent and selective SMARCA2 degraders, exemplified by SMD-3040. SMD-3040 achieved over 90% degradation for SMARCA2 with nanomolar potency, while caused no more than 50% degradation of SMARCA4. SMD-3040 had antiproliferative effects in SMARCA4-deficient cancer cell lines while sparing SMARCA4-wildtype cancer cells. In vivo efficacy studies showed that SMD-3040 effectively inhibited tumor growth in H838 and SK-Mel-5 SMARCA4-deficient xenograft tumor models in mice. These data suggested SMD-3040 as a promising lead compound that warrants further optimization toward a new class of therapies for SMARCA4-deficient human cancers.



ACBI1 **(4)**

SMARCA2 DC_{50} = 6 nM
SMARCA4 DC_{50} = 11 nM
SMARCA2 D_{max} > 95%
SMARCA4 D_{max} > 95%

A947 **(5)**

SMARCA2 DC_{50} = 0.039 nM
SMARCA4 DC_{50} = 1.1 nM
SMARCA2 D_{max} = 96%
SMARCA4 D_{max} = 92%

ACBI2 **(6)**

SMARCA2 DC_{50} = 1 nM
SMARCA4 DC_{50} = 32 nM
SMARCA2 D_{max} = 81%
SMARCA4 D_{max} = 67%

Figure 15. Structures of reported SMARCA degraders

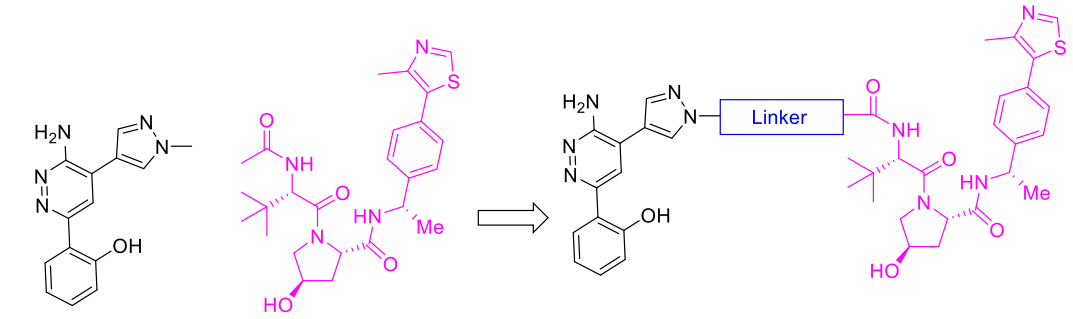
2.2 Results and discussion

2.2.1 Design of Potent and Selective SMARCA2 PROTAC Degraders

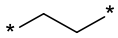
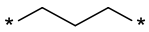
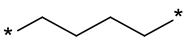
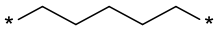
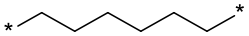
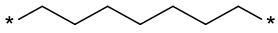
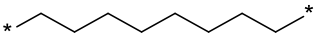
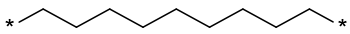
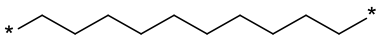
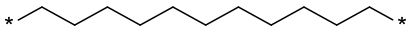
SMARCA bromodomain ligands with distinct chemotypes but lack of selectivity in binding to SMARCA2 or SMARCA4 have been reported.[69, 71, 75, 147] From all of these ligands, compound 3 reported by Genentech showed the highest binding affinity for both SMARCA2 and SMARCA4, and serves as a good SMARCA-recruiting moiety in the design of PROTAC SMARCA degraders. The structure-activity relationships (SARs) around the pyrazole moiety have been extensively studied. In the N1 position of pyrazole, substituents with different sizes at the N1 were shown to be well tolerated, indicating that this position is exposed to solvent when compound **3** binds to SMARCA2 and SMARCA4. Furthermore, in the publication of ACBI1, the co-crystal structure where one of these series of compounds binds to SMARCA2 bromodomain[117] (PDB: 6HAZ) showed similar SARs. All the above evidence collectively supports that the pyrazole site serves as a suitable exit vector to tether a ligand for an E3 ligase for the development of PROTAC degraders.

In choosing the proper E3 ligands for the design of initial SMARCA2 selective PROTAC degraders, we first employed a high-affinity VHL/cullin 2 E3 ligase ligand (**7**, in Table 2) that has been used successfully for the design of PROTAC degraders for a large number of protein targets.[109-110, 150] A series of compounds that could potentially degrade SMARCA2/4 proteins were designed and synthesized incorporating compounds **3** and **7**, tethered with linear alkyl linkers of different lengths (Table 2). Thees potential SMARCA degraders are tested for their potency and efficacy in degrading SMARCA2 and SMARCA4 proteins in HiBit degradation assay,[151] and the data are summarized in Table 2.

Table 2. Determination of the optimal linker length in PROTAC SMARCA2/4 degraders.



SMARCA2/4 Ligand (**3**) VHL Ligand (**7**) PROTAC SMARCA2/4 Degarders

Compound	Linker	SMARCA2 DC_{50} (nM)	SMARCA2 D_{max} (%)	SMARCA4 DC_{50} (nM)	SMARCA4 D_{max} (%)
8		>1000	19	>1000	0
9		132	88	463	84
10		134	85	>1000	57
11		12	93	>1000	73
12		16	89	212	81
13		3	95	23	90
14		3	95	31	93
15		2	93	8	94
16		6	93	47	87
17		3	95	13	96

The data showed that the first 3 compounds **8-10**, containing a linker of 2, 3 or 4 methylene groups respectively, were not very potent or effective at degrading either protein with DC_{50} values above 100 nM. However, when we extended the linker in compound 10 with one more methylene to obtain compound 11, the degradation potency for SMARCA2 greatly improved with a DC_{50} value of 12 nM and D_{max} of 93%. Interestingly, for SMARCA4 protein, compound **11** had a DC_{50} >1000 nM and a Dmax value of 73%, showcasing evidence that selective degradation for

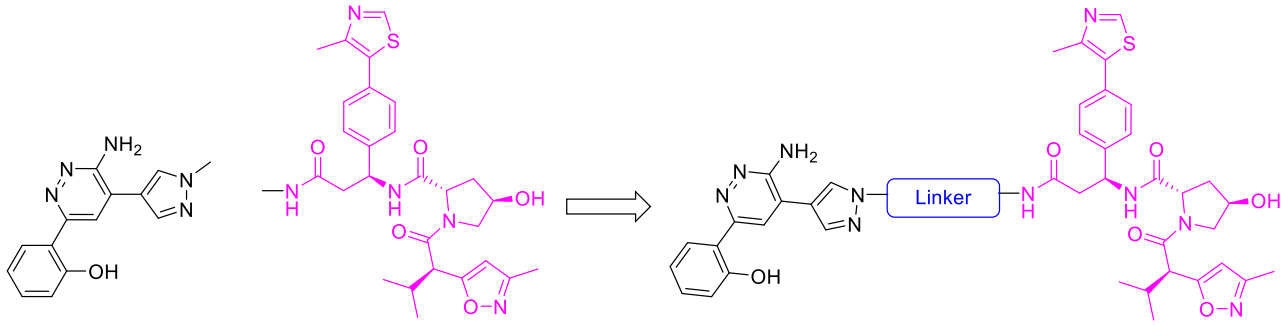
SMARCA2 over SMARCA4 by PROTAC degraders using a non-selective SMARCA2/4 bromodomain ligand could be achieved. Compound **12** with a linker of 6 methylene groups was equipotent with compound **11** for the degradation of SMARCA2, but less selective for the degradation of SMARCA4.

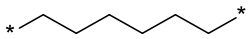
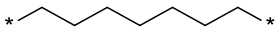
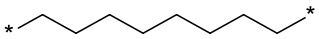
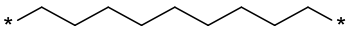
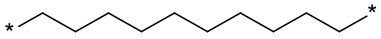
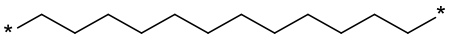
To further investigate the effect of linker length degradation potency and selectivity, we synthesized compounds **13-17** with linkers of 7 to 10 methylene groups. The degradation data showed that all the five compounds could induce over 90% degradation of both SMARCA2 and SMARCA4 proteins, with DC_{50} values of 2-6 nM for SMARCA2 and 8-47 nM for SMARCA4. Compound **15** containing a linker with a 9 methylene groups was the most potent degrader among the five compounds, which displayed a DC_{50} = 2 nM and a D_{max} = 93% for SMARCA2 protein. Although the SMARCA4 DC50 values were slightly higher than those of SMARCA2, the D_{max} values for SMARCA2 and SMARCA4 had no difference, indicating no or low SMARCA2 selectivity for these compounds.

The series of PROTAC degraders shown in Table 2-1 all contained linkers tethering to the terminal acetamide group of the VHL ligand (**7**). From the co-crystal structure of a potent VHL ligand complexed with VHL protein (PDB: 4W9H),[152] it was observed that the (S)-C-methyl group in the benzylic part of the VHL ligand was exposed to the solvent, which could be exploited as an alternative exit site to attach the linker. This linker design strategy had been used in a series of highly potent AR degraders previously reported in our group. Accordingly, we designed and synthesized 6 potential SMARCA degraders, compounds **18-23**, using the same SMARCA bromodomain ligand tethered to the middle methyl portion of a more potent, isoxazole-containing VHL ligand. These compounds were tested by HiBit degradation assay for their ability to reduce

the levels of SMARCA2 and SMARCA4 proteins and the generated results were summarized in Table 3.

Table 3. Investigation of a different linking position in VHL ligand for the design of PROTAC degraders



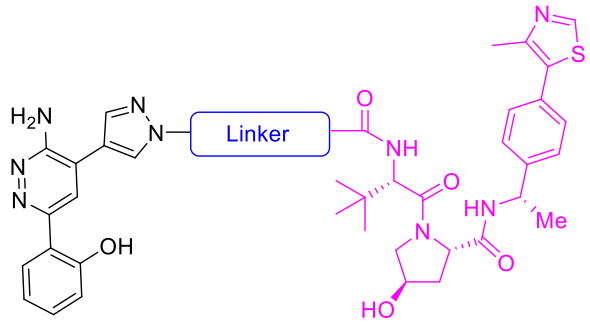
Compound	Linker	SMARCA2 DC_{50} (nM)	SMARCA2 D_{max} (%)	SMARCA4 DC_{50} (nM)	SMARCA4 D_{max} (%)
18		18	86	213	84
19		96	91	91	92
20		67	91	66	93
21		71	94	75	94
22		37	95	53	93
23		46	93	90	89

The data in Table 3 showed that all of these 6 compounds were weaker than compounds **13-17** in Table 1, even though they were able to reduce the level of SMARCA2 protein by over 85%. Compound **18** was the most potent one, achieving DC_{50} = 18 nM. All the compounds in Table 2-2 showed little or no selectivity for SMARCA2 over SMARCA4.

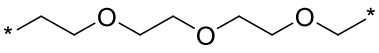
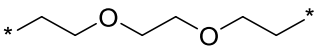
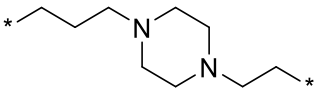
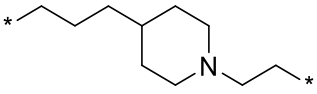
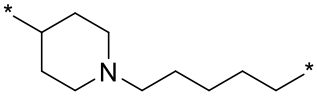
Apart from the linker length, the linker composition was proven to play a crucial role in affecting the degradation potency and selectivity of PROTAC molecules.[109-110, 125, 135-136] Thus, we

designed and synthesized a number of analogues of compound **15** with linkers of the same length but structurally different compositions. Because the linker in compound **15** is entirely hydrophobic, we first tried to introduce polar groups into the linker to increase the solubility. This effort resulted in compounds **24-27** in Table 4.

Table 4. Optimization of the linker composition



PROTAC SMARCA2/4 Degarders

Compound	Linker	SMARCA 2 DC_{50} (nM)	SMARCA 2 D_{max} (%)	SMARCA 4 DC_{50} (nM)	SMARCA 4 D_{max} (%)
24		455	70.5	>1000	46.5
25		313	76.5	>1000	58.5
26		682	62	585	76
27		>1000	12	>1000	0
28		6	94	248	77

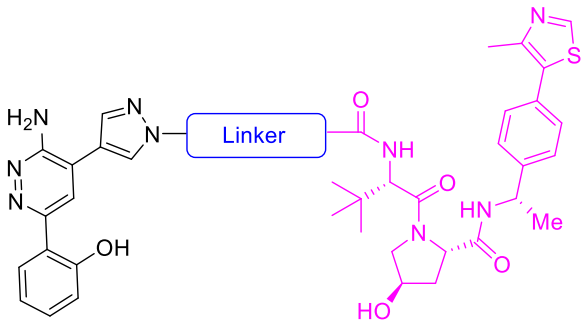
Surprisingly, when we introduced polyethylene glycol (PEG) units to embed in the linker and synthesized compounds **24** and **25**, the HiBit degradation data showed that these two compounds were much less potent than compound **15** with SMARCA2 DC_{50} values of 455 nM and 313 nM, respectively. We next sought to introduce conformational restrictions into the linker because from our previous studies, such strategies could effectively enhance the degradation potency. **40** We therefore incorporated rigid rings containing basic nitrogen atoms into compound **15**, producing compounds **26** with a piperazine ring and **27** with a piperidine ring, respectively in the middle of the linker. The HiBit data showed that while compound **26** had a modest degradation potency with Dmax values above 60% against both proteins, compound **27** was completely inactive in degrading both proteins at concentrations up to 1 μM. Interestingly, when we moved the piperidine group in compound **27** from the middle of the linker to the attachment point in the pyrazole moiety of the SMARCA ligand and resulted compound **28**, it potently degraded SMARCA2 with a DC_{50} = 6 nM and a D_{max} of 94%. Furthermore, compound **28** had a DC_{50} = 248 nM with a D_{max} of 77% againast SMARCA4. Hence, compound **28** demonstrated a selectivity of 40 folds for SMARCA2 over SMARCA4 and a difference of 17% in the D_{max} values.

The promising potency and selectivity data encouraged us to further rigidify the linker of compound **28**. Accordingly, we designed and synthesized compounds **29-32** by incorporating spiro ring systems into the linker (Table 5). The [3.5]azaspiro ring-containing compound **29** (SMD-3040) achieved a DC_{50} value of 12 nM and a D_{max} of 91% against SMARCA2. To our gratification, compound **29** only degraded SMARCA4 with a DC50 >1000 nM and a Dmax = 44 %, implying it was a potent and selective SMARCA2 degrader. By replacing the [3.5]azaspiro group with a [5.5]azaspiro group, we synthesized compound 30, which had a DC_{50} value of 5 nM and a D_{max} value of 90% against SMARCA2 and a DC_{50} value of 219 nM and a D_{max} value of 66% for

SMARCA4. Therefore, compound **30** was 2 times more potent than compound **29** for the degradation of SMARCA2 but less selective for SMARCA4. Removal of the methylene group from the linker in compounds **29** and **30** led to compounds **31** and **32**, respectively. The data showed that both compounds **31** and **32** had a weaker degradation potency against SMARCA2 and less selectivity compared to their counterpart compounds **29** and **30**.

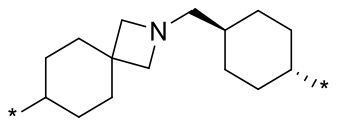
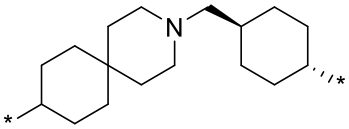
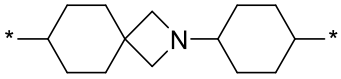
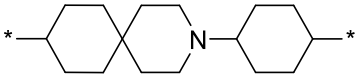
We also evaluated the two recently reported SMARCA2 selective degraders, A947 (**5**) and ACBI2 (**6**) in our HiBit assay (Table 5). A947 (**5**) was a extremely potent SMARCA2 degrader, with DC_{50} = 0.12 nM and D_{max} = 96% for SMARCA2 and DC_{50} = 2 nM and D_{max} = 98% for SMARCA4. ACBI2 (**6**) had DC_{50} values of 1 and 9 nM and D_{max} values of 94 and 92% for SMARCA2 and SMARCA4, respectively. Therefore, A947 and ACBI2 demonstrated a selectivity of 17- and 9-fold for SMARCA2 over SMARCA4, respectively, based upon their DC_{50} values. However, the D_{max} values against both SMARCA2 and SMARCA4 proteins were not distinguishable as they both reached over 90%.

Table 5. Optimization of the linker composition



PROTAC SMARCA2/4 Degarders

Compound	Linker	SMARCA 2 DC_{50} (nM)	SMARCA 2 D_{max} (%)	SMARCA 4 DC_{50} (nM)	SMARCA 4 D_{max} (%)

29 (SMD-3040)		12	91	>1000	44
30		5	90	219	66
31		25	85	>1000	55
32		34	90	315	72
A947 **(5)**	-	0.12	96	2	98
ACBI2 **(6)**	-	1	94	9	92

In summary, our medicinal chemistry efforts have resulted in the identification of the lead compound SMD-3040 as a potent and selective SMARCA2 degrader. We next proceeded to perform extensive biological evaluations of SMD-3040 in vitro and in vivo.

2.2.2 Evaluation of Degradation Kinetics and the Mechanism of Action of SMD-3040

We first examined the kinetics of SMD-3040 in degrading SMARCA2 and SMARCA4 proteins using the HiBit assay (Figure 16). Our results showed that SMD-3040 time- and dose-dependently reduced the levels of SMARCA2 protein, reaching D_{max} of 66, 79, 80, 90 and 94% and DC_{50} values of 250, 63, 44, 10 and 11 nM at 1, 3, 6, 24 and 48 hr time-points, respectively. SMD-3040 also reduced the levels of SMARCA4 protein in a time- and dose-dependent, albeit much less effective manner than for SMARCA2 protein with D_{max} values of 20, 46, 49, 57 and 68% and DC_{50} values of >1 μM, >1 μM, >1 μM, 339 nM and 174 nM at 1, 3, 6, 24 and 48 hr time-points, respectively. These data showed that SMD-3040 displayed a good degradation selectivity

profile against SMARCA2 over SMACRA4 based upon both D_{max} and DC_{50} values at all the time points tested.

We next investigated the mechanism of SMARCA2 and SMARCA4 degradation induced by SMD-3040 using the HiBit assay (Figure 17). Our data showed that SMARCA2 degradation induced by SMD-3040 was significantly attenuated by pre-treatment with the proteasome inhibitor PR171 or the NEDD8-activating E1 enzyme inhibitor MLN4924, indicating that SMARCA2 degradation was proteasome- and neddylation-dependent. SMARCA2/4 degradation by SMD-3040 was also blocked by the pre-treatment of either SMARCA bromodomain ligand (**3**) or VHL ligand (**7**), suggesting that binding to both VHL and SMARCA proteins was required for SMD-3040 to cause SMARCA2/4 degradation. These mechanistic data clearly demonstrate that SMD-3040 is a bona fide PROTAC SMARCA degrader.

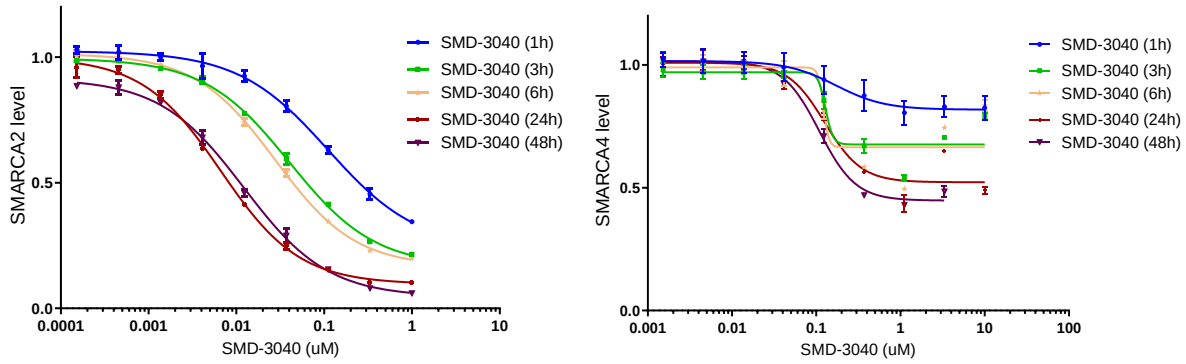


Figure 16. Time course of SMD-3040 in degrading SMARCA2 and SMARCA4 in Hela cells using HiBit assay.

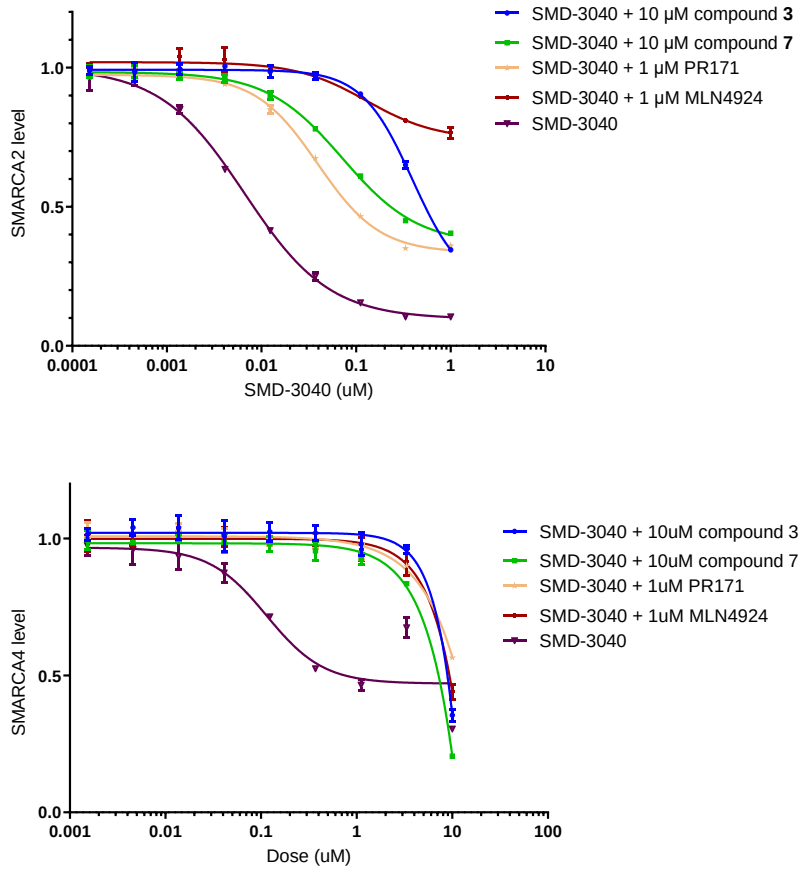


Figure 17. Mechanistic study of SMD-3040 degrading SMARCA2 and SMARCA4 proteins in Hela cells using a HiBit assay.

2.2.3 Evaluation of Degradation Potency and Selectivity of SMD-3040 in Different Cell Lines

We evaluated the degradation potency and selectivity of SMD-3040 in different cell lines by traditional Western Blot experiments. In the SK-Mel-28 melanoma cell line with wildtype SMARCA2/4 proteins, 24 h treatment of SMD-3040 induced potent and complete degradation of SMARCA2 protein, with a DC_{50} value of 35 nM and D_{max} value of 98% (Figure 18). No significant degradation of SMARCA4 was observed up to 1000 nM of SMD-3040 and only a maximum of 24% of SMARCA4 protein was degraded (Figure 18), which was in line with the selectivity of SMD-3040 observed in our HiBit screening efforts.

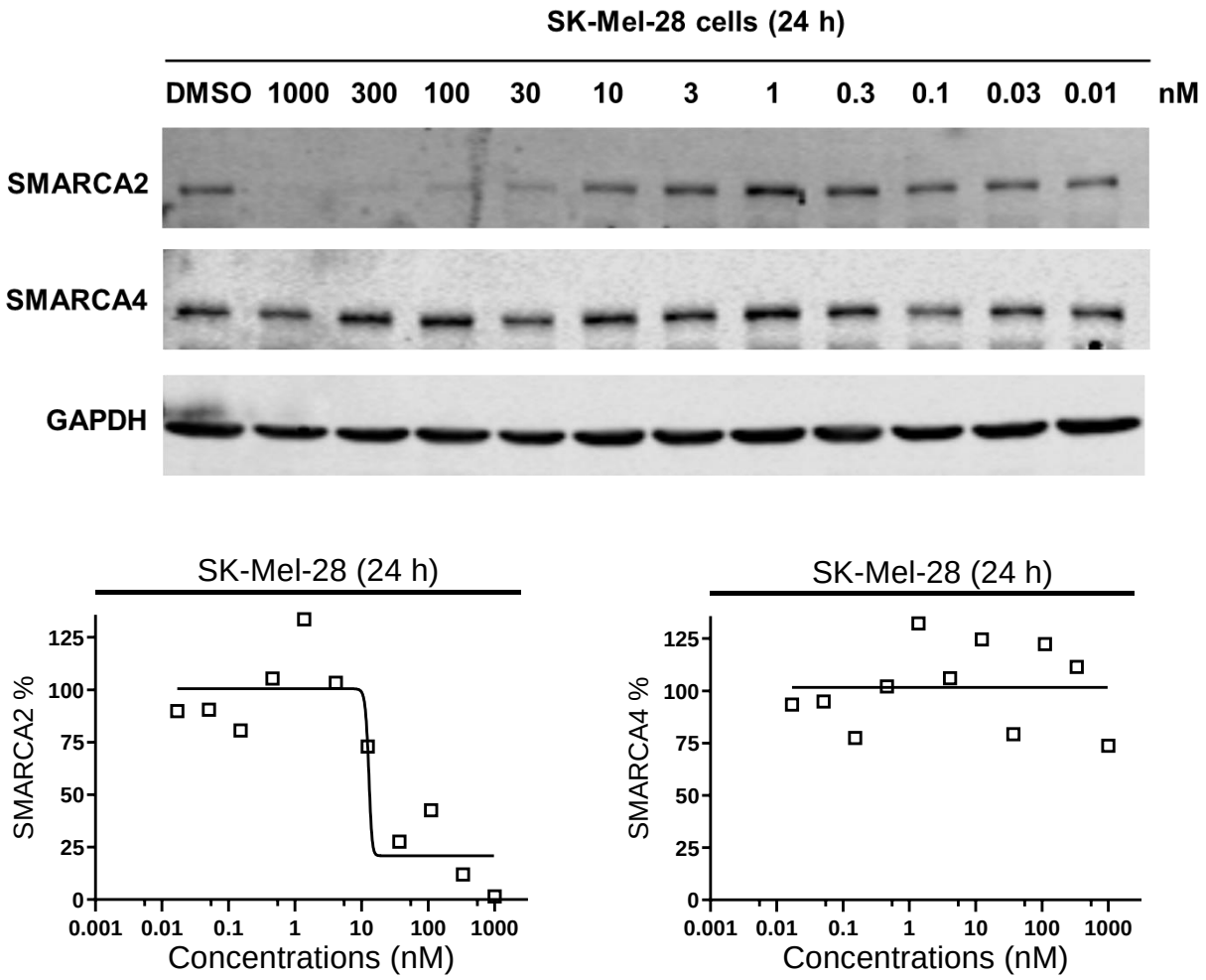
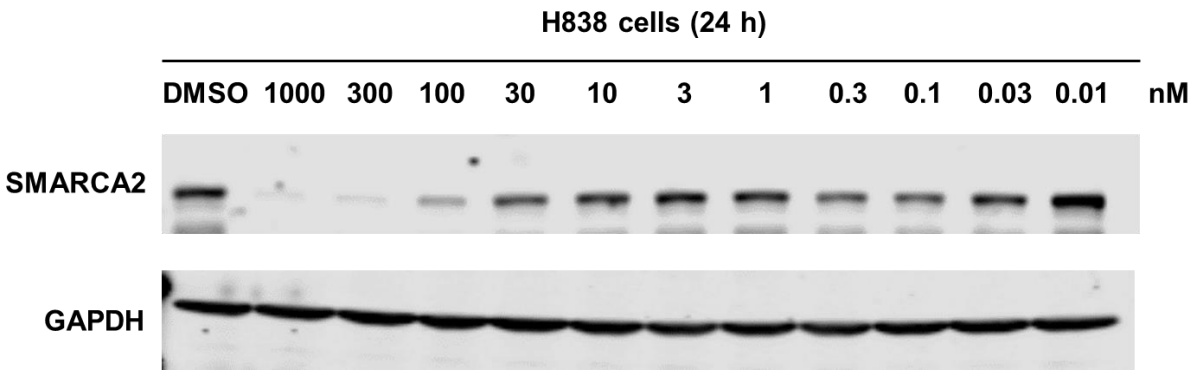
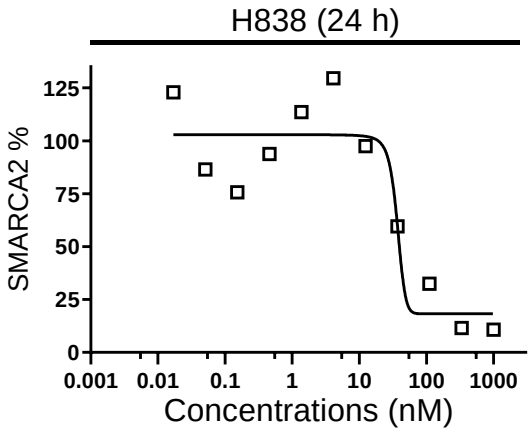
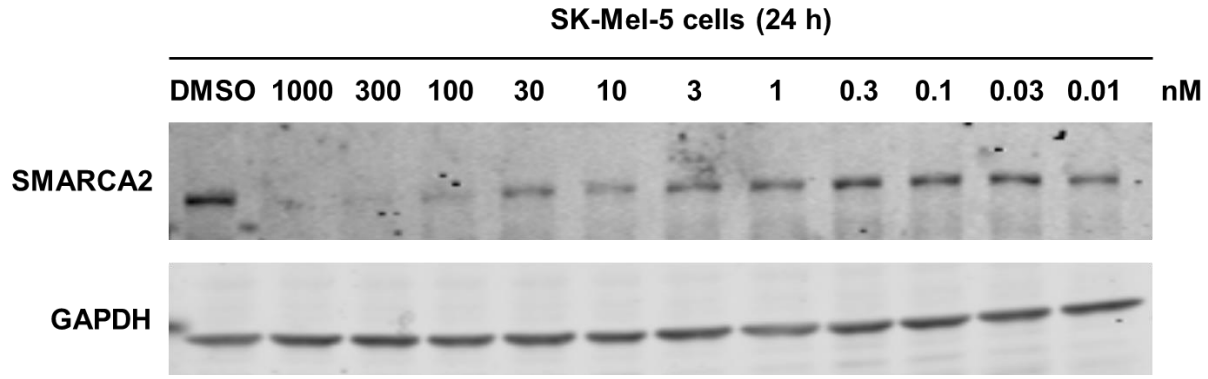


Figure 18. SMARCA2 and SMARCA4 DC_{50} and D_{max} value determination in SK-Mel-28 cell line.

Previous studies have shown that SMARCA4-deleted human cancers are particularly vulnerable to SMARCA2 knockdown.**10-12** Accordingly, we next evaluated SMD-3040 for its ability to degrade SMARCA2 in two cancer cell lines carrying SMARCA4 gene deletion. SMD-3040 was found to achieve DC_{50} values of 62 and 20 nM, with D_{max} values of 90% and 94%, respectively in H838 non-small cell lung cancer cell line and SK-Mel-5 melanoma cell line with a 24 h treatment time (Figure 19). It is noteworthy that the previously reported hook effect[110, 125] was not observed for SMD-3040 up to 1 μM in all three cancer cell lines tested.


H838 cells (24 h)
DMSO 1000 300 100 30 10 3 1 0.3 0.1 0.03 0.01 nM
SMARCA2
GAPDH


H838 (24 h)
SMARCA2 %
125
100
75
50
25
0
0.001 0.01 0.1 1 10 100 1000
Concentrations (nM)


SK-Mel-5 cells (24 h)
DMSO 1000 300 100 30 10 3 1 0.3 0.1 0.03 0.01 nM
SMARCA2
GAPDH

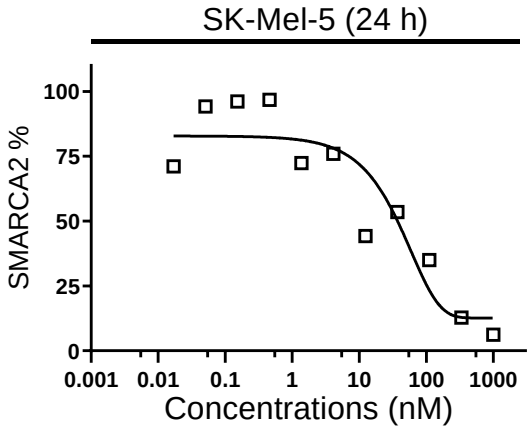


Figure 19. SMARCA2 DC_{50} and D_{max} value determination of SMD-3040 in H838 and SK-Mel-5 cell lines.

2.2.4 Evaluation of Cell Growth Inhibition of SMD-3040 in Different Cell Lines

We then evaluated the cell growth inhibition effect of in a panel of 12 SMARCA4-wildtype or SMARCA4-deficient cell lines. The data obtained were summarized in Figure 20 and Table 6. In selection of cancer lineages, our primary focus was on non-small cell lung cancer (NSCLC) lines and melanoma lines in which the SMARCA4 gene is the most frequently inactivated.

SMD-3040 was effective in inhibiting the cell growth of 6 out of 8 SMARCA4-deficient cell lines that were tested, and achieved GI_{50} (concentration needed to achieve 50% of the maximum of cell growth inhibition rate compared to the control) values of 8.8 - 119 nM, with I_{max} (maximum inhibition) values of 68 - 95% (Figure 20). In comparison, the potent unselective SMARCA2/4 degrader compound 15, had GI_{50} values of 2.5 - 47.9 nM among those 6 cell lines and was 2-4 times more potent than SMD-3040 (Table 6), which was consistent with their degradation potency in HiBit assay. 2 SMARCA4-deficient cell lines, NCI-H1299 and A549, responded to SMD-3040 less effectively, where SMD-3040 showed Imax values of 41 and 51%, respectively. Interestingly, the dual SMARCA2/4 degrader compound 15 had an GI_{50} = 100 nM and I_{max} = 81% in the NCI-H1299 cell line (Table 6), suggesting that partial SMARCA4

functionality might still retained in this cell line, notwithstanding the reported SMARCA4 deletion.[57, 153-154]

Because SMD-3040 showed an excellent SMARCA2 degradation selectivity over SMARCA4 in HiBit assay and Western Blot experiment, we wanted to test its cell growth inhibitory activity in the H647, H1792 and H1975 NSCLC cell lines and the SK-Mel-28 melanoma cell line carrying wildtype SMARCA4 protein. The results showed that SMD-3040 exhibited very weak antiproliferative activity in the H1792, H1975 and SK-Mel-28 cell lines, with GI_{50} >10 μM (Figure 20 and Table 6). In the H647 cell line, SMD-3040 had a modest activity with GI_{50} = 3.1 μM and I_{max} = 74%. Overall, SMD-3040 selectively induced cell growth inhibition in SMARCA4 deficient cancer cell lines, and had minimal effect in SMARCA4 wildtype cancer cell lines. In comparison, the dual degrader, compound **15**, was very potent and effective in inhibiting the cell growth of SMARCA4 wild-type cancer cell lines (Table 6), achieving GI_{50} values of 60, 38, 76 and 32, nM, and I_{max} values of 86, 63, 77 and 90%, in the H1792, H1975, H647 and SK-Mel-28 cell lines, respectively.

We also evaluated A947 and ACBI2 for their cell growth inhibitory activity (Table 6). A947 potently and effectively inhibited cell growth in 8 SMARCA4-deficient cancer cell lines in our evaluation, with GI_{50} values of 0.3 - 31 nM and I_{max} values of 52 - 96%. A947 was also shown to be highly potent and effective in inhibition of cell growth in these 4 SMARCA4 wild-type cancer cell lines, achieving GI_{50} values of 8-18 nM and I_{max} values of 50-92%. ACBI2 attained GI_{50} values of 2.8-116 nM and I_{max} values of 56-96% in these 8 SMARCA4 deficient cancer cell lines and GI_{50} values of 65-165 nM and I_{max} values of 63-80% in these 4 SMARCA4 wildtype cancer cell lines (Table 6). It is of note that a number of SMARCA4-deficient cancer cell lines were highly sensitive to the treatment of dual degraders A947 or ACBI2, compared to SMARCA4 wild-type cancer cell

lines. For example, in the SK-Mel-5, NCI-H1693 and NCI-H1568 SMARCA4-deficient cell lines, A947 achieved GI_{50} values of 0.2-0.4 nM and I_{max} values of 82-96%, which are much better than those achieved in the 4 SMARCA4 wild-type cancer cell lines where the GI_{50} values were 8.1-18 nM and I_{max} values were 50-92%. The same trend was seen for ACBI2 that ACBI2 had much lower GI_{50} values and deeper Imax values in in the SK-Mel-5, NCI-H1693 and NCI-H1568 SMARCA4-deficient cell lines than those values in SMARCA4 wild-type cancer cell lines. The reasons and mechanisms underlying these differences still remain to be elucidated.

Taken together, these data showed that SMD-3040 potently and effectively inhibits cell growth in 6 of 8 SMARCA4 deficient cancer cell lines and had minimal activity in 4 SMARCA4 wild-type cancer cell lines, demonstrating a very high antiproliferative selectivity across cell lines. Our dual SMARCA2/4 degrader, compound **15**, and the reported degraders A947 and ACBI2, were very potent and effective inhibitors of both SMARCA4 deficient and wildtype cancer cell lines.

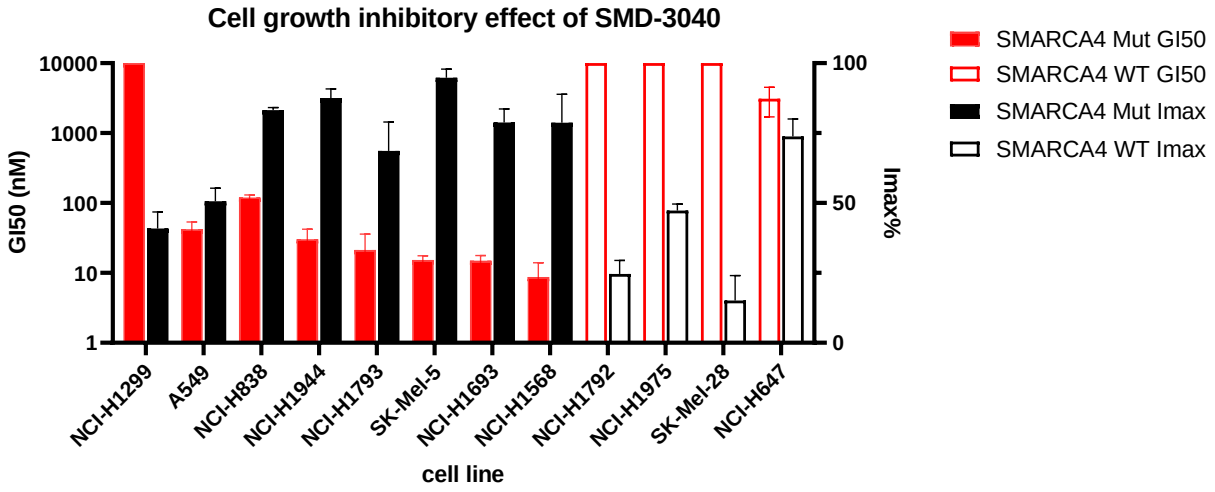


Figure 20. Cell growth inhibition assay results of SMD-3040.

Table 6. Cell growth inhibition activity of SMD-3040, compound **15**, A947 and ACBI2.

Cell line		SMD-3040		Compound **15**		A947		ACBI2	
		GI_{50} (nM)	Imax%	GI_{50} (nM)	Imax%	GI_{50} (nM)	Imax%	GI_{50} (nM)	Imax%
SMARCA4 Deficient	NCI-H1299	>10 μM	41 ± 5	100 ± 40	81 ± 2	31 ± 18	68 ± 4	116 ± 33	74 ± 3
	NCI-H838	119 ± 9	83 ± 1	48 ± 6	91 ± 1	5.0 ± 1.3	93 ± 1	67 ± 23	82 ± 2
	A549	42 ± 9	51 ± 4	16 ± 4	53 ± 4	3.3 ± 1.8	52 ± 1	30 ± 11	56 ± 2
	NCI-H1944	30 ± 10	88 ± 3	4.8 ± 0.7	87 ± 5	0.9 ± 0.2	87 ± 2	13 ± 3	82 ± 5
	NCI-H1793	21 ± 12	69 ± 8	5.0 ± 2.6	72 ± 6	1.0 ± 0.5	67 ± 8	7.3 ± 4.2	68 ± 3
	SK-Mel-5	15 ± 2	95 ± 3	2.5 ± 0.3	95 ± 2	0.4 ± 0.1	96 ± 3	4.9 ± 1.2	96 ± 2
	NCI-H1693	15 ± 2	79 ± 4	3.3 ± 0.6	81 ± 4	0.2 ± 0.1	82 ± 6	2.8 ± 0.6	86 ± 7
	NCI-H1568	8.8 ± 4.3	79 ± 8	2.5 ± 0.9	82 ± 4	0.3 ± 0.2	84 ± 5	2.8 ± 1.1	90 ± 3
SMARCA4 Wild-type	NCI-H1792	>10 μM	25 ± 4	60 ± 13	86 ± 2	17 ± 3	69 ± 3	135 ± 31	65 ± 2
	NCI-H1975	>10 μM	47 ± 2	38 ± 5	63 ± 2	18 ± 3	50 ± 1	65 ± 33	63 ± 7
	SK-Mel-28	>10 μM	15 ± 7	32 ± 4	90 ± 2	8.1 ± 1.9	92 ± 2	>10 μM	50 ± 7
	NCI-H647	3.1 ± 1.2 (μM)	74 ± 5	76 ± 56	77 ± 3	8.1 ± 5.3	68 ± 4	165 ± 116	80 ± 4

2.2.5 Pharmacodynamic evaluation of SMD-3040

We next examined the pharmacodynamics (PD) for SMD-3040 the H838 SMARCA4-deficient xenograft tumors in mice for its ability to induce SMARCA2 degradation in vivo. The

obtained data were summarized in Figure 21 and Table 7. The data showed that a single administration of SMD-3040 at 50 mg/kg via intravenous injection reduced SMARCA2 protein levels in the tumor tissues by 70, 91, 75 and 67% at 3, 24, 48 and 96 h time points, respectively.

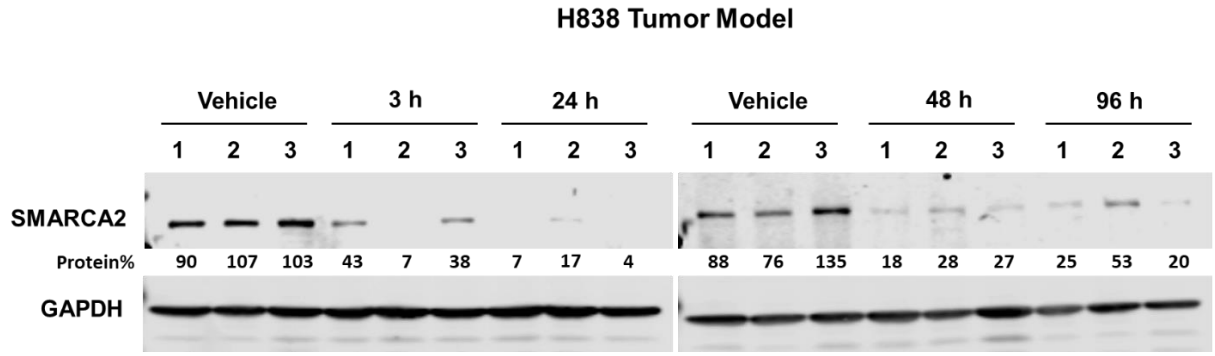


Figure 21. PD effect of SMD-3040 on SMARCA2 protein level in H838 tumors.

Table 7. PD data of SMD-3040 on SMARCA2 protein level in H838 tumors.

H838 **50 mg/kg, IV**	**Samples**	**Relative Protein%**	**Mean Protein %**
		SMARCA2	**SMARCA2**
vehicle	1	90	100 ± 7
	2	107	
	3	103	
3 h	1	43	30 ± 16
	2	7	
	3	38	
24 h	1	7	9 ± 5
	2	17	
	3	4	

48 h	1	18	25 ± 4
	2	28	
	3	27	
96 h	1	25	33 ± 14
	2	53	
	3	20	

To test whether SMD-3040 could selectively degrade SMARCA2 in vivo, we did PD studies of SMD-3040 in the MV4-11 xenograft tumor model, which expresses high levels of SMARCA2 and SMARCA4 proteins, and summarized the data in Figure 22 and Table 8. Single intravenous dose of SMD-3040 at 50 mg/kg induced rapid degradation of SMARCA2 protein within as quickly as 2 h, and the PD effect persisted for 4 days. SMD-3040 reduced the SMARCA2 protein level by 78, 70, 86, 83, 56 and 74% at 2, 6, 24, 48, 72 and 96 h time points, respectively, while the level of SMARCA4 protein was maintained above 70% at all time points tested. These PD data together showed that SMD-3040 could induce a long-lasting PD effect in both the H838 and MV4-11 tumor models by rapidly and effectively degrading SMARCA2 protein. Importantly, excellent selectivity over SMARCA4 protein could be achieved in vivo by SMD-3040 that levels of SMARCA4 protein was reduced only modestly (<30%) at all time points tested in the MV4-11 tumors.

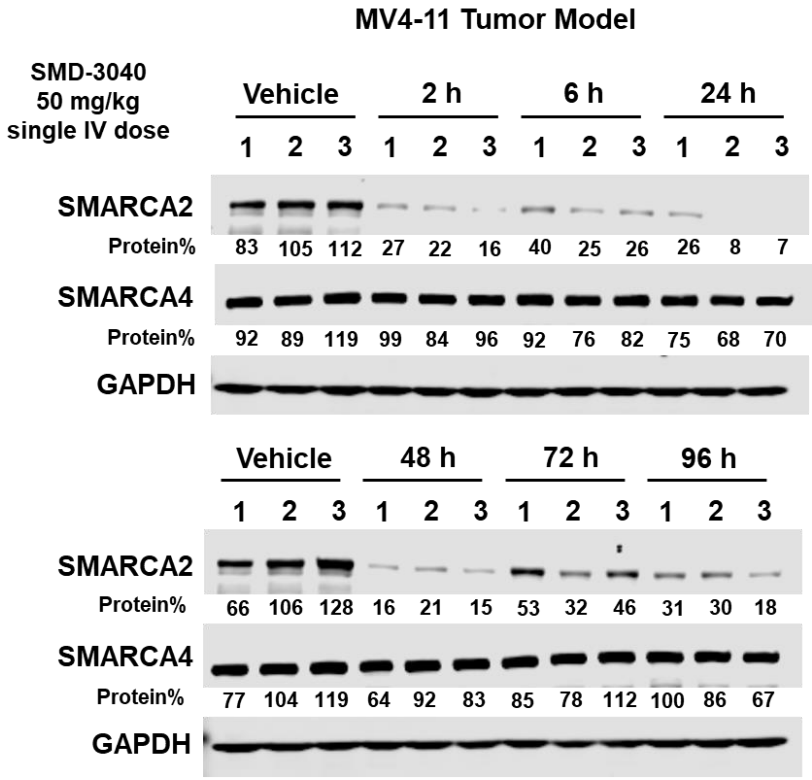


Figure 22. PD effect of SMD-3040 on SMARCA2 and SMARCA4 protein levels in MV4;11 tumors.

Table 8. PD data of SMD-3040 on SMARCA2 and SMARCA4 protein levels in MV4;11 tumors.

	Samples	Relative Protein% SMARCA2	Mean Protein % SMARCA2	Relative Protein% SMARCA4	Mean Protein % SMARCA4
vehicle	1	83	100 ± 15	92	100 ± 16
	2	105		89	
	3	112		119	
2 h	1	27	22 ± 5	99	93 ± 8
	2	22		84	
	3	16		96	
6 h	1	40	30 ± 8	92	83 ± 8

	2	25		76	
	3	26		82	
24 h	1	26	14 ± 11	75	71 ± 3
	2	8		68	
	3	7		70	
48 h	1	16	17 ± 3	64	87 ± 14
	2	21		92	
	3	15		83	
72 h	1	53	44 ± 10	85	91 ± 18
	2	32		78	
	3	46		112	
96 h	1	31	26 ± 7	100	84 ± 17
	2	30		86	
	3	18		67	

To gain insights into the persistent PD effect of SMD-3040, we analyzed drug concentrations in both plasma and tumor tissues in the MV4-11 mice tumor models and summarized the data in Table 9. The data showed that the plasma drug concentration for SMD-3040 was reduced to a very low level after 24 h time point. However, the tumor drug concentration for SMD-3040 was kept at a relatively high level even on day 4. These data indicated that SMD-3040 had a good tumor tissue penetration, resulting in a much slower clearance in the tumor tissue than in the plasma.

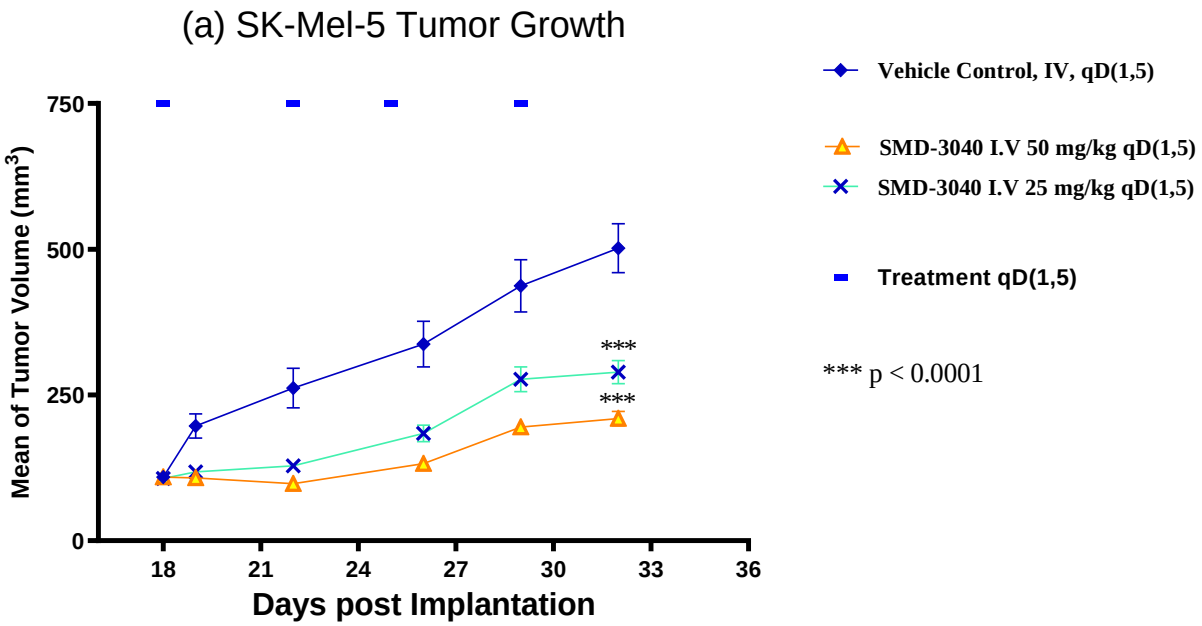
Table 9. Drug concentrations of SMD-3040 in plasma and tumor.

Dose 50mg/kg	Plasma (ng/mL)					Tumor (ng/g)				
Time point (hr)	1	2	3	Mean	SD	1	2	3	Mean	SD
2	1510	3860	2830	2733	1178	2205	4660	3390	3418	1228
6	607	1160	530	766	344	785	1725	795	1102	540
24	85.1	110	460	218	210	2565	3025	3300	2963	371
48	17.6	36.0	128.0	60.5	59.1	715	1170	1050	978	236
72	9.1	9.4	1.7	6.7	4.4	329	510	272	370	124
96	5.8	45.7	7.3	19.6	22.6	620	354	705	560	183

2.2.6 Evaluation of the Efficacy of SMD-3040 in SK-Mel-5 and H838 Xenograft Tumor Models

Based upon the promising PD data, we pursued efficacy studies and evaluated the antitumor activity of SMD-3040 in the SK-Mel-5 xenograft tumor model in mice with an intravenous (I.V.), twice a week (biw) dosing regimen. The data obtained are summarized in Figure 23. SMD-3040 showed dose-dependent tumor growth inhibition in the SK-Mel-5 xenograft model. At 25 and 50 mg/kg, SMD-3040 induces tumor growth inhibition by 54 and 74% on day 32 ($p <$

0.0001), respectively. Although weight loss was observed in all the experimental groups, mice in the two treatments experienced a slighter weight loss (8% and 6%) compared to the vehicle group (12%), suggesting that weight loss might have been caused by the growth of SK-Mel-5 tumors and that treatment of SMD-3040 could potentially have alleviated some of the weight loss effect.



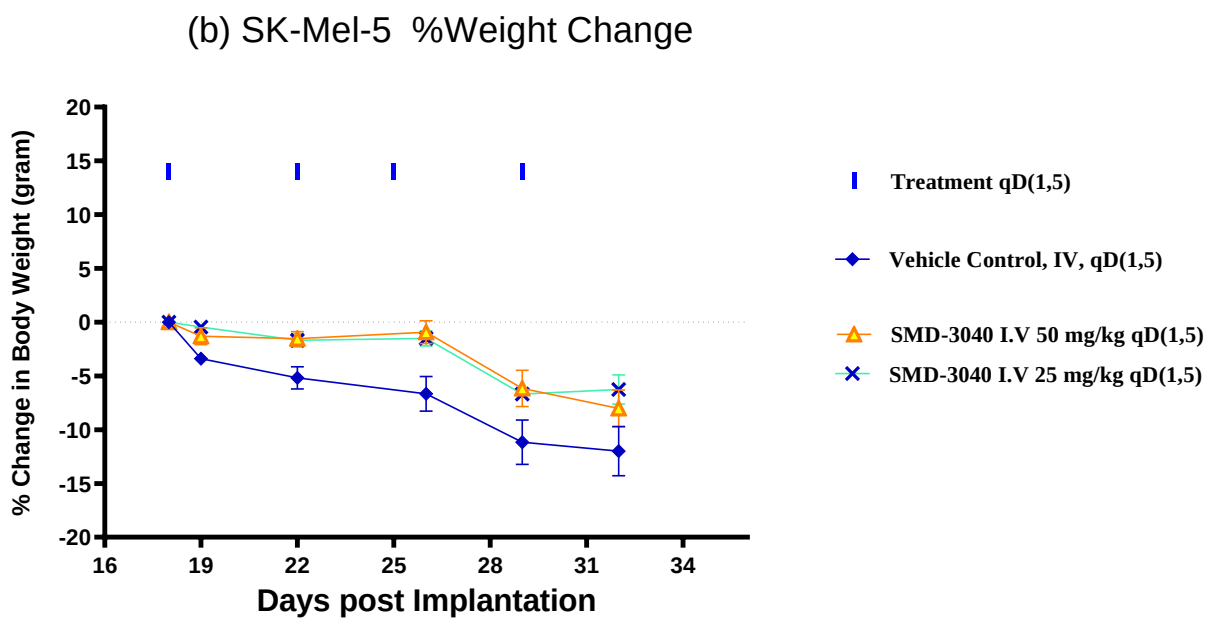


Figure 23. Efficacy study of SMD-3040 in the SK-Mel-5 xenograft tumor model in SCID mice.

SMD-3040 was next evaluated in the SMARCA4-deficient H838 xenograft tumor model for its antitumor activity with an intravenous (I.V.), twice a week(biw) dosing regimen and summarized the data in Figure 24. The data showed that 50 mg/kg of SMD-3040 effectively caused tumor growth inhibition by 81% ($p = 0.0017$) at the last day of the experiment. No significant weight loss was observed during the course of efficacy study in H838 model and SMD-3040 was thus well tolerated. Taken together, SMD-3040 achieved significant in vivo tumor growth inhibition with a well-tolerated safety profile.

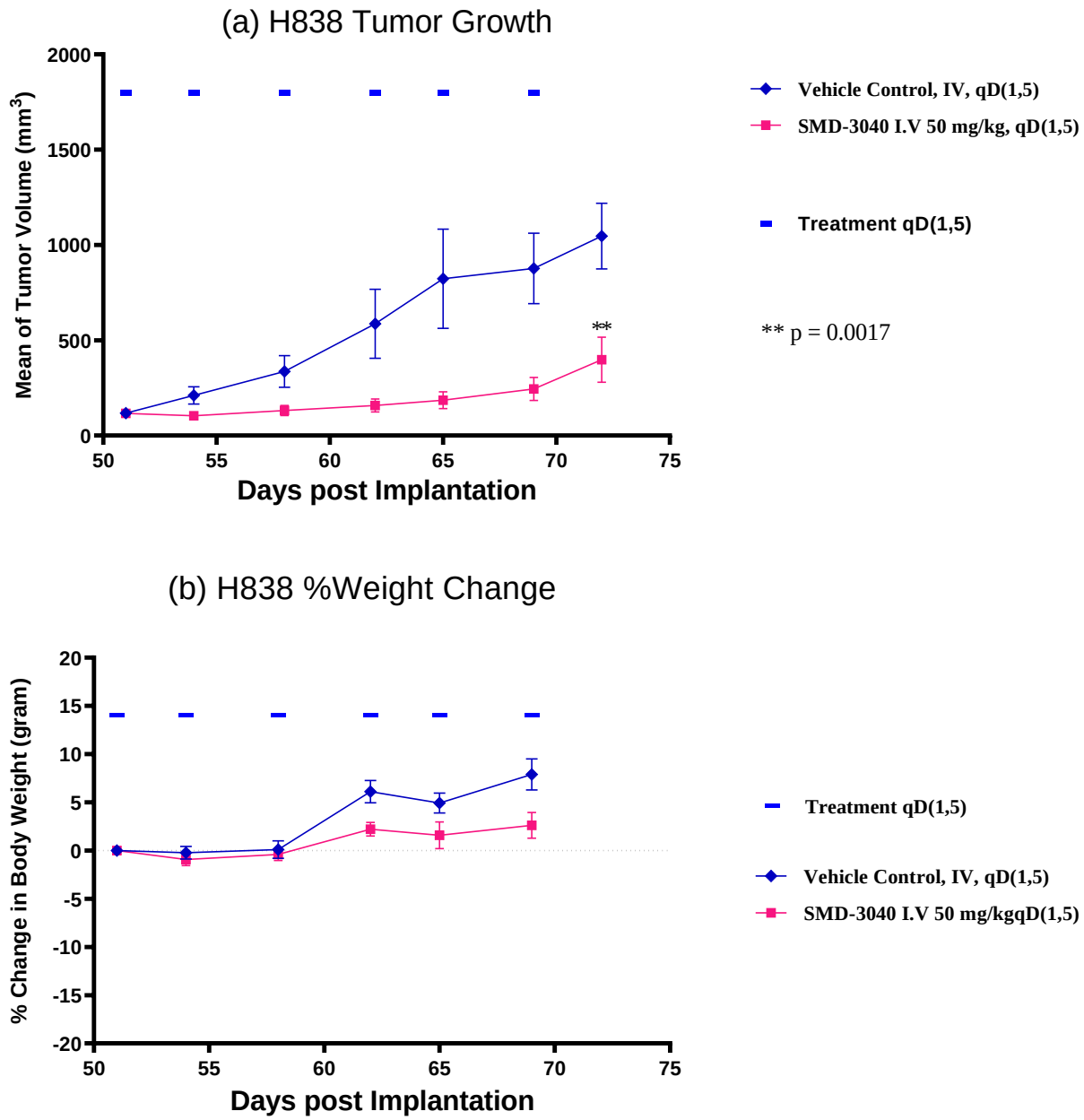


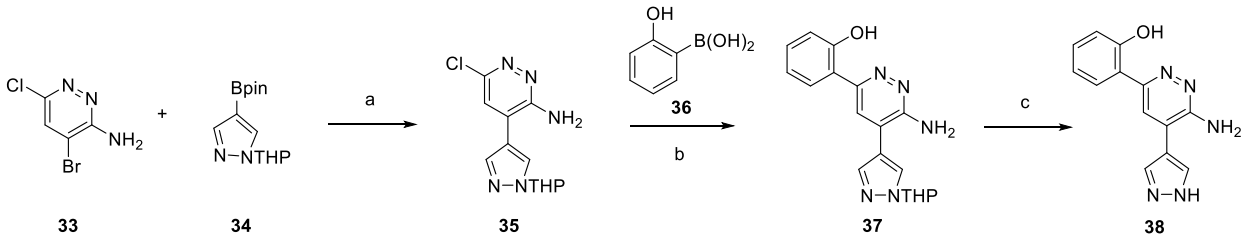
Figure 24. Efficacy study of SMD-3040 in the H838 xenograft tumor model in SCID mice.

2.3 Chemical Synthesis

The synthesis of the key intermediate (**38**) is shown in Scheme 1. Compound **35** was synthesized from 4-bromo-6-chloropyridazin-3-amine (**33**) and 1-(tetrahydro-2H-pyran-2-yl)-4-(4,4,5,5-tetramethyl-1,3,2-dioxaborolan-2-yl)-1H-pyrazole (**34**) by Suzuki coupling. Another

Suzuki coupling of compound (**35**) with (2-hydroxyphenyl)boronic acid (**36**) was carried out to give compound **37**, and this was followed by removal of the THP group to give the intermediate (**38**).

Scheme 1. Synthesis of Compound 38 in chapter 2.

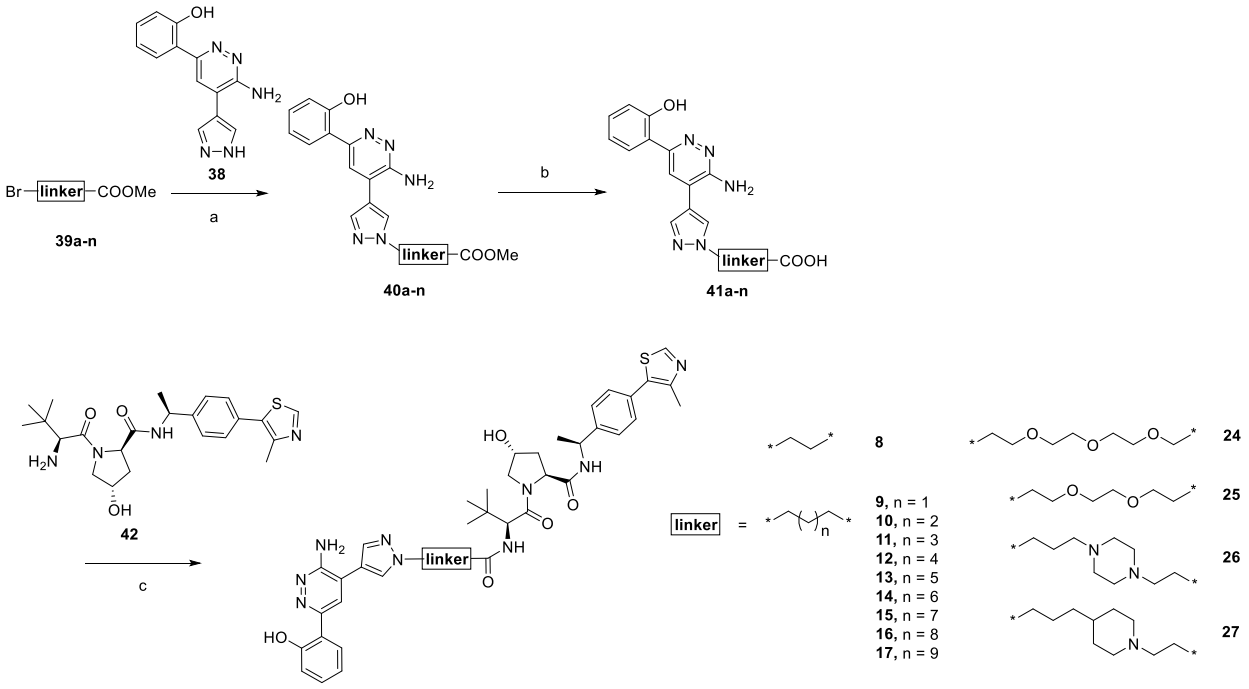


Reaction conditions: (a) $Pd(PPh_3)_4$, K_2CO_3, 1,4-dioxane/H_2O, 100 °C , 6 h. (b) XPhos Pd G3, K_2CO_3, dioxane/H_2O, 95 °C, 12 h. (c) 4N HCl, MeOH, rt, 8 h

Compounds **8-17** and **24-27** were synthesized according to the procedure in Scheme 2. Compounds **40a-n** were prepared through the substitution reaction of 38 with different linkers (**39a-n**). Hydrolysis of the methyl esters gave the corresponding carboxylic acids (**41a-n**). Amide condensation between compounds **41a-n** and the VHL ligand **(42**) afforded the final compounds **8-17** and **24-27**.

Scheme 2-2. Synthesis of Compounds 8-17, 24-27 in chapter 2

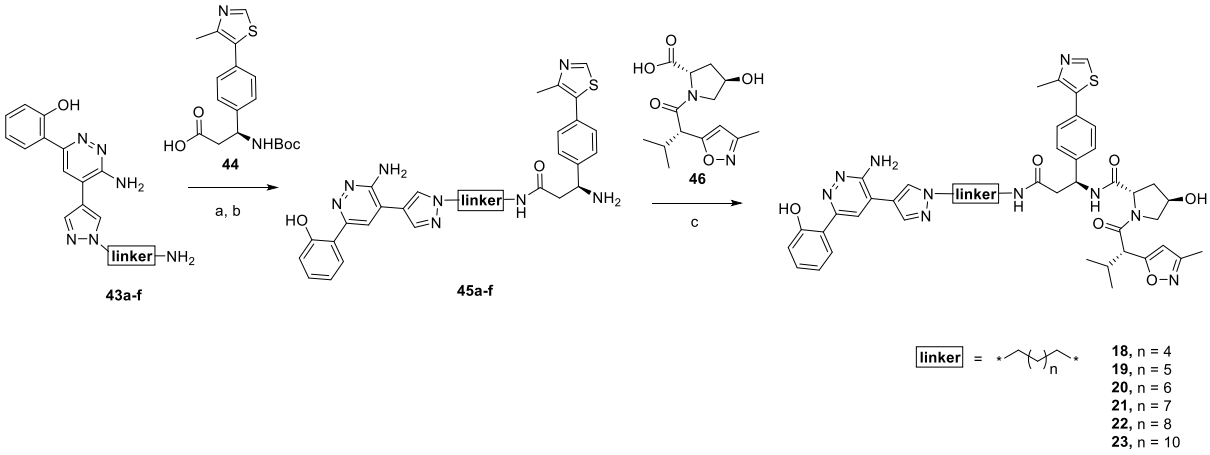
Scheme 2. Synthesis of Compounds 8-17, 24-27 in chapter 2.



Reaction conditions: (a) K_2CO_3, DMF, 60 °C, overnight. (b) LiOH, MeOH/H_2O, 40 °C, 2 h. (c) DIPEA, HATU, DMF, rt, 15 min.

As shown in Scheme 3, the synthesis of compounds **18-23** starts with different linker molecules (**43a-f**). Coupling with a VHL ligand fragment **44** afforded compound **45a-f**. The final compounds **18-23** were obtained through a second amide coupling reaction with another VHL ligand fragment **46**.

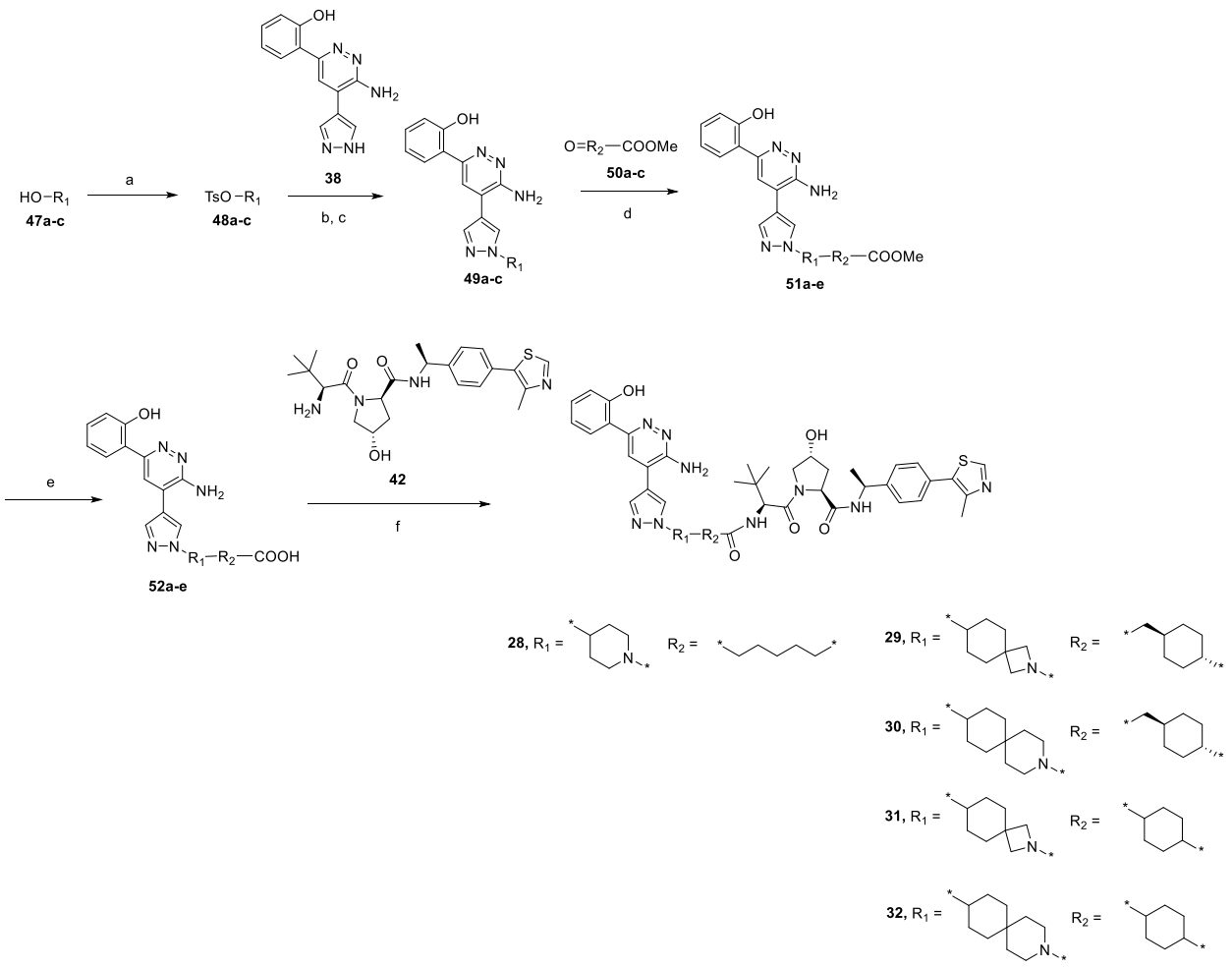
Scheme 3. Synthesis of Compounds 18-23 in chapter 2.



Reaction conditions: (a) K_2CO_3, DMF, 60 °C, 12 h. (b) H_2NNH_2, EtOH/DCM/H_2O, rt, overnight. (c) DIPEA, HATU, DMF, rt, 15 min. (d) 4N HCl in dioxane, rt, 30 min. (e) DIPEA, HATU, DMF, rt, 15 min.

The synthesis of compounds **28-32** is described in Scheme 4. Alcohols **47a-c** were converted into tosylates **48a-c**, followed by substitution with compound **38** to give compounds **49a-c**. Removal of the Boc protecting group and a subsequent reductive amination with compounds **50a-c** result in methyl esters **51a-e**. Hydrolysis of the methyl esters affords free carboxylic acids **52a-e**. A final step of amide coupling with VHL ligand **42** yields compounds **28-32**.

Scheme 4. Synthesis of Compounds 28-32 in chapter 2.



Reaction conditions: (a) TsOH, Et_3N, DMAP, DCM, rt, 12 h. (b) Cs_2CO_3, DMF, 60 °C, 12 h. (c) 4N HCl in dioxane, DCM, rt, 5 h (d) $NaBH(OAc)_3$, AcOH, DCE/DMF, rt, overnight. (e) LiOH, MeOH/THF/H_2O, rt, 12 h. (f) DIPEA, HATU, DMF, rt, 15 min.

2.4 Summary

In summary, we have presented the design, synthesis and biological evaluation of PROTAC degraders of SMARCA proteins. A potent dual SMARCA2/4 bromodomain ligand and VHL ligand were employed in our PROTAC design. Through extensive optimization of linker length, attachment position at the VHL ligand, linker composition and rigidity, we successfully identified a set of potent and selective degraders of SMARCA2 protein over its close paralog SMARCA4, with SMD-3040 (**32**) being the best one. SMD-3040 achieves a low nanomolar DC_{50} value (12 nM) and a high D_{max} value (>90%) for SMARCA2 and demonstrates a good selectivity over SMARCA4 based both on DC_{50} and D_{max} values. Kinetic and mechanistic studies show that SMD-3040 is capable of inducing rapid and complete degradation of SMARCA2 within 6 hours and is a bona fide SMARCA2 PROTAC degrader. In cell growth inhibition assays, SMD-3040 demonstrates potent antiproliferative activity in a panel of SMARCA4-deficient melanoma and non-small cell lung cancer cell lines, while sparing SMARCA4-wildtype cancer cell lines. A single intravenous administration of SMD-3040 could achieve a long-lasting pharmacodynamic effect to reduce SMARCA2 protein while have a modest effect in reducing SMARCA4 protein levels in mice tumor tissues, which is in line with its high and persistent exposure in tumor. SMD-3040 achieves strong tumor growth inhibition in two different SMARCA4-deficient xenograft models at well tolerated doses. Taken together, SMD-3040 is a potent, selective and efficacious SMARCA2 PROTAC degrader in vitro and in vivo, and serves as a promising lead compound for

further optimization for the development of a new therapy targeting human cancers with SMARCA4 deficiency.

2.5 Experimental section

Chemistry: General Experiment and Information. Unless otherwise noted, all purchased reagents were used as received without further purification. ^{1}H NMR and ^{13}C NMR spectra were recorded on a Bruker Avance 400 MHz spectrometer. ^{1}H NMR spectra are reported in parts per million (ppm) downfield from tetramethylsilane. All ^{13}C NMR spectra are reported in ppm and obtained with 1H decoupling. In reported spectral data, the format (δ) chemical shift (multiplicity, J values in Hz, integration) is used with the following abbreviations: s = singlet, d = doublet, t = triplet, q = quartet, m = multiplet. Mass spectral (MS) analysis was carried out with a Waters ultraperformance liquid chromatography (UPLC) mass spectrometer. The final compounds were all purified by C18 reverse-phase preparative high-performance liquid chromatography (HPLC) column with solvent A (0.1% TFA in H_2O) and solvent B (0.1% TFA in CH_3CN) as eluents. The purity of all the final compounds was confirmed to be >95% by UPLC−MS or UPLC.

2-(6-Amino-5-(1*H*-pyrazol-4-yl)pyridazin-3-yl)phenol (**38**)

Into a 250-mL round-bottom flask, was placed a solution of compound **33** (4.16 g, 20 mmol, 1.00 equiv.) in dioxane/H_2O (9:1, 100 mL), compound **34** (7.24 g, 26 mmol, 1.3 equiv.), $Pd(PPh_3)_4$ (2.3 g, 2.0 mmol, 0.10 equiv.), and potassium carbonate (5.52 g, 40 mmol, 2.0 equiv.) under N_2 protection. The resulting solution was stirred at 100 °C for 6 h. Solvent was removed and the residue was applied onto a silica gel column with dichloromethane/methanol (0-10:1). This

resulted in compound **35** as a white solid (5.0 g, 90%). ^{1}H NMR (400 MHz, MeOD) δ 8.38 (d, *J* = 0.6 Hz, 1H), 8.03 (d, *J* = 0.6 Hz, 1H), 7.55 (s, 1H), 5.52 (s, 2H), 5.51 (dd, *J* = 9.9, 2.5 Hz, 1H), 4.09 (ddd, J = 6.4, 5.0, 3.1 Hz, 1H), 3.82 – 3.75 (m, 1H), 2.26 – 2.14 (m, 1H), 2.13 – 2.04 (m, 2H), 1.87 – 1.61 (m, 3H).

Into a 250-mL round-bottom flask, was placed a solution of compound **35** (7.76 g, 20 mmol, 1.00 equiv.) in dioxane/H_2O (5:1, 80 mL), compound **36** (5.51 g, 40 mmol, 1.3 equiv.), XphosPdG3 (1.69 g, 2.0 mmol, 0.10 equiv.), and potassium carbonate (5.52 g, 40 mmol, 2.0 equiv.). The resulting solution was stirred at 95 °C for 12 h. Solvent was removed and the residue was applied onto a silica gel column with dichloromethane/methanol (0-10:1). This resulted in compound **37** as a white solid (4.7 g, 70%). ^{1}H NMR (400 MHz, MeOD) δ 8.49 (s, 1H), 8.37 (s, 1H), 8.09 (s, 1H), 7.73 (d, *J* = 6.8 Hz, 1H), 7.43 (t, *J* = 7.2 Hz, 1H), 7.05 (t, *J* = 7.2 Hz, 2H), 5.56 (dd, *J* = 9.7, 2.3 Hz, 1H), 4.12 (d, *J* = 11.6 Hz, 1H), 3.81 (td, *J* = 11.3, 3.1 Hz, 1H), 2.30 – 2.02 (m, 2H), 1.90 – 1.60 (m, 3H).

Hydrogen chloride solution (4.0 M in dioxane, 10 mL) was added to a stirred solution of compound **37** (4.7 g, 14 mmol, 1.0 equiv.) in MeOH (50 mL) at room temperature (rt). The resulting mixture was stirred for 8 h, then the solvent was evaporated under reduced pressure and the residue was purified by reverse phase flash chromatography (10-100% MeCN in H_2O, 0.1% TFA) to give compound **38** (3.19 g, 90 %). ^{1}H NMR (400 MHz, MeOD) δ 8.52 (s, 1H), 8.40 (s, 2H), 7.92 – 7.86 (m, 1H), 7.61 – 7.53 (m, 1H), 7.20 (M, 2H). ^{13}C NMR (101 MHz, MeOD) δ 157.48, 156.25, 151.56, 135.28, 133.64, 131.72, 130.33, 129.56, 121.24, 119.51, 117.85, 113.84. UPLC−MS calculated for $C_{13}H_{11}N_5O$ $[M + H]^+$: 254.10, found 254.36.

(2S,4R)-1-((S)-2-(3-(4-(3-Amino-6-(2-hydroxyphenyl)pyridazin-4-yl)-1*H*-pyrazol-1-yl)propanamido)-3,3-dimethylbutanoyl)-4-hydroxy-*N*-((S)-1-(4-(4-methylthiazol-5-yl)phenyl)ethyl)pyrrolidine-2-carboxamide (**8**)

Methyl 3-bromopropanoate (**39a**) (100.2 mg, 0.60 mmol, 2.0 equiv.) and K_2CO_3 (145.1 mg, 1.05 mmol, 3.5 equiv.) were added to a solution of compound **38** (76.0 mg, 0.30 mmol, 1.0 equiv.) in DMF (3.5 mL). The reaction mixture was stirred at 60 °C overnight and then diluted with water. The mixture was extracted with EtOAc and the organic layer was separated, washed with brine, and dried and evaporated to afford crude compound **40a** (35.2 mg), which was used without further purification.

Lithium hydroxide monohydrate (16.0 mg, 0.38 mmol, 5.0 equiv.) was added to a solution of **40a** (35.2 mg, 0.076 mmol, 1.0 equiv.) in MeOH (1 mL) and water (0.3 mL). The reaction mixture was stirred at 40 °C for 2 h and cooled in ice bath. 1N HCl was added and the mixture was subjected to HPLC purification to afford compound **41a** (25.3 mg, 74%). ^{1}H NMR (400 MHz, MeOD) δ 8.34 (s, 1H), 8.31 (s, 1H), 8.06 (s, 1H), 7.73 (dd, *J* = 8.2, 1.7 Hz, 1H), 7.40 (td, *J* = 7.8, 1.7 Hz, 1H), 7.03 (t, *J* = 7.3 Hz, 2H), 4.54 (t, *J* = 6.6 Hz, 2H), 2.99 (t, *J* = 6.6 Hz, 2H).

DIPEA (14.1 mg, 0.11 mmol) and HATU (5.0 mg, 0.013 mg, 1.2 equiv.) were added to a solution of compound **41a** (6.7 mg, 0.011 mmol, 1.0 equiv.) and VHL ligand **42** (5.2 mg, 0.011 mmol, 1.0 equiv.) in DMF (1.5 mL). The reaction mixture was stirred at rt for 15 min and then subjected to HPLC purification to afford compound **8** (6.9 mg, 83%). ^{1}H NMR (400 MHz, MeOH-d_4) δ 9.06 – 8.97 (m, 1H), 8.41 – 8.23 (m, 2H), 8.10 – 8.01 (m, 1H), 7.71 (dd, *J* = 8.1, 1.6 Hz, 1H), 7.44 (q, *J* = 8.2 Hz, 4H), 7.36 – 7.23 (m, 1H), 7.08 – 6.95 (m, 2H), 4.71 – 4.46 (m, 4H), 4.43 (dd, *J* = 4.5, 2.4 Hz, 1H), 3.88 (d, *J* = 11.0 Hz, 1H), 3.74 (dd, *J* = 11.0, 3.9 Hz, 1H), 3.05 – 2.83 (m, 2H), 2.50 (s, 3H), 2.45 (s, 1H), 2.24 – 2.14 (m, 1H), 1.93 (dddd, *J* = 25.4, 12.9, 8.7, 4.6 Hz, 1H), 1.53 (dd, *J*

= 23.0, 7.0 Hz, 3H), 1.00 (s, 9H). ^{13}C NMR (101 MHz, MeOD) δ 171.81, 171.01, 170.70, 155.89, 151.96, 144.50, 138.82, 132.49, 131.19, 130.72, 129.26, 129.10, 128.89, 128.35, 126.29, 125.87, 119.97, 119.81, 116.38, 112.64, 69.57, 67.74, 59.34, 59.20, 57.91, 56.58, 48.86, 48.76, 37.40, 36.11, 35.17, 35.01, 25.58, 25.52, 21.22, 20.93, 14.01. UPLC−MS calculated for $C_{39}H_4N_9O_5S$ [M + H]$^+$: 752.33, found 752.41. UPLC-retention time: 4.861 min.

(2S,4R)-1-((S)-2-(4-(4-(3-Amino-6-(2-hydroxyphenyl)pyridazin-4-yl)-1*H*-pyrazol-1-yl)propanamido)-3,3-dimethylbutanoyl)-4-hydroxy-*N*-((S)-1-(4-(4-methylthiazol-5-yl)phenyl)ethyl)pyrrolidine-2-carboxamide (**9**)

Compound **9** was synthesized by a procedure identical to that used for compound **8**. ^{1}H NMR (400 MHz, MeOH-d_4) δ 8.98 (d, J = 5.4 Hz, 1H), 8.38 – 8.28 (m, 2H), 8.10 – 8.02 (m, 1H), 7.71 (dd, J = 8.1, 1.7 Hz, 1H), 7.50 – 7.36 (m, 4H), 7.37 – 7.19 (m, 1H), 7.09 – 6.96 (m, 2H), 5.01 (d, J = 7.0 Hz, 1H), 4.66 – 4.53 (m, 2H), 4.44 (qd, J = 4.1, 2.6, 1.9 Hz, 1H), 4.30 (t, J = 6.9 Hz, 2H), 3.90 (d, J = 11.1 Hz, 1H), 3.76 (dd, J = 11.0, 4.0 Hz, 1H), 2.50 (s, 3H), 2.46 – 2.27 (m, 2H), 2.20 (ddt, J = 11.8, 7.9, 1.9 Hz, 1H), 2.08 – 1.91 (m, 2H), 1.65 (m, 1H), 1.53 (dd, J = 14.2, 7.0 Hz, 3H), 1.04 (s, 9H). UPLC−MS calculated for $C_{40}H_{47}N_9O_5S$ [M + H]$^+$: 766.35, found 766.06. UPLC-retention time: 4.181 min.

(2S,4R)-1-((S)-2-(5-(4-(3-Amino-6-(2-hydroxyphenyl)pyridazin-4-yl)-1*H*-pyrazol-1-yl)propanamido)-3,3-dimethylbutanoyl)-4-hydroxy-*N*-((S)-1-(4-(4-methylthiazol-5-yl)phenyl)ethyl)pyrrolidine-2-carboxamide (**10**)

Compound **10** was synthesized by a procedure identical to that used for compound **8**. ^{1}H NMR (400 MHz, MeOH-d_4) δ 9.01 – 8.93 (m, 1H), 8.41 – 8.27 (m, 2H), 8.09 (d, J = 5.3 Hz, 1H), 7.73 (dd, J = 8.2, 1.7 Hz, 1H), 7.50 – 7.36 (m, 4H), 7.41 – 7.31 (m, 1H), 7.04 (q, J = 7.1 Hz, 2H), 5.00 (q, J = 7.0 Hz, 1H), 4.67 – 4.55 (m, 2H), 4.46 (dq, J = 4.0, 2.1 Hz, 1H), 4.32 (q, J = 6.3 Hz, 2H), 3.97 – 3.88 (m, 1H), 3.77 (dd, J = 11.0, 4.0 Hz, 1H), 3.60 – 3.44 (m, 1H), 2.50 (s, 3H), 2.43 (s, 1H), 2.44 – 2.16 (m, 5H), 2.06 – 1.92 (m, 1H), 1.61 (d, J = 7.0 Hz, 1H), 1.49 (d, J = 7.0 Hz, 2H), 1.07 (s, 9H). UPLC−MS calculated for $C_{41}H_{49}N_9O_5S$ $[M + H]^+$: 780.36, found 780.07 UPLC-retention time: 4.220 min.

(2S,4R)-1-((S)-2-(6-(4-(3-Amino-6-(2-hydroxyphenyl)pyridazin-4-yl)-1*H*-pyrazol-1-yl)propan-amido)-3,3-dimethylbutanoyl)-4-hydroxy-*N*-((S)-1-(4-(4-methylthiazol-5-yl)phenyl)ethyl)-pyrrolidine-2-carboxamide (**11**)

Compound **11** was synthesized by a procedure identical to that used for compound **8**. ^{1}H NMR (400 MHz, MeOH-d_4) δ 8.96 (s, 1H), 8.34 (dd, J = 19.6, 2.6 Hz, 2H), 8.06 (d, J = 8.7 Hz, 1H), 7.72 (dd, J = 8.2, 1.7 Hz, 1H), 7.43 (dd, J = 12.8, 4.2 Hz, 5H), 7.05 (t, J = 7.2 Hz, 2H), 5.01 (td, J = 7.3, 5.1 Hz, 1H), 4.66 – 4.53 (m, 2H), 4.47 – 4.35 (m, 1H), 4.29 (t, J = 6.9 Hz, 2H), 3.87 (d, J = 11.1 Hz, 1H), 3.74 (dd, J = 11.0, 4.0 Hz, 1H), 2.48 (d, J = 13.1 Hz, 3H), 2.39 – 2.24 (m, 2H), 2.21 (m, 1H), 1.97 (dq, J = 9.2, 7.2 Hz, 2H), 1.74 – 1.55 (m, 2H), 1.51 (d, J = 7.0 Hz, 3H), 1.45 – 1.30 (p, J = 7.7 Hz, 3H), 1.03 (s, 9H). UPLC−MS calculated for $C_{42}H_{51}N_9O_5S$ $[M + H]^+$: 794.38, found 794.42 UPLC-retention time: 3.93 min.

(2S,4R)-1-((S)-2-(7-(4-(3-Amino-6-(2-hydroxyphenyl)pyridazin-4-yl)-1*H*-pyrazol-1-yl)propan-amido)-3,3-dimethylbutanoyl)-4-hydroxy-*N*-((S)-1-(4-(4-methylthiazol-5-yl)phenyl)ethyl)-pyrrolidine-2-carboxamide (12)

Compound **12** was synthesized by a procedure identical to that used for compound **8**. ^{1}H NMR (400 MHz, MeOH-d_4) δ 8.95 (s, 1H), 8.36 (s, 2H), 8.07 (d, J = 2.8 Hz, 1H), 7.75 – 7.68 (m, 1H), 7.49 – 7.32 (m, 5H), 7.09 – 7.00 (m, 2H), 5.01 (d, J = 7.0 Hz, 1H), 4.66 – 4.54 (m, 2H), 4.45 (s, 1H), 4.28 (t, J = 7.1 Hz, 2H), 3.89 (d, J = 11.0 Hz, 1H), 3.76 –3.65 (m, 2H), 2.48 (d, J = 15.9 Hz, 3H), 2.38 – 2.23 (m, 2H), 1.97 (ddt, J = 13.9, 11.2, 6.9 Hz, 2H), 1.70 – 1.55 (m, 3H), 1.55 – 1.42 (m, 2H), 1.44 – 1.35 (m, 5H), 1.04 (d, J = 9.3 Hz, 9H). UPLC−MS calculated for $C_{43}H_{53}N_9O_5S$ $[M + H]^+$: 808.39, found 808.42 UPLC-retention time: 4.109 min.

(2S,4R)-1-((S)-2-(8-(4-(3-Amino-6-(2-hydroxyphenyl)pyridazin-4-yl)-1*H*-pyrazol-1-yl)propanamido)-3,3-dimethylbutanoyl)-4-hydroxy-*N*-((S)-1-(4-(4-methylthiazol-5-yl)phenyl)ethyl)pyrrolidine-2-carboxamide (13)

Compound **13** was synthesized by a procedure identical to that used for compound **8**. ^{1}H NMR (400 MHz, MeOH-d_4) δ 8.92 (d, J = 11.8 Hz, 1H), 8.35 (s, 2H), 8.05 (d, J = 8.9 Hz, 1H), 7.71 (td, J = 8.0, 1.7 Hz, 1H), 7.43 (dd, J = 9.5, 2.8 Hz, 5H), 7.11 – 6.99 (m, 2H), 5.07 – 4.96 (m, 1H), 4.67 – 4.54 (m, 2H), 4.44 (tt, J = 4.1, 1.9 Hz, 1H), 4.28 (t, J = 7.1 Hz, 2H), 3.89 (d, J = 11.1 Hz, 1H), 3.76 (dd, J = 11.0, 4.0 Hz, 1H), 2.51 – 2.47 (s, 3H), 2.38 – 2.15 (m, 2H), 1.97 (ddd, J = 15.0, 7.7, 3.2 Hz, 3H), 1.63 (q, J = 7.5, 6.9 Hz, 2H), 1.61 – 1.47 (m, 3H), 1.38 (m, 7H), 1.04 (s, 9H). UPLC−MS calculated for $C_{44}H_{55}N_9O_5S$ $[M + H]^+$: 822.40, found 822.45 UPLC-retention time: 4.353 min.

(2S,4R)-1-((S)-2-(9-(4-(3-Amino-6-(2-hydroxyphenyl)pyridazin-4-yl)-1*H*-pyrazol-1-yl)propan-amido)-3,3-dimethylbutanoyl)-4-hydroxy-*N*-((S)-1-(4-(4-methylthiazol-5-yl)phenyl)ethyl)-pyrrolidine-2-carboxamide (14)

Compound **14** was synthesized by a procedure identical to that used for compound **8**. ^{1}H NMR (400 MHz, MeOH-d_4) δ 8.91 (s, 1H), 8.38 – 8.29 (m, 2H), 8.06 (d, J = 8.3 Hz, 1H), 7.71 (ddd, J = 8.0, 4.4, 1.7 Hz, 1H), 7.44 (qd, J = 7.9, 7.2, 5.4 Hz, 5H), 7.05 (dd, J = 8.0, 6.7 Hz, 2H), 5.01 (q, J = 6.9 Hz, 1H), 4.66 – 4.54 (m, 2H), 4.48 – 4.42 (m, 1H), 4.27 (dt, J = 9.2, 6.7 Hz, 2H), 3.92 – 3.85 (m, 1H), 3.76 (dd, J = 11.0, 4.1 Hz, 1H), 2.50 (s, 3H), 2.37 – 2.15 (m, 2H), 2.03 – 1.91 (m, 3H), 1.68 – 1.56 (m, 2H), 1.55 – 1.47 (m, 3H), 1.43 – 1.28 (m, 9H), 1.04 (d, J = 8.2 Hz, 9H). UPLC−MS calculated for $C_{45}H_{57}N_9O_5S$ $[M + H]^+$: 836.42, found 836.52 UPLC-retention time: 4.610 min.

(2S,4R)-1-((S)-2-(10-(4-(3-Amino-6-(2-hydroxyphenyl)pyridazin-4-yl)-1*H*-pyrazol-1-yl)dec-anamido)-3,3-dimethylbutanoyl)-4-hydroxy-*N*-((S)-1-(4-(4-methylthiazol-5-yl)phenyl)ethyl)-pyrrolidine-2-carboxamide (15)

Compound **15** was synthesized by a procedure identical to that used for compound **8**. ^{1}H NMR (400 MHz, MeOH-d4) δ 8.92 (d, 10.1 Hz, 1H), 8.38 – 8.30 (m, 2H), 8.06 (d, 8.1 Hz, 1H), 7.74 – 7.67 (m, 1H), 7.50 – 7.36 (m, 5H), 7.10 – 7.00 (m, 2H), 5.02 (q, J = 6.9 Hz, 1H), 4.64 (s, 1H), 4.58 (t, J = 8.3 Hz, 1H), 4.50 – 4.40 (m, 1H), 4.28 (t, J = 7.2 Hz, 2H), 3.89 (d, J = 11.1 Hz, 1H), 3.76 (dd, J = 11.0, 3.9 Hz, 1H), 2.49 (d, J = 6.2 Hz, 3H), 2.40 – 2.14 (m, 3H), 1.97 (ddd, J = 13.2, 9.0, 4.6 Hz, 3H), 1.70 – 1.54 (m, 2H), 1.52 (d, J = 7.1 Hz, 3H), 1.42 – 1.29 (m, 10H), 1.04 (d, J =

9.4 Hz, 9H). ^{13}C NMR (101 MHz, MeOD) δ 176.04, 173.25, 172.32, 157.23, 150.99, 139.80, 133.94, 132.15, 131.86, 130.68, 130.52, 129.95, 127.80, 127.62, 121.38, 119.28, 118.23, 117.74, 115.39, 113.99, 70.95, 69.04, 60.78, 60.57, 59.01, 58.34, 57.97, 53.66, 50.17, 49.64, 49.43, 49.21, 49.00, 48.79, 48.57, 48.36, 38.77, 37.57, 36.62, 36.47, 31.16, 30.37, 30.34, 30.26, 30.21, 30.08, 27.51, 27.04, 26.95, 22.36, 14.83. UPLC−MS calculated for $C_{46}H_{59}N_9O_5S$ $[M + H]^+$: 850.44, found 850.56. UPLC-retention time: 4.861 min.

(2S,4R)-1-((S)-2-(11-(4-(3-Amino-6-(2-hydroxyphenyl)pyridazin-4-yl)-1*H*-pyrazol-1-yl)propanamido)-3,3-dimethylbutanoyl)-4-hydroxy-*N*-((S)-1-(4-(4-methylthiazol-5-yl)phenyl)ethyl)pyrrolidine-2-carboxamide (16)

Compound **16** was synthesized by a procedure identicalto that used for compound **8**. ^{1}H NMR (400 MHz, MeOH-d_4) δ 8.96 (d, J = 5.1 Hz, 1H), 8.35 (d, J = 1.4 Hz, 2H), 8.07 (d, J = 5.5 Hz, 1H), 7.71 (dd, J = 8.2, 1.7 Hz, 1H), 7.51 – 7.35 (m, 5H), 7.09 – 7.00 (m, 2H), 5.07 – 4.97 (m, 1H), 4.67 – 4.54 (m, 2H), 4.45 (dt, J = 4.9, 2.5 Hz, 1H), 4.28 (t, J = 7.2 Hz, 1H), 3.94 – 3.85 (m, 1H), 3.76 (dt, J = 11.0, 3.8 Hz, 1H), 3.56 (t, J = 6.6 Hz, 1H), 2.50 (d, J = 2.0 Hz, 3H), 2.39 – 2.15 (m, 4H), 1.97 (ddd, J = 13.3, 9.0, 4.5 Hz, 2H), 1.70 – 1.48 (m, 7H), 1.43 – 1.27 (m, 10H), 1.09 – 1.00 (m, 9H). UPLC−MS calculated for $C_{47}H_{61}N_9O_5S$ $[M + H]^+$: 864.45, found 864.62 UPLC-retention time: 5.150 min.

(2S,4R)-1-((S)-2-(12-(4-(3-Amino-6-(2-hydroxyphenyl)pyridazin-4-yl)-1*H*-pyrazol-1-yl)propanamido)-3,3-dimethylbutanoyl)-4-hydroxy-*N*-((S)-1-(4-(4-methylthiazol-5-yl)phenyl)ethyl)pyrrolidine-2-carboxamide (17)

Compound **17** was synthesized by a procedure identical to that used for compound **8**. ^{1}H NMR (400 MHz, MeOH-d_4) δ 8.95 (q, J = 3.1 Hz, 1H), 8.35 (d, J = 1.3 Hz, 2H), 8.08 (s, 1H), 7.75 – 7.67 (m, 1H), 7.50 – 7.35 (m, 5H), 7.05 (t, J = 7.4 Hz, 2H), 5.06 – 4.97 (m, 1H), 4.68 – 4.54 (m, 2H), 4.45 (dd, J = 4.6, 2.4 Hz, 1H), 4.28 (t, J = 7.2 Hz, 2H), 3.89 (d, J = 11.1 Hz, 1H), 3.76 (dd, J = 11.0, 4.0 Hz, 1H), 2.49 (d, J = 5.4 Hz, 3H), 2.37 – 2.15 (m, 4H), 2.03 – 1.92 (m, 3H), 1.70 – 1.55 (m, 3H), 1.52 (d, J = 7.0 Hz, 3H), 1.43 – 1.23 (m, 12H), 1.04 (d, J = 9.5 Hz, 9H). UPLC−MS calculated for $C_{48}H_{63}N_9O_5S$ $[M + H]^+$: 878.47, found 878.6 UPLC-retention time: 5.435 min.

(2S,4R)-*N*-((S)-3-((6-(4-(3-amino-6-(2-hydroxyphenyl)pyridazin-4-yl)-1*H*-pyrazol-1-yl)hexyl)amino)-1-(4-(4-methylthiazol-5-yl)phenyl)-3-oxopropyl)-4-hydroxy-1-((R)-3-methyl-2-(3-methylisoxazol-5-yl)butanoyl)pyrrolidine-2-carboxamide (18)

Compound **18** was synthesized by a procedure reported previously.[40] ^{1}H NMR (400 MHz, MeOH-d_4) δ 8.88 (d, J = 3.4 Hz, 1H), 8.32 (d, J = 20.9 Hz, 2H), 8.06 (s, 1H), 7.72 (dd, J = 8.0, 1.7 Hz, 1H), 7.51 – 7.35 (m, 5H), 7.04 (dd, J = 8.1, 5.1 Hz, 2H), 6.28 – 6.16 (m, 1H), 5.39 – 5.26 (m, 1H), 4.54 – 4.42 (m, 2H), 4.20 (t, J = 7.0 Hz, 2H), 3.88 (dd, J = 10.8, 4.3 Hz, 1H), 3.83 – 3.70 (m, 1H), 3.60 (dd, J = 10.0, 7.6 Hz, 1H), 3.07 (ddt, J = 19.9, 13.2, 6.7 Hz, 2H), 2.91 – 2.70 (m, 2H), 2.47 (s, 3H), 2.47 – 2.35 (m, 0H), 2.26 (d, J = 8.4 Hz, 3H), 2.22 – 2.11 (m, 1H), 1.97 (ddd, J = 13.2, 7.8, 4.6 Hz, 1H), 1.85 (q, J = 7.2 Hz, 2H), 1.38 (p, J = 6.8 Hz, 2H), 1.26 (td, J = 15.2, 13.8, 7.7 Hz, 6H), 1.06 (d, J = 6.6 Hz, 3H), 0.88 (dd, J = 11.3, 6.0 Hz, 3H). UPLC−MS calculated for $C_{46}H_{54}N_{10}O_6S$ $[M + H]^+$: 875.40, found 875.17 UPLC-retention time: 4.113 min.

(2S,4R)-*N*-((S)-3-((7-(4-(3-Amino-6-(2-hydroxyphenyl)pyridazin-4-yl)-1*H*-pyrazol-1-yl)heptyl)amino)-1-(4-(4-methylthiazol-5-yl)phenyl)-3-oxopropyl)-4-hydroxy-1-((R)-3-methyl-2-(3-methylisoxazol-5-yl)butanoyl)pyrrolidine-2-carboxamide (19)

Compound **19** was synthesized by a procedure identical to that used for compound **18**. ^{1}H NMR (400 MHz, MeOH-d_4) δ 8.91 (s, 1H), 8.34 (d, J = 8.8 Hz, 2H), 8.06 (s, 1H), 7.71 (dd, J = 8.0, 1.7 Hz, 1H), 7.51 – 7.34 (m, 5H), 7.12 – 6.99 (m, 2H), 6.23 (s, 1H), 5.38 – 5.25 (m, 1H), 4.54 – 4.41 (m, 2H), 4.21 (t, J = 7.0 Hz, 2H), 3.88 (dd, J = 10.8, 4.2 Hz, 1H), 3.83 – 3.70 (m, 1H), 3.60 (ddd, J = 9.8, 3.9, 2.1 Hz, 1H), 3.19 – 2.99 (m, 2H), 2.85 (dd, J = 14.2, 6.1 Hz, 1H), 2.75 (dd, J = 14.0, 8.5 Hz, 1H), 2.49 (s, 3H), 2.51 – 2.33 (m, 1H), 2.27 (s, 3H), 2.22 – 2.11 (m, 1H), 1.98 (ddd, J = 13.2, 8.6, 4.9 Hz, 1H), 1.91 – 1.81 (m, 2H), 1.43 – 1.25 (m, 6H), 1.18 (q, J = 6.9 Hz, 2H), 1.07 (dd, J = 6.5, 3.3 Hz, 3H), 0.88 (dd, J = 12.4, 6.7 Hz, 3H). UPLC−MS calculated for $C_{47}H_{56}N_{10}O_6S$ $[M + H]^+$: 889.41, found 889.25 UPLC-retention time: 4.317 min.

(2S,4R)-*N*-((S)-3-((8-(4-(3-Amino-6-(2-hydroxyphenyl)pyridazin-4-yl)-1*H*-pyrazol-1-yl)-heptyl)amino)-1-(4-(4-methylthiazol-5-yl)phenyl)-3-oxopropyl)-4-hydroxy-1-((R)-3-methyl-2-(3-methylisoxazol-5-yl)butanoyl)pyrrolidine-2-carboxamide (20)

Compound **20** was synthesized by a procedure identical to that used for compound **18**. ^{1}H NMR (400 MHz, MeOH-d_4) δ 8.91 (s, 1H), 8.34 (d, J = 8.8 Hz, 2H), 8.06 (s, 1H), 7.71 (dd, J = 8.0, 1.7 Hz, 1H), 7.51 – 7.34 (m, 5H), 7.12 – 6.99 (m, 2H), 6.23 (s, 1H), 5.38 – 5.25 (m, 1H), 4.54 – 4.41 (m, 2H), 4.21 (t, J = 7.0 Hz, 2H), 3.88 (dd, J = 10.8, 4.2 Hz, 1H), 3.83 – 3.70 (m, 1H), 3.60 (ddd, J = 9.8, 3.9, 2.1 Hz, 1H), 3.19 – 2.99 (m, 2H), 2.85 (dd, J = 14.2, 6.1 Hz, 1H), 2.75 (dd, J = 14.0, 8.5 Hz, 1H), 2.49 (s, 3H), 2.51 – 2.33 (m, 1H), 2.27 (s, 3H), 2.22 – 2.11 (m, 1H), 1.98 (ddd, J =

13.2, 8.6, 4.9 Hz, 1H), 1.91 – 1.81 (m, 2H), 1.43 – 1.10 (m, 10H), 1.07 (dd, *J* = 6.5, 3.3 Hz, 3H), 0.88 (dd, *J* = 12.4, 6.7 Hz, 3H). UPLC−MS calculated for $C_{48}H_{58}N_{10}O_6S$ $[M + H]^+$: 903.43, found 903.62 UPLC-retention time: 4.151 min.

(2S,4R)-*N*-((S)-3-((9-(4-(3-Amino-6-(2-hydroxyphenyl)pyridazin-4-yl)-1*H*-pyrazol-1-yl)heptyl)amino)-1-(4-(4-methylthiazol-5-yl)phenyl)-3-oxopropyl)-4-hydroxy-1-((R)-3-methyl-2-(3-methylisoxazol-5-yl)butanoyl)pyrrolidine-2-carboxamide (**21**)

Compound **21** was synthesized by a procedure identical to that used for compound **18**. ^{1}H NMR (400 MHz, MeOH-d_4) δ 8.91 (d, *J* = 1.8 Hz, 1H), 8.35 (s, 2H), 8.08 (s, 1H), 7.71 (dd, *J* = 8.0, 1.7 Hz, 1H), 7.51 – 7.35 (m, 5H), 7.08 – 6.99 (m, 2H), 6.29 – 6.18 (m, 1H), 5.39 – 5.25 (m, 1H), 4.55 – 4.44 (m, 1H), 4.49 – 4.37 (m, 1H), 4.25 (t, *J* = 7.1 Hz, 2H), 3.94 – 3.84 (m, 1H), 3.84 – 3.66 (m, 1H), 3.66 – 3.56 (m, 1H), 3.16 – 2.98 (m, 2H), 2.91 – 2.78 (m, 1H), 2.82 – 2.69 (m, 1H), 2.49 (s, 3H), 2.42 (dq, *J* = 9.7, 6.7 Hz, 1H), 2.26 (d, *J* = 6.0 Hz, 3H), 2.22 – 2.12 (m, 1H), 1.98 (ddd, *J* = 13.2, 8.6, 4.7 Hz, 1H), 1.90 (t, *J* = 7.1 Hz, 2H), 1.39 – 1.17 (m, 10H), 1.14 (d, *J* = 8.3 Hz, 2H), 1.07 (d, *J* = 6.6 Hz, 3H), 0.89 (dd, *J* = 12.2, 6.7 Hz, 3H). UPLC−MS calculated for $C_{49}H_{60}N_{10}O_6S$ $[M + H]^+$: 917.45, found 917.34 UPLC-retention time: 4.874 min.

(2S,4R)-*N*-((S)-3-((10-(4-(3-Amino-6-(2-hydroxyphenyl)pyridazin-4-yl)-1*H*-pyrazol-1-yl)heptyl)amino)-1-(4-(4-methylthiazol-5-yl)phenyl)-3-oxopropyl)-4-hydroxy-1-((R)-3-methyl-2-(3-methylisoxazol-5-yl)butanoyl)pyrrolidine-2-carboxamide (**22**)

Compound **22** was synthesized by a procedure identical to that used for compound **18**. ^{1}H NMR (400 MHz, MeOH-d_4) δ 8.91 (d, *J* = 3.4 Hz, 1H), 8.36 (d, *J* = 1.6 Hz, 2H), 8.08 (s, 1H), 7.71 (dd,

J = 8.1, 1.7 Hz, 1H), 7.51 – 7.35 (m, 5H), 7.05 (t, *J* = 7.2 Hz, 2H), 6.29 – 6.17 (m, 1H), 5.39 – 5.25 (m, 1H), 4.49 (dd, *J* = 17.0, 8.8 Hz, 2H), 4.26 (t, *J* = 7.1 Hz, 2H), 3.94 – 3.85 (m, 1H), 3.84 – 3.70 (m, 1H), 3.59 (dd, *J* = 12.4, 10.2 Hz, 1H), 3.07 (dp, *J* = 20.0, 6.7 Hz, 2H), 2.86 (dd, *J* = 14.0, 5.8 Hz, 1H), 2.75 (dd, *J* = 14.1, 8.5 Hz, 1H), 2.49 (s, 3H), 2.51 – 2.36 (m, 1H), 2.26 (d, *J* = 5.0 Hz, 3H), 2.22 – 2.11 (m, 1H), 2.06 – 1.88 (m, 1H), 1.93 (q, *J* = 7.3, 6.0 Hz, 2H), 1.39 – 1.17 (m, 12H), 1.14 (s, 2H), 1.07 (d, *J* = 6.6 Hz, 3H), 0.89 (dd, *J* = 12.1, 6.7 Hz, 3H). UPLC−MS calculated for $C_{50}H_{62}N_{10}O_6S$ $[M + H]^+$: 931.46, found 931.54 UPLC-retention time: 4.656 min.

(2S,4R)-*N*-((S)-3-((12-(4-(3-Amino-6-(2-hydroxyphenyl)pyridazin-4-yl)-1*H*-pyrazol-1-yl)heptyl)amino)-1-(4-(4-methylthiazol-5-yl)phenyl)-3-oxopropyl)-4-hydroxy-1-((R)-3-methyl-2-(3-methylisoxazol-5-yl)butanoyl)pyrrolidine-2-carboxamide (**23**)

Compound **23** was synthesized by a procedure idnetical to that used for compound **18**. ^{1}H NMR (400 MHz, MeOH-d_4) δ 8.93 (s, 1H), 8.36 (d, *J* = 4.5 Hz, 2H), 8.08 (s, 1H), 7.71 (dd, *J* = 8.0, 1.7 Hz, 1H), 7.51 – 7.35 (m, 5H), 7.11 – 7.00 (m, 2H), 6.23 (s, 1H), 5.32 (ddd, *J* = 21.2, 7.7, 5.4 Hz, 1H), 4.55 – 4.42 (m, 2H), 4.28 (t, *J* = 7.1 Hz, 2H), 3.94 – 3.85 (m, 1H), 3.84 – 3.68 (m, 1H), 3.65 – 3.57 (m, 1H), 3.08 (ddq, *J* = 19.6, 12.9, 6.7 Hz, 2H), 2.93 – 2.79 (m, 1H), 2.83 – 2.68 (m, 1H), 2.49 (s, 3H), 2.51 – 2.34 (m, 1H), 2.27 (s, 3H), 2.24 – 2.10 (m, 1H), 2.06 – 1.88 (m, 3H), 1.41 – 1.15 (m, 18H), 1.07 (dd, *J* = 6.6, 2.6 Hz, 3H), 0.89 (dd, *J* = 12.7, 6.7 Hz, 3H). UPLC−MS calculated for $C_{52}H_{66}N_{10}O_6S$ $[M + H]^+$: 959.49, found 959.38 UPLC-retention time: 5.766 min.

(2S,4R)-1-((S)-14-(4-(3-Amino-6-(2-hydroxyphenyl)pyridazin-4-yl)-1*H*-pyrazol-1-yl)-2-(tert-butyl)-4-oxo-6,9,12-trioxa-3-azatetradecanoyl)-4-hydroxy-*N*-((S)-1-(4-(4-methylthiazol-5-yl)phenyl)ethyl)pyrrolidine-2-carboxamide (**24**)

Compound **24** was synthesized by a procedure identical to that used for compound **8**. ^{1}H NMR (400 MHz, MeOH-d_4) δ 9.36 – 9.27 (m, 1H), 8.45 – 8.32 (m, 2H), 8.07 (d, J = 2.7 Hz, 1H), 7.71 (dt, J = 7.9, 1.9 Hz, 1H), 7.56 – 7.37 (m, 5H), 7.08 – 6.97 (m, 2H), 5.20 – 5.08 (m, 1H), 4.67 – 4.40 (m, 5H), 4.40 – 4.26 (m, 1H), 4.00 – 3.83 (m, 3H), 3.80 – 3.56 (m, 7H), 2.59 – 2.40 (m, 5H), 2.28 – 2.17 (m, 1H), 2.05 – 1.89 (m, 1H), 1.60 – 1.46 (m, 3H), 1.07 – 0.98 (m, 9H). UPLC−MS calculated for $C_{44}H_{55}N_9O_8S$ $[M + H]^+$: 870.39, found 870.59 UPLC-retention time: 3.831 min.

(2S,4R)-1-((S)-2-(3-(2-(2-(4-(3-Amino-6-(2-hydroxyphenyl)pyridazin-4-yl)-1*H*-pyrazol-1-yl)ethoxy)ethoxy)propanamido)-3,3-dimethylbutanoyl)-4-hydroxy-*N*-((S)-1-(4-(4-methylthiazol-5-yl)phenyl)ethyl)pyrrolidine-2-carboxamide (**25**)

Compound **25** was synthesized by a procedure identical to that used for compound **8**. ^{1}H NMR (400 MHz, MeOH-d_4) δ 9.51 – 9.42 (m, 1H), 8.46 – 8.33 (m, 2H), 8.07 (dd, J = 4.3, 0.9 Hz, 1H), 7.69 (td, J = 8.2, 1.6 Hz, 1H), 7.54 – 7.40 (m, 5H), 7.09 – 6.99 (m, 2H), 4.72 – 4.64 (m, 1H), 4.63 – 4.55 (m, 1H), 4.48 (q, J = 4.8 Hz, 2H), 4.01 – 3.91 (m, 4H), 3.71 – 3.60 (m, 8H), 2.55 (d, J = 4.1 Hz, 4H), 2.30 – 2.17 (m, 1H), 2.02 – 1.90 (m, 1H), 1.58 (dd, J = 7.1, 1.9 Hz, 1H), 1.50 (dd, J = 7.0, 1.6 Hz, 3H), 1.09 – 0.97 (m, 9H). UPLC−MS calculated for $C_{43}H_{53}N_9O_7S$ $[M + H]^+$: 840.38, found 840.46 UPLC-retention time: 3.733 min.

(2S,4R)-1-((S)-2-(3-(4-(3-(4-(3-Amino-6-(2-hydroxyphenyl)pyridazin-4-yl)-1*H*-pyrazol-1-yl)propyl)piperazin-1-yl)propanamido)-3,3-dimethylbutanoyl)-4-hydroxy-*N*-((S)-1-(4-(4-methylthiazol-5-yl)phenyl)ethyl)pyrrolidine-2-carboxamide (**26**)

Compound **26** was synthesized by a procedure identical to that used for compound **8**. ^{1}H NMR (400 MHz, MeOH-d_4) δ 8.90 (d, J = 4.5 Hz, 2H), 8.29 (s, 1H), 8.11 (s, 1H), 8.02 – 7.98 (m, 1H), 7.44 (dd, J = 8.9, 4.8 Hz, 5H), 7.02 (d, J = 7.7 Hz, 2H), 5.00 – 4.95 (m, 2H), 4.67 – 4.56 (m, 2H), 3.39 – 3.34 (m, 3H), 3.02 (d, J = 0.5 Hz, 4H), 2.88 (d, J = 0.7 Hz, 4H), 2.53 – 2.45 (m, 6H), 2.02 (s, 3H), 1.52 (t, J = 7.3 Hz, 5H), 1.40 (d, J = 6.8 Hz, 1H), 1.36 – 1.27 (m, 3H), 1.16 (s, 1H), 1.07 (s, 9H), 1.04 (d, J = 3.1 Hz, 2H). UPLC−MS calculated for $C_{46}H_{59}N_{11}O_5S$ $[M + H]^+$: 878.45, found 878.49 UPLC-retention time: 3.177 min.

(2S,4R)-1-((S)-2-(3-(4-(3-(4-(3-Amino-6-(2-hydroxyphenyl)pyridazin-4-yl)-1*H*-pyrazol-1-yl)propyl)piperidin-1-yl)propanamido)-3,3-dimethylbutanoyl)-4-hydroxy-*N*-((S)-1-(4-(4-methylthiazol-5-yl)phenyl)ethyl)pyrrolidine-2-carboxamide (**27**)

Compound **27** was synthesized by a procedure identical to that used for compound **8**. ^{1}H NMR (400 MHz, MeOH-d_4) δ 8.93 (d, J = 7.0 Hz, 1H), 8.39 – 8.25 (m, 2H), 8.10 (s, 1H), 7.71 (dt, J = 8.2, 1.5 Hz, 1H), , 7.47 – 7.34 (m, 5H), 7.10 – 7.00 (m, 2H), 4.65 – 4.44 (m, 3H), 4.38 (s, 1H), 4.30 (t, J = 7.0 Hz, 2H), 4.20 (t, J = 7.1 Hz, 1H), 3.93 (d, J = 11.1 Hz, 1H), 3.75 (dd, J = 10.8, 3.9 Hz, 1H), 3.08 – 2.92 (m, 3H), 2.91 – 2.79 (m, 2H), 2.53 – 2.44 (m, 3H), 2.23 (dd, J = 13.2, 7.7 Hz, 1H), 2.08 – 1.83 (m, 6H), 1.61 (d, J = 7.1 Hz, 2H), 1.52 (dd, J = 7.0, 4.3 Hz, 3H), 1.45 (d, J = 12.4 Hz, 1H), 1.44 – 1.29 (m, 3H), 1.07 (d, J = 12.2 Hz, 9H). UPLC−MS calculated for $C_{47}H_{60}N_{10}O_5S$ $[M + H]^+$: 877.45, found 877.44 UPLC-retention time: 2.957 min.

(2S,4R)-1-((S)-2-(6-(4-(4-(3-Amino-6-(2-hydroxyphenyl)pyridazin-4-yl)-1*H*-pyrazol-1-yl)piperidin-1-yl)hexanamido)-3,3-dimethylbutanoyl)-4-hydroxy-*N*-((S)-1-(4-(4-methylthiazol-5-yl)phenyl)ethyl)pyrrolidine-2-carboxamide (**28**)

DMAP (0.22 g, 1.8 mmol, 0.20 equiv.) and TEA (1.6 mL, 11 mmol, 1.3 equiv.) were added to a stirred solution of *tert*-butyl 4-hydroxypiperidine-1-carboxylate (1.7 g, 8.7 mmol, 1.0 equiv.) and p-toluenesulfonyl chloride (2.1 g, 11 mmol, 1.3 equiv.) in DCM (40 mL) at 0 °C. The resulting mixture was allowed to warm to rt then stirred for 12 h. The reaction was then quenched with water, and the aqueous layer was extracted with DCM. The combined organic extracts were washed with 1 N HCl and dried over anhydrous Na_2SO_4. Concentration *in vacuo* followed by column chromatography (EtOAc/hexane) gave pure compound **48a** (2.8 g, 90%). ^{1}H NMR (400 MHz, MeOD) δ 7.87 – 7.79 (m, 2H), 7.50 – 7.43 (m, 2H), 4.72 (tt, *J* = 7.4, 3.7 Hz, 1H), 3.57 (ddd, *J* = 12.0, 7.4, 4.0 Hz, 2H), 3.33 – 3.25 (m, 2H), 2.48 (s, 3H), 1.78 (m, 2H), 1.70 – 1.56 (m, 2H), 1.45 (s, 9H).

Cs_2CO_3 (631 mg, 1.94 mmol, 3.2 equiv.) was added to a solution of compound **38** (224 mg, 0.6 mmol, 1.0 equiv.) and compound **48a** (412 mg, 1.16 mmol, 1.9 equiv.) in DMF (8 mL) at rt. The resulting mixture was stirred for 12 h at 60 °C. The residue was applied onto a silica gel column with dichloromethane/methanol (0-10:1). The corresponding product was redissolved in DCM (4 mL). Hydrogen chloride solution (4.0 M in dioxane, 2 mL) was added to the resulting mixture which was then stirred for 5 h. The solvent was evaporated under reduced pressure to yield the corresponding crude product **49a** (151 mg, 67% over 2 steps). ^{1}H NMR (400 MHz, MeOD) δ 8.46 (s, 1H), 8.37 (s, 1H), 8.11 (s, 1H), 7.72 (dd, *J* = 8.3, 1.7 Hz, 1H), 7.43 (ddd, *J* = 8.2, 7.4, 1.7 Hz,

1H), 7.05 (dd, *J* = 7.6, 6.9 Hz, 2H), 4.80 – 4.68 (m, 1H), 3.69 – 3.57 (m, 2H), 3.32 – 3.24 (m, 2H), 2.55 – 2.34 (m, 4H).

HOAc (35 µL, 0.61 mmol, 1.5 equiv.) was added at rt to a stirred solution of compound **49a** (151 mg, 0.4 mmol, 1.0 equiv.) and methyl 6-oxohexanoate (**50a**) (117 mg, 0.81 mmol, 2.0 equiv.) in DMF/DCE (1:1, 4 mL). The resulting mixture was stirred for 4 h and $NaBH(OAc)_3$ (341 mg, 1.6 mmol, 4.0 equiv.) was added, and the mixture was stirred overnight. The residue was applied to a silica gel column with dichloromethane/methanol (0-10:1). The corresponding product was redissolved into THF/MeOH/H_2O (4 mL). Lithium hydroxide monohydrate (170 mg, 4.0 mmol, 10 equiv.) was added to the resulting mixture, which was then stirred for 10 h at rt. The residue was subject to HPLC purification to afford compound **52a** (150 mg, 82% over 2 steps). ^{1}H NMR (400 MHz, MeOD) δ 8.40 (s, 1H), 8.33 (s, 1H), 8.10 (d, *J* = 0.7 Hz, 1H), 7.72 (dd, *J* = 8.0, 1.7 Hz, 1H), 7.41 (ddd, *J* = 8.3, 7.3, 1.7 Hz, 1H), 7.09 – 6.94 (m, 2H), 4.70 (m, 1H), 3.80 (d, *J* = 12.5 Hz, 2H), 3.21 (t, *J* = 8.4 Hz, 4H), 2.47 (t, *J* = 6.2 Hz, 4H), 2.37 (t, *J* = 7.2 Hz, 2H), 1.97 – 1.76 (m, 2H), 1.71 (p, *J* = 7.3 Hz, 2H), 1.58 – 1.40 (m, 2H).

HATU (57 mg, 0.15 mmol, 1.1 equiv.) and DIPEA (188 µL, 1.1 mmol, 8.0 equiv.) were added at rt to a stirred solution of compound **52a** (75 mg, 0.14 mmol, 1.0 equiv.) in DMF (4 mL). The resulting mixture was stirred for 5 min then VHL-1 (74 mg, 0.154 mmol, 1.1 equiv.) was added, and stirred for 15 min. The residue was subject to HPLC purification to afford compound **28** (85 mg, 57%). ^{1}H NMR (400 MHz, MeOD) δ 8.96 (s, 1H), 8.44 – 8.27 (m, 2H), 8.10 (d, J = 0.7 Hz, 1H), 7.75 – 7.66 (m, 1H), 7.49 – 7.37 (m, 5H), 7.09 – 6.98 (m, 2H), 5.02 (q, J = 7.0 Hz, 1H), 4.66 (d, J = 9.9 Hz, 1H), 4.59 (dd, J = 9.0, 7.7 Hz, 1H), 4.46 (dp, J = 4.4, 2.0 Hz, 1H), 3.89 (s, 1H), 3.86 – 3.46 (m, 4H), 3.23 (m, 4H), 2.50 (s, 3H), 2.46 (d, J = 8.8 Hz, 3H), 2.36 (qd, J = 7.1, 3.4 Hz, 2H), 2.27 – 2.11 (m, 1H), 1.99 (ddd, J = 13.1, 8.9, 4.4 Hz, 1H), 1.89 – 1.76 (m, 2H), 1.71 (p, J = 7.3 Hz,

2H), 1.53 (d, J = 7.0 Hz, 3H), 1.46 (dq, J = 15.2, 7.7 Hz, 2H), 1.06 (d, J = 6.4 Hz, 9H). ^{13}C NMR (100 MHz, MeOD) δ 174.18, 171.85, 170.95, 155.90, 154.61, 152.01, 149.94, 144.57, 138.91, 132.42, 130.97, 129.59, 129.21, 129.10, 128.18, 126.31, 119.93, 118.21, 116.39, 112.65, 69.58, 59.40, 59.22, 57.74, 57.02, 56.62, 56.50, 56.31, 51.26, 51.21, 48.77, 37.47, 35.07, 34.56, 29.32, 25.66, 25.61, 24.59, 23.44, 20.96, 14.00. UPLC−MS calculated for $C_{47}H_{60}N_{10}O_5S$ $[M + H]^+$: 877.45, found 877.74 UPLC-retention time: 3.129 min.

(2S,4R)-1-((S)-2-((1r,4S)-4-((7-(4-(3-Amino-6-(2-hydroxyphenyl)pyridazin-4-yl)-1*H*-pyrazol-1-yl)-2-azaspiro[3.5]nonan-2-yl)methyl)cyclohexane-1-carboxamido)-3,3-dimethylbutanoyl)-4-hydroxy-*N*-((S)-1-(4-(4-methylthiazol-5-yl)phenyl)ethyl)pyrrolidine-2-carboxamide (**29**)

Compound **29** was synthesized by a procedure identical to that used for compound **28**. ^{1}H NMR (400 MHz, MeOD) δ 8.89 (s, 1H), 8.29 (d, *J* = 0.6 Hz, 1H), 8.10 (s, 1H), 8.06 (d, *J* = 0.6 Hz, 1H), 7.87 (dd, *J* = 8.3, 1.5 Hz, 1H), 7.49 – 7.37 (m, 4H), 7.31 – 7.25 (m, 1H), 6.96 (ddd, *J* = 6.6, 3.6, 1.0 Hz, 2H), 5.02 (q, *J* = 7.0 Hz, 1H), 4.63 (s, 1H), 4.58 (dd, *J* = 15.1, 7.0 Hz, 1H), 4.48 – 4.43 (m, 1H), 4.30 – 4.20 (m, 1H), 3.88 (d, *J* = 11.2 Hz, 1H), 3.77 (dd, *J* = 11.0, 3.9 Hz, 1H), 3.27 (s, 2H), 3.15 (s, 2H), 2.51 – 2.46 (m, 4H), 2.34 (t, *J* = 12.0 Hz, 1H), 2.25 – 2.07 (m, 5H), 2.02 – 1.79 (m, 8H), 1.73 – 1.63 (m, 2H), 1.53 (d, *J* = 7.0 Hz, 3H), 1.51 – 1.39 (m, 3H), 1.33 – 1.29 (m, 2H), 1.05 (d, *J* = 10.3 Hz, 9H). ^{13}C NMR (100 MHz, MeOD) δ 178.57, 173.16, 172.29, 159.59, 158.09, 154.82, 152.79, 149.03, 145.58, 139.20, 133.30, 131.63, 131.47, 130.44, 129.25, 127.60, 127.18, 123.72, 123.70, 120.28, 119.08, 118.73, 116.05, 70.95, 67.89, 66.63, 65.30, 62.01, 60.58, 58.70, 57.98, 50.08, 45.68, 38.76, 37.34, 36.66, 36.04, 31.72, 31.51, 30.81, 30.71, 30.54, 29.79, 27.05, 22.38, 15.83. UPLC−MS calculated for $C_{51}H_{65}N_{10}O_5S$ $[M + H]^+$: 930.20, found 930.43. UPLC-

retention time: 3.641 min. UPLC−MS calculated for $C_{52}H_{66}N_{10}O_5S$ $[M + H]^+$: 943.49, found 943.37. UPLC-retention time: 3.509 min.

(2S,4R)-1-((S)-2-((1r,4S)-4-((9-(4-(3-Amino-6-(2-hydroxyphenyl)pyridazin-4-yl)-1*H*-pyrazol-1-yl)-3-azaspiro[5.5]undecan-3-yl)methyl)cyclohexane-1-carboxamido)-3,3-dimethylbutanoyl)-4-hydroxy-*N*-((S)-1-(4-(4-methylthiazol-5-yl)phenyl)ethyl)pyrrolidine-2-carboxamide (**30**)

Compound **30** was synthesized by a procedure identical to that used for compound **28**. ^{1}H NMR (400 MHz, MeOD) δ 9.02 (s, 1H), 8.38 (s, 1H), 8.33 (s, 1H), 8.07 (d, *J* = 0.5 Hz, 1H), 7.73 – 7.68 (m, 1H), 7.47 – 7.37 (m, 5H), 7.05 – 6.98 (m, 2H), 5.01 (q, *J* = 7.0 Hz, 1H), 4.65 – 4.53 (m, 2H), 4.44 (s, 1H), 4.32 (ddd, *J* = 15.7, 10.7, 4.9 Hz, 1H), 3.86 (d, *J* = 11.2 Hz, 1H), 3.75 (dd, *J* = 11.0, 3.9 Hz, 1H), 3.52 – 3.41 (m, 2H), 3.18 – 3.06 (m, 2H), 3.06 – 2.98 (m, 2H), 2.49 (s, 3H), 2.42 – 2.26 (m, 3H), 2.25 – 2.16 (m, 1H), 2.14 – 2.00 (m, 4H), 2.00 – 1.79 (m, 8H), 1.70 – 1.53 (m, 7H), 1.51 (d, *J* = 7.0 Hz, 3H), 1.36 (td, *J* = 13.5, 4.7 Hz, 1H), 1.21 – 1.10 (m, 2H), 1.04 (s, 9H). ^{13}C NMR (100 MHz, MeOD) δ 178.13, 173.21, 172.26, 157.28, 156.10, 153.31, 151.18, 145.93, 139.71, 133.85, 131.92, 131.08, 130.61, 130.50, 129.85, 127.68, 127.50, 121.33, 119.49, 117.77, 113.70, 70.97, 63.75, 62.97, 60.60, 58.83, 57.99, 50.14, 45.01, 39.18, 38.81, 37.31, 36.66, 33.53, 30.92, 30.71, 30.43, 30.22, 29.61, 29.21, 28.85, 27.02, 22.37, 15.43. UPLC−MS calculated for $C_{54}H_{71}N_{10}O_5S$ $[M + H]^+$: 972.28, found 972.37. UPLC-retention time: 4.472 min.

(2S,4R)-1-((S)-2-(4-(7-(4-(3-Amino-6-(2-hydroxyphenyl)pyridazin-4-yl)-1*H*-pyrazol-1-yl)-2-azaspiro[3.5]nonan-2-yl)cyclohexane-1-carboxamido)-3,3-dimethylbutanoyl)-4-hydroxy-*N*-((S)-1-(4-(4-methylthiazol-5-yl)phenyl)ethyl)pyrrolidine-2-carboxamide (31)

Compound **31** was synthesized by a procedure identical to that used for compound **28**. ^{1}H NMR (400 MHz, MeOD) δ 8.90 (s, 1H), 8.35 (s, 1H), 8.31 (s, 1H), 8.08 – 8.04 (m, 1H), 7.72 – 7.67 (m, 1H), 7.47 – 7.37 (m, 5H), 7.05 – 6.99 (m, 2H), 5.01 (q, *J* = 6.8 Hz, 1H), 4.66 – 4.53 (m, 2H), 4.44 (d, *J* = 1.7 Hz, 1H), 4.32 (t, *J* = 11.2 Hz, 1H), 4.20 – 4.12 (m, 1H), 4.01 (dd, *J* = 10.4, 5.4 Hz, 1H), 3.95 (d, *J* = 5.2 Hz, 2H), 3.85 (d, *J* = 11.1 Hz, 1H), 3.75 (dd, *J* = 11.1, 3.8 Hz, 1H), 2.48 (s, 3H), 2.44 – 2.35 (m, 1H), 2.31 (d, *J* = 11.2 Hz, 1H), 2.25 – 2.08 (m, 6H), 2.07 – 1.91 (m, 5H), 1.91 – 1.73 (m, 5H), 1.58 (dd, *J* = 14.3, 7.2 Hz, 2H), 1.51 (d, *J* = 7.0 Hz, 3H), 1.37 – 1.23 (m, 2H), 1.05 (s, 9H). UPLC−MS calculated for $C_{51}H_{65}N_{10}O_5S$ $[M + H]^+$: 930.20, found 930.18. UPLC-retention time: 3.551 min.

(2S,4R)-1-((S)-2-(4-(9-(4-(3-Amino-6-(2-hydroxyphenyl)pyridazin-4-yl)-1*H*-pyrazol-1-yl)-3-azaspiro[5.5]undecan-3-yl)cyclohexane-1-carboxamido)-3,3-dimethylbutanoyl)-4-hydroxy-*N*-((S)-1-(4-(4-methylthiazol-5-yl)phenyl)ethyl)pyrrolidine-2-carboxamide (32)

Compound **32** was synthesized by a procedure identical to that used for compound **28**. ^{1}H NMR (400 MHz, MeOD) δ 8.99 (d, *J* = 2.8 Hz, 1H), 8.40 (s, 1H), 8.34 (s, 1H), 8.09 (s, 1H), 7.75 – 7.67 (m, 1H), 7.54 – 7.37 (m, 5H), 7.05 (t, *J* = 7.3 Hz, 2H), 5.03 (dd, *J* = 13.2, 6.3 Hz, 1H), 4.70 – 4.54 (m, 2H), 4.44 (s, 1H), 4.39 – 4.26 (m, 1H), 3.96 – 3.83 (m, 1H), 3.78 (dt, *J* = 11.0, 3.8 Hz, 1H), 3.54 – 3.36 (m, 2H), 3.28 – 3.10 (m, 3H), 2.52 – 2.40 (m, 4H), 2.32 – 2.18 (m, 3H), 2.18 – 1.94 (m, 9H), 1.89 – 1.75 (m, 2H), 1.75 – 1.57 (m, 7H), 1.53 (d, *J* = 7.0 Hz, 3H), 1.43 – 1.28 (m, 2H),

1.06 (s, 9H). UPLC−MS calculated for $C_{53}H_{69}N_{10}O_5S$ $[M + H]^+$: 958.25, found 958.22. UPLC-retention time: 3.411 min.

HiBit degradation assay. Hela cells were genetically modified by CRISPR/Cas9 to fuse HiBit to the carboxy terminus of SMARCA2 (Promega CS302365) or SMARCA4 (Promega CS3023225). Cells were cultured in DMEM containing 10% FBS and 1% (Vol:Vol) penicillin-streptomycin. At the time of the experiment, cells were seeded at a density of 20,000 cells per well in a 96-well plate (Corning Cat. #3903) and treated with serial dilutions of testing compounds for 24 h. At the end of the experiment, levels of SMARCA2 or SMARCA4 expression were assessed with Nano-Glo® HiBiT Lytic Detection Assay (Promega N3050). IC_{50} values were obtained using the GraphPad Prism data analysis software.

Cell Lines and Cell Culture. All the cells used were purchased from American Type Culture Collection (ATCC) and grown in RPMI 1640 medium (Invitrogen) supplemented with 10% fetal bovine serum (Invitrogen). All the cells were cultured at 37 °C in a humidified 5% CO_2 incubator.

Western Blot Analysis. 1.5 - 2 × 10^6 cells/well were plated in 12-well plates and treated with compounds at the indicated concentrations and times. Cells were collected, washed with PBS, and lysed in Radioimmunoprecipitation Assay Protein Lysis and Extraction Buffer containing proteinase inhibitor cocktail (Roche Diagnostics, Mannheim, Germany). Twenty micrograms of lysate were electrophoresed through 4-12% Tris-glycine SDS-PAGE gels (Invitrogen) and blotted into PVDF (polyvinylidene difluoride) membranes (MilliporeSigma, IPFL00010). The

membranes were blocked with Intercept Blocking Buffer (LI-COR Biosciences, 927-70001) for 1 hour at room temperature and then washed with 1× Tris-buffered saline Tween 20 four times for 5 minutes each. The membranes were incubated overnight at 4 °C in Intercept Blocking Buffer supplemented with Tween 20 (dilution 1:500). Rabbit SMARCA2 antibody (CST, cat# 11966, 1:1000), rabbit SMARCA4 antibody (Bethyl, cat# A700-106, 1:2000) or mouse GAPDH antibody (Santa Cruz Biotechnology, sc-47724, 1:1,000) were used for immunoblotting. The membranes were washed with TBST buffer for 5 minutes four times and incubated in Intercept Blocking Buffer supplemented with Tween 20 (dilution 1:500) and 10% SDS solution (dilution 1:500) for 1 hour at room temperature. IRDye 800CW goat anti-mouse secondary antibody (LI-COR Biosciences, 1:20000), IRDye 680RD goat anti-rabbit secondary antibody (LI-COR Biosciences, 1:20000) were used for immunoblotting. The membranes were then washed with TBST for 5 minutes four times and scanned by Odyssey CLx Imaging System (LI-COR Biosciences). The immunoblots were finally quantified by the software and the readings were fitted using a nonlinear regression analysis with the GraphPad Prism 8 software to obtain the DC_{50} value.

Cell growth assay. 500-2000 cells/well were seeded in a 96-well tissue culture plate with a final volume of 200 μL/well and treated with indicated doses of compounds in a 3-fold serially diluted manner. The cells were incubated for 7 days at 37 °C in an atmosphere of 5% CO_2. Cell growth was evaluated by WST-8 assay (Dojindo Molecular Technologies, MD). An adequate volume of WST-8 reagent was added to each well, incubated for at least 1 h in the cell culture incubator, and read at 450 nm in a Tecan Infinite M1000 multimode microplate reader (Tecan, Morrisville, NC). The readings were normalized to the DMSO-treated cells and fitted using a nonlinear regression analysis with the GraphPad Prism 8 software to obtain the IC_{50} value.

Toxicity, PK/PD and efficacy studies. All *in vivo* studies were performed under an animal protocol (PRO00009463) approved by the Institutional Animal Care and Use Committee (IACUC) of the University of Michigan, in accordance with the recommendations in the Guide for the Care and Use of Laboratory Animals of the National Institutes of Health. CB.17 SCID breeders and Balb/c mice were obtained from Charles River Laboratories, CB.17 SCID mice were bred by University of Michigan Unit for Laboratory Animal Medicine (ULAM) Breeding Core.

For toxicity studies, female Balb/C mice were treated with SMD-3040 or vehicle control (25% PCP:33% of 10 part of PEG400 + 3 part of Cremchol, and PBS, pH was adjusted to 7 with 0.5 N NaOH) with indicated doses. Mouse body weights were measured every 2-3 days.

For PD studies, female SCID mice (6-10 weeks old) were injected subcutaneously with 5×10^6 MV4-11 cells in 5 mg/mL Matrigel (Corning) for tumor growth. SMD-3040 was administered in animals by intravenous (IV) injection using 25% PCP as the dosing vehicle when tumors reached approximately 200 mm^3. Mice with similar-sized tumors were grouped and assigned to different experimental groups and treated with indicated doses. At the indicated timepoints, mice were euthanized, and blood and tumor samples were collected for analysis. Isolated tumor samples were placed in a Precellys tube (CK28-R) and immediately frozen in liquid nitrogen. All plasma and tumor samples (about 200 μL) were stored at -80 °C until analysis. For the analysis of SMARCA protein levels in tumor samples, resected xenograft tumor tissues were ground into powder in liquid nitrogen and lysed in Radioimmunoprecipitation Assay Protein Lysis and Extraction Buffer containing proteinase inhibitor cocktail (Roche Diagnostics, Mannheim, Germany). Twenty micrograms of lysate were electrophoresed through 4-12% Tris-glycine SDS-PAGE gels (Invitrogen) and blotted into PVDF (polyvinylidene difluoride) membranes (MilliporeSigma,

IPFL00010). The membranes were blocked with Intercept Blocking Buffer (LI-COR Biosciences, 927-70001) for 1 h at rt and then washed with 1× Tris-buffered saline Tween 20 four times for 5 min each. The membranes were incubated overnight at 4 °C in Intercept Blocking Buffer supplemented with Tween 20 (dilution 1:500). Rabbit SMARCA2 antibody (CST, cat# 11966, 1:1,000), rabbit SMARCA4 antibody (Bethyl, cat# A700-106, 1:2,000) or mouse GAPDH antibody (Santa Cruz Biotechnology, sc-47724, 1:1,000) were used for immunoblotting. The membranes were washed with TBST buffer for 5 min four times and incubated in Intercept Blocking Buffer supplemented with Tween 20 (dilution 1:500) and 10% SDS solution (dilution 1:500) for 1 h at rt. IRDye 800CW goat anti-mouse secondary antibody (LI-COR Biosciences, 1:20000), IRDye 680RD goat anti-rabbit secondary antibody (LI-COR Biosciences, 1:20000) were used for immunoblotting. The membranes were then washed with TBST for 5 min four times and scanned by Odyssey CLx Imaging System (LI-COR Biosciences). The immunoblots were finally quantified by the software and the readings were fitted using a nonlinear regression analysis with the GraphPad Prism 8 software to obtain the DC_{50} value.

For efficacy studies, female SCID mice (6-8 weeks old) were injected subcutaneously with 5×10^6 H838 cells or 5×10^6 SK-Mel-5 cells in 5 mg/mL Matrigel (Corning) for tumor growth. When tumors reached an average volume of 100 mm^3, mice were tumor size matched and randomly assigned to different experimental groups with 8 mice for each group. Drugs or vehicle control were given at the dose schedule as indicated using 25% PCP as the dosing vehicle. Tumor sizes and animal weights were measured 2–3 times per week. Tumor volume (mm^3) = (length × $width^2$)/2. Tumor growth inhibition was calculated as TGI (%) = $(V_c - V_t)/(V_c - Vo)*100$, where V_c, V_t are the medians of the control and treated groups at the end of the treatment

respectively, and V_0 at the start. Tumor volumes at the end of treatment were statistically analyzed using a two-tailed, unpaired *t*-test (GraphPad Prism 9.0).

To prepare tumor samples for LCMS analysis, mixed ultrapure water and acetonitrile solution (4:1) were added to the defrosted tumor tissue samples 5:1, v/w, in order to facilitate homogenization with a Precellys evolution homogenizer at 4 °C. The homogenized tissues solution was denatured using cold acetonitrile (1:3, v/v) with vortex and centrifuged at 13000 rpm 4 °C for 10 min. Following protein precipitation, the final supernatants were collected for LC–MS analysis.

To determine drug concentrations in plasma and tumor samples, a LC–MS/MS method was developed and validated. The LC–MS/MS method consisted of a Shimadzu HPLC system, and chromatographic separation of a test compound was achieved using a Waters XBridge-C18 column (5 cm × 2.1 mm, 3.5 μm). An AB Sciex QTrap 5500 mass spectrometer equipped with an electrospray ionization source (Applied Biosystems, Toronto, Canada) in the positive-ion multiple reaction monitoring mode was used for detection. For example, the precursor/product ion transitions were monitored at m/z 942.5 for SMD-3040 and internal standard, respectively, in the positive electrospray ionization mode. The mobile phases used on HPLC were 0.1% formic acid in purified water (A) and 0.1% formic acid in acetonitrile (B). The gradient (B) was held at 10% (0–0.3 min), increased to 95% at 0.7 min, then kept at an isocratic 95% B for 2.3 min, and then immediately stepped back down to 10% for 2 min re-equilibration. The flow rate was set at 0.4 mL/min.

Chapter 3 Development of Novel Spiro SMARCA Bromodomain Ligands and Spiro SMARCA2 Selective PROTAC Degraders

3.1 Introduction

Epigenetic dysregulation is a feature prevalent in almost all human cancers, and targeting epigenetic regulators has been increasingly recognized as a useful therapeutic strategy to combat human cancers, as well as other diseases.[1] The pursuit of developing epigenetic inhibitors has been a journey of a half century, with clinical approvals of the first DNMT inhibitor azacitidine[2] and first HDAC inhibitor vorinostat[3] in the 2000s and more recently the EZH2 inhibitor tazemetostat.[5] Nevertheless, small molecule inhibitors of epigenetic regulators have met substantial clinical setbacks, due to reasons that they often lack isoform selectivity among many epigenetic protein families such as HDACs and BET proteins[155] and that small molecule inhibitors are intrinsically ineffective to target cancers driven by epigenetic regulators harboring loss-of-function (LOF) mutations.

SMARCA4, together with SMARCA2, are two mutually exclusive catalytic subunits of the mammalian SWItch/Sucrose Non-Fermentable (SWI/SNF) complexes, and they function as ATPases to enable the mSWI/SNF complexes to exert the chromatin remodeling process.[156] Studies have shown that SMARCA4 LOF mutations are highly prevalent in various types of cancers, including ovarian cancer, melanoma, and non-small cell lung cancer (NSCLC).[38, 54-61]

Importantly, large scale genome sequencing in patient samples revealed that SMARCA4 is frequently mutated in NSCLC patient populations with a rate of 9-13%, which reflects a large group of patients lacking targeted treatment regimens.[54, 60, 62] Several studies have reported that cancer cells with SMARCA4 LOF deficiencies are highly dependent on SMARCA2 for their survival by RNAi-based functional genomic screenings.[54-56] Therefore, numerous endeavors have been made to develop SMARCA2 small molecule inhibitors based on these findings. Early reported SMARCA2 inhibitors focused on targeting its bromodomain have no antiproliferative effects against SMARCA4-deficient cancer cells, while following biological investigations proved that it was the ATPase domain, rather than bromodomain of SMARCA2 that maintained the survival of cancer cells without SMARCA4 functionalities.[70] Accordingly, a number of inhibitors targeting the ATPase activities of SMARCA2 were subsequently disclosed, with one such inhibitor FHD-286 being advanced into Phase 1 clinical trials recently.[76, 80] Nevertheless, dose-limiting toxicities were observed in preclinical efficacy studies of these inhibitors with no selectivity between highly homologous SMARCA2 and SMARAC4 ATPase domains, which is consistent with the findings that concurrent loss of SMARCA2 and SNARCA4 were detrimental to normal cells and tissues.[77-78, 157-158]

To develop therapeutics that could selectively target SMARCA2 protein, we turned our attentions on the proteolysis targeting chimera (PROTAC) technology. In this case, PROTACs offer two distinct advantages over small-molecule inhibitors to achieve selective SMARCA2 targeting, one being that PROTACs could remove the whole disease-related protein by their unique mode of action which might potentially recapitulate the cellular phenotypes generated by RNAi or CRISPR knockout experiments,[159] the other being that PROTACs have the ability to selectively degrade one protein over its highly homologous proteins even by incorporating a pan-inhibitor

with no selectivity.[93, 116] Several SMARCA2-targeting PROTACs have been reported in the scientific literature, but most of these molecules still lack sufficient selectivity for SMARCA2 over SMARCA4.[89, 117-118] Our group recently reported a selective SMARCA2 degrader, SMD-3040,[87] which to our knowledge, possesses the best selectivity profile among all SMARCA degraders disclosed to date. However, further development and in vivo characterization of SMD-3040 were impeded by its mediocre in vitro degradation potency for SMARCA2 protein (DC_{50} = 12 nM) and poor ADME properties. To address these issues, we have designed and synthesized a new class of high-affinity small-molecule ligands of SMARCA2/4 proteins, and employed these novel ligands to successfully discover a series of exceptionally selective SMARCA2 degraders with improved drug-like properties, exemplified by SMD-3236. SMD-3236 showed a DC_{50} of 0.57nM and D_{max} of 96% against SMARCA2 protein with less than 50% degradation and over 1000-fold selectivity for SMARCA4 protein. In cell growth inhibition studies, SMD-3236 potently inhibited cell growth in SMARCA4-deficient cancer cell lines while sparing SMARCA4 wild-type cancer cells. SMD-3236 has a well-balanced pharmacokinetic profile and can achieve week-long SMARCA2 reduction in tumor tissues with a single dose of intravenous administration in mice. Once a week (qw) administration of SMD-3236 is well tolerated and can cause significant tumor growth inhibition in SMARCA4-deficient xenograft tumor models. Our data demonstrates SMD-3236 is a promising intravenous lead compound towards a SMARCA2-targeted developmental candidate for the treatment of SMARCA4-deficient human cancers.

3.2 Results and discussion

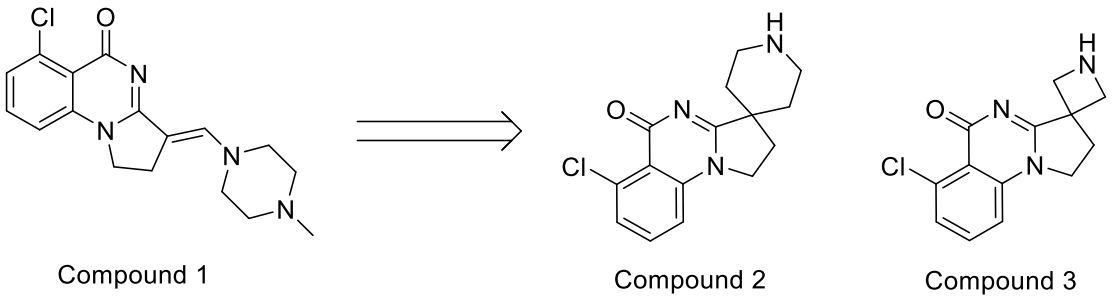
3.2.1 Structure guided design of novel spiro SMARCA bromodomain ligands

The development of SMARCA2 selective PROTAC degraders as potential targeted therapeutics against human cancers with SMARCA4 loss-of-function mutations has attracted tremendous interest in the drug discovery community. However, up to now most reported SMARCA PROTAC degraders have adopted the aminopyridazine class of compounds as the ligand for recruitment of SMARCA proteins.[87, 89, 118] This type of aminopyridazine SMARCA ligands possess high number of hydrogen bond donors, high tPSA, and a number of metabolic labile functional groups, such as the oxidation- and glucuronidation-prone phenol moiety. In order to obtain SMARCA2 PROTAC molecules with better physicochemical properties and metabolic stability, we set out to first discover a new class of SMARCA ligands that target SMARCA bromodomains and then use them to design novel SMARCA2 selective degraders with improved potency and ADME properties.

Instead of continuing to optimize the aminopyridazine-based SMARCA bromodomain ligands, we chose to switch to molecules with a different chemotype. In 2016, a series of 2,3-Dihydropyrrolo[1,2-a]quinazolin-5(*1H*)-one inhibitors targeting the bromodomains of SMARCA2/SMARCA4/PBRM1 were reported.[75] Compound **1**, as an example, has no hydrogen bond donor and a relatively low tPSA, which serves as a good starting point for our design of a new class of SMARCA bromodomain ligands. To remove the chemically unstable imine moiety in compound **1**, we elected to incorporate spirocyclic scaffolds to address this issue as well as to increase the sp^3 carbon fraction (Fsp^3) of the molecule.[160] Accordingly, we designed and

synthesized compounds **2** and **3** to test this initial idea, and tested their binding affinity to the SMARCA bromodomain using bio-layer interferometry (BLI) assay (Table 10).

Table 10. Design of spiro-containing SMARCA bromodomain ligands.



Compound	SMARCA2 BLI K_d	SMARCA4 BLI K_d
1	262 nM (ITC K_d)	417 nM (ITC K_d)
2	1.3 μM	0.9 μM
3	>10 μM	>10 μM

Compound **2**, containing a [4.5]azaspiro moiety, had K_d values of 1.3 μM for SMARCA2 BD and 0.9 μM for SMARCA4 BD, respectively. As we narrow the spiro ring size from a 6-membered ring to a 4-membered ring-containing compound **3**, its binding affinity for the SMARCA bromodomain significantly decreased, and showed no binding to either SMARCA2 or SMARCA4 bromodomains up to concentrations of 10 μM. Although compound **2** is still a weak SMARCA BD binder, it proved that our design strategy is viable that this alternative scaffold could lead to potent compounds after further medicinal chemistry optimizations. We next performed computational modeling analysis by docking compound **2** into a co-crystal structure of the SMARCA4 BD complexed with a SMARCA bromodomain ligand.[89] (PDB: 6HAZ) In the modeled structure, the amide group in the quinazolinone ring of compound **2** formed a bifurcated hydrogen bond with Asn1464. The chlorine atom was in close proximity to the backbone carbonyl

of Leu1456 (3.3 Å) and the oxygen in the residue of Tyr1421 (3.1 Å), indicating strong halogen bond interactions.

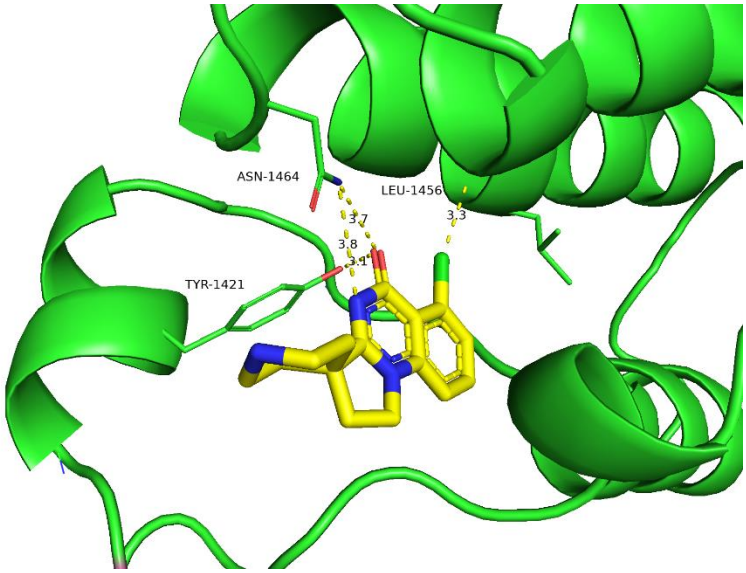


Figure 25. Modeled structure of compound 2 docked into SMARCA2 bromodomain.

In the disclosure of SMARCA2 PROTAC molecule ACBI2 recently published by Boehringer Ingelheim/U of Dundee, the authors described a class of new small molecule ligands for SMARCA BD that also originated from compound **1**.[117] In their medicinal chemistry campaign on discovering these ligands, compound **4** (Figure 26) was the most potent one with a K_d value of 46 nM for SMARCA2 BD in the SPR assay. Interestingly, introduction of the piperazine ring in compound **4** resulted in a 23-fold increase in K_d value compared to the precursor compound with no piperidine ring. From the disclosed co-crystal structure of nor-methyl analog of compound **4** in complex with SMARCA2 BD, the increase of the binding affinity could be attributed to the additional captured hydrogen bond interaction of Glu1417 to the piperidine. To test whether this strategy could be employed in our hands aiming at further improving the binding affinity of compound **2**, we tentatively introduced a phenylpiperidine moiety to the core spiro ring in compound **2** to get compound **5**. (Table 11) To our disappointment, the anticipated improvement

in binding affinity for compound **5** was not observed. In contrast, incorporation of the phenylpiperidine group resulted in loss of binding to SMARCA BD by 3 folds for SMARCA2 and over 10 folds for SMARCA4.

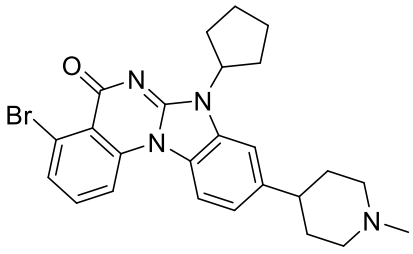
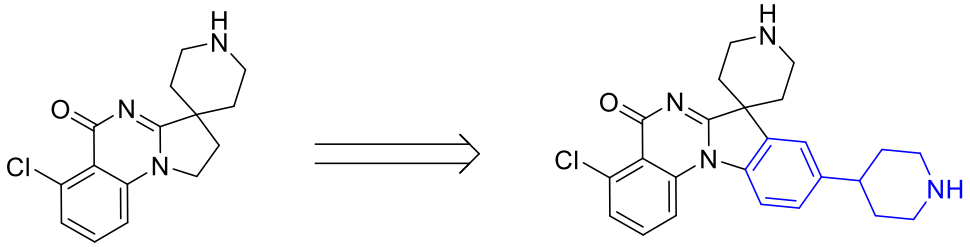


Figure 26. Chemical structure of new small molecule ligand (4) for SMARCA bromodomain from Boehringer Ingelheim.

Table 11. Desing and binding affinity testing of compound 5.



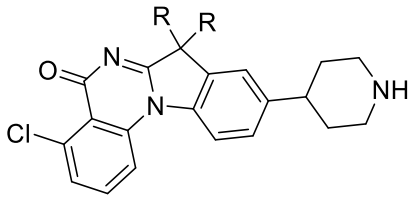
Compound 2 Compound 5

Compound	SMARCA2	SMARCA4
2	1.3 µM (BLI K_d)	0.9 µM (BLI K_d)
5	4.7 µM (TR_FRET IC_{50})	>10 µM (TR_FRET IC_{50})

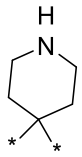
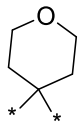
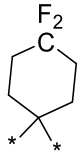
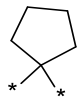
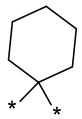
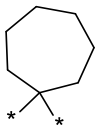
From our modeled structure, the spiro piperidine in compound **3** was positioned towards the surface area of SMARCA4 bromodomain. Careful examination of the interactions of spiro piperidine with SMARCA4 BD revealed that although there are no defined binding pockets for the spiro piperidine ring to occupy with, the amino acids in close contact with spiro piperidine ring

are mostly consist of hydrophobic residues. We thus reasoned that modification of the positive charge-containing spiro piperidine ring into non-polar ring systems would be helpful in improving its binding to the protein. Accordingly, we synthesized compounds **6-10** with different hydrophobic substituents and summarized the binding data in Table 12. The TR-FRET data showed that substituting the piperidine in compound **5** by a tetrahydro pyran group resulted in over 30-fold increase the binding to SMARCA bromodomain, as the corresponding compound 6 had IC_{50} values of 140 nM for SMARCA2 and 380 nM for SMARCA4. Introduction of di-fluoro substituents significantly reduced the binding affinity compared to the pyran ring presumably attributed to increased steric hinderance. Compound **8** with a cyclopentyl and compound **9** with a cyclohexyl bound well to SMARCA2/4, with IC_{50} values of 5nM and 9.5 nM for SMARCA2 BD respectively, and IC_{50} values of 30 nM and 8.2 nM for SMARCA4 respectively. Further increase of the ring size was shown to be detrimental to the binding, as compound **10** with a 7-membered cycloheptyl substituent achieved IC_{50} values of 440 nM for SMARCA2 and 310 nM for SMARCA4, which was about 40-fold weaker than the 6-member ring-containing compound **9**. Collectively, these SAR data demonstrates that hydrophobic groups with defined sizes are well tolerated in the spiro ring position with 6-membered ring being the best one, while polar groups tend to result in significant or complete loss of binding affinity.

Table 12. Design and binding affinity testing of compounds 6-10.

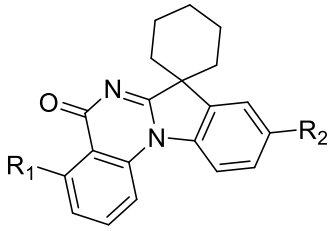


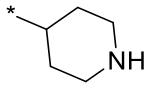
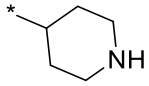
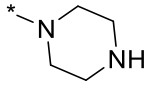
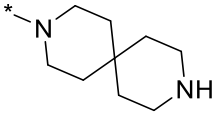
Compound	R	SMARCA2 TR_FRET IC_{50}	SMARCA4 TR_FRET IC_{50}

5		4.7 μM	>10 μM
6		140 nM	380 nM
7		>10 μM	790 nM
8		5 nM	30 nM
9		9.5 nM	8.2 nM
10		440 nM	310 nM

Next, we tested the SAR around other regions of our new SMARCA bromodomain ligand using compound **9** as a template. The data were summarized in Table 13. Replacing the chlorine in compound **9** with a bromine atom in compound **11** led to 2-fold loss is its binding to either SMARCA2 or SMARCA4 BD. Compound **12** containing a piperazine group or compound **13** containing a [5.5]diazaspiro group drastically abolished the binding with a over 1000-fold decrease in SMARCA2 BD affinity and approximately 100-fold decrease in SMARCA4 BD affinity, compared to compound **9**. Further SAR explorations in these regions are still required to yield potent ligands for SMARCA bromodomain.

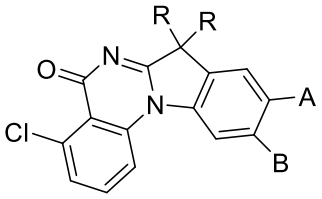
Table 13. Design and binding affinity testing of compounds 11-13.

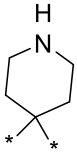
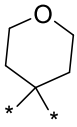
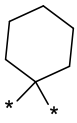


Compound	R_1	R_2	SMARCA2 TR_FRET IC_{50}	SMARCA4 TR_FRET IC_{50}
9	Cl		9.5 nM	8.2 nM
11	Br		15 nM	21 nM
12	Cl		>10 μM	1.2 μM
13	Cl		>10 μM	710 nM

Apart from the previous series of molecules where the piperidine ring is attached in a fixed position, we next investigated an alternative position in the phenyl ring for the attachment of the piperidine group, generating compounds **14-17** in Table 14. The data showed that compared to compounds **5-6** and compounds **8-9** where the piperidine group in at position A, their corresponding analogs **14-17** where the piperidine group in at position B were 3-fold to 10-fold weaker in binding to SMARCA bromodomains, as suggested by their IC_{50} values, while similar SAR around the R spiro substituents were observed.

Table 14. Design and binding affinity testing of compounds 14-17.



Compound	R	Position of Piperidine	SMARCA2 TR_FRET IC_{50}	SMARCA4 TR_FRET IC_{50}
5		A	4.7 μM	>10 μM
14		B	>10 μM	>10 μM
6		A	140 nM	380 nM
15		B	1.3 μM	1.6 μM
8		A	5 nM	30 nM
16		B	43 nM	100 nM
9		A	9.5 nM	8.2 nM
17		B	17 nM	44 nM

In order to gain further insights into the binding mode of our novel SMARCA bromodomain ligands, we successfully solved the co-crystal structure of one of these analogs, compound **17**, in complex with SMARCA2 bromodomain at a 1.74 Å resolution. (Figure 27, PDB undeposited) In the co-crystal structure, the quinazolinone core forms bidentate hydrogen bonds with Asn1464, and an additional hydrogen bond interaction is observed between the carbonyl oxygen and Tyr1421. An unusual halogen-bonding interaction is formed between the chlorine and

the Leu1456 backbone carbonyl. The Cl-phenyl moiety is positioned vertically to Phe1409, suggesting the existence of edge-face π–π interactions. The middle phenyl sits between the hydrophobic cleft formed by Pro1413 and Val1408, whereas the cyclohexyl group fits into a large, hydrophobic surface surrounded by Leu1418, Phe1463 and Ile1470. The piperidinyl group is exposed to solvent and could be utilized as the exit vector for PROTAC linker attachment. Interestingly, hydrogen bond interactions between the piperidine group and Glu1417 were not observed as was shown in the BI SMARCA ligand (**3**). Instead, the basic nitrogen in piperidinyl group formed weak polar interactions with Gln1411. The co-crystal structure, together with the SAR data, provides us with a solid basis for the next design of selective SMARCA2 PROTAC degraders based upon these series of scaffolds.

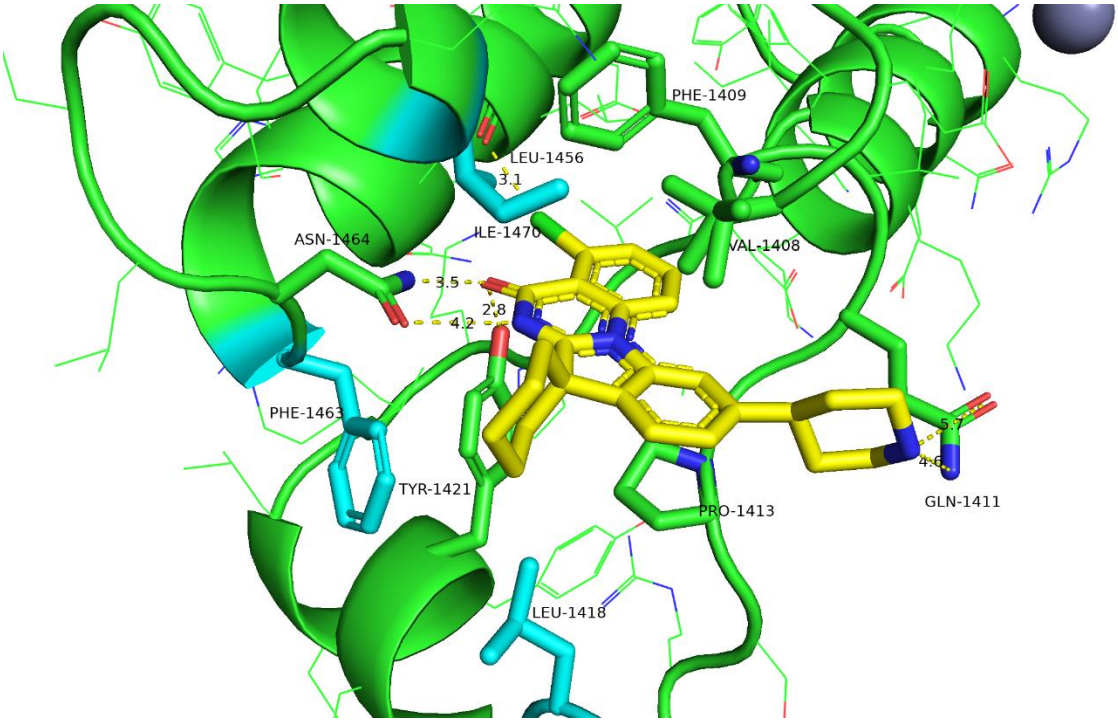


Figure 27. Co-crystal structure of SMARCA2 bromodomain complexed with compound 17.

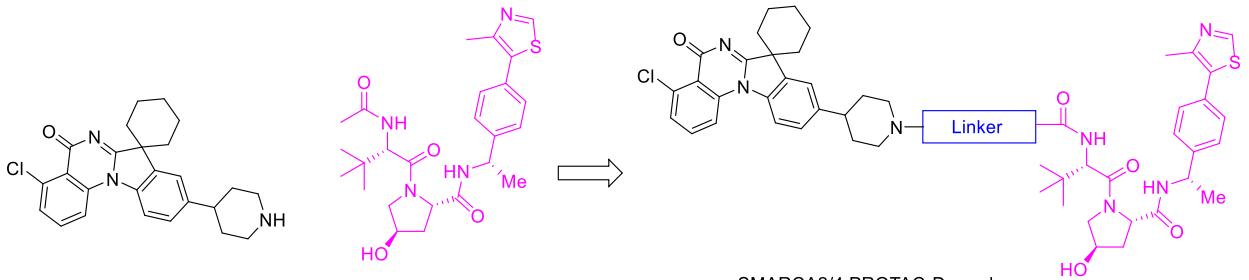
3.2.2 Design of selective SMARCA2 PROTAC degraders based on novel spiro SMARCA bromodomain ligands

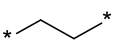
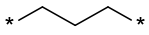
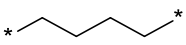
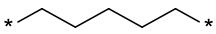
According to our co-crystal structure of compound **17** with SMARCA2 bromodomain (Figure 29), the piperidine group is exposed to solvent environment, making this position a suitable site at which to anchor a chemical linker for the design of selective SMARCA2 PROTAC degraders. We first selected compound **9** as the SMARCA protein recruitment moiety, which showed the best binding affinity (IC_{50} = 9.5 nM for SMARCA2 and 8.2 nM for SMARCA4) among all the new SMARCA bromodomain ligand we have synthesized. In our previous studies, we have successfully employed VHL/cullin 2 E3 ligase ligands to develop potent and selective SMARCA2 PROTAC degrader SMD-3040. Hence, we kept using these VHL ligands for our design of SMARCA2 selective PROTAC degraders and synthesized compounds **19-23** containing all-alkyl linkers with different lengths, and tested their degradation potency for SMARCA2 and SMARCA4 proteins in our HiBit assay. (Table 15)

The data showed that compound **19** with the shortest linker containing only one methylene, was very potent in degrading both SMARCA2 and SMARCA4 protein with DC_{50} values of 8 nM and 19 nM, respectively. However, near complete (98%) degradation of SMARCA2 and SMARCA4 were observed for compound **19** with identical D_{max} values, indicating that there was no SMARCA2 selectivity for compound **19**. By extending the linker length to 2, 3, and 4 methylene groups, we obtained compounds **20-22**. These three compounds were 25-35 times less potent than compound **19** in degrading SMARCA2 and were thus much weaker SMARCA2 degraders. Interestingly, compounds **21** and **22** only reduced the level of SMARCA4 protein by 18.5 %, with ΔD_{max} values (the difference between SMARCA2 D_{max} and SMARCA4 D_{max}) of 61% and 63% respectively. Compound **23** with a 5-methylene linker was 3-fold more potent than

compound **20**, but 9-fold less potent than compound **19** in inducing the degradation of SMARCA2 protein, with a DC_{50} value of 76 nM and a D_{max} value of 93%. Importantly, the SMARCA4 protein was degraded less than 50 % by compound **23** and a ΔD_{max} value of 43 was obtained. Among all these compounds we profiled, compound **23** showed a decent degradation potency for SMARCA2 and selectivity over SMARCA4, and we decided to select compound **23** for further linker optimization.

Table 15. Investigation of the optimal linker length in PROTAC SMARCA2/4 degraders.

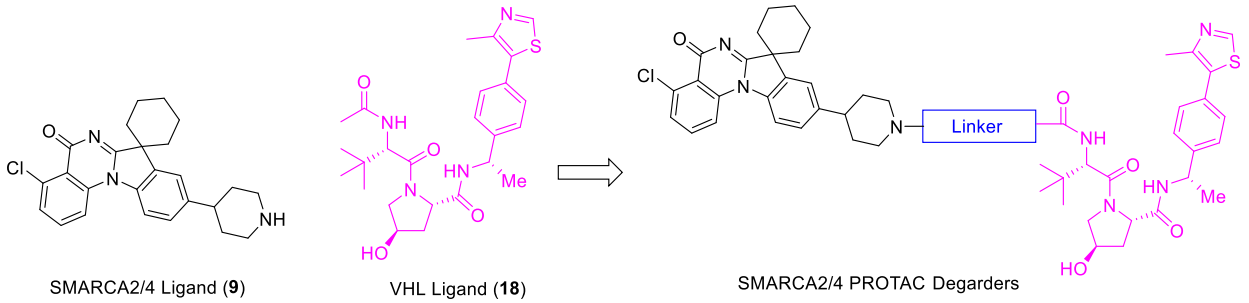


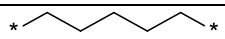
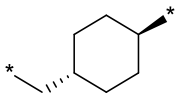
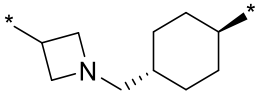
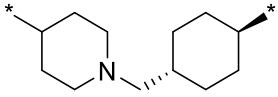
Compound	Linker	SMARCA2 DC_{50} (nM)	SMARCA2 D_{max} (%)	SMARCA4 DC_{50} (nM)	SMARCA4 D_{max} (%)	S2/S4 DC_{50} ratio	ΔD_{max} (%)
19		8	98	19	98	1.4	0
20		216	87.5	714	68.5	3.3	19
21		240	79.5	>1000	18.5	>4.2	61
22		275	81	1106	18.5	4.0	63
23		76	93	1000	50	13.2	43

In our previous studies of SMD-3040, we used a rigid, cyclohexyl group in the linker to achieve an 80-fold SMARCA2 selectivity over SMARCA4 protein. Based upon the success of SMD-3040, we tried to employ this design strategy in compound **23** to further increase the potency and selectivity. Accordingly, we designed and synthesized compounds **24-26** in Table 16.

Cyclization of the 5-methylene linear linker in compound **23** has yielded compound **24** with the cyclohexyl group. To our delight, the degradation potency for SMARCA2 was increased 12 folds compared to compound **23**, with partial loss SMARCA4 selectivity as a of 29.5-fold difference in DC_{50} ratio and ΔD_{max} of 24.5 were still retained. Introduction of basic nitrogen-containing 4-membered azetidine ring or 6-membered piperidine ring resulted in more than 10 folds of loss of SMARCA2 degradation potencies as were shown by HiBit results of compounds **25** and **26**, which precluded us to further pursue these modifications.

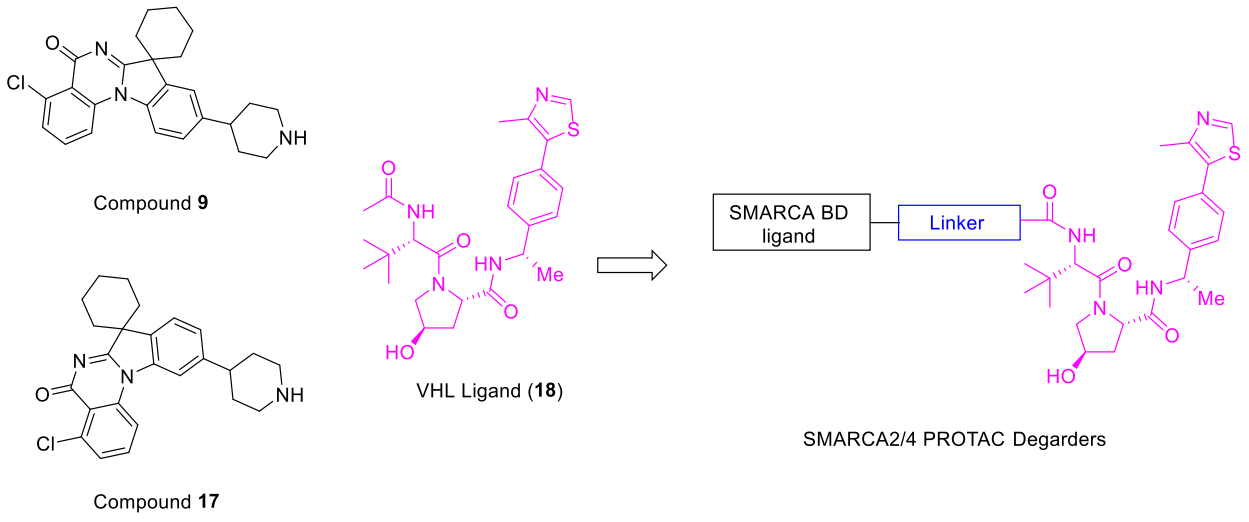
Table 16. Investigation of the linker composition in PROTAC SMARCA2/4 degraders.

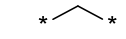
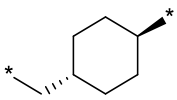
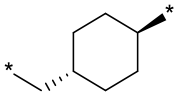


Compound	Linker	SMARCA2 DC_{50} (nM)	SMARCA2 D_{max} (%)	SMARCA4 DC_{50} (nM)	SMARCA4 D_{max} (%)	S2/S4 DC_{50} ratio	ΔD_{max} (%)
23		76	93	1000	50	13.2	43
24		6	92	177	67.5	29.5	24.5
25		191	88.5	819	52	4.3	36.5
26		50	88.5	>1000	38	>20	53.5

So far, all our designed PROTAC degraders have employed compound **9** as the ligand of SMARCA proteins. From the co-crystal structure we solved, compound **17** with a different exit vector in the piperidine position provides us with an alternative opportunity for the design of potential SMARCA2 selective PROTAC degraders with distinct molecular geometries. To investigate how these changes might impact the degradation potency and selectivity, compounds **27** and **28** utilizing the same linkers in compounds **19** and **24** but utilizing compound **17** as the SMARCA ligand, were synthesized and tested with data summarized in Table 17. Compared with compound **19**, compound **27** had minimal differences in its degradation potency for SMARCA2 with DC_{50} = 6 nM and D_{max} = 92%, while the SMARCA4 selectivity was slightly increased as indicated by the 5.8-fold S2/S4 DC_{50} ratio and the 6.5 % ΔD_{max} value. Surprisingly, when comparing compounds **24** and **28** which both contain a cyclohexyl linker, compound **28** showed a SMARCA4 D_{max} value of only 10% in comparison to the 67.5% SMARCA4 D_{max} for compound **24**, indicating the SMARCA4 degradation activity in compound **28** was almost completely abolished while the SMARCA2 degradation potency could be maintained, by merely changing the SMARCA ligand conformation.

Table 17. Investigation of the exit vector positions in the SMARCA bromodomain.

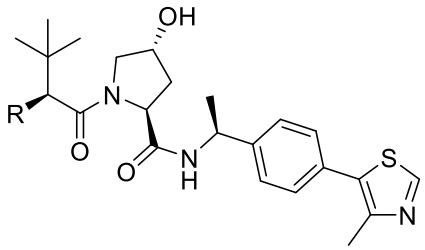


Compound	Ligand	Linker	SMARCA2 DC_{50} (nM)	SMARCA2 D_{max} (%)	SMARCA4 DC_{50} (nM)	SMARCA4 D_{max} (%)	S2/S4 DC_{50} ratio	ΔD_{max} (%)
19	**9**		8	98	19	98	1.4	0
24	**9**		6	92	177	67.5	29.5	24.5
27	**17**		13	97	76	91.5	5.8	6.5
28	**17**		13	87.5	>1000	10	>76.9	77.5

Despite the exceptional selectivity of compound **28**, its degradation potency (DC_{50} = 13 nM) and efficacy (D_{max} = 87.5%) for SMARCA2 were yet to be optimal. Aiming at a DC_{50} value lower than 1 nM and a D_{max} value above 95%, we next set out to optimize the VHL ligand portion of our SMARCA PROTAC degraders. During the course of this work, a series of triazolo VHL ligands with improved binding affinity and cell permeability were disclosed by Genentech.[161] One such ligand (**29**), tested in our fluorescence polarization (FP) binding assay, showed a K_i value of 14 nM which is >10 times more potent then out amide-containing VHL ligand **18**. (Table 18) Encouraged by the high binding affinity of VHL ligand **29**, we further extended its usage in our selective compound **28** by replacing the VHL ligand **18**, which led to compound **30**. (Table 19) The HiBit degradation data showed that introduction of triazolo VHL ligand in compound **30** dramatically improved the degradation potency. Compound **30** was able to achieve DC_{50} of 0.3 nM and D_{max} of 99% for SMARCA2, which was >40-fold more potent than compound **28**. Although a 383-fold S2/S4 DC_{50} ratio and 29% ΔD_{max} was suboptimal, we decided to proceed

compound **30** into in vivo studies to gather initial PK/PD data. Nevertheless, during the formulation step, compound **30** was found to be insoluble at the 30 mg/kg dosage group which impeded us from further in vivo characterization. To address this solubility issue, we elected to introduce polar substituents into compound **30**.

Table 18. Comparison of the binding affinity of VHL ligands.



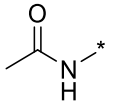
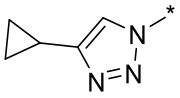
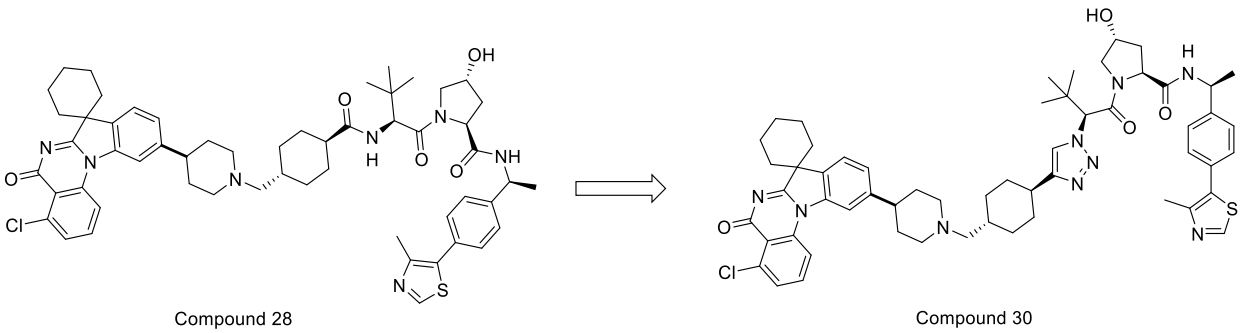
Compound	R	Fluorescence Polarization K_i
18		164 nM
29		14 nM

Table 19. Optimization of the VHL ligands in PROTAC SMARCA2/4 degraders.



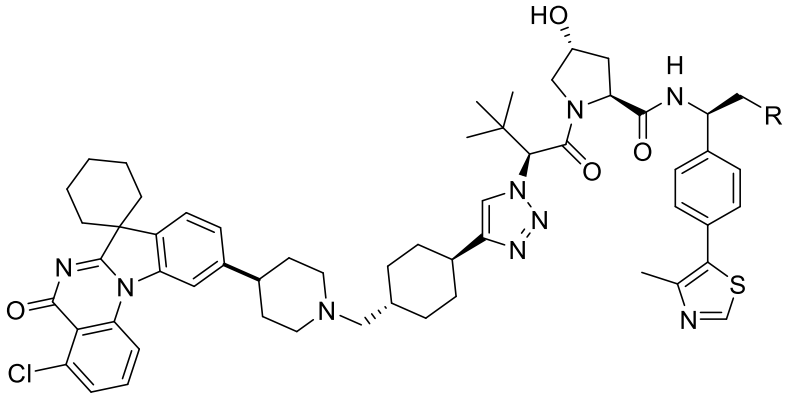
Compound 28 Compound 30

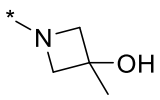
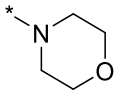
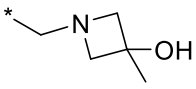
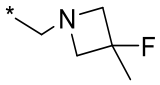
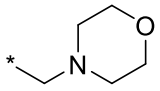
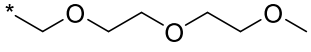
Compound	SMARCA2 DC_{50} (nM)	SMARCA2 D_{max} (%)	SMARCA4 DC_{50} (nM)	SMARCA4 D_{max} (%)	S2/S4 DC_{50} ratio	ΔD_{max} (%)

28	13	87.5	>1000	10	>76.9	77.5
30	0.3	99	115	70	383	29

According to the co-crystal structure of a representative VHL ligand bound to the VHL protein reported by Ciulli group,[152] (PDB: 4W9H) the (S)-methyl group of those VHL ligands used in our SMARCA PROTAC degraders is exposed to the solvent, making it an ideal position for attaching polar and hydrophilic substituents. We therefore synthesized compounds **31-37** with various types of soluble groups in the methyl position. (Table 20) Compounds 30 containing a 3-methyl-3-hydroxyl azetidinyl and compound **32** containing a 3-methyl-3-fluoro azetidinyl were weaker compounds in inducing the degradation of SMARCA2 protein compared to compound **30**. Unexpectedly, introduction of these two soluble groups resulted in increase in the selectivity for SMARCA4 by the lowering of both DC_{50} and D_{max} values. Compound **33** (SMD-3236) containing a morpholinyl group was equally potent to compound **30**, while demonstrating the best SMARCA4 selectivity property among all the three new analogs prepared, as was shown by a SMARCA4 D_{max} value of 41%, a S2/S4 DC_{50} ratio of >2000 folds, and a ΔD_{max} value of 55%. Extending the length by one more methylene resulted in compounds **34-36**, which were weaker in degrading SMARCA2 protein than their corresponding compounds **31-33** by several folds. When we switched to neutral, polyethylene glycol substituents and synthesized compound **37**, it was still 2-fold less potent than compound **33** albeit demonstrating a similar extent of SMARCA4 selectivity.

Table 20. Optimization of the solubility of PROTAC SMARCA2/4 degraders.



Compound	R	SMARCA2 DC_{50} (nM)	SMARCA2 D_{max} (%)	SMARCA4 DC_{50} (nM)	SMARCA4 D_{max} (%)	S2/S4 DC_{50} ratio	ΔD_{max} (%)
30	H	0.3	99	115	70	383	29
31		2	95	> 1000	62	>500	33
32		1	96	> 1000	52.5	>1000	43.5
33 (SMD-3236)		0.5	96	> 1000	41	>2000	55
34		6	83	> 1000	52.5	>167	30.5
35		19	82.5	> 1000	58	>53	24.5
36		1	94.5	> 1000	26.5	>1000	68
37		1	95	> 1000	53	>1000	42

In summary, our efforts have yielded SMD-3236 (**33**) as a potent and selective SMARCA2 PROTAC degrader, which prompted us to perform biological experiments for the evaluation of its activities in vitro and in vivo.

3.2.3 Evaluation of Degradation Kinetics and the Mechanism of Action of SMD-3040.

We evaluated the kinetics of SMD-3236 in induction SMARCA2 and SMARCA4 degradation at different time points and the data were summarized in Figure 28 and Table 21. Our HiBit data showed that SMD-3236 could induce the degradation of SMARCA2 protein in a time- and dose-dependent manner, achieving DC_{50} values of 10 nM, 3 nM, 1 nM, 1 nM, 0,45 nM and 0.24 nM at 2, 4, 6, 8, 24, 48 h time points and a >90% D_{max} after 8 h time point. SMD-3236 demonstrated an excellent selectivity profile against SMARCA4 protein, with maximum degradation values of <5%, 22.5%, 34.5%, 45.5%, 55% and 58.5% attained at at 2, 4, 6, 8, 24, 48 h time points, respectively.

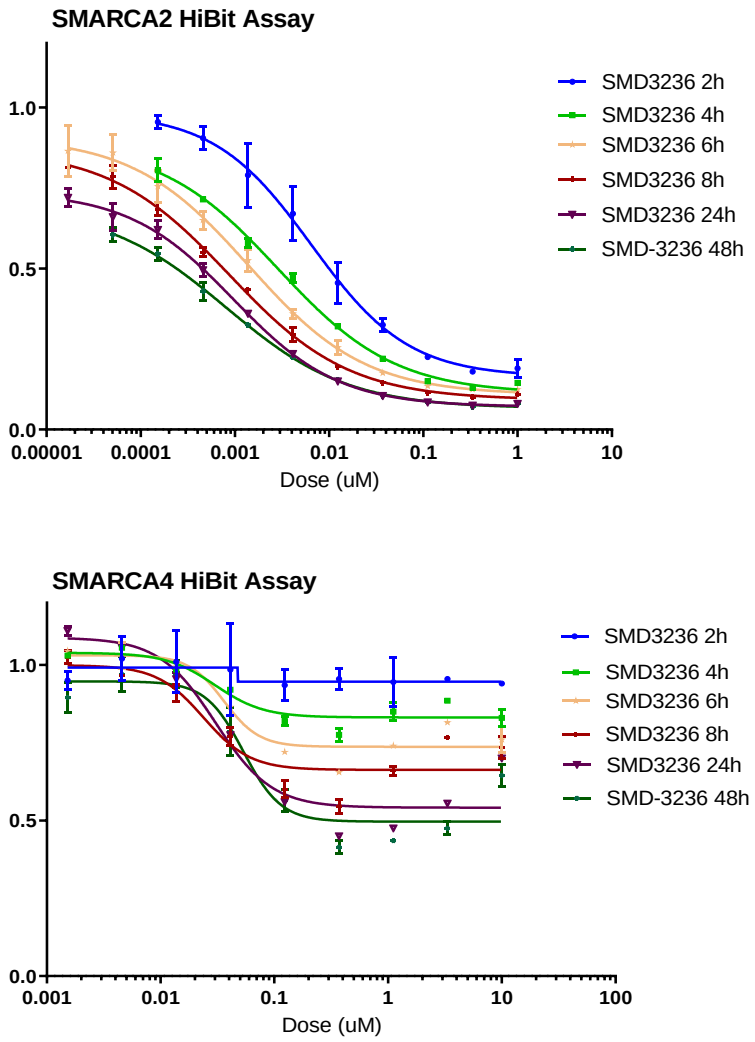


Figure 28. Time course of SMD-3236 in degrading SMARCA2 and SMARCA4 in Hela cells using HiBit assay.

Table 21. SMD-3236 kinetic degradation data.

Time point	SMARCA2 DC_{50} (nM)	SMARCA2 D_{max} (%)	SMARCA4 DC_{50} (nM)	SMARCA4 D_{max} (%)	ΔD_{max} (%)
2 h	10	82	> 10000	No deg	82
4 h	3	87	> 10000	22.5	64.5

6 h	1	87.5	> 10000	34.5	53
8 h	1	90	> 10000	45.5	44.5
24 h	0.45	92.5	> 10000	55	37.5
48 h	0.24	93	338	58.5	34.5

We next investigated the mechanism of SMARCA2 degradation induced by SMD-3236 using the HiBit assay (Figure 29). Our data showed that SMARCA2 degradation by SMD-3236 was effectively attenuated by SMARCA bromodomain ligand (**17**) or VHL ligand (**29**), indicating that the binding of both VHL and SMARCA is required for degradation. Pre-treatment of the NEDD8-activating E1 enzyme inhibitor MLN4924 or the proteasome inhibitor PR171 also blocked the SMARCA2 degradation induced by SMD-3236, confirming that SMARCA2 degradation was neddylation- and proteasome-dependent. These mechanistic data clearly demonstrate that SMD-3236 is a bona fide PROTAC SMARCA degrader.

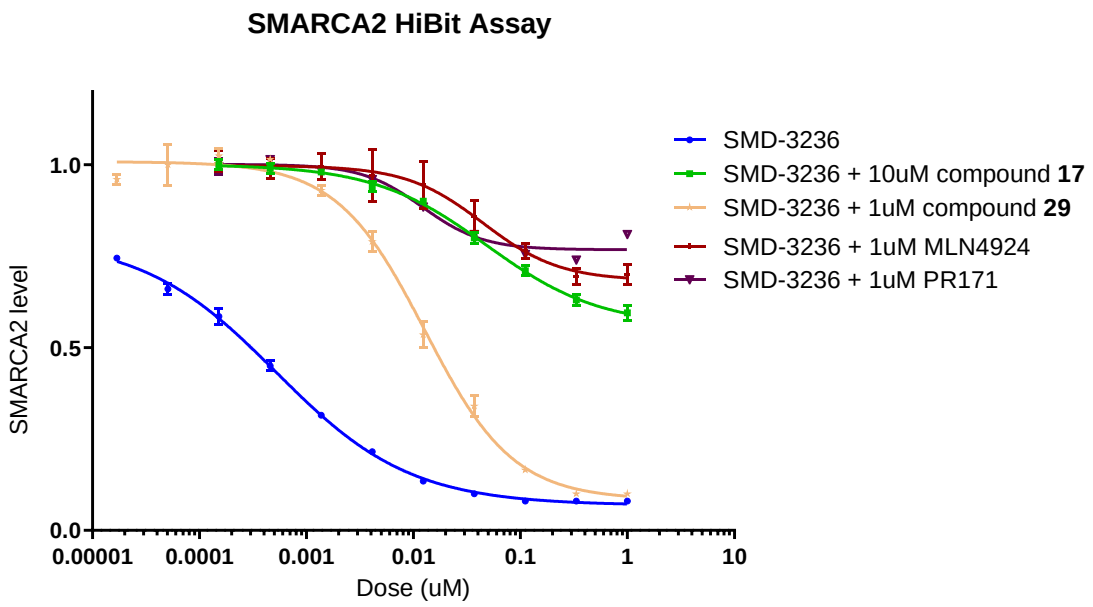


Figure 29. Mechanistic study of SMD-3236 degrading SMARCA2 protein in Hela cells using a HiBit assay.

3.2.4 Evaluation of Cell Growth Inhibition of SMD-3040 in Different Cell Lines

We next evaluated SMD-3236 for its antiproliferative effects in a panel of 5 SMARCA4-deficient cell lines and 3 SMARCA4-wildtype cell lines and obtained the data summarized in Table 22. In the 5 SMARCA4-deficient cell lines evaluated, SMD-3236 was able to achieve GI_{50} values of 1.5 – 9.8 nM, with Imax values of 71 - 95%. In comparison, we tested our previously reported selective SMARCA2 degrader SMD-3040 in parallel to SMD-3236. SMD-3040 had GI_{50} values of 12 - 152 nM among those 5 cell lines and is 9-16 times less potent than SMD-3236, but showed no difference than SMD-3236 in terms of Imax values.

In SK-Mel-28 melanoma cell line, H1792 and H1975 NSCLC cell lines carrying wildtype SMARCA4 protein, SMD-3236 exhibited GI_{50} values of >10 uM and Imax values of 55 - 80% in these three cell lines. Although the SMD-3236 Imax values of 55 - 80% were higher than those of

SMD-3040 (15 - 40%), the weak cell growth GI_{50} values confirmed its excellent selectivity for inhibiting SMARCA4-deficient cancer cell liens over SMARCA4 wild-type cancer cell lines.

Table 22. Cell growth inhibition activity of SMD-3236 and SMD-3040 in 5 SMARCA4 deficient and 3 SMARCA4 wild-type cancer cell lines.

Cell line		SMD-3040		SMD-3236	
		GI_{50} (nM)	Imax%	GI_{50} (nM)	Imax%
SMARCA4 deficient	SK-Mel-5	16 ± 1	96 ± 1	1.5 ± 0.4	95 ± 1
	NCI-H838	152 ± 40	77 ± 8	9.5 ± 1.1	80 ± 6
	NCI-H1568	12 ± 3	87 ± 6	2.2 ± 0.6	86 ± 6
	NCI-H1944	123 ± 58	70 ± 13	9.8 ± 6.6	71 ± 12
	NCI-H1693	43 ± 22	81 ± 5	4.8 ± 2.5	85 ± 6
SMARCA4 wildtype	NCI-H1792	>10 uM	25 ± 4	>10 uM	80 ± 9
	SK-Mel-28	>10 uM	15 ± 7	>10 uM	55 ± 7
	NCI-H1975	>10 uM	40 ± 10	>10 uM	65 ± 19

3.2.5 Pharmacodynamic evaluation of SMD-3236

We next proceeded for evaluation of the pharmacodynamics effects of SMD-3236 in mice. We first tested SMD-3236 for its SMARCA2 degradation activity in H838 SMARCA4-deficient xenograft tumor model in mice. Mice were administered with a single dose of SMD-3236 at 10mg/kg intravenously and data points at 6 h, 48 h and 168 h were generated and summarized in Table 23. From the PD data, the level of SMARCA2 in tumor tissues was reduced by 46%, 72% and 78% at 6 h, 48 h and 168 h time points, respectively. Another SMARCA4-deficient H1299 xenograft tumors model was also used for the evaluation of the PD effect of SMD-3236. In this model, SMARCA2 protein levels were reduced by 62%, 91% and 70% at 6 h, 48 h and 168 h time points, respectively, with a single 30 mg/kg intravenous dose of SMD-3236. (Table 24)

Table 23. PD data of SMARCA2 protein level upon treatment of SMD-3236 in H838 tumors.

H838 **10 mg/kg, IV**	**Samples**	**Relative Protein%**	**Mean Protein %**
		SMARCA2	**SMARCA2**
vehicle	1	79	100 ± 30
	2	87	
	3	134	
6 h	1	51	54 ± 23
	2	33	
	3	78	
48 h	1	32	28 ± 7
	2	20	
	3	33	
168 h	1	13	22 ± 8
	2	28	
	3	25	

Table 24. PD data of SMARCA2 protein level upon treatment of SMD-3236 in H1299 tumors.

H1299 **30 mg/kg, IV**	**Samples**	**Relative Protein%**	**Mean Protein %**
		SMARCA2	**SMARCA2**
vehicle	1	112	100 ± 35
	2	127	
	3	61	
6 h	1	39	38 ± 15
	2	52	

	3	22	
48 h	1	0	9 ± 10
	2	7	
	3	20	
168 h	1	31	30 ± 20
	2	9	
	3	49	

To test the in vivo degradation selectivity of SMD-3236, we next evaluated its PD effect in MV4-11 xenograft tumor model which expresses a high level of wildtype SMARCA4 protein. Mice bearing MV4;11 xenograft tumors were administered with a single dose of SMD-3040 at 30 mg/kg intravenously and were sacrificed at 24, 48 and 168 h time points after the treatment. Western blotting experiments were carried out to analyze the SMARCA2 and SMARCA4 protein levels in collected tumor samples and the obtained data were summarized in Table 25. SMD-3236 effectively reduced the level of SMARCA2 protein in MV4-11 tumor tissues by 97%, 85% and 89% at 24 h, 48 h and 168 h time points, respectively. On the contrary, the level of SMARCA4 protein was increased by 131%, 110% and 45% at 24 h, 48 h and 168 h time points, respectively. The extent of SMARCA4 protein level increment was attenuated at later time points, indicating a stronger compensate effects taking place upon the rapid degradation of SMARCA2 protein by overexpression of SMARCA4 protein. Further investigations are needed to elucidate the precise mechanism of this SMARCA4 upregulation induced by SMD-3236.

Table 25. PD data of SMARCA2 and SMARCA4 protein level upon treatment of SMD-3236 in MV4-11 tumors.

MV4-11 30mg/kg, IV	**Samples**	**Relative Protein% SMARCA2**	**Mean Protein % SMARCA2**	**Relative Protein% SMARCA4**	**Mean Protein % SMARCA4**
vehicle	1	139	100 ± 34	85	100 ± 14
	2	79		102	
	3	83		113	
24 h	1	8	3 ± 5	289	231 ± 80
	2	0		141	
	3	0		264	
48 h	1	38	15 ± 20	229	210 ± 57
	2	4		256	
	3	4		147	
168 h	1	0	11 ± 16	147	145 ± 20
	2	5		164	
	3	29		125	

Taken together, these PD data demonstrated that a single intravenous dose of SMD-3236 could induce effective and long-lasting reduction of SMARCA2 protein in H838 and H1299 SMARCA4-deficient tumor models as well as MV4-11 SMARCA4-wildtype tumor model with the effect persisting for 7 days. Importantly, SMD-3236 did not cause the reduction of the levels of SMARCA4 protein in the MV4-11 SMARCA4-wildtype tumor model at all time points in the experiment cycle. SMD-3236 is therefore an effective and selective degrader of SMARCA2 protein in vivo.

3.2.6 Stability, CYP inhibition, hERG inhibition and Pharmacokinetic (PK) Evaluation of SMD-3236

As SMD-3236 showed an excellent selectivity and efficacy in degrading SMARCA2 protein in a number of tumor xenograft models, we next proceeded for the evaluation of its plasma and microsomal stability in different species and obtained the data summarized in Table 26. Our data indicated that SMD-3236 exhibited exceptional plasma stability with half-life >120 min across all three species studied and exceptional liver microsomal stability with half-life >60 min across all three species studied.

Table 26. Plasma and liver microsomal stability data of SMD-3236.

SMD-3236	Plasma Stability			Liver Microsomal Stability		
Species	Mouse	Rat	Human	Mouse	Rat	Human
Half-life (min)	>120	>120	>120	>60	>60	>60

We evaluated SMD-3236 for its cytochrome P450 (CYP) inhibitory activity to avoid potential drug-drug interaction risks. For all the 7 major CYP isoforms tested, SMD-3236 showed no significant effect (IC_{50} > 50 μM) in inhibiting the enzymatic activities. (Table 27)

Human ether-à-go-go-related gene human (hERG) inhibition can cause QT prolongation and lead to fatal ventricular tachyarrhythmia in the clinic. Therefore, we also tested the SMD-3236 for its hERG inhibitory activity. (Table 27) Our data showed that SMD-3236 had a moderate hERG activity with an IC_{50} value of 6.9 μM in the hERG inhibition assay. Further optimization of SMD-3236 might be necessary to eradicate the hERG activity.

Table 27. CYP and hERG inhibition data of SMD-3236.

SMD-3236	CYP inhibition							hERG inhibition
CYP enzyme	1A2	2B6	2C8	2C9	2C19	2D6	3A4	-
IC_{50} (μM)	>100	>100	>100	>100	>100	65	>100	6.9

In addition to the stability and in vitro safety data for SMD-3236, we further evaluated its pharmacokinetics (PK) in mice and rats, and have obtained the PK data summarized in Table 28. In mice, SMD-3236 had a very low clearance (Cl = 9.2 mL/min/kg), an excellent volume of distribution (V_{ss} = 1.9L/kg), a long half-life of 8.4 h and a reasonable exposure (AUC = 1743 h*ng/mL and C_{max} = 2232 ng/mL). In rats, SMD-3236 had a moderately low clearance (Cl = 21.9 mL/min/kg), a good volume of distribution (V_{ss} = 0.9 L/kg), a long half-life of 6.3 h and a moderate exposure (AUC = 753 h*ng/mL and C_{max} = 2417 ng/mL). Overall, these initial PK data showed that SMD-3236 had a well-balanced PK profile in mice and rats.

Table 28. Summary of PK data for SMD-3236 in mice and rats.

Species	Route	Dose Level	$T_{1/2}$	C_{max}	$AUC_{(0-t)}$	V_{ss}	Cl
		mg/kg	h	ng/mL	h*ng/mL	L/kg	mL/min/kg
Mouse	IV	1	8.4	2232	1743	1.9	9.2
Rat	IV	1	6.3	2417	753	0.9	21.9

3.2.7 Antitumor Efficacy of SMD-3236 in H838 and H1299 Mice Xenograft Tumor Models

Based upon the promising PK/PD data of SMD-3236, we decided to evaluate its antitumor activity in the SMARCA4-deficient H838 and H1299 NSCLC tumor xenograft models in mice with a once per week, intravenous dosing regimen, and the data were summarized in Figures 30 and 31.

In the H838 model, SMD-3236 demonstrated effective and dose-dependent tumor growth inhibition. SMD-3236 at 10 mg/kg and 30mg/kg suppressed the tumor growth by 64% and 68%, respectively, at the end day of treatment. In the H1299 model, SMD-3236 achieved tumor growth inhibition by 53% and 60% over the vehicle control treatment, respectively, at 10 mg/kg and 30 mg/kg, respectively. Of note, SMD-3236 at these doses didn't cause any weight loss or other signs of toxicity during the entire experiment in both tumor xenograft models. Taken together, SMD-3236 exhibited significant tumor growth inhibitory activity in H838 and H1299 SMARCA4-deficient xenograft models and was well tolerated in these efficacy experiments.

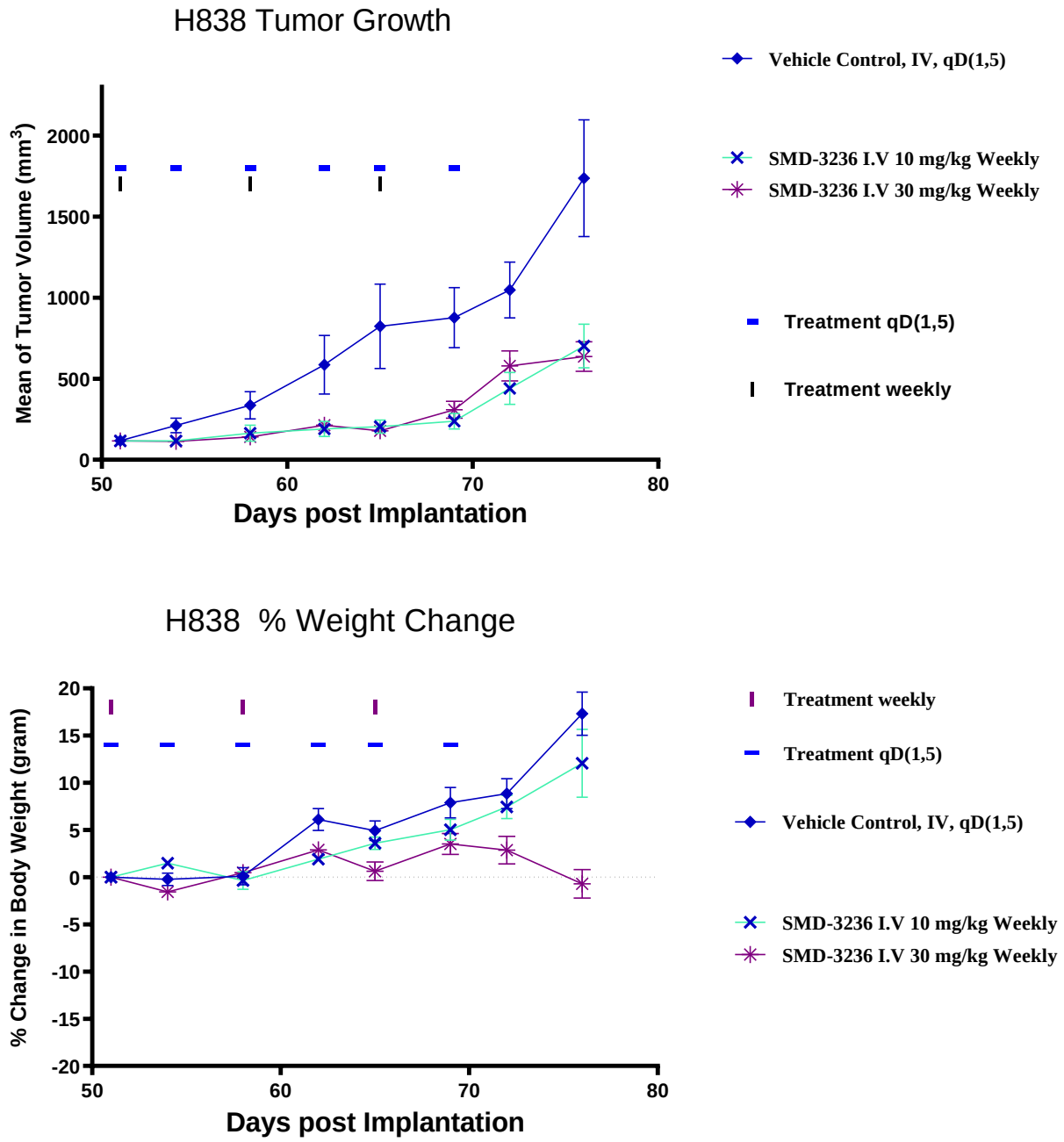


Figure 30. Efficacy study of SMD-3236 in the H838 xenograft tumor model in SCID mice.

.

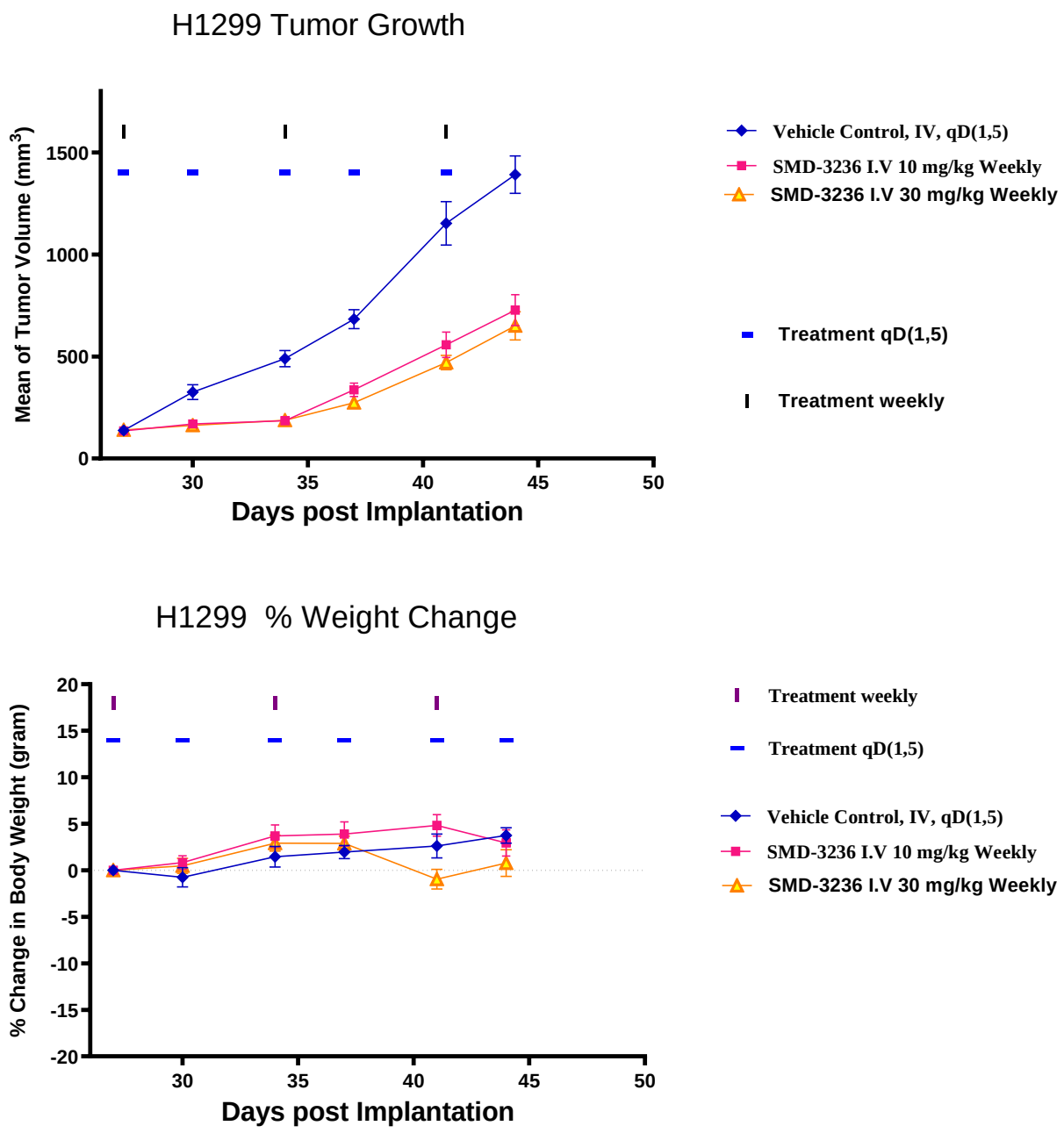


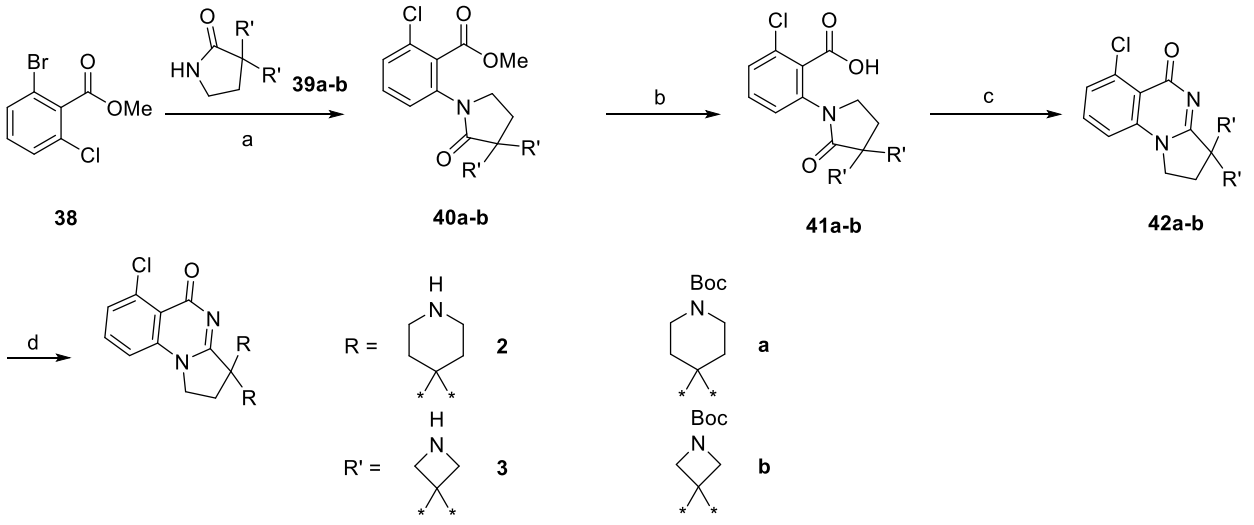
Figure 31. Efficacy study of SMD-3236 in the H1299 xenograft tumor model in SCID mice.

3.3 Chemical synthesis

The synthesis of the compounds **2-3** is shown in Scheme 5. Compounds **40a-b** were synthesized from methyl 2-bromo-6-chlorobenzoate (**38**) and spiro lactams (**39a-b**) by Buchwald-

Hartwig coupling. Basic hydrolysis of compounds **40a-b** resulted in free acids (**41a-b**), followed by imination and amide condensation to give cyclized compounds **42a-b**. Final deprotection of the Boc group gave compounds **1-2**.

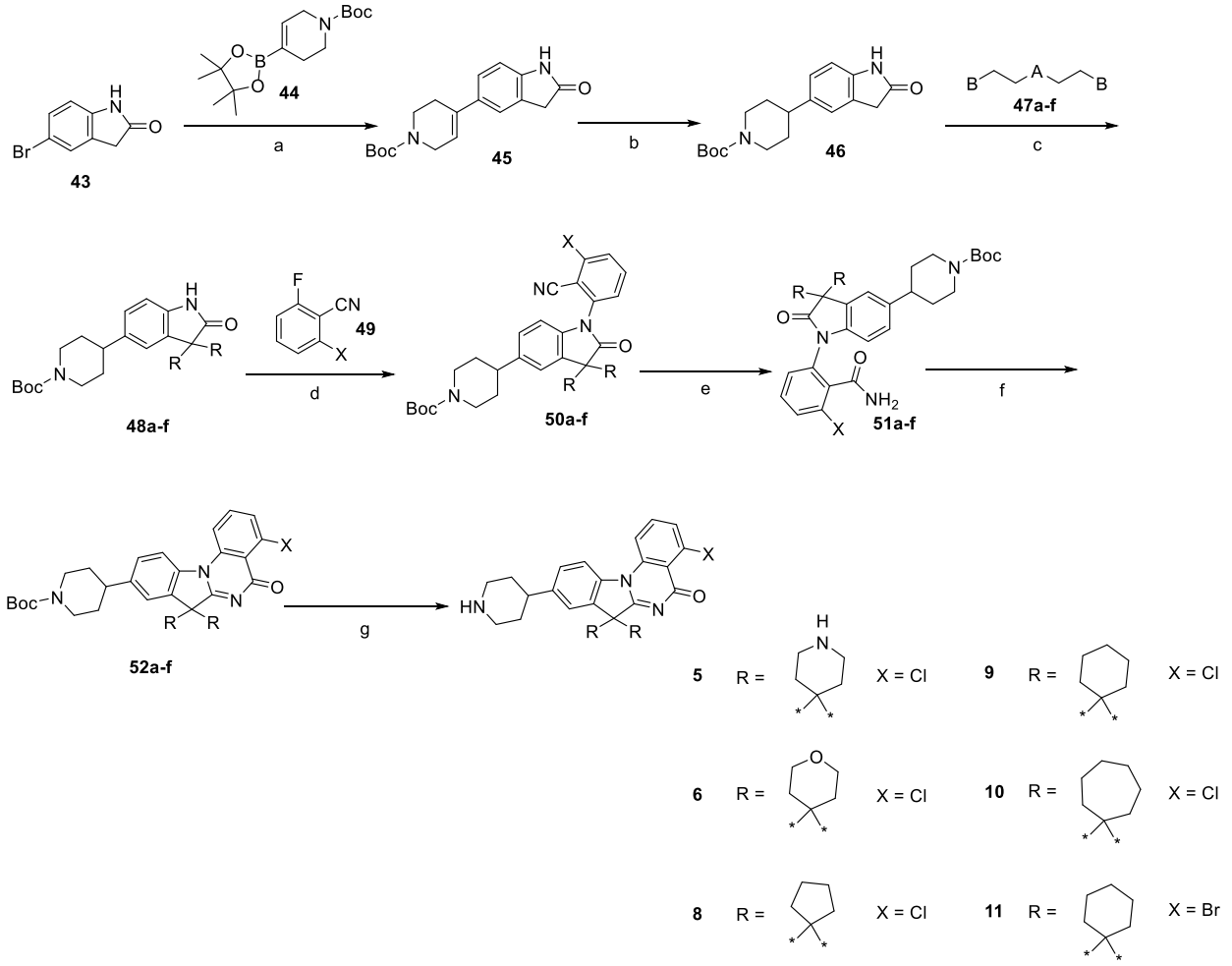
Scheme 5. Synthesis of Compounds 2-3 in chapter 3.



Reaction conditions: (a) Xantphos, $Pd_2(dba)_3$, Cs_2CO_3, dioxane, 100 °C, 16 h. (b) NaOH, MeOH/H_2O, rt, 3 h. (c) DIPEA, HATU, NH_3, CH_3CN, rt, 30 min. (d) TFA, DCM, rt, 30 min.

Compounds **5-6** and **8-11** were synthesized according to the procedure in Scheme 6. Compound **46** were prepared through the Suzuki coupling of compound **43** with boronic ester (**44**) and the following hydrogenation of double bond in compound **45**. Alkylation of compound **46** with different di-halo compounds (**47a-f**) gave the corresponding spiro compounds **48a-f**. Aromatic nucleophilic substitution of compounds **48a-f** with 2-chloro-6-fluorobenzonitrile (**49**) afforded compounds **50a-f**, which were then converted into amides (**51a-f**) through hydrogen peroxide mediated hydrolysis. Base assisted cyclization of final deprotection of compounds **51a-f** yielded compounds **5-6** and **8-11**.

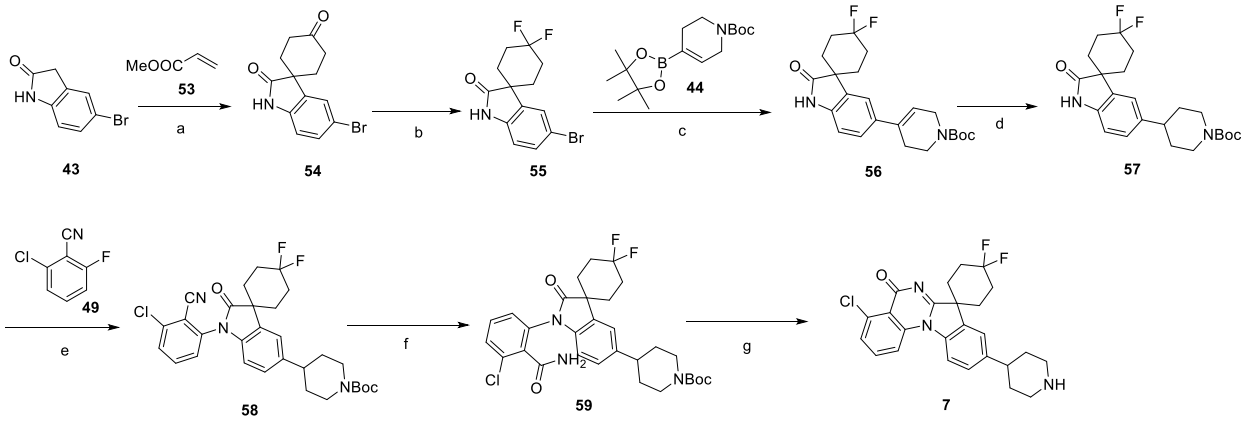
Scheme 6. Synthesis of Compounds 5-6, 8-11 in chapter 3.



Reaction conditions: (a) $Pd(dppf)Cl_2$, K_2CO_3, dioxane/H_2O, 100 °C, 10 h. (b) H_2, Pd/C, MeOH, rt, overnight. (c) LHMDS, THF, -78 °C to rt to 50 °C, 6 h. (d) Cs_2CO_3, CH_3CN, 80 °C, overnight. (e) H_2O_2, K_2CO_3, DMSO, 50 °C, 3 h. (f) NaOMe, MeOH, 65 °C, overnight. (g) TFA, DCM, rt, 0.5 h.

The synthesis of compound **7** is described in Scheme 7. Compound **43** was converted to spiro ketone (**54**) through a cascade of Micheal addition with Methyl acrylate, Dieckmann condensation and decarboxylation reaction, which was then turned into difluoro compound **55**. Compound **7** was then obtained following the similar steps described in Scheme 2.

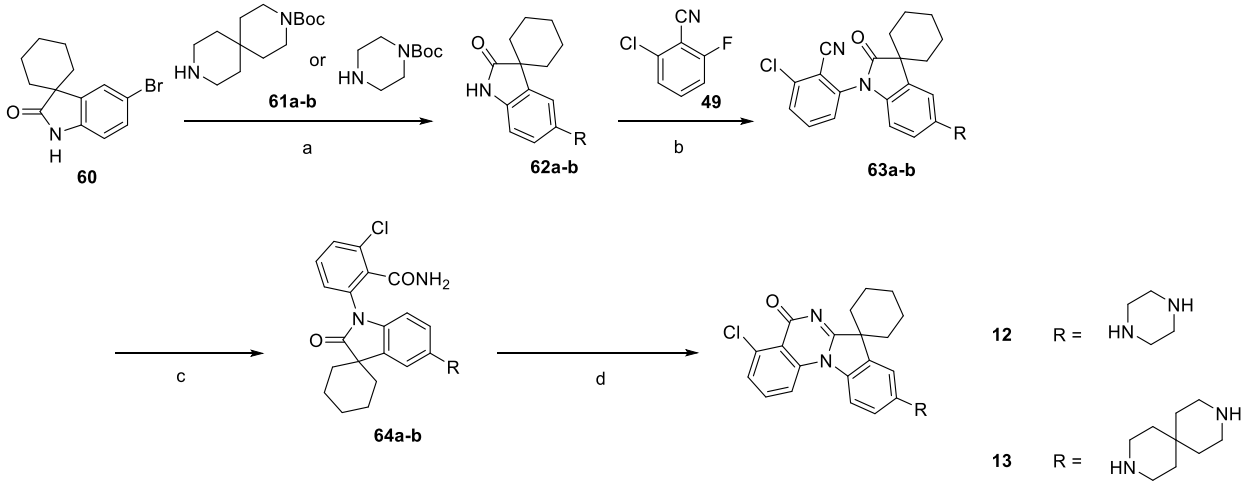
Scheme 7. Synthesis of Compound 7 in chapter 3.



Reaction conditions: (a) tBuOK, DMSO, rt to 45 °C to 85 °C in H_2O, 6 h. (b) DAST, DCM, rt, overnight. (c) $Pd(dppf)Cl_2$, K_2CO_3, dioxane/H_2O, 100 °C, 10 h. (d) H_2, Pd/C, MeOH, rt, overnight. (e) Cs_2CO_3, CH_3CN, 80 °C, overnight. (f) H_2O_2, K_2CO_3, DMSO, 50 °C, 3 h. (g) NaOMe, MeOH, 65 °C, overnight then TFA, DCM, rt, 0.5 h.

The synthesis of compounds **12-13** is shown in Scheme 8. Spiro oxindole (**60**) and compounds **61a-b** were coupled by Buchwald-Hartwig coupling reaction to afford compound **62a-b**, followed by similar steps described in Scheme 2 to give compounds **12-13**.

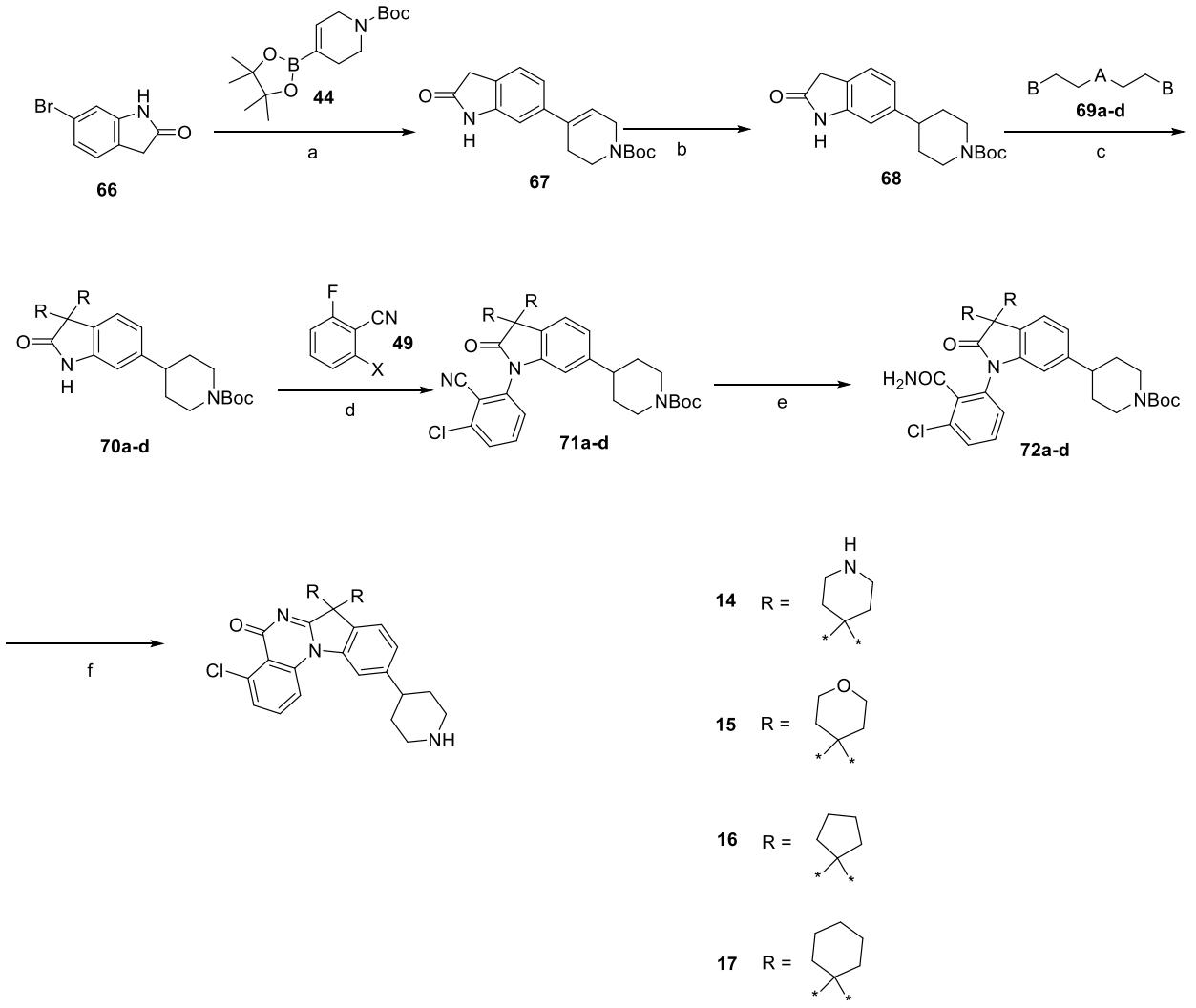
Scheme 8. Synthesis of Compounds 12-13 in chapter 3.



Reaction conditions: (a) Xphos, $Pd_2(dba)_3$, NaOtBu, dioxane, *mw*, 110 °C, 12 h. (b) NaH, DMF, 60 °C, 6 h. (c) H_2O_2, K_2CO_3, DMSO, 50 °C, 3 h. (d) NaOMe, MeOH, 65 °C, overnight then TFA, DCM, rt, 0.5 h.

As described in Scheme 9, synthesis of compounds **14-17** started from compound **66** with the bromide located at a different position, followed a similar procedure that was used in the synthesis of compounds **5-6**, **8-11**.

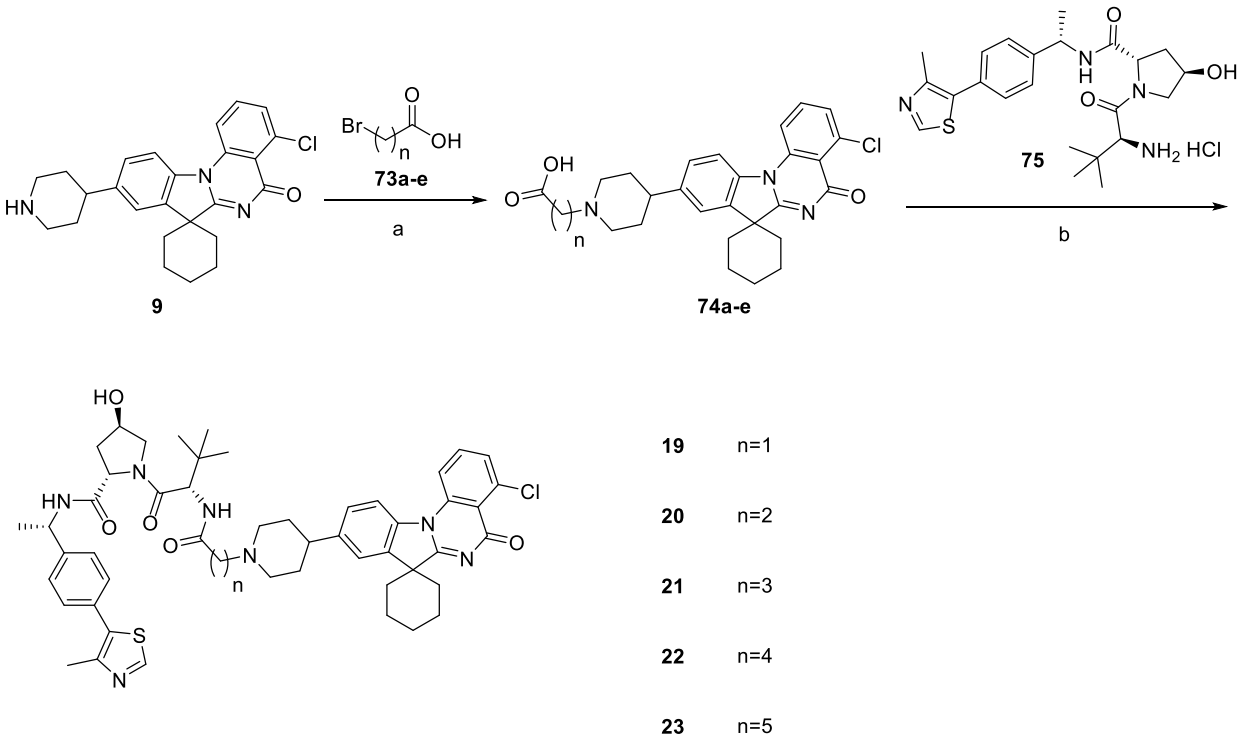
Scheme 9. Synthesis of Compounds 14-17 in chapter 3.



Reaction conditions: (a) $Pd(dppf)Cl_2$, K_2CO_3, dioxane/H_2O, 100 °C, 10 h. (b) H_2, Pd/C, MeOH, rt, overnight. (c) LHMDS, THF, -78 °C to rt to 50 °C, 6 h. (d) Cs_2CO_3, CH_3CN, 80 °C, overnight. (e) H_2O_2, K_2CO_3, DMSO, 50 °C, 3 h. (f) NaOMe, MeOH, 65 °C, overnight then TFA, DCM, rt, 0.5 h.

The synthesis of compounds **19-23** is described in Scheme 10. Bromo carboxylic acids (**73a-e**) were installed into compound **9** to give intermediates **74a-e**, which underwent a subsequent step of amide coupling with VHL ligand **75** to yield compounds **19-23**.

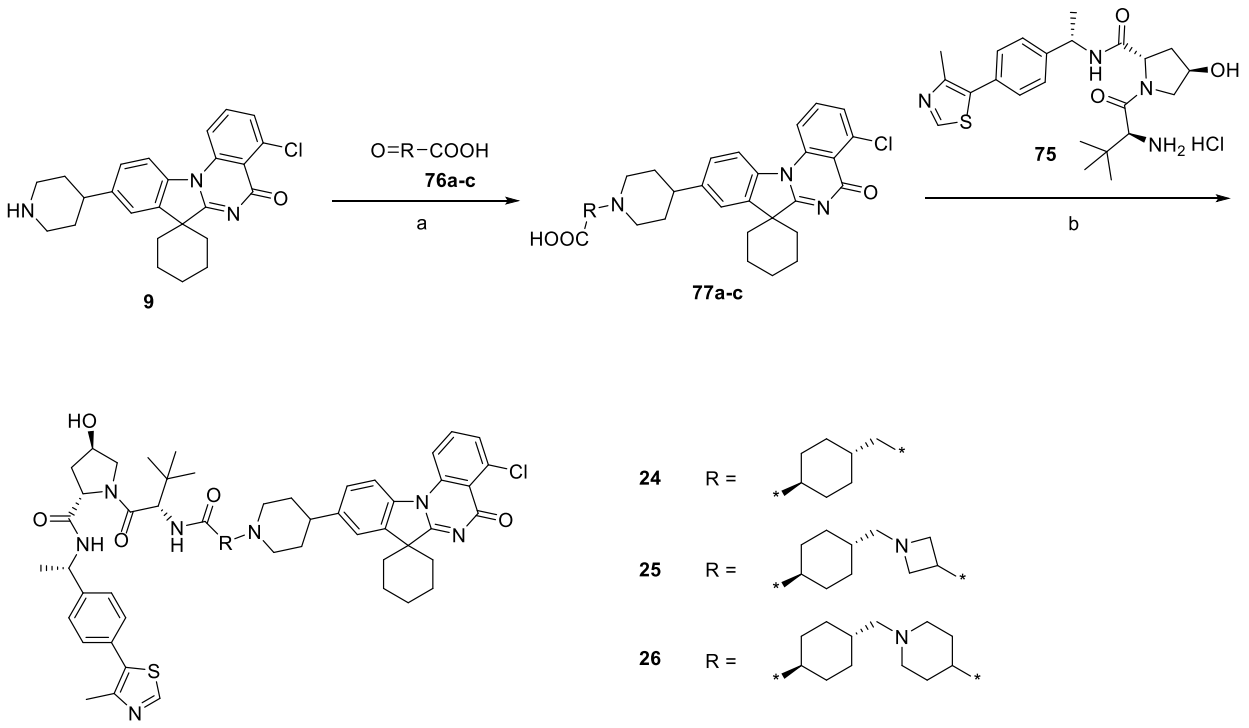
Scheme 10. Synthesis of Compounds 19-23 in chapter 3.



Reaction conditions: (a) DIPEA, DMF, 60 °C, 1 h. (b) HATU, DIPEA, DMF, rt, 30 min.

Compounds **24-26** were synthesized following the procedure in Scheme 11. Compound **9** was converted into substituted carboxylate acids **77a-c** by reductive amination with ketones or aldehydes **76a-c**. A final step of amide coupling with VHL ligand **75** yielded compounds **24-26**.

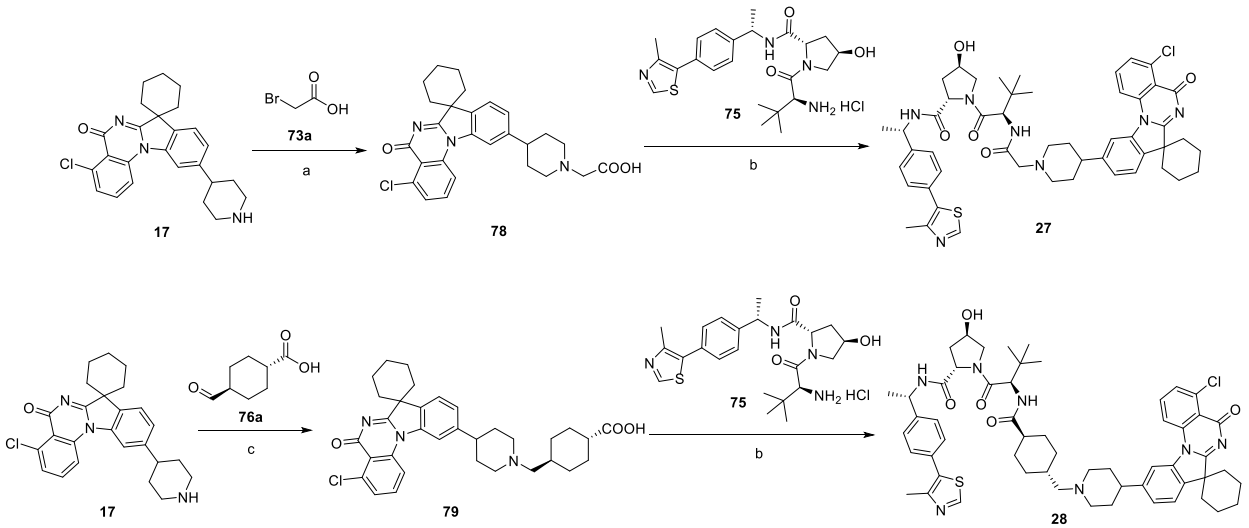
Scheme 11. Synthesis of Compounds 24-26 in chapter 3.



Reaction conditions: (a) $NaBH(OAc)_3$, AcOH, DCE/DMF, rt, 6 h. (b) HATU, DIPEA, DMF, rt, 30 min.

The synthesis of compounds **27** and **28** is shown in Scheme 12, which was similar to that for compounds **19** and **24**, but using a different SMARCA ligand (**17**).

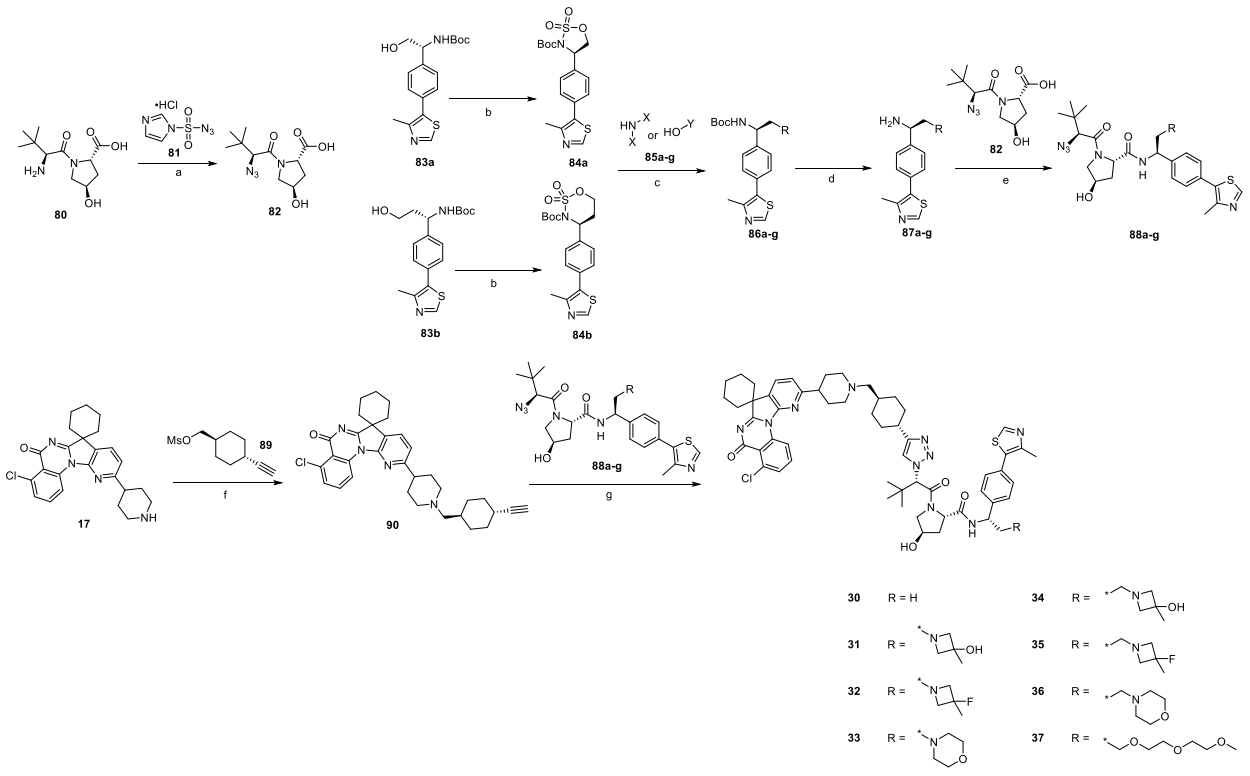
Scheme 12. Synthesis of Compounds 27 and 28 in chapter 3.



Reaction conditions: (a) DIPEA, DMF, 60 °C, 1 h. (b) HATU, DIPEA, DMF, rt, 30 min. (c) $NaBH(OAc)_3$, AcOH, DCE/DMF, rt, 6 h.

The synthesis of compounds **30-37** is shown in Scheme 13. Azide-containing VHL ligand fragment **82** was synthesized by compound **80** reacting with 1*H*-imidazole-1-sulfonyl azide hydrochloride (**81**). VHL ligand fragments **88a-g** were synthesized from commercially available compounds **83a-b**, followed by sequential conversion to cyclized compounds **84a-b**, ring opening by compounds **85a-g**, deprotection of Boc and amide coupling with fragment **82**. Compound **17** reacted with alkyne **89** to yield compound **90**, followed by conjugating with VHL ligand fragments **88a-g** via click reaction to afford compounds **30-37**.

Scheme 13. Synthesis of Compounds 30-37 in chapter 3.



Reaction conditions: (a) K_2CO_3, $CuSO_4$, MeOH, rt, 18 h. (b) $SOCl_2$, TEA, imidazole, DCM, -78 °C to rt, 3 h then $NaIO_4$, $RuCl_3$, CH_3CN/H_2O, 0 °C, 1 h. (c) DIPEA, CH_3CN, rt, 3 h. (d) TFA, DCM, rt, 0.5 h. (e) DIPEA, HATU, DMF, rt, 15 min. (f) DIPEA, DMF, 90 °C, 12 h. (g) $CuSO_4$, (+)-Sodium L-ascorbate, $tBuOH/H_2O$, rt, 12 h.

3.4 Summary

In this study, we aimed to identify a new class of potent and selective SMARCA2 PROTAC degraders with improved ADME properties. We first designed a novel series of spiro SMARCA bromodomain ligands using structure-based strategy with some of the best compounds demonstrating low nanomolar binding affinities, which were then employed in the synthesis of our next-generation selective SMARCA2 PROTAC degraders. Through extensive optimization of the linker length, linker composition, exit vector position in the SMARCA bromodomain ligand, as well as the binding affinity and solubility of the VHL ligand, our efforts have culminated in the identification of compound 33 (SMD-3236). SMD-3236 achieves DC_{50} = 0.5 nM and D_{max} = 96% for SMARCA2 protein in the HiBit degradation assay. Impressively, SMD-3236 only has a D_{max} = 41% for SMARCA4 protein, which translates into a S2/S4 DC_{50} ratio of over 1000 folds and a ΔD_{max} of 55%. Mechanistic and kinetic studies show that SMD-3236 is a bona fide SMARCA2 selective degrader with a rapid degradation profile. SMD-3236 potently inhibits the growth of SMARCA4-deficient cancer cells while has minimal effects in inhibiting the growth of SMARCA4-wildtype cancer cells, and is 9-16 times more potent than our previously reported SMD-3040. SMD-3236 achieves durable a pharmacodynamic effect in reducing SMARCA2 protein levels while increasing SMARCA4 protein levels in mice tumor models upon a single intravenous dosage. SMD-3236 displays excellent plasma and microsomal stability and little CYP inhibition or hERG liability. SMD-3236 has an excellent intravenous PK profile in mice and rats. Once a week intravenous administration of SMD-3236 effectively inhibits the tumor growth in SMARCA4-deficient H1299 and H838 xenograft tumor models in mice without showing any sign of toxicity. Collectively, our data demonstrate that SMD-3236 is a highly potent and selective

SMARCA2 PROTAC degrader suitable for advanced preclinical studies, and future optimization of SMD-3236 might lead to development candidates for the treatment of human cancers with SMARCA4 deficiency.

3.5 Experimental section

Chemistry: General Experiment and Information. Unless otherwise noted, all purchased reagents were used as received without further purification. ^{1}H NMR and ^{13}C NMR spectra were recorded on a Bruker Avance 400 MHz spectrometer. ^{1}H NMR spectra are reported in parts per million (ppm) downfield from tetramethylsilane. All ^{13}C NMR spectra are reported in ppm and obtained with 1H decoupling. In reported spectral data, the format (δ) chemical shift (multiplicity, J values in Hz, integration) is used with the following abbreviations: s = singlet, d = doublet, t = triplet, q = quartet, m = multiplet. Mass spectral (MS) analysis was carried out with a Waters ultraperformance liquid chromatography (UPLC) mass spectrometer. The final compounds were all purified by C18 reverse-phase preparative high-performance liquid chromatography (HPLC) column with solvent A (0.1% TFA in H_2O) and solvent B (0.1% TFA in CH_3CN) as eluents. The purity of all the final compounds was confirmed to be >95% by UPLC−MS or UPLC.

6'-chloro-1',2'-dihydro-5'H-spiro[piperidine-4,3'-pyrrolo[1,2-a]quinazolin]-5'-one (2)

To a solution of compound **38** (500 mg, 2 mmol, 1 equiv) in dioxane (30 mL) was added compound **39a** (560 mg, 2.2 mmol, 1.1 equiv), $Pd_2(dba)_3$ (88 mg, 0.1 mmol, 0.05 equiv), (9,9-dimethyl-9H-xanthene-4,5-diyl)bis(diphenylphosphane) (116 mg, 0.2, 0.1 equiv), Cs_2CO_3 (1.3 g, 4.0 mmol, 2 equiv). Under protection of nitrogen, the mixture was refluxed for 16 h. After cooling to room temperature, the mixture was filtered and the filtrate was purified by C-18 reversal column (elution solvents: CH_3CN/H_2O from 10% to 100%, 0.1%TFA) to get compound **40a** (620 mg, 73%). ESI MS m/z: 423.16 $[M+H]^+$.

To a solution of tert-butyl compound **40a** (620 mg, 1.47 mmol, 1 equiv) in a mixture solution of $MeOH/H_2O$ (30/3 mL) was added NaOH (175 mg, 4.4 mmol, 3 equiv). The mixture was stirred for 3 h at room temperature. After reaction, the methanol was removed under reduce pressure. The residue aqueous phase was neutralized by TFA to week acidic (pH: 3-4). Extraction with DCM twice, combined DCM phases was washed by brine once, after dried and removing, the crude product **41a** (600 mg, 99%) was obtained and can be used in the next step directly. ESI MS m/z: 409.16 $[M+H]^+$.

To a solution of received acid product **41a** (600 mg, 1.47 mmol, 1.0 equiv) in CH_3CN (20 mL) was added HATU (725 mg, 1.91 mmol, 1.3 equiv) and DIPEA (570 mg, 4.4 mmol, 3.0 equiv). under stirring, the mixture was bubbled by NH_3 gas for 2 minutes. Then let mixture stirred for 30 min at room temperature. The reaction solution was purified by prepared HPLC C-18 reversal column to get compound **42a** (160 mg, 28%). ESI MS m/z: 390.16 $[M+H]^+$.

The obtained compound **42a** (160 mg, 0.26 mmol) was dissolved into DCM (5 mL), then TFA (5 mL) was added. The mixture was stirred for 30 minutes. After concentrating, the residue was

purified by prepared HPLC C-18 reversal column to get compound **2** (60 mg, 81%). ESI MS m/z: 290.10 $[M+H]^+$.

6'-chloro-1',2'-dihydro-5'H-spiro[azetidine-3,3'-pyrrolo[1,2-a]quinazolin]-5'-one (3)

Compound **3** was synthesized by a procedure identical to that used for compound **2**. ESI MS m/z: 262.04 $[M+H]^+$.

4-chloro-9-(piperidin-4-yl)-5H-spiro[indolo[1,2-a]quinazoline-7,4'-piperidin]-5-one (5)

To a flask was added compound **43** (2.00 g, 9.40 mmol, 1.0 eq), compound **44** (2.92 g, 9.40 mmol, 1.0 eq), $Pd(dppf)Cl_2$ (692 mg, 0.94 mmol, 0.1 eq), K_2CO_3 (2.61 g, 18.80 mmol, 2.0 eq). Then a mixture solvent of dioxane and water (50 mL and 10 mL) was added to the flask. The suspension was protected by nitrogen and heated to reflux for 10 h. LC-MS showed the reaction completed. The reaction mixture was diluted by ethyl acetate (the formed solid was removed by celite filtration), washed by brine. After removing solvent, the residue was purified directly by C-18 reversal column chromatography (elution solvents: CH_3CN/H_2O from 10% to 100%, 0.1%TFA) to get compound **45** (2.45 g, 86%) as a slight yellow solid. ESI MS m/z: 315.16 $[M+H]^+$.

Under nitrogen protection, to a solution of compound **45** (2.40 g, 7.63 mmol, 1.0 eq) in methanol (50 mL) was added palladium on carbon (0.6 g, 50% wt water, 10% wt palladium) cautiously. Then mixture was stirred overnight under hydrogen atmosphere (1 atm). After reaction, the mixture was filtered by celite. After removing solvent, the residue was purified by silica-gel column chromatography (ethyl acetate/hexane = 1/1) to obtained compound **46** (2.10 g, 87%) as a white solid. ESI MS m/z: 317.18 $[M+H]^+$. 1H NMR (400 MHz, CDCl3) δ 8.26 (s, 1H), 7.18 – 6.98 (m,

2H), 6.83 (d, J = 8.0 Hz, 1H), 4.26 (d, J = 12.3 Hz, 2H), 3.53 (d, J = 1.1 Hz, 2H), 2.81 (t, J = 12.7 Hz, 2H), 2.62 (tt, J = 12.0, 3.7 Hz, 1H), 1.80 (m, 2H), 1.60 (dd, J = 12.6, 4.2 Hz, 2H), 1.50 (s, 9H). Under nitrogen protection, to a solution of compound **46** (2.10 g, 6.64 mmol, 1.0 eq) in dry THF (40 mL) was added LHMDS (21.9 mL, 21.9 mmol, 3.3 eq) slowly at -78 °C. Then mixture was stirred 30 min. After that, compound **47a** (1.61 g, 6.64 mmol, 1.0 eq) was added. The mixture was warmed to rt and kept for 2 h, then the mixture was heated to 50 °C for 4 h. After reaction, the mixture was quenched by NH_4Cl solution, diluted by ethyl acetate (50 mL). the organic phase was collected, dried by anhydrous Na_2SO_4. After removing solvent, the residue was purified by silica-gel column chromatography (ethyl acetate/hexane = 1/1) to obtain compound **48a** (650 mg, 20%) as a white solid. ESI MS m/z: 486.30 $[M+H]^+$.

To a flask was added compound **48a** (600 mg, 1.24 mmol, 1.0 eq), compound **49** (211 mg, 1.36 mmol, 1.1 eq), Cs_2CO_3 (805 g, 2.47 mmol, 2.0 eq). Then CH_3CN (80 mL and 10 mL) was added to the flask. The suspension was refluxed overnight. After concentration, the residue was redissolved into a mixture of ethyl acetate and water. The organic layer was collected. After concentration, the residue was purified directly by C-18 reversal column chromatography (elution solvents: CH_3CN/H_2O from 10% to 100%, 0.1%TFA) to get target product compound **50a** (720 mg, 94%) as a slight yellow solid. ESI MS m/z: 621.28 $[M+H]^+$.

To a solution of DMSO (10 mL) was added compound **50a** (300 mg, 0.48 mmol, 1 eq), K_2CO_3 (133 mg, 0.97 mmol, 2 eq) and H_2O_2 (2 mL). The mixture was warmed to 50 °C and stirred for 16 h. after reaction, the mixture was transferred to C-18 reversal column (elution solvents: CH_3CN/H_2O from 10% to 100%, 0.1%TFA) to purify directly to get compound **51a** (278 mg, 90%). ESI MS m/z: 639.30 $[M+H]^+$.

Compound **51a** (250 mg, 0.39 mmol, 1 eq) was dissolved into dry methanol (30 mL), then a MeONa (211 mg,3.9 mmol, 10 eq) was added. Followed by refluxing overnight under anhydrous condition, LC-MS showed about 50% conversion. The reaction solution was cooled by dry-ice, then TFA (0.5 mL) was added to neutralized the MeONa. The solvent was removed under rotatory evaporator and the received residue was dissolved into a mixture of DCM and water, the DCM layer was collected and dried by anhydrous Na_2SO_4. After removing solvent, the residue was purified by C-18 (elution solvents: CH_3CN/H_2O from 10% to 100%, 0.1%TFA) directly to get compound **52a** (110 mg, 45 %). ESI MS m/z: 521.28 $[M\text{-Boc}+H]^+$.

To a solution of compound **52a** (10 mg, 0.24 mmol, 1 equiv) in DCM (5 mL) was added TFA (5 mL). The mixture was stirred for 0.5 h. After removing solvent, the mixture was purified by pre-HPLC C-18 reversal column to get target product compound **5** as a white solid (86 mg, 86%). ESI MS m/z: 421.17 $[M+H]^+$.

4-chloro-9-(piperidin-4-yl)-2',3',5',6'-tetrahydro-5H-spiro[indolo[1,2-a]quinazoline-7,4'-pyran]-5-one (6)

Compound **6** was synthesized by a procedure identical to that used for compound **5**. ESI MS m/z: 422.16 $[M+H]^+$. ^1H NMR (400 MHz, DMSO) δ 8.72 (d, J = 11.6 Hz, 1H), 8.45 (s, 1H), 8.39 (d, J = 8.6 Hz, 1H), 8.12 (d, J = 8.6 Hz, 1H), 7.83 (t, J = 8.3 Hz, 1H), 7.72 (d, J = 1.8 Hz, 1H), 7.64 (d, J = 7.8 Hz, 1H), 7.37 (dd, J = 8.5, 1.8 Hz, 1H), 4.31 (ddd, J = 12.0, 8.6, 3.6 Hz, 2H), 3.89 (dt, J = 11.8, 4.6 Hz, 2H), 3.43 (d, J = 12.5 Hz, 2H), 3.14 – 2.91 (m, 3H), 2.12 – 1.76 (m, 8H).

4'-chloro-4,4-difluoro-9'-(piperidin-4-yl)-5'H-spiro[cyclohexane-1,7'-indolo[1,2-a]quinazolin]-5'-one (7)

To a flask was added compound **43** (3 g, 14.2 mmol, 1.0 eq) and DMSO (7 mL). Potassium tert-butoxide (0.085 g, 0.80 mmol, 0.05 eq) was added and the mixture was stirred at room temperature for 10 minutes. The mixture was heated to 45 °C and methyl acrylate (4.00 mL, 44.4 mmol, 3.1 eq) was added dropwise over 70 minutes. After addition, the mixture was stirred at 45 °C for 1 hour and then further potassium tert-butoxide (955 mg, 8.5 mmol, 0.6 eq) was added four times over 30 minutes keeping the temperature below 50 °C. The mixture was then heated to 100 °C and stirred for 1.5 hours and water (45 mL) was added and heating was continued at 85 °C for 4 hours. After cooling to room temperature, the mixture was extracted with EtOAc (50 mL) 3 times and the combined organic layer was washed with water (100 mL) and saturated brine (100 mL), dried over Na_2SO_4 and filtered. Solvent was removed and the residue was purified by column chromatography (0-60% 0-60% Ethyl acetate in hexanes) to give compound **54** (960 mg, 23%).

To a solution of compound **54** (130 mg, 0.44 mmol, 1.0 eq) in DCM (4 mL) was added (Diethylamino)sulfur trifluoride (0.17 mL, 1.30 mmol, 3.0 eq) dropwise. The mixture was stirred at room temperature overnight and then added dropwise to an ice-water mixture. After stirring for 20 minutes, saturated sodium bicarbonate solution (5 mL) was added and the mixture was extracted with DCM (5 mL) 3 times. The combined organic layer was dried over $MgSO_4$. Solvent was removed and the residue was purified by flash chromatography (0-60% Ethyl acetate in hexanes) to give compound **55** (90 mg, 64 %).

The rest of the synthetic procedure for compound **7** was identical to that used for compound **5**. ESI MS m/z: 456.18 $[M+H]^+$. ^1H NMR (400 MHz, MeOD) δ 7.95 – 7.87 (m, 1H), 7.83 (dd, J = 8.3, 1.1 Hz, 1H), 7.65 (dd, J = 7.9, 1.1 Hz, 1H), 7.36 (d, J = 1.8 Hz, 1H), 7.22 (dd, J = 8.2, 1.8 Hz, 1H),

6.70 (d, *J* = 8.1 Hz, 1H), 4.59 (s, 1H), 3.56 – 3.49 (m, 2H), 3.16 (td, *J* = 13.0, 3.0 Hz, 2H), 2.97 (tt, *J* = 12.3, 3.6 Hz, 1H), 2.73 – 2.56 (m, 2H), 2.30 – 2.05 (m, 8H), 1.92 (qd, *J* = 13.3, 4.0 Hz, 2H).

4'-chloro-9'-(piperidin-4-yl)-5'H-spiro[cyclopentane-1,7'-indolo[1,2-a]quinazolin]-5'-one (8)

Compound **8** was synthesized by a procedure identical to that used for compound **5**. ESI MS m/z: 406.16 $[M+H]^+$. ^{1}H NMR (400 MHz, MeOD) δ 8.41 (dd, J = 8.7, 1.0 Hz, 1H), 8.10 (d, J = 8.5 Hz, 1H), 7.87 (dd, J = 8.6, 7.9 Hz, 1H), 7.68 (dd, J = 8.0, 0.9 Hz, 1H), 7.53 (d, J = 1.9 Hz, 1H), 7.46 (dd, J = 8.6, 1.9 Hz, 1H), 3.56 (d, J = 12.9 Hz, 2H), 3.20 (t, J = 12.7 Hz, 2H), 3.13 – 3.02 (m, 1H), 2.40 (dd, J = 12.3, 5.0 Hz, 2H), 2.28 (s, 2H), 2.14 (d, J = 9.3 Hz, 6H), 1.99 (qd, J = 13.3, 4.2 Hz, 2H), 1.20 (t, J = 7.1 Hz, 1H).

4'-chloro-9'-(piperidin-4-yl)-5'H-spiro[cyclohexane-1,7'-indolo[1,2-a]quinazolin]-5'-one (9)

Compound **9** was synthesized by a procedure identical to that used for compound **5**. ESI MS m/z: 420.18 $[M+H]^+$. ^{1}H NMR (400 MHz, MeOD) δ 8.35 (dd, J = 8.8, 1.0 Hz, 1H), 8.03 (d, J = 8.5 Hz, 1H), 7.82 (dd, J = 8.7, 7.9 Hz, 1H), 7.75 (d, J = 1.9 Hz, 1H), 7.61 (dd, J = 7.9, 0.9 Hz, 1H), 7.45 (dd, J = 8.5, 1.8 Hz, 1H), 3.63 – 3.54 (m, 2H), 3.22 (td, J = 12.9, 3.1 Hz, 2H), 3.08 (tt, J = 12.1, 3.7 Hz, 1H), 2.23 – 1.92 (m, 8H), 1.92 – 1.60 (m, 6H).

4'-chloro-9'-(piperidin-4-yl)-5'H-spiro[cycloheptane-1,7'-indolo[1,2-a]quinazolin]-5'-one (10)

Compound **10** was synthesized by a procedure identical to that used for compound **5**. ESI MS m/z: 434.20 $[M+H]^+$. ^{1}H NMR (400 MHz, MeOD) δ 8.38 (dd, J = 8.7, 1.0 Hz, 1H), 8.06 (d, J = 8.5 Hz, 1H), 7.89 – 7.80 (m, 1H), 7.69 – 7.62 (m, 2H), 7.46 (dd, J = 8.5, 1.9 Hz, 1H), 3.64 – 3.53 (m, 2H),

3.21 (td, J = 12.9, 3.0 Hz, 2H), 3.08 (tt, J = 12.2, 3.7 Hz, 1H), 2.25 – 2.09 (m, 6H), 2.09 – 1.70 (m, 11H).

4'-bromo-9'-(piperidin-4-yl)-5'H-spiro[cyclohexane-1,7'-indolo[1,2-a]quinazolin]-5'-one (11)

Compound **11** was synthesized by a procedure identical to that used for compound **5**. ESI MS m/z: 644.14 $[M+H]^+$. ^1H NMR (400 MHz, MeOD) δ 8.40 (dd, J = 8.6, 1.0 Hz, 1H), 8.04 (d, J = 8.5 Hz, 1H), 7.85 (dd, J = 7.9, 0.9 Hz, 1H), 7.78 – 7.72 (m, 1H), 7.72 – 7.67 (m, 1H), 7.44 (dd, J = 8.5, 1.9 Hz, 1H), 3.59 (dt, J = 11.5, 2.7 Hz, 2H), 3.22 (td, J = 12.9, 3.1 Hz, 2H), 3.08 (tt, J = 12.1, 3.7 Hz, 1H), 2.29 – 1.93 (m, 8H), 1.93 – 1.58 (m, 6H).

4'-chloro-9'-(piperazin-1-yl)-5'H-spiro[cyclohexane-1,7'-indolo[1,2-a]quinazolin]-5'-one (12)

To a microwave tube was added added compound **60** (70 mg, 0.25 mmol, 1.0 eq), tert-butyl piperazine-1-carboxylate **61a** (92 mg, 0.50 mmol, 2.0 eq), $Pd_2(dba)_3$ (23 mg, 0.025 mmol, 0.1 eq), XPhos (12 mg, 0.025 mmol, 0.1 eq), NaOtBu (48 mg, 0.50 mmol, 2.0 eq). Dioxane(2 mL) was added and the microwave tube was flushed with nitrogen. The mixture was stirred at 110°C in microwave reactor for 12 h. After cooling to room temperature, solvent was removed and the residue was purified by flash chromatography (0-100 % Ethyl acetate in hexanes) to give compound **62a** (30 mg, 31 %).

To a stirred solution of compound **62a** (30 mg, 0.077 mmol, 1.0 eq) in DMF (1 mL) was added NaH (60% wt in mineral oil, 4.6 mg, 0.12 mmol, 1.5 eq). The reaction mixture was stirred at room temperature for 15 min, then compound **49** (13 mg, 0.085 mmol, 1.1 eq) was added. The reaction mixture was stirred at 60°C for 6 h. After cooling to room temperature, the mixture was diluted with saturated NH_4Cl solution (5 mL) and extracted with ethyl acetate (5 mL) 3 times. The organic

layer was washed with water (10 mL) and saturated brine (10 mL), dried over Na_2SO_4 and filtered. The solvent was removed and the residue was purified by flash chromatography (0-100 % Ethyl acetate in hexanes) to give compound **63a** (28 mg, 69 %).

To a stirred solution of compound **63a** (28 mg, 0.054 mmol, 1.0 eq) in DMSO (1mL) was added H_2O_2 (30% wt in H_2O, 0.2 mL) and K_2CO_3 (15 mg, 0.11 mmol, 2.0 eq). The reaction mixture was stirred at 50°C for 6 h. After cooling to room temperature, the mixture was purified by reverse phase flash chromatography (10-100% MeCN in H_2O, 0.1% TFA) to give compound **64a** (20 mg, 69 %).

To a stirred solution of compound **64a** (20 mg, 0.036 mmol, 1.0 eq) in dry MeOH (2 mL) was added sodium methoxide solution (0.5 M in MeOH, 1 mL, 0.50 mmol, 14 eq). The reaction mixture was stirred at 65°C for 12 h. After cooling to -78°C, TFA was added to adjust pH to 3 and the solvent was removed. The residue was dissolved in DCM (1 mL) and TFA (0.5 mL) and the rection mixture was stirred at room temperature for 2 h. The solvent was removed and the residue was purified by Prep-HPLC (20-100 % MeCN in H_2O, 0.1 % TFA) to give compound **12** (3.1 mg, 20 %). ESI MS m/z: 421.19 $[M+H]^+$. ^{1}H NMR (400 MHz, MeOD) δ 7.87 (t, *J* = 8.1 Hz, 1H), 7.79 (dd, *J* = 8.3, 1.1 Hz, 1H), 7.59 (dd, *J* = 8.0, 1.1 Hz, 1H), 7.30 (d, *J* = 2.4 Hz, 1H), 6.94 (dd, *J* = 8.5, 2.4 Hz, 1H), 6.64 (d, *J* = 8.5 Hz, 1H), 3.45 – 3.34 (m, 8H), 2.11 – 2.02 (m, 2H), 2.01 – 1.88 (m, 2H), 1.87 – 1.77 (m, 2H), 1.77 – 1.66 (m, 6H).

4'-chloro-9'-(3,9-diazaspiro[5.5]undecan-3-yl)-5'H-spiro[cyclohexane-1,7'-indolo[1,2-a]quinazolin]-5'-one (13)

Compound **13** was synthesized by a procedure identical to that used for compound **12**. ESI MS m/z: 489.28 $[M+H]^+$. ^{1}H NMR (400 MHz, MeOD) δ 7.96 – 7.88 (m, 1H), 7.88 (d, *J* = 2.4 Hz, 1H), 7.84 (dd, *J* = 8.3, 1.1 Hz, 1H), 7.63 (dd, *J* = 7.9, 1.1 Hz, 1H), 7.55 (dd, *J* = 8.6, 2.4 Hz, 1H), 6.85 (d, *J* = 8.6 Hz, 1H), 3.70 – 3.62 (m, 4H), 3.31 – 3.24 (m, 4H), 2.14 – 2.03 (m, 6H), 2.03 – 1.91 (m, 6H), 1.91 – 1.68 (m, 6H).

4-chloro-10-(piperidin-4-yl)-5H-spiro[indolo[1,2-a]quinazoline-7,4'-piperidin]-5-one (14)

Compound **14** was synthesized by a procedure identical to that used for compound **5**. ESI MS m/z: 421.19 $[M+H]^+$. ^{1}H NMR (400 MHz, MeOD) δ 8.46 (d, *J* = 8.5 Hz, 1H), 8.04 (s, 1H), 7.90 (t, *J* = 8.2 Hz, 1H), 7.71 (d, *J* = 7.8 Hz, 1H), 7.66 (d, *J* = 7.7 Hz, 1H), 7.42 (d, *J* = 7.6 Hz, 1H), 4.19 (t, *J* = 12.0 Hz, 2H), 3.58 (d, *J* = 12.4 Hz, 2H), 3.46 (d, *J* = 12.9 Hz, 2H), 3.30 – 3.15 (m, 3H), 2.45 (t, *J* = 12.4 Hz, 2H), 2.20 (d, *J* = 14.4 Hz, 4H), 2.07 (q, *J* = 13.1 Hz, 2H).

4-chloro-10-(piperidin-4-yl)-2',3',5',6'-tetrahydro-5H-spiro[indolo[1,2-a]quinazoline-7,4'-pyran]-5-one (15)

Compound **15** was synthesized by a procedure identical to that used for compound **5**. ESI MS m/z: 422.14 $[M+H]^+$. ^{1}H NMR (400 MHz, MeOD) δ 8.44 (dd, *J* = 8.6, 0.9 Hz, 1H), 8.02 (d, *J* = 1.3 Hz, 1H), 7.92 – 7.80 (m, 2H), 7.73 – 7.62 (m, 1H), 7.42 – 7.33 (m, 1H), 4.50 – 4.42 (m, 2H), 4.00 (dt, *J* = 11.8, 4.8 Hz, 2H), 3.58 (d, *J* = 12.6 Hz, 2H), 3.28 – 3.11 (m, 3H), 2.62 (s, 1H), 2.21 (d, *J* = 14.1 Hz, 2H), 2.15 – 1.99 (m, 6H).

4'-chloro-10'-(piperidin-4-yl)-5'H-spiro[cyclopentane-1,7'-indolo[1,2-a]quinazolin]-5'-one (16)

Compound **16** was synthesized by a procedure identical to that used for compound **5**. ESI MS m/z: 406.20 $[M+H]^+$. ^1H NMR (400 MHz, MeOD) δ 8.41 (dd, *J* = 8.6, 1.0 Hz, 1H), 7.97 (d, *J* = 1.5 Hz, 1H), 7.86 (dd, *J* = 8.6, 7.9 Hz, 1H), 7.66 (dd, *J* = 7.9, 0.9 Hz, 1H), 7.61 (d, *J* = 7.8 Hz, 1H), 7.36 (dd, *J* = 7.9, 1.3 Hz, 1H), 3.58 (d, *J* = 13.0 Hz, 2H), 3.22 (td, *J* = 13.1, 3.1 Hz, 2H), 3.17 – 3.09 (m, 1H), 2.42 – 2.31 (m, 2H), 2.31 – 2.17 (m, 4H), 2.17 – 2.03 (m, 4H), 2.03 – 1.96 (m, 2H).

4'-chloro-10'-(piperidin-4-yl)-5'H-spiro[cyclohexane-1,7'-indolo[1,2-a]quinazolin]-5'-one (17)

Compound **17** was synthesized by a procedure identical to that used for compound **5**. ESI MS m/z: 420.18 $[M+H]^+$. ^1H NMR (400 MHz, MeOD) δ 8.42 (dd, *J* = 8.6, 1.0 Hz, 1H), 8.02 – 7.97 (s, 1H), 7.92 – 7.81 (m, 2H), 7.66 (dd, *J* = 8.0, 0.8 Hz, 1H), 7.36 (dd, *J* = 7.9, 1.4 Hz, 1H), 3.59 (d, *J* = 12.6 Hz, 2H), 3.28 – 3.09 (m, 3H), 2.22 (d, *J* = 14.2 Hz, 2H), 2.15 – 2.01 (m, 6H), 1.95 – 1.87 (m, 3H), 1.77 (q, *J* = 6.7, 5.7 Hz, 3H).

(2S,4R)-1-((S)-2-(2-(4-(4'-chloro-5'-oxo-5'H-spiro[cyclohexane-1,7'-indolo[1,2-a]quinazolin]-9'-yl)piperidin-1-yl)acetamido)-3,3-dimethylbutanoyl)-4-hydroxy-N-((S)-1-(4-(4-methylthiazol-5-yl)phenyl)ethyl)pyrrolidine-2-carboxamide (19)

To a solution of compound **9** (50 mg, 0.12 mmol, 1.0 equiv.) in DMF (2 mL) was added compound **73a** (16.5 mg, 0.12mmol, 0.1 equiv.) and DIPEA (46.2 mg, 0.36 mmol, 3.0 equiv.). The mixture was stirred for 1 h at 60 °C. The residue was purified by C-18 reversal column (elution solvents: CH_3CN/H_2O from 10% to 100%, 0.1%TFA) to get compound **74a** (36 mg, 63%). ESI MS m/z: 478.18 $[M+H]^+$.

To a solution of compound **74a** (20 mg, 0.041 mmol, 1.0 equiv.) and VHL ligand **75** (13.8 mg, 0.041 mmol, 1.0 equiv.) in DMF (2 mL) was added HATU (24.0 mg, 0.063 mmol, 1.5 equiv.) and DIPEA (16.2 mg, 0.13 mmol, 3 equiv.). The mixture was stirred for 1 h. Water (10 mL) was added to quench the reaction and product was extracted with ethyl acetate twice (10 mL×2). Combined organic phases were washed by brine twice, dried by anhydrous Na_2SO_4. After removing solvent, the received crude product was purified by pre-HPLC to get compound **19** (23.0 mg, 61%). ESI MS m/z: 904.40 $[M+H]^+$.

(2S,4R)-1-((S)-2-(3-(4-(4'-chloro-5'-oxo-5'H-spiro[cyclohexane-1,7'-indolo[1,2-a]quinazolin]-9'-yl)piperidin-1-yl)propanamido)-3,3-dimethylbutanoyl)-4-hydroxy-N-((S)-1-(4-(4-methylthiazol-5-yl)phenyl)ethyl)pyrrolidine-2-carboxamide (20)

Compound **20** was synthesized by a procedure identical to that used for compound **19**. ESI MS m/z: 918.41 $[M+H]^+$.

(2S,4R)-1-((S)-2-(4-(4-(4'-chloro-5'-oxo-5'H-spiro[cyclohexane-1,7'-indolo[1,2-a]quinazolin]-9'-yl)piperidin-1-yl)butanamido)-3,3-dimethylbutanoyl)-4-hydroxy-N-((S)-1-(4-(4-methylthiazol-5-yl)phenyl)ethyl)pyrrolidine-2-carboxamide (21)

Compound **21** was synthesized by a procedure identical to that used for compound **19**. ESI MS m/z: 932.42 $[M+H]^+$.

(2S,4R)-1-((S)-2-(5-(4-(4'-chloro-5'-oxo-5'H-spiro[cyclohexane-1,7'-indolo[1,2-a]quinazolin]-9'-yl)piperidin-1-yl)pentanamido)-3,3-dimethylbutanoyl)-4-hydroxy-N-((S)-1-(4-(4-methylthiazol-5-yl)phenyl)ethyl)pyrrolidine-2-carboxamide (22)

Compound **22** was synthesized by a procedure identical to that used for compound **19**. ESI MS m/z: 946.45 $[M+H]^+$.

(2S,4R)-1-((S)-2-(6-(4-(4'-chloro-5'-oxo-5'H-spiro[cyclohexane-1,7'-indolo[1,2-a]quinazolin]-9'-yl)piperidin-1-yl)hexanamido)-3,3-dimethylbutanoyl)-4-hydroxy-N-((S)-1-(4-(4-methylthiazol-5-yl)phenyl)ethyl)pyrrolidine-2-carboxamide (23)

Compound **23** was synthesized by a procedure identical to that used for compound **19**. ESI MS m/z: 960.45 $[M+H]^+$.

(2S,4R)-1-((S)-2-((1r,4S)-4-((4-(4'-chloro-5'-oxo-5'H-spiro[cyclohexane-1,7'-indolo[1,2-a]quinazolin]-9'-yl)piperidin-1-yl)methyl)cyclohexane-1-carboxamido)-3,3-dimethylbutanoyl)-4-hydroxy-N-((S)-1-(4-(4-methylthiazol-5-yl)phenyl)ethyl)pyrrolidine-2-carboxamide (24)

To a solution of compound **9** (50 mg, 0.12 mmol, 1 equiv.) in DCE/DMF (2/2 mL) was added compound **76a** (28.0 mg, 0.18 mmol, 1.5 equiv.). The mixture was stirred for 15 min. then $NaBH(OAc)_3$ (75 mg, 0.36 mmol, 3 equiv.) was added. let the reaction mixture stirred for additional 15 min. After reaction, TFA (0.5 mL) was added to quench the reaction. The DCE was removed under rotatory evaporator. The residue was purified by C-18 reversal column (elution solvents: CH_3CN/H_2O from 10% to 100%, 0.1%TFA) to get compound **77a** (46 mg, 69%). ESI MS m/z: 560.26 $[M+H]^+$.

To a solution of compound **77a** (20 mg, 0.036 mmol, 1.0 equiv.) and VHL ligand **75** (11.8 mg, 0.036 mmol, 1.0 equiv.) in DMF (2 mL) was added HATU (20.4 mg, 0.054 mmol, 1.5 equiv.) and DIPEA (13.8 mg, 0.11 mmol, 3 equiv.). The mixture was stirred for 1 h. Water (10 mL) was added

to quench the reaction and product was extracted with ethyl acetate twice (10 mL×2). Combined organic phases were washed by brine twice, dried by anhydrous Na_2SO_4. After removing solvent, the received crude product was purified by pre-HPLC to get compound **24** (21.0 mg, 60%). ESI MS m/z: 986.45 $[M+H]^+$.

(2S,4R)-1-((S)-2-((1r,4S)-4-((3-(4-(4'-chloro-5'-oxo-5'H-spiro[cyclohexane-1,7'-indolo[1,2-a]quinazolin]-9'-yl)piperidin-1-yl)azetidin-1-yl)methyl)cyclohexane-1-carboxamido)-3,3-dimethylbutanoyl)-4-hydroxy-N-((S)-1-(4-(4-methylthiazol-5-yl)phenyl)ethyl)pyrrolidine-2-carboxamide (25)

Compound **25** was synthesized by a procedure identical to that used for compound **24**. ESI MS m/z: 1041.51 $[M+H]^+$.

(2S,4R)-1-((S)-2-((1r,4S)-4-((4-(4'-chloro-5'-oxo-5'H-spiro[cyclohexane-1,7'-indolo[1,2-a]quinazolin]-9'-yl)-[1,4'-bipiperidin]-1'-yl)methyl)cyclohexane-1-carboxamido)-3,3-dimethylbutanoyl)-4-hydroxy-N-((S)-1-(4-(4-methylthiazol-5-yl)phenyl)ethyl)pyrrolidine-2-carboxamide (26)

Compound **26** was synthesized by a procedure identical to that used for compound **24**. ESI MS m/z: 1069.54 $[M+H]^+$.

(2S,4R)-1-((S)-2-(2-(4-(4'-chloro-5'-oxo-5'H-spiro[cyclohexane-1,7'-indolo[1,2-a]quinazolin]-10'-yl)piperidin-1-yl)acetamido)-3,3-dimethylbutanoyl)-4-hydroxy-N-((S)-1-(4-(4-methylthiazol-5-yl)phenyl)ethyl)pyrrolidine-2-carboxamide (27)

Compound **27** was synthesized by a procedure identical to that used for compound **24**. ESI MS m/z: 1041.53 $[M+H]^+$.

(2S,4R)-1-((S)-2-((1r,4S)-4-((4-(4'-chloro-5'-oxo-5'H-spiro[cyclohexane-1,7'-indolo[1,2-a]quinazolin]-10'-yl)piperidin-1-yl)methyl)cyclohexane-1-carboxamido)-3,3-dimethylbutanoyl)-4-hydroxy-N-((S)-1-(4-(4-methylthiazol-5-yl)phenyl)ethyl)pyrrolidine-2-carboxamide (28)

Compound **28** was synthesized by a procedure identical to that used for compound **24**. ESI MS m/z: 1069.55 $[M+H]^+$.

(2S,4R)-1-((S)-2-(4-((1r,4S)-4-((4-(4'-bromo-5'-oxo-5'H-spiro[cyclohexane-1,7'-indolo[1,2-a]quinazolin]-10'-yl)piperidin-1-yl)methyl)cyclohexyl)-1H-1,2,3-triazol-1-yl)-3,3-dimethylbutanoyl)-4-hydroxy-N-((S)-1-(4-(4-methylthiazol-5-yl)phenyl)ethyl)pyrrolidine-2-carboxamide (30)

To a stirred solution of compound **17** (50 mg 0.086 mmol, 1.0 eq) and compound **89** (37.3 mg, 0.172 mmol, 2.0 eq) in DMF (1 mL) was added DIPEA (0.133 mL, 10 eq) and the reaction mixture was stirred at 90 °C for 12 hours. After cooling to room temperature, the mixture was subjected to reverse phase flash chromatography (10-100% MeCN in H_2O, 0.1% TFA) to give compound **90** (16.6 mg, 30 %).

To a stirred solution of compound **90** (16.6mg, 0.025 mmol, 1.0 eq), compound **88** (17.8 mg, 0.030 mg. 1.2 eq) in tBuOH (0.5 mL) and water (0.5 mL) was added $CuSO_4$ (5.3 mg, 0.033 mmol, 1.3 eq) and (+)-Sodium L-ascorbate (20.1 mg, 0.101 mmol, 4.0 eq). The reaction mixture was stirred

at room temperature for 12 hours. The mixture was subjected to Prep-HPLC (35-100% MeCN in H_2O, 0.1 % TFA) to give compound **30** (17.0 mg, 67 %). ESI MS m/z: 1054.42 $[M+H]^+$.

(2S,4R)-1-((S)-2-(4-((1r,4S)-4-((4-(4'-chloro-5'-oxo-5'H-spiro[cyclohexane-1,7'-indolo[1,2-a]quinazolin]-10'-yl)piperidin-1-yl)methyl)cyclohexyl)-1H-1,2,3-triazol-1-yl)-3,3-dimethylbutanoyl)-4-hydroxy-N-((R)-2-(3-hydroxy-3-methylazetidin-1-yl)-1-(4-(4-methylthiazol-5-yl)phenyl)ethyl)pyrrolidine-2-carboxamide (31)

To a flask was added compound **80** (416 mg, 1.7 mmol, 1.0 eq), 1H-imidazole-1-sulfonyl azide hydrochloride (**81**) (391 mg, 1.87 mmol, 1.1 eq), K_2CO_3 (586 mg, 4.25 mmol, 2.5 eq), $CuSO_4$ (27 mg, 0.17 mmol, 0.1 eq). Then the solvent of MeOH (9 mL) was added to the flask. The suspension was stirred at rt for 8 h. After removing solvent, the residue was purified directly by C-18 reversal column chromatography (elution solvents: CH_3CN/H_2O from 10% to 100%, 0.1%TFA) to afford compound **82** (201 mg, 44%) as a withe solid.

Compound **83a** (2.2 g, 1.0 eq.) in CH_2Cl_2 (15 mL) was added dropwise to a stirred solution of $SOCl_2$ (1.1 eq.), TEA (2.2 eq.) and imidazole (4 eq.) in CH_2Cl_2 (15 mL) at -78 °C (CO_2 and EtOH) and the resulting solution was stirred at -78 °C for 3 h. The reaction mixture was warmed to room temperature, quenched by addition of water, phases separated, organic phase washed with brine, dried (Na_2SO_4) and concentrated in vacuo to give the crude cyclic sulfamidite. The crude cyclic sulfamidite was dissolved in MeCN (0.13 M) at rt, $NaIO_4$ (1.6 eq) $RuCl_3$ (0.5 mol%) and water (0.16 M) were added sequentially and the resulting solution was stirred until completion was indicated by TLC. The reaction mixture was diluted with water (equal volume to that used in reaction), extracted with Et_2O, washed with brine, dried (Na_2SO_4) and concentrated in vacuo to give the crude compound **84a** (2.3 g, 88% for two steps).

To a solution of compound **84a** (47 mg, 0.12 mmol, 1 equiv.) in CH_3CN (1.2 mL) was added compound **85a** (31 mg, 0.36 mmol, 3 equiv.) and DIPEA (150 μL, 0.96 mmol, 8.0 equiv.). The mixture was stirred at rt for 3 h. After reaction, the solvent was removed, the residue was purified by silica gel column chromatography (elution solvents: ethyl acetate/hexane = 1/1) to get compound **86a** (41.5 mg, 86%).

To a solution of compound **86a** (41.5 mg, 0.10 mmol, 1 equiv.) in DCM (1 mL), was added TFA (1 mL) and the mixture was stirred 30 min. After removing solvent, the crude product **87a** was received and can be used in the next step directly. ESI MS m/z: 304.14 $[M+H]^+$.

To a solution of crude compound **87a** (0.10 mmol, 1.0 equiv.) and compound **82** (32.4 mg, 0.12 mmol, 1.2 equiv.) in DMF (2 mL) was added HATU (38.1 mg, 0.10 mmol, 1.0 equiv.) and DIPEA (126 μL, 0.80 mmol, 8 equiv.). The mixture was stirred for 10 min. The reaction is quenched by TFA, the residue was purified by pre-HPLC to get pure compound **88a** (42.2 mg, 76%). The rest of the synthetic procedure for compound **31** was identical to that used for compound **30**. ESI MS m/z: 1095.55 $[M+H]^+$.

(2S,4R)-1-((S)-2-(4-((1r,4S)-4-((4-(4'-chloro-5'-oxo-5'H-spiro[cyclohexane-1,7'-indolo[1,2-a]quinazolin]-10'-yl)piperidin-1-yl)methyl)cyclohexyl)-1H-1,2,3-triazol-1-yl)-3,3-dimethylbutanoyl)-N-((R)-2-(3-fluoro-3-methylazetidin-1-yl)-1-(4-(4-methylthiazol-5-yl)phenyl)ethyl)-4-hydroxypyrrolidine-2-carboxamide (32)

Compound **32** was synthesized by a procedure identical to that used for compound **31**. ESI MS m/z: 1097.87 $[M+H]^+$.

(2S,4R)-1-((S)-2-(4-((1r,4S)-4-((4-(4'-chloro-5'-oxo-5'H-spiro[cyclohexane-1,7'-indolo[1,2-a]quinazolin]-10'-yl)piperidin-1-yl)methyl)cyclohexyl)-1H-1,2,3-triazol-1-yl)-3,3-dimethylbutanoyl)-4-hydroxy-N-((R)-1-(4-(4-methylthiazol-5-yl)phenyl)-2-morpholinoethyl)pyrrolidine-2-carboxamide (33)

Compound **33** was synthesized by a procedure identical to that used for compound **31**. ESI MS m/z: 1095.55 $[M+H]^+$.

(2S,4R)-1-((S)-2-(4-((1r,4S)-4-((4-(4'-chloro-5'-oxo-5'H-spiro[cyclohexane-1,7'-indolo[1,2-a]quinazolin]-10'-yl)piperidin-1-yl)methyl)cyclohexyl)-1H-1,2,3-triazol-1-yl)-3,3-dimethylbutanoyl)-4-hydroxy-N-((S)-3-(3-hydroxy-3-methylazetidin-1-yl)-1-(4-(4-methylthiazol-5-yl)phenyl)propyl)pyrrolidine-2-carboxamide (34)

Compound **34** was synthesized by a procedure identical to that used for compound **31**. ESI MS m/z: 1109.42 $[M+H]^+$.

(2S,4R)-1-((S)-2-(4-((1r,4S)-4-((4-(4'-chloro-5'-oxo-5'H-spiro[cyclohexane-1,7'-indolo[1,2-a]quinazolin]-10'-yl)piperidin-1-yl)methyl)cyclohexyl)-1H-1,2,3-triazol-1-yl)-3,3-dimethylbutanoyl)-N-((S)-3-(3-fluoro-3-methylazetidin-1-yl)-1-(4-(4-methylthiazol-5-yl)phenyl)propyl)-4-hydroxypyrrolidine-2-carboxamide (35)

Compound **35** was synthesized by a procedure identical to that used for compound **31**. ESI MS m/z: 1111.79 $[M+H]^+$.

(2S,4R)-1-((S)-2-(4-((1r,4S)-4-((4-(4'-chloro-5'-oxo-5'H-spiro[cyclohexane-1,7'-indolo[1,2-a]quinazolin]-10'-yl)piperidin-1-yl)methyl)cyclohexyl)-1H-1,2,3-triazol-1-yl)-3,3-

dimethylbutanoyl)-4-hydroxy-N-((S)-1-(4-(4-methylthiazol-5-yl)phenyl)-3-morpholinopropyl)pyrrolidine-2-carboxamide (36)

Compound **36** was synthesized by a procedure identical to that used for compound **31**. ESI MS m/z: 1109.66 $[M+H]^+$.

(2S,4R)-1-((S)-2-(4-((1r,4S)-4-((4-(4'-chloro-5'-oxo-5'H-spiro[cyclohexane-1,7'-indolo[1,2-a]quinazolin]-10'-yl)piperidin-1-yl)methyl)cyclohexyl)-1H-1,2,3-triazol-1-yl)-3,3-dimethylbutanoyl)-4-hydroxy-N-((S)-3-(2-(2-methoxyethoxy)ethoxy)-1-(4-(4-methylthiazol-5-yl)phenyl)propyl)pyrrolidine-2-carboxamide (37)

Compound **37** was synthesized by a procedure identical to that used for compound **31**. ESI MS m/z: 1142.78 $[M+H]^+$.

BLI binding assay. Purified recombinant SMARCA2/4 protein was biotinylated using the Thermo EZ-Link long-chain biotinylation reagent. Briefly, protein and biotinylation reagent were mixed with 1:1 molar ratio in PBS at 4 °C. Low biotinylation reagent concentration was applied to avoid protein over-biotinylation. This reaction mixture was incubated at 4°C for 2 hours to allow reaction being finished. Reaction mixture was then dialyzed using Fishersci 10K MWCO dialysis cassettes to remove unreacted biotinylation reagent. Bio-Layer Interferometry (BLI) assays were performed using an OctetRED96 instrument from PALL/ForteBio. All assays were run at 30 °C with continuous 1000 RPM shaking. PBS with 0.1% BSA, 0.01% Tween-20 and 2% DMSO was used as the assay buffer. Biotinylated DCN1 protein was tethered on Super Streptavidin (SSA) biosensors (ForteBio) by dipping sensors into 50 μg/mL protein solutions. Average saturation response level of 4-5 nm was achieved in 15 minutes. Biotinylated blocked Super Streptavidin

(SSA) biosensors were prepared as well by following the protocol provided by the manufacturer which were used as the inactive reference controls. Sensors with proteins tethered were washed in assay buffer for 10 minutes to eliminate loose nonspecific bound protein molecules and establish stable base line before starting association-dissociation cycles of compound. Different association and dissociation times were used depending on the potencies of compounds being tested. DMSO only reference was included in all assays. Raw kinetic data collected were processed in the Data Analysis software provided by the manufacturer using double reference subtraction in which both DMSO only reference and inactive protein reference were subtracted. Resulting data were analyzed based on 1:1 binding model from which kon and koff values were obtained and then Kd values were calculated.

HTRF assay. Compounds were serially diluted in DMSO and 0.02 µL volume was transferred to white non-binding 384-well plate. The reaction was conducted in total volume of 20 µL with addition of 5 uL of SMARCA4 at 0.12 ng/ul followed (or SMARCA2 at 0.5 ng/uL) by 30 min incubation at 25 ºC. 5 uL of 120-fold diluted bromodomain ligand 2 for SMARCA4 or 90-fold diluted bromodomain ligand 2 for SMARCA2 was added followed by addition of diluted Tb-labeled donor and 5 uL of diluted dye-labeled acceptor (BPS Biosciences cat# 40341). After 120 min incubation at 25C, the HTRF signals were read on Envision reader (Perkin Elemer) at 340 nm excitation and 620 nm and 665 nm emission. Data was analyzed using XLfit using four parameters dose response curve to determine IC_{50}s.

HiBit degradation assay. Hela cells were genetically modified by CRISPR/Cas9 to fuse HiBit to the carboxy terminus of SMARCA2 (Promega CS302365) or SMARCA4 (Promega CS3023225).

Cells were cultured in DMEM containing 10% FBS and 1% (Vol:Vol) penicillin-streptomycin. At the time of the experiment, cells were seeded at a density of 20,000 cells per well in a 96-well plate (Corning Cat. #3903) and treated with serial dilutions of testing compounds for 24 h. At the end of the experiment, levels of SMARCA2 or SMARCA4 expression were assessed with Nano-Glo® HiBiT Lytic Detection Assay (Promega N3050). IC_{50} values were obtained using the GraphPad Prism data analysis software.

Cell Lines and Cell Culture. All the cells used were purchased from American Type Culture Collection (ATCC) and grown in RPMI 1640 medium (Invitrogen) supplemented with 10% fetal bovine serum (Invitrogen). All the cells were cultured at 37 °C in a humidified 5% CO_2 incubator.

Western Blot Analysis. 1.5 - 2 × 10^6 cells/well were plated in 12-well plates and treated with compounds at the indicated concentrations and times. Cells were collected, washed with PBS, and lysed in Radioimmunoprecipitation Assay Protein Lysis and Extraction Buffer containing proteinase inhibitor cocktail (Roche Diagnostics, Mannheim, Germany). Twenty micrograms of lysate were electrophoresed through 4-12% Tris-glycine SDS-PAGE gels (Invitrogen) and blotted into PVDF (polyvinylidene difluoride) membranes (MilliporeSigma, IPFL00010). The membranes were blocked with Intercept Blocking Buffer (LI-COR Biosciences, 927-70001) for 1 hour at room temperature and then washed with 1× Tris-buffered saline Tween 20 four times for 5 minutes each. The membranes were incubated overnight at 4 °C in Intercept Blocking Buffer supplemented with Tween 20 (dilution 1:500). Rabbit SMARCA2 antibody (CST, cat# 11966, 1:1000), rabbit SMARCA4 antibody (Bethyl, cat# A700-106, 1:2000) or mouse GAPDH antibody

(Santa Cruz Biotechnology, sc-47724, 1:1,000) were used for immunoblotting. The membranes were washed with TBST buffer for 5 minutes four times and incubated in Intercept Blocking Buffer supplemented with Tween 20 (dilution 1:500) and 10% SDS solution (dilution 1:500) for 1 hour at room temperature. IRDye 800CW goat anti-mouse secondary antibody (LI-COR Biosciences, 1:20000), IRDye 680RD goat anti-rabbit secondary antibody (LI-COR Biosciences, 1:20000) were used for immunoblotting. The membranes were then washed with TBST for 5 minutes four times and scanned by Odyssey CLx Imaging System (LI-COR Biosciences). The immunoblots were finally quantified by the software and the readings were fitted using a nonlinear regression analysis with the GraphPad Prism 8 software to obtain the DC_{50} value.

Cell growth assay. 500-2000 cells/well were seeded in a 96-well tissue culture plate with a final volume of 200 μL/well and treated with indicated doses of compounds in a 3-fold serially diluted manner. The cells were incubated for 7 days at 37 °C in an atmosphere of 5% CO_2. Cell growth was evaluated by WST-8 assay (Dojindo Molecular Technologies, MD). An adequate volume of WST-8 reagent was added to each well, incubated for at least 1 h in the cell culture incubator, and read at 450 nm in a Tecan Infinite M1000 multimode microplate reader (Tecan, Morrisville, NC). The readings were normalized to the DMSO-treated cells and fitted using a nonlinear regression analysis with the GraphPad Prism 8 software to obtain the IC_{50} value.

Microsomal Metabolic Stability Studies Pooled human and rat microsomes (10 μL aliquot) were prepared and stored at −80 °C prior to use. Master-mix containing microsome, phosphate buffer, and test compound solution was made as follows: (1) 10 μL of microsome (20 mg/mL) was diluted

with 330 μL 0.1 M phosphate buffer (3.3 mM $MgCl_2$); (2) about 3.3 mg of NADPH was dissolved in 200 μL of 0.1 M phosphate buffer (3.3 mM $MgCl_2$); (3) 40 μL of 10 μM SMD-3236 PBS solution, was added to microsome; (4) the master solution was pre-warmed at 37 °C for 5 min. NADPH (20 μL) was added to the abovementioned master solution to initiate the reaction. The final concentration of SMD-3236 in the reaction system was 1 μM. Aliquot of 40 μL was pipetted from the reaction solution and stopped by the addition of 160 μL cold MeCN containing 25 nM of CE302 as an internal standard at the designated time points (0, 5, 10, 15, 30, 45, and 60 min). The incubation solution was vortexed-mixed (800 rpm/10 min) and centrifuged at 3500 rpm for 10 min to precipitate proteins. The supernatant was collected and used for the LC/MS/MS analysis. The natural log peak area ratio (compound peak area/internal standard peak area) was plotted against time and the gradient of the line was determined.

CYP inhibition assay The CYP inhibition of SMD-3236 was studied in human liver microsomes in Medicilon Inc (Shanghai, China). Briefly, 0.2 mg/mL human liver microsome stock solution was prepared by adding 10 μL of 20 mg/mL microsome to 990 μL of 0.1 M KH_2PO_4 (pH 7.4). In general, human liver microsomes were mixed with buffer (0.1 M K-buffer), a test compound or a reference inhibitor, and warmed to 37 °C in a 96-well temperature-controlled heater block for 5 min. Aliquots of this mixture (30 μL and in duplicate) were delivered to each well of a 96-well polypropylene polymerase chain reaction plate maintained at 37 °C, followed by adjoining of a substrate (15 μL) as applicable. Final organic solvent concentration was 1% (v/v) or less. Incubation was commenced with addition of NADPH stock solution (15 μL, 8 mM, pre-incubated at 37 °C) to a final incubation volume of 60 μL and maintained at 37 °C for a period (5 min for 3A4, 10 min for 1A2, 2B6, and 2C9, 20 min for 2C8 and 2D6, and 45 min for 2C19). Incubations

were typically terminated by adding 180 μL of cold CAN-containing IS. After quenching, the plates were shaken at the vibrator for 10 min (600 rpm/min) and then centrifuged at 6000 rpm for 15 min. 80 μL of the supernatant was transferred from each well into a 96-well sample plate containing 120 μL of ultra-pure water for LC/MS analysis. Phenacetin, amfebutamone HCl, paclitaxel, diclofenac, S-mephenytoin, and dextromethorphan were used as substrates for CYP 1A2, 2B6, 2C8, 2C9, 2C19, and 2D6 isoforms, respectively, and midazolam and testosterone as substrates for CYP 3A4. α-Naphthoflavon, ticlopidine, montelukast, sulfaphenazole, omeprazole, quinidine, and ketoconazole were used as reference inhibitor controls for CYP 1A2, 2B6, 2C8, 2C9, 2C19, 2D6, and 3A4, respectively.

hERG Assay SMD-3236 was tested for its effect on hERG potassium channels in a HEK 293 cell line stably expressed hERG using a manual patch-clamp technique. In brief, SMD-3236 was tested at 3 and 30 μM in duplicate, with terfenadine included as the positive control. SMD-3236 or the positive article was tested at room temperature using the whole-cell patch-clamp technique with a PatchMaster patch-clamp system (HEKA Elektronik, Germany).

Toxicity, PK/PD and efficacy studies. All *in vivo* studies were performed under an animal protocol (PRO00009463) approved by the Institutional Animal Care and Use Committee (IACUC) of the University of Michigan, in accordance with the recommendations in the Guide for the Care and Use of Laboratory Animals of the National Institutes of Health. CB.17 SCID breeders and Balb/c mice were obtained from Charles River Laboratories, CB.17 SCID mice were bred by University of Michigan Unit for Laboratory Animal Medicine (ULAM) Breeding Core.

For toxicity studies, female Balb/C mice were treated with SMD-3040 or vehicle control (25% PCP:33% of 10 part of PEG400 + 3 part of Cremchol, and PBS, pH was adjusted to 7 with 0.5 N NaOH) with indicated doses. Mouse body weights were measured every 2-3 days.

For PD studies, female SCID mice (6-10 weeks old) were injected subcutaneously with 5×10^6 MV4-11 cells in 5 mg/mL Matrigel (Corning) for tumor growth. SMD-3040 was administered in animals by intravenous (IV) injection using 25% PCP as the dosing vehicle when tumors reached approximately 200 mm^3. Mice with similar-sized tumors were grouped and assigned to different experimental groups and treated with indicated doses. At the indicated timepoints, mice were euthanized, and blood and tumor samples were collected for analysis. Isolated tumor samples were placed in a Precellys tube (CK28-R) and immediately frozen in liquid nitrogen. All plasma and tumor samples (about 200 μL) were stored at -80 °C until analysis. For the analysis of SMARCA protein levels in tumor samples, resected xenograft tumor tissues were ground into powder in liquid nitrogen and lysed in Radioimmunoprecipitation Assay Protein Lysis and Extraction Buffer containing proteinase inhibitor cocktail (Roche Diagnostics, Mannheim, Germany). Twenty micrograms of lysate were electrophoresed through 4-12% Tris-glycine SDS-PAGE gels (Invitrogen) and blotted into PVDF (polyvinylidene difluoride) membranes (MilliporeSigma, IPFL00010). The membranes were blocked with Intercept Blocking Buffer (LI-COR Biosciences, 927-70001) for 1 h at rt and then washed with 1× Tris-buffered saline Tween 20 four times for 5 min each. The membranes were incubated overnight at 4 °C in Intercept Blocking Buffer supplemented with Tween 20 (dilution 1:500). Rabbit SMARCA2 antibody (CST, cat# 11966, 1:1,000), rabbit SMARCA4 antibody (Bethyl, cat# A700-106, 1:2,000) or mouse GAPDH antibody (Santa Cruz Biotechnology, sc-47724, 1:1,000) were used for immunoblotting. The membranes were washed with TBST buffer for 5 min four times and incubated in Intercept

Blocking Buffer supplemented with Tween 20 (dilution 1:500) and 10% SDS solution (dilution 1:500) for 1 h at rt. IRDye 800CW goat anti-mouse secondary antibody (LI-COR Biosciences, 1:20000), IRDye 680RD goat anti-rabbit secondary antibody (LI-COR Biosciences, 1:20000) were used for immunoblotting. The membranes were then washed with TBST for 5 min four times and scanned by Odyssey CLx Imaging System (LI-COR Biosciences). The immunoblots were finally quantified by the software and the readings were fitted using a nonlinear regression analysis with the GraphPad Prism 8 software to obtain the DC_{50} value.

For efficacy studies, female SCID mice (6-8 weeks old) were injected subcutaneously with 5×10^6 H838 cells or 5×10^6 SK-Mel-5 cells in 5 mg/mL Matrigel (Corning) for tumor growth. When tumors reached an average volume of 100 mm^3, mice were tumor size matched and randomly assigned to different experimental groups with 8 mice for each group. Drugs or vehicle control were given at the dose schedule as indicated using 25% PCP as the dosing vehicle. Tumor sizes and animal weights were measured 2–3 times per week. Tumor volume (mm^3) = (length × $width^2$)/2. Tumor growth inhibition was calculated as TGI (%) = $(V_c - V_t)/(V_c - V_o)*100$, where V_c, V_t are the medians of the control and treated groups at the end of the treatment respectively, and V_o at the start. Tumor volumes at the end of treatment were statistically analyzed using a two-tailed, unpaired *t*-test (GraphPad Prism 9.0).

To prepare tumor samples for LCMS analysis, mixed ultrapure water and acetonitrile solution (4:1) were added to the defrosted tumor tissue samples 5:1, v/w, in order to facilitate homogenization with a Precellys evolution homogenizer at 4 °C. The homogenized tissues solution was denatured using cold acetonitrile (1:3, v/v) with vortex and centrifuged at 13000 rpm 4 °C for 10 min. Following protein precipitation, the final supernatants were collected for LC–MS analysis.

To determine drug concentrations in plasma and tumor samples, a LC–MS/MS method was developed and validated. The LC–MS/MS method consisted of a Shimadzu HPLC system, and chromatographic separation of a test compound was achieved using a Waters XBridge-C18 column (5 cm × 2.1 mm, 3.5 μm). An AB Sciex QTrap 5500 mass spectrometer equipped with an electrospray ionization source (Applied Biosystems, Toronto, Canada) in the positive-ion multiple reaction monitoring mode was used for detection. For example, the precursor/product ion transitions were monitored at m/z 942.5 for SMD-3040 and internal standard, respectively, in the positive electrospray ionization mode. The mobile phases used on HPLC were 0.1% formic acid in purified water (A) and 0.1% formic acid in acetonitrile (B). The gradient (B) was held at 10% (0–0.3 min), increased to 95% at 0.7 min, then kept at an isocratic 95% B for 2.3 min, and then immediately stepped back down to 10% for 2 min re-equilibration. The flow rate was set at 0.4 mL/min.

Chapter 4 General Discussion and Future Directions

4.1 Achievements in this dissertation

1) We reported the discovery efforts of a potent and selective SMARCA2 PROTAC degrader, SMD-3040, which demonstrates strong in vivo antitumor activity and possesses the best selectivity profile among all disclosed SMARCA degraders in the literature.

2) We developed a novel series of spiro SMARCA bromodomain ligands through structure-based drug design and crystallography studies.

3) Using the novel spiro SMARCA bromodomain ligands, we discovered a next-generation selective SMARCA2 PROTAC degrader, SMD-3236, which shows improved potency and excellent DMPK properties compared to SMD-3040. SMD-3236 is currently undergoing extensive advanced preclinical studies.

4.2 Future directions

4.2.1 Development of orally available SMARCA2 selective degraders

Up to now, all SMARCA (selective) degraders with in vivo data,[87, 117-118] including one that recently entered clinical trial,[145] adopt the intravenous method for drug administration. For small molecule drug discovery, developing an orally available agent is the utmost goal for its advantagesin patient compliances, manufacturing costs and complication risks over any other administration routes.[162] The major hurdle for developing orally available SMARCA PROTAC degraders is that those reported SMARCA PROTAC degraders widely make use of VHL ligands as the E3 ligase recruiting moiety. Generally, the VHL ligands used stem from the initial scaffolds reported by the Crews group and Ciulli group.[103, 105, 162] These VHL ligands belong to the type of peptidomimetic molecules with features such as multiple hydrogen bond donors and rotatable bonds, which are naturally undesirable for developing an orally available drug. In fact, all the orally available PROTAC degraders in clinical trials with disclosed chemical structures use the thalidomide analogs as the recruitment ligand for the cereblon E3 ligase (see Table 1). Thalidomide, as an example of cereblon E3 ligase ligand, has a low molecular weight of 258 with only one hydrogen bond donor in the molecule, making it an ideal E3 ligase ligand for the design of orally available PROTAC degraders. Therefore, one prominent solution would be the adoption of cereblon ligands in the pursuit of developing orally available SMARCA2 selective PROTAC degraders. Currently, our group is working on the discovery of selective and orally available SMARCA2 PROTAC degraders and has achieved certain milestones with promising in vivo data. These progresses will be reported in due course.

During the past few years, the targeted protein degradation community has seen tremendous progress made in expending the targetable E3 ligase scope that could be redirected for protein degradation, with the discovery of small molecule ligands for a variety of different E3 ligases.[163-167] (Figure 34) Nevertheless, these ligands bear a number of defects, such as high molecular weights, low target specificity or poor physicochemical properties. Further medicinal chemistry optimizations are required to assure these ligands being applied in the development of orally available PROTAC degraders.

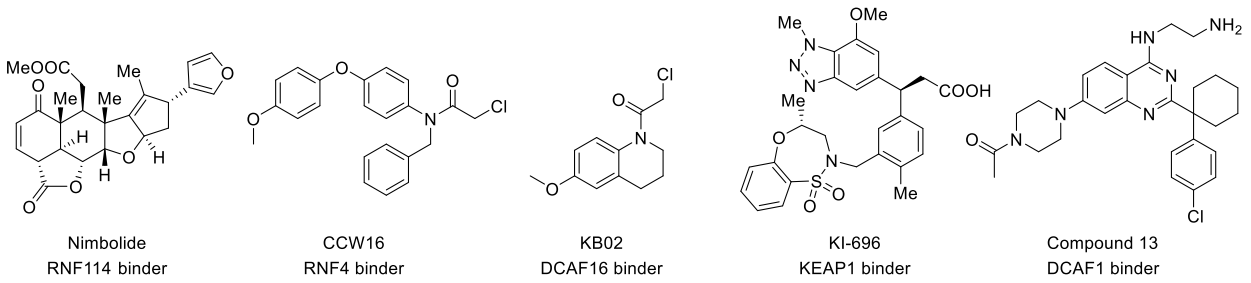


Figure 32. Chemical structures of representative novel E3 ligase ligands.

4.2.2 SMARCA2 selectivity: from serendipity to rational design

PROTAC degrader molecules have the potential to achieve high degradation selectivity for one specific protein over its closed related homologs with high sequence similarity. This advantage has been exploited for the discovery of several highly isoform-selective PROTAC degraders, such as BRD4 degrader, STAT3 degrader and STAT5 degrader.[88, 93, 131] In this thesis, we also reported two highly selective SMARCA2 PROTAC degrader molecules. Admittedly, our successes in identifying SMARCA2 selective PROTAC degrades mainly come from serendipity, while the mechanisms underlying the selectivity remained largely understudied. Here, we discuss our thoughts on future aspects that might assist us to elucidate the SMARCA2 selectivity and potential enabling technologies for the rational design of selectivity.

For proteins with a high sequence homology, it is relatively difficult to develop selective inhibitors because their small molecule binding sites likely share very conserved amino acid sequences. However, unlike small molecules which only occupy a defined small binding pocket, PROTAC molecules induce large protein-protein interactions between the E3 ligase and the target protein, where the residues are normally not well conserved even among highly homologous proteins. These differentiated residue patterns could potentially discriminate the large protein-protein interaction landscape in the process of ternary complex formation with E3 ligase and PROTAC molecule for one target protein over its homologs. Therefore, the HTRF-based ternary complex formation assay could be used as a routine screening effort for the identification of PROTAC molecules that specifically form ternary complex with the desired protein isoform. Other biochemical assays, including SPR and TR-FRET, could be used as orthogonal assays for the conformation of the formation of cooperative ternary complexes.

After finding the selective lead PROTAC molecule, crystallography studies, especially E3-PROTAC-POI ternary complex solvation, would be necessary in the next step for characterizing key structural features in the protein-protein interaction interface that contribute to the selectivity. Site mutagenesis experiments, followed by determination of the binding affinity of each mutated target protein with E3 ligase in the presence of PROTAC molecule, will provide further structural basis of the isoform selectivity by in the single amino acid resolution. Of note, one prominent caveat of current X-ray crystallography is the requirement of crystal growing, which must be done in an in vitro setting and thus might not reflect the protein conformations in their native state. Cryo-EM offers an alternative but attractive method for the determination of large and dynamic macromolecular assemblies, such as ternary complexes, without the requirement of obtaining

crystals.[168] We believe that cryo-EM could serve as a powerful tool for the structure-based selective PROTAC design with the technical advances to push the resolution limits of cryo-EM.

In addition to wet lab experiments, a set of in silico tools provide a repertoire for ternary complex structural analysis. Some of the widely used in silico docking programs, such as FRODOCK,[169] RDKit, VoroMQA,[170] and RosettaDock[171] could help in predicting the conformation of productive ternary complexes and guiding the design of potential PROTAC molecules with suitable linker attachment position, length and compositions. After the best-scored docking models are established, molecular dynamic (MD) simulation studies will further structural details in the protein-protein interaction interfaces that affect the degradation selectivity among closely related protein homologs.

4.2.3 Toxicity related to SMARCA2 selective PROTAC degraders

In recent years, more and more attention has been brought to the off-target effects of PROTAC molecules as the knowledge and understanding in the targeted protein degradation field deepens. In several individual reports, a number of phthalimide-based PROTAC degraders failed to degrade their intended target protein, yet displayed potent cell growth inhibition effects in a degradation independent manner. These observations led to the discovery that these PROTAC degraders induce the inadvertent degradation of translation termination factor GSPT1 in a molecular glue-like mode of action, which lead to profound off-target cytotoxicity.[172-173] Of note, off-target degradation of VHL-based PROTAC degraders has not been described to data, indicating that they are less prone to exhibit the molecular glue type of mode of action compared to phthalimide-based PROTAC degraders. Nevertheless, to avoid the peril of potential degradation of off-target proteins of our SMARCA2 selective PROTAC degraders, unbiased whole-cell

proteomic experiments are critically needed to assess the selectivity of PROTAC molecules in a proteome-wide scope, which has been included in most of the PROTAC related literatures in the field.

Other than off-target toxicity, the SMARCA2 selective PROTAC degraders bear their intrinsic on-target toxicity liabilities: the concurrent degradation of SMARCA4 protein. Studies have shown that loss of both SMARCA2 and SMARCA4 may disrupt the function of normal cells and tissues.[77-78] Consistent with these findings, non-selective SMARCA2/4 inhibitors have been reported to be toxic in preclinical models and in human clinical trials.[76, 81] Therefore, minimizing the SMARCA4 degradation is of critical importance for the development of SMARCA2 selective PROTAC degraders to circumvent toxicity issues. To evaluate the degradation of SMARCA2 and SMARCA4 protein in the cellular level, traditional western blot analysis or HiBit degradation assay are often used as the routine screening effort. However, the consensus degree of maximum SMARCA4 degradation that would lead to in vivo toxicities is still not clear because of a number of reasons. First, the compound triage threshold and parameters in early screening campaigns varies vastly from different assays or even different institutions. In our HiBit degradation assay, we employed four parameters, DC_{50}, D_{max}, S4/S2 DC_{50} ratio and ΔD_{max} for comprehensive evaluation of our degraders, and only compounds with SMARCA2 $DC_{50} < 10$ nM, SMARCA2 $D_{max} > 85\%$, SMARCA4 $D_{max} < 60\%$ and $\Delta D_{max} > 40\%$ will be proceeded into further cell growth and in vivo characterizations. Second, how well the in vitro SMARCA4 degradation data correlates with in vivo SMARCA4 degradation profile is not established. In the evaluation of in vivo protein degradation, our methods are limited to the low-robustness and low-throughput western blot experiments, which severely impacts the quality and effectiveness of data generation. In addition, PK properties, tissue distribution and plasma protein binding also could greatly alter the in vivo

degradation activity and result in disconnection with in vitro data. Third, how the function of individual tissues and organs would be affected, especially in humans, by global perturbation of SMARCA4 protein is not clear yet. Cardio and intestine toxicities in mice caused by genetic knockout of SMARCA4 protein have already been reported in the literature, suggesting that these organs might be more sensitive to SMARCA4 degradation than other tissues. The tissue distribution of potential SMARCA2 selective PROTAC degrader will need to be optimized in order to avoid the drug accumulation in such sensitive tissues that might lead to toxicity.

4.2.4 Clinical development considerations

Previous studies have reported that SMARCA4 loss-of-function mutations, including homozygous hotspot missense mutations, frameshift indels and nonsense (stop gain, stop loss) mutations, are found in multiple cancer types with high frequencies.[57-58, 174-176] However, these genomics studies are generally based on open-sourced data base such as TCGA or other small-scale pan-cancer analysis, indicating an incomplete understanding of the SMARCA4 mutational status with only 927 SMARCA4 variants being identified in these literatures thus far. To understand status of SMARCA4 LOF mutations and functional consequences in order for successful translation of SMARCA2 targeted therapies into the clinic, it is imperative to comprehensively analyze the SMARCA4 mutational landscape in a more clinically relevant setting. Recently, Genentech published a result of targeted exome sequencing data from 131668 cancer patients with diverse lineages.[62] SMARCA4 mutations are found to be mutated in 9434 patients with the identification of 10562 SMARCA4 variants including 6289 missense mutations clustering at hotspots in SNF2 domain and ATPase helicase domain. Importantly, some of the SMARCA4 hotspot missense mutants that were previously deemed LOF are able to partially or even fully rescue cell viability and chromatin accessibility after SMARCA2 knockdown in SMARCA4-

deficient H1944 cell line. These findings provide key insights on patient selection criteria in the clinic: patients with frameshift indels, nonsense or truncating mutations that confer a clear SMARCA4 LOF are potential population eligible for SMARCA2 targeted therapies. For homozygous SMARCA4 missense mutations, careful functional assessments of each individual mutation are needed. Patients with pseudo-LOF-mutation SMARCA4 proteins where their cellular functionalities are retained should be excluded from the clinical trial cohort because they might not likely benefit from SMARCA2-direcred therapies. However, the percentage of patients that carry authentic LOF SMARCA4 missense mutations among all SMARCA4-mutated patients remains unclear yet, and future clinical safety and efficacy data might shed light on this field.

References

(1) Pfister, S. X.; Ashworth, A. Marked for death: targeting epigenetic changes in cancer. *Nat Rev Drug Discov* **2017**, *16,* 241-263.
(2) Stresemann, C.; Lyko, F. Modes of action of the DNA methyltransferase inhibitors azacytidine and decitabine. *Int J Cancer* **2008**, *123,* 8-13.
(3) Gabbara, S.; Bhagwat, A. S. The mechanism of inhibition of DNA (cytosine-5-)-methyltransferases by 5-azacytosine is likely to involve methyl transfer to the inhibitor. *Biochem J* **1995**, *307,* 87-92.
(4) Mann, B. S.; Johnson, J. R.; Cohen, M. H.; Justice, R.; Pazdur, R. FDA approval summary: vorinostat for treatment of advanced primary cutaneous T-cell lymphoma. *The Oncologist* **2007**, *12,* 1247-1252.
(5) Hoy, S. M. Tazemetostat: First Approval. *Drugs* **2020**, *80,* 513-521.
(6) Feng, S.; De Carvalho, D. D. Clinical advances in targeting epigenetics for cancer therapy. *FEBS J* **2022**, *289,* 1214-1239.
(7) Euskirchen, G.; Auerbach, R. K.; Snyder, M. SWI/SNF chromatin-remodeling factors: multiscale analyses and diverse functions. *J Biol Chem* **2012**, *287,* 30897-30905.
(8) Kwon, H.; Imbalzano, A. N.; Khavari, P. A.; Kingston, R. E.; Green, M. R. Nucleosome disruption and enhancement of activator binding by a human SW1/SNF complex. *Nature* **1994**, *370,* 477-481.
(9) Schick, S.; Rendeiro, A. F.; Runggatscher, K.; Ringler, A.; Boidol, B.; Hinkel, M.; Majek, P.; Vulliard, L.; Penz, T.; Parapatics, K.; Schmidl, C.; Menche, J.; Boehmelt, G.; Petronczki, M.; Muller, A. C.; Bock, C.; Kubicek, S. Systematic characterization of BAF mutations provides insights into intracomplex synthetic lethalities in human cancers. *Nat Genet* **2019**, *51,* 1399-1410.
(10) Barisic, D.; Stadler, M. B.; Iurlaro, M.; Schubeler, D. Mammalian ISWI and SWI/SNF selectively mediate binding of distinct transcription factors. *Nature* **2019**, *569,* 136-140.
(11) Menon, D. U.; Shibata, Y.; Mu, W.; Magnuson, T. Mammalian SWI/SNF collaborates with a polycomb-associated protein to regulate male germline transcription in the mouse. *Development* **2019**, *146,* dev174094.
(12) Alver, B. H.; Kim, K. H.; Lu, P.; Wang, X.; Manchester, H. E.; Wang, W.; Haswell, J. R.; Park, P. J.; Roberts, C. W. The SWI/SNF chromatin remodelling complex is required for maintenance of lineage specific enhancers. *Nat Commun* **2017**, *8,* 14648.
(13) Wang, X.; Lee, R. S.; Alver, B. H.; Haswell, J. R.; Wang, S.; Mieczkowski, J.; Drier, Y.; Gillespie, S. M.; Archer, T. C.; Wu, J. N.; Tzvetkov, E. P.; Troisi, E. C.; Pomeroy, S. L.; Biegel, J. A.; Tolstorukov, M. Y.; Bernstein, B. E.; Park, P. J.; Roberts, C. W. SMARCB1-mediated SWI/SNF complex function is essential for enhancer regulation. *Nat Genet* **2017**, *49,* 289-295.
(14) Nakayama, R. T.; Pulice, J. L.; Valencia, A. M.; McBride, M. J.; McKenzie, Z. M.; Gillespie, M. A.; Ku, W. L.; Teng, M.; Cui, K.; Williams, R. T.; Cassel, S. H.; Qing, H.; Widmer, C. J.; Demetri, G. D.; Irizarry, R. A.; Zhao, K.; Ranish, J. A.; Kadoch, C. SMARCB1 is required for widespread BAF complex-mediated activation of enhancers and bivalent promoters. *Nat Genet* **2017**, *49,* 1613-1623.
(15) Hodges, C.; Kirkland, J. G.; Crabtree, G. R. The Many Roles of BAF (mSWI/SNF) and PBAF Complexes in Cancer. *Cold Spring Harb Perspect Med* **2016**, *6,*
(16) Brownlee, P. M.; Meisenberg, C.; Downs, J. A. The SWI/SNF chromatin remodelling complex: Its role in maintaining genome stability and preventing tumourigenesis. *DNA Repair (Amst)* **2015**, *32,* 127-133.
(17) Dykhuizen, E. C.; Hargreaves, D. C.; Miller, E. L.; Cui, K.; Korshunov, A.; Kool, M.; Pfister, S.; Cho, Y. J.; Zhao, K.; Crabtree, G. R. BAF complexes facilitate decatenation of DNA by topoisomerase IIalpha. *Nature* **2013**, *497,* 624-627.

(18) Meisenberg, C.; Pinder, S. I.; Hopkins, S. R.; Wooller, S. K.; Benstead-Hume, G.; Pearl, F. M. G.; Jeggo, P. A.; Downs, J. A. Repression of Transcription at DNA Breaks Requires Cohesin throughout Interphase and Prevents Genome Instability. *Mol Cell* **2019**, *73,* 212-223 e217.
(19) Niimi, A.; Chambers, A. L.; Downs, J. A.; Lehmann, A. R. A role for chromatin remodellers in replication of damaged DNA. *Nucleic Acids Res* **2012**, *40,* 7393-7403.
(20) Clapier, C. R.; Cairns, B. R. The biology of chromatin remodeling complexes. *Annu Rev Biochem* **2009**, *78,* 273-304.
(21) Wang, W.; Côté, J.; Xue, Y.; Zhou, S.; Khavari, P. A.; Biggar, S. R.; Muchardt, C.; Kalpana, G. V.; Goff, S. P.; Yaniv, M.; Workman, J. L.; Crabtree, G. R. Purification and biochemical heterogeneity of the mammalian SWI-SNF complex. *EMBO J* **1996**, *15,* 5370-5382.
(22) Lemon, B.; Inouye, C.; King, D. S.; Tjian, R. Selectivity of chromatin-remodelling cofactors for ligand-activated transcription. *Nature* **2001**, *414,* 924-928.
(23) Raab, J. R.; Resnick, S.; Magnuson, T. Genome-Wide Transcriptional Regulation Mediated by Biochemically Distinct SWI/SNF Complexes. *PLoS Genet* **2015**, *11,* e1005748.
(24) Alpsoy, A.; Dykhuizen, E. C. Glioma tumor suppressor candidate region gene 1 (GLTSCR1) and its paralog GLTSCR1-like form SWI/SNF chromatin remodeling subcomplexes. *J Biol Chem* **2018**, *293,* 3892-3903.
(25) Brien, G. L.; Remillard, D.; Shi, J.; Hemming, M. L.; Chabon, J.; Wynne, K.; Dillon, E. T.; Cagney, G.; Van Mierlo, G.; Baltissen, M. P.; Vermeulen, M.; Qi, J.; Frohling, S.; Gray, N. S.; Bradner, J. E.; Vakoc, C. R.; Armstrong, S. A. Targeted degradation of BRD9 reverses oncogenic gene expression in synovial sarcoma. *elife* **2018**, *7,*
(26) Wang, X.; Wang, S.; Troisi, E. C.; Howard, T. P.; Haswell, J. R.; Wolf, B. K.; Hawk, W. H.; Ramos, P.; Oberlick, E. M.; Tzvetkov, E. P.; Ross, A.; Vazquez, F.; Hahn, W. C.; Park, P. J.; Roberts, C. W. M. BRD9 defines a SWI/SNF sub-complex and constitutes a specific vulnerability in malignant rhabdoid tumors. *Nat Commun* **2019**, *10,* 1881.
(27) Michel, B. C.; D'Avino, A. R.; Cassel, S. H.; Mashtalir, N.; McKenzie, Z. M.; McBride, M. J.; Valencia, A. M.; Zhou, Q.; Bocker, M.; Soares, L. M. M.; Pan, J.; Remillard, D. I.; Lareau, C. A.; Zullow, H. J.; Fortoul, N.; Gray, N. S.; Bradner, J. E.; Chan, H. M.; Kadoch, C. A non-canonical SWI/SNF complex is a synthetic lethal target in cancers driven by BAF complex perturbation. *Nat Cell Biol* **2018**, *20,* 1410-1420.
(28) Wang, W.; Xue, Y.; Zhou, S.; Kuo, A.; Cairns, B. R.; Crabtree, G. R. Diversity and specialization of mammalian SWI/SNF complexes. *Genes Dev* **1996**, *10,* 2117-2130.
(29) Centore, R. C.; Sandoval, G. J.; Soares, L. M. M.; Kadoch, C.; Chan, H. M. Mammalian SWI/SNF Chromatin Remodeling Complexes: Emerging Mechanisms and Therapeutic Strategies. *Trends Genet* **2020**, *36,* 936-950.
(30) Nie, Z.; Xue, Y.; Yang, D.; Zhou, S.; Deroo, B. J.; Archer, T. K.; Wang, W. A Specificity and Targeting Subunit of a Human SWI/SNF Family-Related Chromatin-Remodeling Complex. *Mol Cell Biol* **2000**, *20,* 8879-8888.
(31) Middeljans, E.; Wan, X.; Jansen, P. W.; Sharma, V.; Stunnenberg, H. G.; Logie, C. SS18 together with animal-specific factors defines human BAF-type SWI/SNF complexes. *PLoS One* **2012**, *7,* e33834.
(32) He, S.; Wu, Z.; Tian, Y.; Yu, Z.; Yu, J.; Wang, X.; Li, J.; Liu, B.; Xu, Y. Structure of nucleosome-bound human BAF complex. *Science* **2020**, *367,* 875-881.
(33) Mashtalir, N.; Suzuki, H.; Farrell, D. P.; Sankar, A.; Luo, J.; Filipovski, M.; D'Avino, A. R.; St Pierre, R.; Valencia, A. M.; Onikubo, T.; Roeder, R. G.; Han, Y.; He, Y.; Ranish, J. A.; DiMaio, F.; Walz, T.; Kadoch, C. A Structural Model of the Endogenous Human BAF Complex Informs Disease Mechanisms. *Cell* **2020**, *183,* 802-817 e824.
(34) Yuan, J.; Chen, K.; Zhang, W.; Chen, Z. Structure of human chromatin-remodelling PBAF complex bound to a nucleosome. *Nature* **2022**, *605,* 166-171.
(35) Wang, L.; Yu, J.; Yu, Z.; Wang, Q.; Li, W.; Ren, Y.; Chen, Z.; He, S.; Xu, Y. Structure of nucleosome-bound human PBAF complex. *Nat Commun* **2022**, *13,* 7644.
(36) Varga, J.; Kube, M.; Luck, K.; Schick, S. The BAF chromatin remodeling complexes: structure, function, and synthetic lethalities. *Biochem Soc Trans* **2021**, *49,* 1489-1503.

(37) Mashtalir, N.; D'Avino, A. R.; Michel, B. C.; Luo, J.; Pan, J.; Otto, J. E.; Zullow, H. J.; McKenzie, Z. M.; Kubiak, R. L.; St Pierre, R.; Valencia, A. M.; Poynter, S. J.; Cassel, S. H.; Ranish, J. A.; Kadoch, C. Modular Organization and Assembly of SWI/SNF Family Chromatin Remodeling Complexes. *Cell* **2018**, *175,* 1272-1288 e1220.
(38) Shain, A. H.; Pollack, J. R. The spectrum of SWI/SNF mutations, ubiquitous in human cancers. *PLoS One* **2013**, *8,* e55119.
(39) Kadoch, C.; Hargreaves, D. C.; Hodges, C.; Elias, L.; Ho, L.; Ranish, J.; Crabtree, G. R. Proteomic and bioinformatic analysis of mammalian SWI/SNF complexes identifies extensive roles in human malignancy. *Nat Genet* **2013**, *45,* 592-601.
(40) Bailey, M. H.; Tokheim, C.; Porta-Pardo, E.; Sengupta, S.; Bertrand, D.; Weerasinghe, A.; Colaprico, A.; Wendl, M. C.; Kim, J.; Reardon, B.; Ng, P. K.; Jeong, K. J.; Cao, S.; Wang, Z.; Gao, J.; Gao, Q.; Wang, F.; Liu, E. M.; Mularoni, L.; Rubio-Perez, C.; Nagarajan, N.; Cortes-Ciriano, I.; Zhou, D. C.; Liang, W. W.; Hess, J. M.; Yellapantula, V. D.; Tamborero, D.; Gonzalez-Perez, A.; Suphavilai, C.; Ko, J. Y.; Khurana, E.; Park, P. J.; Van Allen, E. M.; Liang, H.; Group, M. C. W.; Cancer Genome Atlas Research, N.; Lawrence, M. S.; Godzik, A.; Lopez-Bigas, N.; Stuart, J.; Wheeler, D.; Getz, G.; Chen, K.; Lazar, A. J.; Mills, G. B.; Karchin, R.; Ding, L. Comprehensive Characterization of Cancer Driver Genes and Mutations. *Cell* **2018**, *173,* 371-385 e318.
(41) Zehir, A.; Benayed, R.; Shah, R. H.; Syed, A.; Middha, S.; Kim, H. R.; Srinivasan, P.; Gao, J.; Chakravarty, D.; Devlin, S. M.; Hellmann, M. D.; Barron, D. A.; Schram, A. M.; Hameed, M.; Dogan, S.; Ross, D. S.; Hechtman, J. F.; DeLair, D. F.; Yao, J.; Mandelker, D. L.; Cheng, D. T.; Chandramohan, R.; Mohanty, A. S.; Ptashkin, R. N.; Jayakumaran, G.; Prasad, M.; Syed, M. H.; Rema, A. B.; Liu, Z. Y.; Nafa, K.; Borsu, L.; Sadowska, J.; Casanova, J.; Bacares, R.; Kiecka, I. J.; Razumova, A.; Son, J. B.; Stewart, L.; Baldi, T.; Mullaney, K. A.; Al-Ahmadie, H.; Vakiani, E.; Abeshouse, A. A.; Penson, A. V.; Jonsson, P.; Camacho, N.; Chang, M. T.; Won, H. H.; Gross, B. E.; Kundra, R.; Heins, Z. J.; Chen, H. W.; Phillips, S.; Zhang, H.; Wang, J.; Ochoa, A.; Wills, J.; Eubank, M.; Thomas, S. B.; Gardos, S. M.; Reales, D. N.; Galle, J.; Durany, R.; Cambria, R.; Abida, W.; Cercek, A.; Feldman, D. R.; Gounder, M. M.; Hakimi, A. A.; Harding, J. J.; Iyer, G.; Janjigian, Y. Y.; Jordan, E. J.; Kelly, C. M.; Lowery, M. A.; Morris, L. G. T.; Omuro, A. M.; Raj, N.; Razavi, P.; Shoushtari, A. N.; Shukla, N.; Soumerai, T. E.; Varghese, A. M.; Yaeger, R.; Coleman, J.; Bochner, B.; Riely, G. J.; Saltz, L. B.; Scher, H. I.; Sabbatini, P. J.; Robson, M. E.; Klimstra, D. S.; Taylor, B. S.; Baselga, J.; Schultz, N.; Hyman, D. M.; Arcila, M. E.; Solit, D. B.; Ladanyi, M.; Berger, M. F. Mutational landscape of metastatic cancer revealed from prospective clinical sequencing of 10,000 patients. *Nat Med* **2017**, *23,* 703-713.
(42) Wiegand, K. C.; Shah, S. P.; Al-Agha, O. M.; Zhao, Y.; Tse, K.; Zeng, T.; Senz, J.; McConechy, M. K.; Anglesio, M. S.; Kalloger, S. E.; Yang, W.; Heravi-Moussavi, A.; Giuliany, R.; Chow, C.; Fee, J.; Zayed, A.; Prentice, L.; Melnyk, N.; Turashvili, G.; Delaney, A. D.; Madore, J.; Yip, S.; McPherson, A. W.; Ha, G.; Bell, L.; Fereday, S.; Tam, A.; Galletta, L.; Tonin, P. N.; Provencher, D.; Miller, D.; Jones, S. J.; Moore, R. A.; Morin, G. B.; Oloumi, A.; Boyd, N.; Aparicio, S. A.; Shih Ie, M.; Mes-Masson, A. M.; Bowtell, D. D.; Hirst, M.; Gilks, B.; Marra, M. A.; Huntsman, D. G. ARID1A mutations in endometriosis-associated ovarian carcinomas. *N Engl J Med* **2010**, *363,* 1532-1543.
(43) Jones, S.; Wang, T.-L.; Shih, I.-M.; Mao, T.-L.; Nakayama, K.; Roden, R.; Glas, R.; Slamon, D.; Diaz, L. A.; Vogelstein, B.; Kinzler, K. W.; Velculescu, V. E.; Papadopoulos, N. Frequent Mutations of Chromatin Remodeling Gene ARID1A in Ovarian Clear Cell Carcinoma. *Science* **2010**, *330,* 228-231.
(44) Varela, I.; Tarpey, P.; Raine, K.; Huang, D.; Ong, C. K.; Stephens, P.; Davies, H.; Jones, D.; Lin, M. L.; Teague, J.; Bignell, G.; Butler, A.; Cho, J.; Dalgliesh, G. L.; Galappaththige, D.; Greenman, C.; Hardy, C.; Jia, M.; Latimer, C.; Lau, K. W.; Marshall, J.; McLaren, S.; Menzies, A.; Mudie, L.; Stebbings, L.; Largaespada, D. A.; Wessels, L. F.; Richard, S.; Kahnoski, R. J.; Anema, J.; Tuveson, D. A.; Perez-Mancera, P. A.; Mustonen, V.; Fischer, A.; Adams, D. J.; Rust, A.; Chan-on, W.; Subimerb, C.; Dykema, K.; Furge, K.; Campbell, P. J.; Teh, B. T.; Stratton, M. R.; Futreal, P. A. Exome sequencing identifies frequent mutation of the SWI/SNF complex gene PBRM1 in renal carcinoma. *Nature* **2011**, *469,* 539-542.

(45) Versteege, I.; Sévenet, N.; Lange, J.; Rousseau-Merck, M.-F.; Ambros, P.; Handgretinger, R.; Aurias, A.; Delattre, O. Truncating mutations of hSNF5/INI1 in aggressive paediatric cancer. *Nature* **1998**, *394,* 203-206.
(46) Biegel, J. A.; Zhou, J. Y.; Rorke, L. B.; Stenstrom, C.; Wainwright, L. M.; Fogelgren, B. Germ-line and acquired mutations of INI1 in atypical teratoid and rhabdoid tumors. *Cancer Res* **1999**, *59,* 74-79.
(47) Sévenet, N.; Sheridan, E.; Amram, D.; Schneider, P.; Handgretinger, R.; Delattre, O. Constitutional mutations of the hSNF5/INI1 gene predispose to a variety of cancers. *Am J Hum Genet* **1999**, *65,* 1342-1348.
(48) Lu, B.; Shi, H. An In-Depth Look at Small Cell Carcinoma of the Ovary, Hypercalcemic Type (SCCOHT): Clinical Implications from Recent Molecular Findings. *J Cancer* **2019**, *10,* 223-237.
(49) Hartwell, L. H.; Szankasi, P.; Roberts, C. J.; Murray, A. W.; Friend, S. H. Integrating genetic approaches into the discovery of anticancer drugs. *Science* **1997**, *278,* 1064-1068.
(50) Kim, G.; Ison, G.; McKee, A. E.; Zhang, H.; Tang, S.; Gwise, T.; Sridhara, R.; Lee, E.; Tzou, A.; Philip, R.; Chiu, H. J.; Ricks, T. K.; Palmby, T.; Russell, A. M.; Ladouceur, G.; Pfuma, E.; Li, H.; Zhao, L.; Liu, Q.; Venugopal, R.; Ibrahim, A.; Pazdur, R. FDA Approval Summary: Olaparib Monotherapy in Patients with Deleterious Germline BRCA-Mutated Advanced Ovarian Cancer Treated with Three or More Lines of Chemotherapy. *Clin Cancer Res* **2015**, *21,* 4257-4261.
(51) Lord, C. J.; Ashworth, A. PARP inhibitors: Synthetic lethality in the clinic. *Science* **2017**, *355,* 1152-1158.
(52) Mathur, R.; Alver, B. H.; San Roman, A. K.; Wilson, B. G.; Wang, X.; Agoston, A. T.; Park, P. J.; Shivdasani, R. A.; Roberts, C. W. ARID1A loss impairs enhancer-mediated gene regulation and drives colon cancer in mice. *Nat Genet* **2017**, *49,* 296-302.
(53) Helming, K. C.; Wang, X.; Wilson, B. G.; Vazquez, F.; Haswell, J. R.; Manchester, H. E.; Kim, Y.; Kryukov, G. V.; Ghandi, M.; Aguirre, A. J.; Jagani, Z.; Wang, Z.; Garraway, L. A.; Hahn, W. C.; Roberts, C. W. ARID1B is a specific vulnerability in ARID1A-mutant cancers. *Nat Med* **2014**, *20,* 251-254.
(54) Oike, T.; Ogiwara, H.; Tominaga, Y.; Ito, K.; Ando, O.; Tsuta, K.; Mizukami, T.; Shimada, Y.; Isomura, H.; Komachi, M.; Furuta, K.; Watanabe, S.; Nakano, T.; Yokota, J.; Kohno, T. A synthetic lethality-based strategy to treat cancers harboring a genetic deficiency in the chromatin remodeling factor BRG1. *Cancer Res* **2013**, *73,* 5508-5518.
(55) Hoffman, G. R.; Rahal, R.; Buxton, F.; Xiang, K.; McAllister, G.; Frias, E.; Bagdasarian, L.; Huber, J.; Lindeman, A.; Chen, D.; Romero, R.; Ramadan, N.; Phadke, T.; Haas, K.; Jaskelioff, M.; Wilson, B. G.; Meyer, M. J.; Saenz-Vash, V.; Zhai, H.; Myer, V. E.; Porter, J. A.; Keen, N.; McLaughlin, M. E.; Mickanin, C.; Roberts, C. W.; Stegmeier, F.; Jagani, Z. Functional epigenetics approach identifies BRM/SMARCA2 as a critical synthetic lethal target in BRG1-deficient cancers. *Proc Natl Acad Sci U S A* **2014**, *111,* 3128-3133.
(56) Wilson, B. G.; Helming, K. C.; Wang, X.; Kim, Y.; Vazquez, F.; Jagani, Z.; Hahn, W. C.; Roberts, C. W. Residual complexes containing SMARCA2 (BRM) underlie the oncogenic drive of SMARCA4 (BRG1) mutation. *Mol Cell Biol* **2014**, *34,* 1136-1144.
(57) Jelinic, P.; Mueller, J. J.; Olvera, N.; Dao, F.; Scott, S. N.; Shah, R.; Gao, J.; Schultz, N.; Gonen, M.; Soslow, R. A.; Berger, M. F.; Levine, D. A. Recurrent SMARCA4 mutations in small cell carcinoma of the ovary. *Nat Genet* **2014**, *46,* 424-426.
(58) Ramos, P.; Karnezis, A. N.; Craig, D. W.; Sekulic, A.; Russell, M. L.; Hendricks, W. P.; Corneveaux, J. J.; Barrett, M. T.; Shumansky, K.; Yang, Y.; Shah, S. P.; Prentice, L. M.; Marra, M. A.; Kiefer, J.; Zismann, V. L.; McEachron, T. A.; Salhia, B.; Prat, J.; D'Angelo, E.; Clarke, B. A.; Pressey, J. G.; Farley, J. H.; Anthony, S. P.; Roden, R. B.; Cunliffe, H. E.; Huntsman, D. G.; Trent, J. M. Small cell carcinoma of the ovary, hypercalcemic type, displays frequent inactivating germline and somatic mutations in SMARCA4. *Nat Genet* **2014**, *46,* 427-429.
(59) Hodis, E.; Watson, I. R.; Kryukov, G. V.; Arold, S. T.; Imielinski, M.; Theurillat, J. P.; Nickerson, E.; Auclair, D.; Li, L.; Place, C.; Dicara, D.; Ramos, A. H.; Lawrence, M. S.; Cibulskis, K.; Sivachenko, A.; Voet, D.; Saksena, G.; Stransky, N.; Onofrio, R. C.; Winckler, W.; Ardlie, K.; Wagle, N.; Wargo, J.; Chong, K.; Morton, D. L.; Stemke-Hale, K.; Chen, G.; Noble, M.; Meyerson, M.; Ladbury, J. E.; Davies, M. A.;

Gershenwald, J. E.; Wagner, S. N.; Hoon, D. S.; Schadendorf, D.; Lander, E. S.; Gabriel, S. B.; Getz, G.; Garraway, L. A.; Chin, L. A landscape of driver mutations in melanoma. *Cell* **2012**, *150,* 251-263.
(60) Imielinski, M.; Berger, A. H.; Hammerman, P. S.; Hernandez, B.; Pugh, T. J.; Hodis, E.; Cho, J.; Suh, J.; Capelletti, M.; Sivachenko, A.; Sougnez, C.; Auclair, D.; Lawrence, M. S.; Stojanov, P.; Cibulskis, K.; Choi, K.; de Waal, L.; Sharifnia, T.; Brooks, A.; Greulich, H.; Banerji, S.; Zander, T.; Seidel, D.; Leenders, F.; Ansén, S.; Ludwig, C.; Engel-Riedel, W.; Stoelben, E.; Wolf, J.; Goparju, C.; Thompson, K.; Winckler, W.; Kwiatkowski, D.; Johnson, B. E.; Jänne, P. A.; Miller, V. A.; Pao, W.; Travis, W. D.; Pass, H. I.; Gabriel, S. B.; Lander, E. S.; Thomas, R. K.; Garraway, L. A.; Getz, G.; Meyerson, M. Mapping the hallmarks of lung adenocarcinoma with massively parallel sequencing. *Cell* **2012**, *150,* 1107-1120.
(61) Medina, P. P.; Carretero, J.; Fraga, M. F.; Esteller, M.; Sidransky, D.; Sanchez-Cespedes, M. Genetic and epigenetic screening for gene alterations of the chromatin-remodeling factor, SMARCA4/BRG1, in lung tumors. *Genes Chromosomes Cancer* **2004**, *41,* 170-177.
(62) Fernando, T. M.; Piskol, R.; Bainer, R.; Sokol, E. S.; Trabucco, S. E.; Zhang, Q.; Trinh, H.; Maund, S.; Kschonsak, M.; Chaudhuri, S.; Modrusan, Z.; Januario, T.; Yauch, R. L. Functional characterization of SMARCA4 variants identified by targeted exome-sequencing of 131,668 cancer patients. *Nat Commun* **2020**, *11,* 5551.
(63) Filippakopoulos, P.; Picaud, S.; Mangos, M.; Keates, T.; Lambert, J. P.; Barsyte-Lovejoy, D.; Felletar, I.; Volkmer, R.; Müller, S.; Pawson, T.; Gingras, A. C.; Arrowsmith, C. H.; Knapp, S. Histone recognition and large-scale structural analysis of the human bromodomain family. *Cell* **2012**, *149,* 214-231.
(64) Brand, M.; Measures, A. R.; Wilson, B. G.; Cortopassi, W. A.; Alexander, R.; Höss, M.; Hewings, D. S.; Rooney, T. P.; Paton, R. S.; Conway, S. J. Small molecule inhibitors of bromodomain-acetyl-lysine interactions. *ACS Chem Biol* **2015**, *10,* 22-39.
(65) Shorstova, T.; Foulkes, W. D.; Witcher, M. Achieving clinical success with BET inhibitors as anti-cancer agents. *Br J Cancer* **2021**, *124,* 1478-1490.
(66) Andrieu, G.; Belkina, A. C.; Denis, G. V. Clinical trials for BET inhibitors run ahead of the science. *Drug Discov Today Technol* **2016**, *19,* 45-50.
(67) Vidler, L. R.; Brown, N.; Knapp, S.; Hoelder, S. Druggability analysis and structural classification of bromodomain acetyl-lysine binding sites. *J Med Chem* **2012**, *55,* 7346-7359.
(68) Fedorov, O.; Castex, J.; Tallant, C.; Owen, D. R.; Martin, S.; Aldeghi, M.; Monteiro, O.; Filippakopoulos, P.; Picaud, S.; Trzupek, J. D.; Gerstenberger, B. S.; Bountra, C.; Willmann, D.; Wells, C.; Philpott, M.; Rogers, C.; Biggin, P. C.; Brennan, P. E.; Bunnage, M. E.; Schüle, R.; Günther, T.; Knapp, S.; Müller, S. Selective targeting of the BRG/PB1 bromodomains impairs embryonic and trophoblast stem cell maintenance. *Sci Adv* **2015**, *1,* e1500723.
(69) Gerstenberger, B. S.; Trzupek, J. D.; Tallant, C.; Fedorov, O.; Filippakopoulos, P.; Brennan, P. E.; Fedele, V.; Martin, S.; Picaud, S.; Rogers, C.; Parikh, M.; Taylor, A.; Samas, B.; O'Mahony, A.; Berg, E.; Pallares, G.; Torrey, A. D.; Treiber, D. K.; Samardjiev, I. J.; Nasipak, B. T.; Padilla-Benavides, T.; Wu, Q.; Imbalzano, A. N.; Nickerson, J. A.; Bunnage, M. E.; Müller, S.; Knapp, S.; Owen, D. R. Identification of a Chemical Probe for Family VIII Bromodomains through Optimization of a Fragment Hit. *J Med Chem* **2016**, *59,* 4800-4811.
(70) Vangamudi, B.; Paul, T. A.; Shah, P. K.; Kost-Alimova, M.; Nottebaum, L.; Shi, X.; Zhan, Y.; Leo, E.; Mahadeshwar, H. S.; Protopopov, A.; Futreal, A.; Tieu, T. N.; Peoples, M.; Heffernan, T. P.; Marszalek, J. R.; Toniatti, C.; Petrocchi, A.; Verhelle, D.; Owen, D. R.; Draetta, G.; Jones, P.; Palmer, W. S.; Sharma, S.; Andersen, J. N. The SMARCA2/4 ATPase Domain Surpasses the Bromodomain as a Drug Target in SWI/SNF-Mutant Cancers: Insights from cDNA Rescue and PFI-3 Inhibitor Studies. *Cancer Res* **2015**, *75,* 3865-3878.
(71) Albrecht, B. K.; Cote, A.; Crawford, T.; Duplessis, M.; Good, A. C.; Leblanc, Y.; Magnuson, S. R.; Nasveschuk, C. G.; Romero, F. A.; Tang, Y.; Taylor, A. M. Preparation of therapeutic pyridazine compounds useful as inhibitors of BRG1, BRM and PB1. WO2016138114, 2016.
(72) Taylor, A. M.; Bailey, C.; Belmont, L. D.; Campbell, R.; Cantone, N.; Côté, A.; Crawford, T. D.; Cummings, R.; DeMent, K.; Duplessis, M.; Flynn, M.; Good, A. C.; Huang, H. R.; Joshi, S.; Leblanc, Y.; Murray, J.; Nasveschuk, C. G.; Neiss, A.; Poy, F.; Romero, F. A.; Sandy, P.; Tang, Y.; Tsui, V.; Zawadzke,

L.; Sims, R. J., 3rd; Audia, J. E.; Bellon, S. F.; Magnuson, S. R.; Albrecht, B. K.; Cochran, A. G. GNE-064: A Potent, Selective, and Orally Bioavailable Chemical Probe for the Bromodomains of SMARCA2 and SMARCA4 and the Fifth Bromodomain of PBRM1. *J Med Chem* **2022**, *65,* 11177-11186.
(73) Ji, N.; Zhang, Y.; Sintchak, M. D. Preparation of heterocyclic compounds as SMARCA inhibitors and uses thereof. WO2020251974, 2020.
(74) Ji, N.; Zhang, Y.; Sintchak, M. D.; Fleming, P. R. Preparation of heterocyclic compounds as SMARCA degraders and uses thereof. WO2020251972, 2020.
(75) Sutherell, C. L.; Tallant, C.; Monteiro, O. P.; Yapp, C.; Fuchs, J. E.; Fedorov, O.; Siejka, P.; Müller, S.; Knapp, S.; Brenton, J. D.; Brennan, P. E.; Ley, S. V. Identification and Development of 2,3-Dihydropyrrolo[1,2-a]quinazolin-5(1H)-one Inhibitors Targeting Bromodomains within the Switch/Sucrose Nonfermenting Complex. *J Med Chem* **2016**, *59,* 5095-5101.
(76) Papillon, J. P. N.; Nakajima, K.; Adair, C. D.; Hempel, J.; Jouk, A. O.; Karki, R. G.; Mathieu, S.; Mobitz, H.; Ntaganda, R.; Smith, T.; Visser, M.; Hill, S. E.; Hurtado, F. K.; Chenail, G.; Bhang, H. C.; Bric, A.; Xiang, K.; Bushold, G.; Gilbert, T.; Vattay, A.; Dooley, J.; Costa, E. A.; Park, I.; Li, A.; Farley, D.; Lounkine, E.; Yue, Q. K.; Xie, X.; Zhu, X.; Kulathila, R.; King, D.; Hu, T.; Vulic, K.; Cantwell, J.; Luu, C.; Jagani, Z. Discovery of Orally Active Inhibitors of Brahma Homolog (BRM)/SMARCA2 ATPase Activity for the Treatment of Brahma Related Gene 1 (BRG1)/SMARCA4-Mutant Cancers. *J Med Chem* **2018**, *61,* 10155-10172.
(77) Bultman, S. J.; Holley, D. W.; G, G. d. R.; Pizzo, S. V.; Sidorova, T. N.; Murray, K. T.; Jensen, B. C.; Wang, Z.; Bevilacqua, A.; Chen, X.; Quintana, M. T.; Tannu, M.; Rosson, G. B.; Pandya, K.; Willis, M. S. BRG1 and BRM SWI/SNF ATPases redundantly maintain cardiomyocyte homeostasis by regulating cardiomyocyte mitophagy and mitochondrial dynamics in vivo. *Cardiovasc Pathol* **2016**, *25,* 258-269.
(78) Holik, A. Z.; Krzystyniak, J.; Young, M.; Richardson, K.; Jardé, T.; Chambon, P.; Shorning, B. Y.; Clarke, A. R. Brg1 is required for stem cell maintenance in the murine intestinal epithelium in a tissue-specific manner. *Stem Cells* **2013**, *31,* 2457-2466.
(79) Richard, C. C.; Luis, M. M. S.; Salih, T.; Rishi, G. V.; Kana, I.; Zhifang, L.; Hong, F.; Jeremy, W. S.; David, L. L.; Laura, E. Z.; Xueying, C.; Kimberly, D. B.; Jordana, M.; Neville, A.; Gabriel, J. S.; Katharine, F.; GiNell, E.; Ammar, A.; David, H.; Yunji, D.; Shawn, S.; Kevin, J. W.; Johannes, V.; Lan, X.; Martin, H.; David, S. M.; Ho Man, C.; Carl, P. D.; Ryan, G. K.; Steven, F. B. Pharmacologic inhibition of BAF chromatin remodeling complexes as a therapeutic approach to transcription factor-dependent cancers. *bioRxiv* **2023**, 2023.2009.2011.557162.
(80) *FHD-286 as Monotherapy or Combination Therapy in Subjects With Advanced Hematologic Malignancies*. 2023. https://clinicaltrials.gov/study/NCT04891757?term=FHD-286&rank=2 (accessed Nov 5 2023).
(81) *Death triggers FDA hold on Foghorn blood cancer clinical trial, shrouding timing of data drop*. 2022. https://www.fiercebiotech.com/biotech/death-triggers-fda-hold-foghorn-blood-cancer-clinical-trial-shrouding-timing-data-drop (accessed 2023 Oct 2).
(82) Stanton, B. Z.; Chory, E. J.; Crabtree, G. R. Chemically induced proximity in biology and medicine. *Science* **2018**, *359,*
(83) Cruz Walma, D. A.; Chen, Z.; Bullock, A. N.; Yamada, K. M. Ubiquitin ligases: guardians of mammalian development. *Nat Rev Mol Cell Biol* **2022**, *23,* 350-367.
(84) Békés, M.; Langley, D. R.; Crews, C. M. PROTAC targeted protein degraders: the past is prologue. *Nat Rev Drug Discov* **2022**, *21,* 181-200.
(85) Han, X.; Zhao, L.; Xiang, W.; Qin, C.; Miao, B.; Xu, T.; Wang, M.; Yang, C. Y.; Chinnaswamy, K.; Stuckey, J.; Wang, S. Discovery of Highly Potent and Efficient PROTAC Degraders of Androgen Receptor (AR) by Employing Weak Binding Affinity VHL E3 Ligase Ligands. *J Med Chem* **2019**, *62,* 11218-11231.
(86) Bondeson, D. P.; Mares, A.; Smith, I. E.; Ko, E.; Campos, S.; Miah, A. H.; Mulholland, K. E.; Routly, N.; Buckley, D. L.; Gustafson, J. L.; Zinn, N.; Grandi, P.; Shimamura, S.; Bergamini, G.; Faelth-Savitski, M.; Bantscheff, M.; Cox, C.; Gordon, D. A.; Willard, R. R.; Flanagan, J. J.; Casillas, L. N.; Votta, B. J.; den Besten, W.; Famm, K.; Kruidenier, L.; Carter, P. S.; Harling, J. D.; Churcher, I.; Crews, C. M. Catalytic in vivo protein knockdown by small-molecule PROTACs. *Nat Chem Biol* **2015**, *11,* 611-617.

(87) Yang, L.; Tu, W.; Huang, L.; Miao, B.; Kaneshige, A.; Jiang, W.; Leng, L.; Wang, M.; Wen, B.; Sun, D.; Wang, S. Discovery of SMD-3040 as a Potent and Selective SMARCA2 PROTAC Degrader with Strong in vivo Antitumor Activity. *Journal of Medicinal Chemistry* **2023**, *66,* 10761-10781.
(88) Bai, L.; Zhou, H.; Xu, R.; Zhao, Y.; Chinnaswamy, K.; McEachern, D.; Chen, J.; Yang, C. Y.; Liu, Z.; Wang, M.; Liu, L.; Jiang, H.; Wen, B.; Kumar, P.; Meagher, J. L.; Sun, D.; Stuckey, J. A.; Wang, S. A Potent and Selective Small-Molecule Degrader of STAT3 Achieves Complete Tumor Regression In Vivo. *Cancer Cell* **2019**, *36,* 498-511.e417.
(89) Farnaby, W.; Koegl, M.; Roy, M. J.; Whitworth, C.; Diers, E.; Trainor, N.; Zollman, D.; Steurer, S.; Karolyi-Oezguer, J.; Riedmueller, C.; Gmaschitz, T.; Wachter, J.; Dank, C.; Galant, M.; Sharps, B.; Rumpel, K.; Traxler, E.; Gerstberger, T.; Schnitzer, R.; Petermann, O.; Greb, P.; Weinstabl, H.; Bader, G.; Zoephel, A.; Weiss-Puxbaum, A.; Ehrenhofer-Wolfer, K.; Wohrle, S.; Boehmelt, G.; Rinnenthal, J.; Arnhof, H.; Wiechens, N.; Wu, M. Y.; Owen-Hughes, T.; Ettmayer, P.; Pearson, M.; McConnell, D. B.; Ciulli, A. BAF complex vulnerabilities in cancer demonstrated via structure-based PROTAC design. *Nat Chem Biol* **2019**, *15,* 672-680.
(90) Saenz, D. T.; Fiskus, W.; Qian, Y.; Manshouri, T.; Rajapakshe, K.; Raina, K.; Coleman, K. G.; Crew, A. P.; Shen, A.; Mill, C. P.; Sun, B.; Qiu, P.; Kadia, T. M.; Pemmaraju, N.; DiNardo, C.; Kim, M. S.; Nowak, A. J.; Coarfa, C.; Crews, C. M.; Verstovsek, S.; Bhalla, K. N. Novel BET protein proteolysis-targeting chimera exerts superior lethal activity than bromodomain inhibitor (BETi) against post-myeloproliferative neoplasm secondary (s) AML cells. *Leukemia* **2017**, *31,* 1951-1961.
(91) Nowak, R. P.; DeAngelo, S. L.; Buckley, D.; He, Z.; Donovan, K. A.; An, J.; Safaee, N.; Jedrychowski, M. P.; Ponthier, C. M.; Ishoey, M.; Zhang, T.; Mancias, J. D.; Gray, N. S.; Bradner, J. E.; Fischer, E. S. Plasticity in binding confers selectivity in ligand-induced protein degradation. *Nat Chem Biol* **2018**, *14,* 706-714.
(92) Gadd, M. S.; Testa, A.; Lucas, X.; Chan, K. H.; Chen, W.; Lamont, D. J.; Zengerle, M.; Ciulli, A. Structural basis of PROTAC cooperative recognition for selective protein degradation. *Nat Chem Biol* **2017**, *13,* 514-521.
(93) Hu, J.; Hu, B.; Xu, F.; Wang, M.; Qin, C.; McEachern, D.; Stuckey, J.; Wang, S. Precise Conformational Control Yielding Highly Potent and Exceptionally Selective BRD4 Degraders with Strong Antitumor Activity. *J Med Chem* **2023**, *66,* 8222-8237.
(94) Sakamoto, K. M.; Kim, K. B.; Kumagai, A.; Mercurio, F.; Crews, C. M.; Deshaies, R. J. Protacs: chimeric molecules that target proteins to the Skp1-Cullin-F box complex for ubiquitination and degradation. *Proc Natl Acad Sci U S A* **2001**, *98,* 8554-8559.
(95) Schneekloth, J. S., Jr.; Fonseca, F. N.; Koldobskiy, M.; Mandal, A.; Deshaies, R.; Sakamoto, K.; Crews, C. M. Chemical genetic control of protein levels: selective in vivo targeted degradation. *J Am Chem Soc* **2004**, *126,* 3748-3754.
(96) Toure, M.; Crews, C. M. Small-Molecule PROTACS: New Approaches to Protein Degradation. *Angew Chem Int Ed Engl* **2016**, *55,* 1966-1973.
(97) Schneekloth, A. R.; Pucheault, M.; Tae, H. S.; Crews, C. M. Targeted intracellular protein degradation induced by a small molecule: En route to chemical proteomics. *Bioorg Med Chem Lett* **2008**, *18,* 5904-5908.
(98) Vassilev, L. T.; Vu, B. T.; Graves, B.; Carvajal, D.; Podlaski, F.; Filipovic, Z.; Kong, N.; Kammlott, U.; Lukacs, C.; Klein, C.; Fotouhi, N.; Liu, E. A. In vivo activation of the p53 pathway by small-molecule antagonists of MDM2. *Science* **2004**, *303,* 844-848.
(99) Itoh, Y.; Ishikawa, M.; Naito, M.; Hashimoto, Y. Protein knockdown using methyl bestatin-ligand hybrid molecules: design and synthesis of inducers of ubiquitination-mediated degradation of cellular retinoic acid-binding proteins. *J Am Chem Soc* **2010**, *132,* 5820-5826.
(100) Demizu, Y.; Okuhira, K.; Motoi, H.; Ohno, A.; Shoda, T.; Fukuhara, K.; Okuda, H.; Naito, M.; Kurihara, M. Design and synthesis of estrogen receptor degradation inducer based on a protein knockdown strategy. *Bioorg Med Chem Lett* **2012**, *22,* 1793-1796.

(101) Demizu, Y.; Shibata, N.; Hattori, T.; Ohoka, N.; Motoi, H.; Misawa, T.; Shoda, T.; Naito, M.; Kurihara, M. Development of BCR-ABL degradation inducers via the conjugation of an imatinib derivative and a cIAP1 ligand. *Bioorg Med Chem Lett* **2016**, *26,* 4865-4869.
(102) Ivan, M.; Kondo, K.; Yang, H.; Kim, W.; Valiando, J.; Ohh, M.; Salic, A.; Asara, J. M.; Lane, W. S.; Kaelin, W. G., Jr. HIFalpha targeted for VHL-mediated destruction by proline hydroxylation: implications for O2 sensing. *Science* **2001**, *292,* 464-468.
(103) Buckley, D. L.; Gustafson, J. L.; Van Molle, I.; Roth, A. G.; Tae, H. S.; Gareiss, P. C.; Jorgensen, W. L.; Ciulli, A.; Crews, C. M. Small-molecule inhibitors of the interaction between the E3 ligase VHL and HIF1α. *Angew Chem Int Ed Engl* **2012**, *51,* 11463-11467.
(104) Buckley, D. L.; Van Molle, I.; Gareiss, P. C.; Tae, H. S.; Michel, J.; Noblin, D. J.; Jorgensen, W. L.; Ciulli, A.; Crews, C. M. Targeting the von Hippel-Lindau E3 ubiquitin ligase using small molecules to disrupt the VHL/HIF-1α interaction. *J Am Chem Soc* **2012**, *134,* 4465-4468.
(105) Frost, J.; Galdeano, C.; Soares, P.; Gadd, M. S.; Grzes, K. M.; Ellis, L.; Epemolu, O.; Shimamura, S.; Bantscheff, M.; Grandi, P.; Read, K. D.; Cantrell, D. A.; Rocha, S.; Ciulli, A. Potent and selective chemical probe of hypoxic signalling downstream of HIF-α hydroxylation via VHL inhibition. *Nat Commun* **2016**, *7,* 13312.
(106) Zengerle, M.; Chan, K. H.; Ciulli, A. Selective Small Molecule Induced Degradation of the BET Bromodomain Protein BRD4. *ACS Chem Biol* **2015**, *10,* 1770-1777.
(107) Zoppi, V.; Hughes, S. J.; Maniaci, C.; Testa, A.; Gmaschitz, T.; Wieshofer, C.; Koegl, M.; Riching, K. M.; Daniels, D. L.; Spallarossa, A.; Ciulli, A. Iterative Design and Optimization of Initially Inactive Proteolysis Targeting Chimeras (PROTACs) Identify VZ185 as a Potent, Fast, and Selective von Hippel-Lindau (VHL) Based Dual Degrader Probe of BRD9 and BRD7. *J Med Chem* **2019**, *62,* 699-726.
(108) Salami, J.; Alabi, S.; Willard, R. R.; Vitale, N. J.; Wang, J.; Dong, H.; Jin, M.; McDonnell, D. P.; Crew, A. P.; Neklesa, T. K.; Crews, C. M. Androgen receptor degradation by the proteolysis-targeting chimera ARCC-4 outperforms enzalutamide in cellular models of prostate cancer drug resistance. *Commun Biol* **2018**, *1,* 100.
(109) Han, X.; Wang, C.; Qin, C.; Xiang, W.; Fernandez-Salas, E.; Yang, C. Y.; Wang, M.; Zhao, L.; Xu, T.; Chinnaswamy, K.; Delproposto, J.; Stuckey, J.; Wang, S. Discovery of ARD-69 as a Highly Potent Proteolysis Targeting Chimera (PROTAC) Degrader of Androgen Receptor (AR) for the Treatment of Prostate Cancer. *J Med Chem* **2019**, *62,* 941-964.
(110) Hu, J.; Hu, B.; Wang, M.; Xu, F.; Miao, B.; Yang, C. Y.; Wang, M.; Liu, Z.; Hayes, D. F.; Chinnaswamy, K.; Delproposto, J.; Stuckey, J.; Wang, S. Discovery of ERD-308 as a Highly Potent Proteolysis Targeting Chimera (PROTAC) Degrader of Estrogen Receptor (ER). *J Med Chem* **2019**, *62,* 1420-1442.
(111) Popow, J.; Arnhof, H.; Bader, G.; Berger, H.; Ciulli, A.; Covini, D.; Dank, C.; Gmaschitz, T.; Greb, P.; Karolyi-Özguer, J.; Koegl, M.; McConnell, D. B.; Pearson, M.; Rieger, M.; Rinnenthal, J.; Roessler, V.; Schrenk, A.; Spina, M.; Steurer, S.; Trainor, N.; Traxler, E.; Wieshofer, C.; Zoephel, A.; Ettmayer, P. Highly Selective PTK2 Proteolysis Targeting Chimeras to Probe Focal Adhesion Kinase Scaffolding Functions. *J Med Chem* **2019**, *62,* 2508-2520.
(112) Law, R. P.; Nunes, J.; Chung, C. W.; Bantscheff, M.; Buda, K.; Dai, H.; Evans, J. P.; Flinders, A.; Klimaszewska, D.; Lewis, A. J.; Muelbaier, M.; Scott-Stevens, P.; Stacey, P.; Tame, C. J.; Watt, G. F.; Zinn, N.; Queisser, M. A.; Harling, J. D.; Benowitz, A. B. Discovery and Characterisation of Highly Cooperative FAK-Degrading PROTACs. *Angew Chem Int Ed Engl* **2021**, *60,* 23327-23334.
(113) Yu, X.; Li, D.; Kottur, J.; Shen, Y.; Kim, H. S.; Park, K. S.; Tsai, Y. H.; Gong, W.; Wang, J.; Suzuki, K.; Parker, J.; Herring, L.; Kaniskan, H.; Cai, L.; Jain, R.; Liu, J.; Aggarwal, A. K.; Wang, G. G.; Jin, J. A selective WDR5 degrader inhibits acute myeloid leukemia in patient-derived mouse models. *Sci Transl Med* **2021**, *13,* eabj1578.
(114) Dölle, A.; Adhikari, B.; Krämer, A.; Weckesser, J.; Berner, N.; Berger, L. M.; Diebold, M.; Szewczyk, M. M.; Barsyte-Lovejoy, D.; Arrowsmith, C. H.; Gebel, J.; Löhr, F.; Dötsch, V.; Eilers, M.; Heinzlmeir, S.; Kuster, B.; Sotriffer, C.; Wolf, E.; Knapp, S. Design, Synthesis, and Evaluation of WD-Repeat-Containing Protein 5 (WDR5) Degraders. *J Med Chem* **2021**, *64,* 10682-10710.

(115) Khan, S.; Zhang, X.; Lv, D.; Zhang, Q.; He, Y.; Zhang, P.; Liu, X.; Thummuri, D.; Yuan, Y.; Wiegand, J. S.; Pei, J.; Zhang, W.; Sharma, A.; McCurdy, C. R.; Kuruvilla, V. M.; Baran, N.; Ferrando, A. A.; Kim, Y. M.; Rogojina, A.; Houghton, P. J.; Huang, G.; Hromas, R.; Konopleva, M.; Zheng, G.; Zhou, D. A selective BCL-X(L) PROTAC degrader achieves safe and potent antitumor activity. *Nat Med* **2019**, *25,* 1938-1947.
(116) Burslem, G. M.; Smith, B. E.; Lai, A. C.; Jaime-Figueroa, S.; McQuaid, D. C.; Bondeson, D. P.; Toure, M.; Dong, H.; Qian, Y.; Wang, J.; Crew, A. P.; Hines, J.; Crews, C. M. The Advantages of Targeted Protein Degradation Over Inhibition: An RTK Case Study. *Cell Chem Biol* **2018**, *25,* 67-77.e63.
(117) Kofink, C.; Trainor, N.; Mair, B.; Wohrle, S.; Wurm, M.; Mischerikow, N.; Roy, M. J.; Bader, G.; Greb, P.; Garavel, G.; Diers, E.; McLennan, R.; Whitworth, C.; Vetma, V.; Rumpel, K.; Scharnweber, M.; Fuchs, J. E.; Gerstberger, T.; Cui, Y.; Gremel, G.; Chetta, P.; Hopf, S.; Budano, N.; Rinnenthal, J.; Gmaschitz, G.; Mayer, M.; Koegl, M.; Ciulli, A.; Weinstabl, H.; Farnaby, W. A selective and orally bioavailable VHL-recruiting PROTAC achieves SMARCA2 degradation in vivo. *Nat Commun* **2022**, *13,* 5969.
(118) Cantley, J.; Ye, X.; Rousseau, E.; Januario, T.; Hamman, B. D.; Rose, C. M.; Cheung, T. K.; Hinkle, T.; Soto, L.; Quinn, C.; Harbin, A.; Bortolon, E.; Chen, X.; Haskell, R.; Lin, E.; Yu, S. F.; Del Rosario, G.; Chan, E.; Dunlap, D.; Koeppen, H.; Martin, S.; Merchant, M.; Grimmer, M.; Broccatelli, F.; Wang, J.; Pizzano, J.; Dragovich, P. S.; Berlin, M.; Yauch, R. L. Selective PROTAC-mediated degradation of SMARCA2 is efficacious in SMARCA4 mutant cancers. *Nat Commun* **2022**, *13,* 6814.
(119) Ito, T.; Ando, H.; Suzuki, T.; Ogura, T.; Hotta, K.; Imamura, Y.; Yamaguchi, Y.; Handa, H. Identification of a primary target of thalidomide teratogenicity. *Science* **2010**, *327,* 1345-1350.
(120) Krönke, J.; Udeshi, N. D.; Narla, A.; Grauman, P.; Hurst, S. N.; McConkey, M.; Svinkina, T.; Heckl, D.; Comer, E.; Li, X.; Ciarlo, C.; Hartman, E.; Munshi, N.; Schenone, M.; Schreiber, S. L.; Carr, S. A.; Ebert, B. L. Lenalidomide causes selective degradation of IKZF1 and IKZF3 in multiple myeloma cells. *Science* **2014**, *343,* 301-305.
(121) Petzold, G.; Fischer, E. S.; Thomä, N. H. Structural basis of lenalidomide-induced CK1α degradation by the CRL4(CRBN) ubiquitin ligase. *Nature* **2016**, *532,* 127-130.
(122) Winter, G. E.; Buckley, D. L.; Paulk, J.; Roberts, J. M.; Souza, A.; Dhe-Paganon, S.; Bradner, J. E. DRUG DEVELOPMENT. Phthalimide conjugation as a strategy for in vivo target protein degradation. *Science* **2015**, *348,* 1376-1381.
(123) Lu, J.; Qian, Y.; Altieri, M.; Dong, H.; Wang, J.; Raina, K.; Hines, J.; Winkler, J. D.; Crew, A. P.; Coleman, K.; Crews, C. M. Hijacking the E3 Ubiquitin Ligase Cereblon to Efficiently Target BRD4. *Chem Biol* **2015**, *22,* 755-763.
(124) Zhou, B.; Hu, J.; Xu, F.; Chen, Z.; Bai, L.; Fernandez-Salas, E.; Lin, M.; Liu, L.; Yang, C. Y.; Zhao, Y.; McEachern, D.; Przybranowski, S.; Wen, B.; Sun, D.; Wang, S. Discovery of a Small-Molecule Degrader of Bromodomain and Extra-Terminal (BET) Proteins with Picomolar Cellular Potencies and Capable of Achieving Tumor Regression. *J Med Chem* **2018**, *61,* 462-481.
(125) Qin, C.; Hu, Y.; Zhou, B.; Fernandez-Salas, E.; Yang, C. Y.; Liu, L.; McEachern, D.; Przybranowski, S.; Wang, M.; Stuckey, J.; Meagher, J.; Bai, L.; Chen, Z.; Lin, M.; Yang, J.; Ziazadeh, D. N.; Xu, F.; Hu, J.; Xiang, W.; Huang, L.; Li, S.; Wen, B.; Sun, D.; Wang, S. Discovery of QCA570 as an Exceptionally Potent and Efficacious Proteolysis Targeting Chimera (PROTAC) Degrader of the Bromodomain and Extra-Terminal (BET) Proteins Capable of Inducing Complete and Durable Tumor Regression. *J Med Chem* **2018**, *61,* 6685-6704.
(126) Su, S.; Yang, Z.; Gao, H.; Yang, H.; Zhu, S.; An, Z.; Wang, J.; Li, Q.; Chandarlapaty, S.; Deng, H.; Wu, W.; Rao, Y. Potent and Preferential Degradation of CDK6 via Proteolysis Targeting Chimera Degraders. *J Med Chem* **2019**, *62,* 7575-7582.
(127) Robb, C. M.; Contreras, J. I.; Kour, S.; Taylor, M. A.; Abid, M.; Sonawane, Y. A.; Zahid, M.; Murry, D. J.; Natarajan, A.; Rana, S. Chemically induced degradation of CDK9 by a proteolysis targeting chimera (PROTAC). *Chem Commun (Camb)* **2017**, *53,* 7577-7580.
(128) Qiu, X.; Li, Y.; Yu, B.; Ren, J.; Huang, H.; Wang, M.; Ding, H.; Li, Z.; Wang, J.; Bian, J. Discovery of selective CDK9 degraders with enhancing antiproliferative activity through PROTAC conversion. *Eur J Med Chem* **2021**, *211,* 113091.

(129) Jaime-Figueroa, S.; Buhimschi, A. D.; Toure, M.; Hines, J.; Crews, C. M. Design, synthesis and biological evaluation of Proteolysis Targeting Chimeras (PROTACs) as a BTK degraders with improved pharmacokinetic properties. *Bioorg Med Chem Lett* **2020**, *30,* 126877.
(130) Xue, G.; Chen, J.; Liu, L.; Zhou, D.; Zuo, Y.; Fu, T.; Pan, Z. Protein degradation through covalent inhibitor-based PROTACs. *Chem Commun (Camb)* **2020**, *56,* 1521-1524.
(131) Kaneshige, A.; Bai, L.; Wang, M.; McEachern, D.; Meagher, J. L.; Xu, R.; Wang, Y.; Jiang, W.; Metwally, H.; Kirchhoff, P. D.; Zhao, L.; Jiang, H.; Wang, M.; Wen, B.; Sun, D.; Stuckey, J. A.; Wang, S. A selective small-molecule STAT5 PROTAC degrader capable of achieving tumor regression in vivo. *Nat Chem Biol* **2023**, *19,* 703-711.
(132) Papatzimas, J. W.; Gorobets, E.; Maity, R.; Muniyat, M. I.; MacCallum, J. L.; Neri, P.; Bahlis, N. J.; Derksen, D. J. From Inhibition to Degradation: Targeting the Antiapoptotic Protein Myeloid Cell Leukemia 1 (MCL1). *J Med Chem* **2019**, *62,* 5522-5540.
(133) Zhang, X.; Thummuri, D.; He, Y.; Liu, X.; Zhang, P.; Zhou, D.; Zheng, G. Utilizing PROTAC technology to address the on-target platelet toxicity associated with inhibition of BCL-X(L). *Chem Commun (Camb)* **2019**, *55,* 14765-14768.
(134) Zhang, C.; Han, X. R.; Yang, X.; Jiang, B.; Liu, J.; Xiong, Y.; Jin, J. Proteolysis Targeting Chimeras (PROTACs) of Anaplastic Lymphoma Kinase (ALK). *Eur J Med Chem* **2018**, *151,* 304-314.
(135) Xiang, W.; Zhao, L.; Han, X.; Qin, C.; Miao, B.; McEachern, D.; Wang, Y.; Metwally, H.; Kirchhoff, P. D.; Wang, L.; Matvekas, A.; He, M.; Wen, B.; Sun, D.; Wang, S. Discovery of ARD-2585 as an Exceptionally Potent and Orally Active PROTAC Degrader of Androgen Receptor for the Treatment of Advanced Prostate Cancer. *J Med Chem* **2021**, *64,* 13487-13509.
(136) Han, X.; Zhao, L.; Xiang, W.; Qin, C.; Miao, B.; McEachern, D.; Wang, Y.; Metwally, H.; Wang, L.; Matvekas, A.; Wen, B.; Sun, D.; Wang, S. Strategies toward Discovery of Potent and Orally Bioavailable Proteolysis Targeting Chimera Degraders of Androgen Receptor for the Treatment of Prostate Cancer. *J Med Chem* **2021**, *64,* 12831-12854.
(137) Chen, Z.; Hu, B.; Rej, R. K.; Wu, D.; Acharyya, R. K.; Wang, M.; Xu, T.; Lu, J.; Metwally, H.; Wang, Y.; McEachern, D.; Bai, L.; Gersch, C. L.; Wang, M.; Zhang, W.; Li, Q.; Wen, B.; Sun, D.; Rae, J. M.; Wang, S. Discovery of ERD-3111 as a Potent and Orally Efficacious Estrogen Receptor PROTAC Degrader with Strong Antitumor Activity. *J Med Chem* **2023**, *66,* 12559-12585.
(138) Lai, A. C.; Toure, M.; Hellerschmied, D.; Salami, J.; Jaime-Figueroa, S.; Ko, E.; Hines, J.; Crews, C. M. Modular PROTAC Design for the Degradation of Oncogenic BCR-ABL. *Angew Chem Int Ed Engl* **2016**, *55,* 807-810.
(139) Schiedel, M.; Herp, D.; Hammelmann, S.; Swyter, S.; Lehotzky, A.; Robaa, D.; Oláh, J.; Ovádi, J.; Sippl, W.; Jung, M. Chemically Induced Degradation of Sirtuin 2 (Sirt2) by a Proteolysis Targeting Chimera (PROTAC) Based on Sirtuin Rearranging Ligands (SirReals). *J Med Chem* **2018**, *61,* 482-491.
(140) Yang, K.; Song, Y.; Xie, H.; Wu, H.; Wu, Y. T.; Leisten, E. D.; Tang, W. Development of the first small molecule histone deacetylase 6 (HDAC6) degraders. *Bioorg Med Chem Lett* **2018**, *28,* 2493-2497.
(141) Qu, X.; Liu, H.; Song, X.; Sun, N.; Zhong, H.; Qiu, X.; Yang, X.; Jiang, B. Effective degradation of EGFR(L858R+T790M) mutant proteins by CRBN-based PROTACs through both proteosome and autophagy/lysosome degradation systems. *Eur J Med Chem* **2021**, *218,* 113328.
(142) Yu, X.; Cheng, M.; Lu, K.; Shen, Y.; Zhong, Y.; Liu, J.; Xiong, Y.; Jin, J. Exploring Degradation of Mutant and Wild-Type Epidermal Growth Factor Receptors Induced by Proteolysis-Targeting Chimeras. *J Med Chem* **2022**, *65,* 8416-8443.
(143) Soares, P.; Gadd, M. S.; Frost, J.; Galdeano, C.; Ellis, L.; Epemolu, O.; Rocha, S.; Read, K. D.; Ciulli, A. Group-Based Optimization of Potent and Cell-Active Inhibitors of the von Hippel-Lindau (VHL) E3 Ubiquitin Ligase: Structure-Activity Relationships Leading to the Chemical Probe (2S,4R)-1-((S)-2-(1-Cyanocyclopropanecarboxamido)-3,3-dimethylbutanoyl)-4-hydroxy-N-(4-(4-methylthiazol-5-yl)benzyl)pyrrolidine-2-carboxamide (VH298). *J Med Chem* **2018**, *61,* 599-618.
(144) Xiao, L.; Parolia, A.; Qiao, Y.; Bawa, P.; Eyunni, S.; Mannan, R.; Carson, S. E.; Chang, Y.; Wang, X.; Zhang, Y.; Vo, J. N.; Kregel, S.; Simko, S. A.; Delekta, A. D.; Jaber, M.; Zheng, H.; Apel, I. J.; McMurry, L.; Su, F.; Wang, R.; Zelenka-Wang, S.; Sasmal, S.; Khare, L.; Mukherjee, S.; Abbineni, C.; Aithal, K.;

Bhakta, M. S.; Ghurye, J.; Cao, X.; Navone, N. M.; Nesvizhskii, A. I.; Mehra, R.; Vaishampayan, U.; Blanchette, M.; Wang, Y.; Samajdar, S.; Ramachandra, M.; Chinnaiyan, A. M. Targeting SWI/SNF ATPases in enhancer-addicted prostate cancer. *Nature* **2022**, *601,* 434-439.
(145) *A Study of PRT3789 in Participants With Select Advanced or Metastatic Solid Tumors With a SMARCA4 Mutation*. 2023. https://www.clinicaltrials.gov/study/NCT05639751 (accessed Nov 5 2023).
(146) Li, Y. Y.; Hanna, G. J.; Laga, A. C.; Haddad, R. I.; Lorch, J. H.; Hammerman, P. S. Genomic analysis of metastatic cutaneous squamous cell carcinoma. *Clin Cancer Res* **2015**, *21,* 1447-1456.
(147) Lu, T.; Hu, J. C.; Lu, W. C.; Han, J.; Ding, H.; Jiang, H.; Zhang, Y. Y.; Yue, L. Y.; Chen, S. J.; Jiang, H. L.; Chen, K. X.; Chai, H. F.; Luo, C. Identification of small molecule inhibitors targeting the SMARCA2 bromodomain from a high-throughput screening assay. *Acta Pharmacol Sin* **2018**, *39,* 1544-1552.
(148) Bondeson, D. P.; Smith, B. E.; Burslem, G. M.; Buhimschi, A. D.; Hines, J.; Jaime-Figueroa, S.; Wang, J.; Hamman, B. D.; Ishchenko, A.; Crews, C. M. Lessons in PROTAC Design from Selective Degradation with a Promiscuous Warhead. *Cell Chem Biol* **2018**, *25,* 78-87.e75.
(149) Smith, B. E.; Wang, S. L.; Jaime-Figueroa, S.; Harbin, A.; Wang, J.; Hamman, B. D.; Crews, C. M. Differential PROTAC substrate specificity dictated by orientation of recruited E3 ligase. *Nat Commun* **2019**, *10,* 131.
(150) Diehl, C. J.; Ciulli, A. Discovery of small molecule ligands for the von Hippel-Lindau (VHL) E3 ligase and their use as inhibitors and PROTAC degraders. *Chem Soc Rev* **2022**, *51,* 8216-8257.
(151) Riching, K. M.; Mahan, S. D.; Urh, M.; Daniels, D. L. High-Throughput Cellular Profiling of Targeted Protein Degradation Compounds using HiBiT CRISPR Cell Lines. *J Vis Exp* **2020**,
(152) Galdeano, C.; Gadd, M. S.; Soares, P.; Scaffidi, S.; Van Molle, I.; Birced, I.; Hewitt, S.; Dias, D. M.; Ciulli, A. Structure-guided design and optimization of small molecules targeting the protein-protein interaction between the von Hippel-Lindau (VHL) E3 ubiquitin ligase and the hypoxia inducible factor (HIF) alpha subunit with in vitro nanomolar affinities. *J Med Chem* **2014**, *57,* 8657-8663.
(153) Kim, K. H.; Kim, W.; Howard, T. P.; Vazquez, F.; Tsherniak, A.; Wu, J. N.; Wang, W.; Haswell, J. R.; Walensky, L. D.; Hahn, W. C.; Orkin, S. H.; Roberts, C. W. SWI/SNF-mutant cancers depend on catalytic and non-catalytic activity of EZH2. *Nat Med* **2015**, *21,* 1491-1496.
(154) Xue, Y.; Meehan, B.; Fu, Z.; Wang, X. Q. D.; Fiset, P. O.; Rieker, R.; Levins, C.; Kong, T.; Zhu, X.; Morin, G.; Skerritt, L.; Herpel, E.; Venneti, S.; Martinez, D.; Judkins, A. R.; Jung, S.; Camilleri-Broet, S.; Gonzalez, A. V.; Guiot, M. C.; Lockwood, W. W.; Spicer, J. D.; Agaimy, A.; Pastor, W. A.; Dostie, J.; Rak, J.; Foulkes, W. D.; Huang, S. SMARCA4 loss is synthetic lethal with CDK4/6 inhibition in non-small cell lung cancer. *Nat Commun* **2019**, *10,* 557.
(155) Arrowsmith, C. H.; Bountra, C.; Fish, P. V.; Lee, K.; Schapira, M. Epigenetic protein families: a new frontier for drug discovery. *Nat Rev Drug Discov* **2012**, *11,* 384-400.
(156) Jancewicz, I.; Siedlecki, J. A.; Sarnowski, T. J.; Sarnowska, E. BRM: the core ATPase subunit of SWI/SNF chromatin-remodelling complex-a tumour suppressor or tumour-promoting factor? *Epigenetics Chromatin* **2019**, *12,* 68.
(157) Willis, M. S.; Homeister, J. W.; Rosson, G. B.; Annayev, Y.; Holley, D.; Holly, S. P.; Madden, V. J.; Godfrey, V.; Parise, L. V.; Bultman, S. J. Functional redundancy of SWI/SNF catalytic subunits in maintaining vascular endothelial cells in the adult heart. *Circ Res* **2012**, *111,* e111-122.
(158) Takada, Y.; Fukuda, A.; Chiba, T.; Seno, H. Brg1 plays an essential role in development and homeostasis of the duodenum through regulation of Notch signaling. *Development* **2016**, *143,* 3532-3539.
(159) Gechijian, L. N.; Buckley, D. L.; Lawlor, M. A.; Reyes, J. M.; Paulk, J.; Ott, C. J.; Winter, G. E.; Erb, M. A.; Scott, T. G.; Xu, M.; Seo, H. S.; Dhe-Paganon, S.; Kwiatkowski, N. P.; Perry, J. A.; Qi, J.; Gray, N. S.; Bradner, J. E. Functional TRIM24 degrader via conjugation of ineffectual bromodomain and VHL ligands. *Nat Chem Biol* **2018**, *14,* 405-412.
(160) Wei, W.; Cherukupalli, S.; Jing, L.; Liu, X.; Zhan, P. Fsp(3): A new parameter for drug-likeness. *Drug Discov Today* **2020**, *25,* 1839-1845.
(161) Fuhrmann, J.; Wu, H.; Fairbrother, W. J. Preparation of 1-[2-(4-cyclopropyl-1H-1,2,3-triazol-1-yl)acetyl]-4-hydroxy-N-benzylpyrrolidine -2-carboxamide derivatives as VHL inhibitors for treating anemia and cancer. WO2022103411, 2022.

(162) Cyriac, J. M.; James, E. Switch over from intravenous to oral therapy: A concise overview. *J Pharmacol Pharmacother* **2014**, *5,* 83-87.
(163) Spradlin, J. N.; Hu, X.; Ward, C. C.; Brittain, S. M.; Jones, M. D.; Ou, L.; To, M.; Proudfoot, A.; Ornelas, E.; Woldegiorgis, M.; Olzmann, J. A.; Bussiere, D. E.; Thomas, J. R.; Tallarico, J. A.; McKenna, J. M.; Schirle, M.; Maimone, T. J.; Nomura, D. K. Harnessing the anti-cancer natural product nimbolide for targeted protein degradation. *Nat Chem Biol* **2019**, *15,* 747-755.
(164) Ward, C. C.; Kleinman, J. I.; Brittain, S. M.; Lee, P. S.; Chung, C. Y. S.; Kim, K.; Petri, Y.; Thomas, J. R.; Tallarico, J. A.; McKenna, J. M.; Schirle, M.; Nomura, D. K. Covalent Ligand Screening Uncovers a RNF4 E3 Ligase Recruiter for Targeted Protein Degradation Applications. *ACS Chem Biol* **2019**, *14,* 2430-2440.
(165) Zhang, X.; Crowley, V. M.; Wucherpfennig, T. G.; Dix, M. M.; Cravatt, B. F. Electrophilic PROTACs that degrade nuclear proteins by engaging DCAF16. *Nat Chem Biol* **2019**, *15,* 737-746.
(166) Wei, J.; Meng, F.; Park, K. S.; Yim, H.; Velez, J.; Kumar, P.; Wang, L.; Xie, L.; Chen, H.; Shen, Y.; Teichman, E.; Li, D.; Wang, G. G.; Chen, X.; Kaniskan, H.; Jin, J. Harnessing the E3 Ligase KEAP1 for Targeted Protein Degradation. *J Am Chem Soc* **2021**, *143,* 15073-15083.
(167) Vulpetti, A.; Holzer, P.; Schmiedeberg, N.; Imbach-Weese, P.; Pissot-Soldermann, C.; Hollingworth, G. J.; Radimerski, T.; Thoma, C. R.; Stachyra, T. M.; Wojtynek, M.; Maschlej, M.; Chau, S.; Schuffenhauer, A.; Fernández, C.; Schröder, M.; Renatus, M. Discovery of New Binders for DCAF1, an Emerging Ligase Target in the Targeted Protein Degradation Field. *ACS Med Chem Lett* **2023**, *14,* 949-954.
(168) Renaud, J. P.; Chari, A.; Ciferri, C.; Liu, W. T.; Rémigy, H. W.; Stark, H.; Wiesmann, C. Cryo-EM in drug discovery: achievements, limitations and prospects. *Nat Rev Drug Discov* **2018**, *17,* 471-492.
(169) Ramírez-Aportela, E.; López-Blanco, J. R.; Chacón, P. FRODOCK 2.0: fast protein-protein docking server. *Bioinformatics* **2016**, *32,* 2386-2388.
(170) Olechnovič, K.; Venclovas, Č. VoroMQA: Assessment of protein structure quality using interatomic contact areas. *Proteins* **2017**, *85,* 1131-1145.
(171) Lyskov, S.; Gray, J. J. The RosettaDock server for local protein-protein docking. *Nucleic Acids Res* **2008**, *36,* W233-238.
(172) Ishoey, M.; Chorn, S.; Singh, N.; Jaeger, M. G.; Brand, M.; Paulk, J.; Bauer, S.; Erb, M. A.; Parapatics, K.; Müller, A. C.; Bennett, K. L.; Ecker, G. F.; Bradner, J. E.; Winter, G. E. Translation Termination Factor GSPT1 Is a Phenotypically Relevant Off-Target of Heterobifunctional Phthalimide Degraders. *ACS Chem Biol* **2018**, *13,* 553-560.
(173) Yang, J.; Li, Y.; Aguilar, A.; Liu, Z.; Yang, C. Y.; Wang, S. Simple Structural Modifications Converting a Bona fide MDM2 PROTAC Degrader into a Molecular Glue Molecule: A Cautionary Tale in the Design of PROTAC Degraders. *J Med Chem* **2019**, *62,* 9471-9487.
(174) Medina, P. P.; Romero, O. A.; Kohno, T.; Montuenga, L. M.; Pio, R.; Yokota, J.; Sanchez-Cespedes, M. Frequent BRG1/SMARCA4-inactivating mutations in human lung cancer cell lines. *Hum Mutat* **2008**, *29,* 617-622.
(175) Network, T. C. G. A. R. Comprehensive molecular profiling of lung adenocarcinoma. *Nature* **2014**, *511,* 543-550.
(176) Le Loarer, F.; Watson, S.; Pierron, G.; de Montpreville, V. T.; Ballet, S.; Firmin, N.; Auguste, A.; Pissaloux, D.; Boyault, S.; Paindavoine, S.; Dechelotte, P. J.; Besse, B.; Vignaud, J. M.; Brevet, M.; Fadel, E.; Richer, W.; Treilleux, I.; Masliah-Planchon, J.; Devouassoux-Shisheboran, M.; Zalcman, G.; Allory, Y.; Bourdeaut, F.; Thivolet-Bejui, F.; Ranchere-Vince, D.; Girard, N.; Lantuejoul, S.; Galateau-Sallé, F.; Coindre, J. M.; Leary, A.; Delattre, O.; Blay, J. Y.; Tirode, F. SMARCA4 inactivation defines a group of undifferentiated thoracic malignancies transcriptionally related to BAF-deficient sarcomas. *Nat Genet* **2015**, *47,* 1200-1205.